TAL TECH

DOCTORAL THESIS

Fully Automated Tuning of Microwave Coaxial Cavity Filters

Even Sekhri

TALLINNA TEHNIKAÜLIKOOL
TALLINN UNIVERSITY OF TECHNOLOGY
TALLINN 2024

TALLINN UNIVERSITY OF TECHNOLOGY
DOCTORAL THESIS
20/2024

Fully Automated Tuning of Microwave Coaxial Cavity Filters

EVEN SEKHRI

TAL TECH PRESS

TALLINN UNIVERSITY OF TECHNOLOGY
School of Engineering
Department of Electrical Power Engineering and Mechatronics
This dissertation was accepted for the defence of the degree 22/04/2024

Supervisors: Prof. Mart Tamre
School of Engineering
Tallinn University of Technology, Tallinn, Estonia

Prof. Rajiv Kapoor
Electronics and Communication Department
Delhi Technological University, New Delhi, India

Prof. Anton Rassõlkin
School of Engineering
Tallinn University of Technology, Tallinn, Estonia

Industry Expert: Robert Hudjakov, Ph.D.
Software Developer
IPTE Automation OÜ, Tallinn, Estonia

Opponents: Dr Levon Gevorkov
Power Systems Group
Catalonia Institute for Energy Research (IREC), Spain, Barcelona

Dr Pēteris Apse-Apsītis
Institute of Industrial Electronics and Electrical Engineering,
Riga Technical University, Riga, Latvia

Defence of the thesis: 30/05/2024, Tallinn

Declaration:
Hereby I declare that this doctoral thesis, my original investigation and achievement, submitted for the doctoral degree at Tallinn University of Technology has not been submitted for doctoral or equivalent academic degree.

Even Sekhri

---
signature

European Union
European Regional Development Fund

Investing in your future

ISSN 2585-6898 (publication)
ISBN 978-9916-80-138-3 (publication)
ISSN 2585-6901 (PDF)
ISBN 978-9916-80-139-0 (PDF)
DOI https://doi.org/10.23658/taltech.20/2024
Printed by Koopia Niini & Rauam

Sekhri, E. (2024). *Fully Automated Tuning of Microwave Coaxial Cavity Filters* [TalTech Press]. https://doi.org/10.23658/taltech.20/2024

TALLINNA TEHNIKAÜLIKOOL
DOKTORITÖÖ
20/2024

Mikrolaine-koaksiaalfiltrite täisautomaatne häälestamine

EVEN SEKHRI

TAL TECH
KIRJASTUS

Contents

List of Publications

I M. Vu, M. Tamre and **E. Sekhri**, "Modeling and Robust Control Algorithm for a Linear Belt Driven System," *Open Computer Science,* vol. 8, pp. 142–153, 2018, doi: 10.1515/comp-2018-0010.

II **E. Sekhri**, M. Tamre and R. Kapoor, "Optimal Q-Learning Approach for Tuning the Cavity Filters," *2019 20th International Conference on Research and Education in Mechatronics (REM), Wels, Austria*, 2019, pp. 1–5, doi: 10.1109/REM.2019.8744118.

III **E. Sekhri**, R. Kapoor and M. Tamre, "Double Deep Q-Learning Approach for Tuning Microwave Cavity Filters using Locally Linear Embedding Technique," *2020 International Conference on Mechatronic Systems and Materials (MSM), Bialystok, Poland*, 2020, pp. 1–6, doi: 10.1109/MSM49833.2020.9202393.

IV **E. Sekhri**, M. Tamre, R. Kapoor and D. C. Liyanage, "Novel Band-Subtraction Technique to Differentiate Screws for Microwave Cavity Filter Tuning," *2023 3rd International Conference on Electrical, Computer, Communications and Mechatronics Engineering (ICECCME)*, Tenerife, Canary Islands, Spain, 2023, pp. 1–6, doi: 10.1109/ICECCME57830.2023.10253048.

V **E. Sekhri**, M. Tamre, R. Kapoor and R. Kumar, "A Novel Real-time Parametric Tracking Approach for Robust Microwave Filter Tuning," *2023 The IEEE International Conference on Artificial Intelligence, Blockchain and Internet of Things (AIBThings)*, Mount Pleasant, MI, USA, 2023, pp. 1–5, doi: 10.1109/AIBThings58340.2023.10292473.

VI **E. Sekhri**, M. Tamre and R. Kapoor, "Data-Driven Approaches Based Microwave Filter Tuning – A Review," *3rd International Conference on Artificial-Business Analytics, Quantum and Machine Learning: Trends, Perspectives, and Prospects (COM-IT-CON 2023),* Faridabad, India, 2023, pp. 1–14.

VII **E. Sekhri**, M. Tamre and R. Kapoor, "An Efficient Assistance in Cavity Filter Tuning using Filter Screw Classification," *3rd International Conference on Artificial-Business Analytics, Quantum and Machine Learning: Trends, Perspectives, and Prospects (COM-IT-CON 2023),* Faridabad, India, 2023, pp. 1–9.

VIII **E. Sekhri**, R. Kapoor and M. Tamre, "Review of State-of-the-Art Microwave Filter Tuning Techniques and Implementation of a Novel Tuning algorithm using Expert-based Hybrid Learning," *Wireless Personal Communications*, pp. 1–57, 2024, doi: 10.1007/s11277-024-10894-x

IX **E. Sekhri,** M. Tamre, R. Kapoor, "A Robotic System and Method for Automated Tuning of a Cavity Filter", Estonian Patent Application No. P202400005, filed Apr. 30, 2024.

Author's Contribution to the Publications

I. Even Sekhri implemented the robust controller to control the linear toothed-belt conveyor system in this work. This system is similar to the one designed under the scope of this thesis. Also, he had major contribution in writing this journal article.

II. Even Sekhri is the first author of this paper in which he was responsible for reviewing the related literature, simulating the filter tuning process and ensuring that the system reaches the global minima. Additionally, he had a major contribution in writing the paper. He presented this paper at 20th International Conference on Research and Education in Mechatronics (REM 2019), Wels, Austria.

III. Even Sekhri is the first author of this paper. The author was responsible for literature review, collecting the data for training the agent, implementing locally linear embedding (LLE) technique for dimensional reduction. He presented this paper at 20th International Conference on Mechatronic Systems and Materials (MSM 2020), Bialystok, Poland.

IV. Even Sekhri is the first author of this paper. He was responsible for conducting the experiments using the hyperspectral camera and monochrome camera and had major contribution in writing the paper. He presented this paper at 3rd International Conference on Electrical, Computer, Communications and Mechatronics Engineering (ICECCME 2023), Tenerife, Canary Islands, Spain.

V. Even Sekhri is the first author of this paper where he generated the labelled dataset for training the algorithm and collected the videos for testing the novel algorithm. In addition, he had major contribution in writing the paper. He presented this paper at 3rd International Conference on Artificial Intelligence, Blockchain and Internet of Things (AIBThings 2023), Mount Pleasant, MI, USA.

VI. Even Sekhri is the first author of this paper in which he reviewed the various data-driven approaches for tuning the filters. He had major contribution in collecting and segregating the data as well as in writing the paper. He presented this paper at the 3rd International Conference on Artificial-Business Analytics, Quantum and Machine Learning: Trends, Perspectives, and Prospects, Faridabad, India.

VII. Even Sekhri is the first author of this paper in which he had major role in generating the dataset, labelling the dataset and implementing the state-of-the-art ML algorithms in addition to writing the paper. He presented this paper at the 3rd International Conference on Artificial-Business Analytics, Quantum and Machine Learning: Trends, Perspectives, and Prospects, Faridabad, India. This paper was awarded as the best paper in the conference.

VIII. Even Sekhri is the first author of this article in which he was responsible for compiling the literature review for the various filter tuning techniques. He had major role in writing the article and comparing the state-of-the-art filter tuning techniques. Additionally, he also implemented a novel filter tuning technique in which expert-based hybrid learning was used to tune a 5th order filter.

IX. Even Sekhri is the first author of this patent application. The patent application has been submitted to the Estonian Patent Office and is under review at the moment. He had a major role in drafting the patent.

Abbreviations

AI	Artificial Intelligence
ANFIS	Adaptive Neuro-Fuzzy Inference System
ANN	Artificial Neural Network
ASM	Aggressive Space Mapping
BP	Band Pass
BPNN	Back Propagation Neural Network
CAT	Computer-Aided Tuning
CM	Coupling Matrix
CNN	Convolutional Neural Network
DoH	Determinant of Hessian
DR	Dielectric Resonator
DS	Direct Search
DT	Decision Tree
DQN	Deep Q-Network
DDPG	Deep-Deterministic Policy Gradient
DDQN	Double Deep Q-Network
EM	Electromagnetic
FAT	Fully Automated Tuning
FD	Frequency Domain
FF	Feed-Forward
FIR	Finite Impulse Response
FL	Fuzzy Logic
FLS	Fuzzy Logic System
FNN	Fuzzy Neural Network
FVC	Frequency-Variant Coupling
GA	Genetic Algorithm
GD	Group Delay
GE	Generalisation Error
HSI	Hyperspectral Imaging
IAFTT	Intelligent Automatic Filter Tuning Tool
IFFT	Inverse Fast Fourier Transform
IL	Insertion Loss
ISM	Implicit Space Mapping
KNN	K-Nearest Neighbours
LLE	Locally Linear Embedding
LP	Low Pass
LSM	Least-Squares Method
MDP	Markov Decision Process
ML	Machine Learning

MSE	Mean Squared Error
MW	Microwave
NFS	Neuro-Fuzzy System
NN	Neural Network
PCA	Principal Component Analysis
PE	Parameter Extraction
PF	Particle Filter
PIM	Passive Inter-Modulation
Q_{ext}	External Q
Q_u	Unloaded Q
RBS	Radio Base Stations
RF	Radio Frequency
RL	Return Loss
RLS	Recursive Least Square
RZ	Reflection Zero
SA	Simulated Annealing
SCARA	Selective Compliance Articulated Robot Arm
SGD	Stochastic Gradient Descent
S-Parameters	Scattering Parameters
SIR	Stepped Impedance Resonator
SIW	Substrate Integrated Waveguide
SM	Space Mapping
SNA	Scalar Network Analyser
S-L	Source-Load
SQP	Sequential Quadratic Programming
SVD	Singular Value Decomposition
SVM	Support Vector Machine
TD	Time Domain
TL	Transmission Line
TLS	Total Least Square
TZ	Transmission Zero
VF	Vector Fitting
VNA	Vector Network Analyser
WBS	Wireless Base Station
w.r.t	with respect to
Y-Parameters	Admittance Parameters
YZ-Parameters	Immittance Parameters

1 Introduction

1.1 Motivation and Background

Microwave (MW) or Radio Frequency (RF) filters play a sterling role in space and ground-based wireless communication systems. They are used to separate the desired frequency from a broad spectrum of frequencies. The production of numerous MW/RF filter designs, including as waveguide filters, co-axial filters, microstrip-line filters, dielectric resonator filters, varactor-based filters, etc., was prompted by the substantial rise in the demand for communications systems. In Wireless Base Station (WBS)/Radio Base Station (RBS) systems installations, the most prevalent is the cavity bandpass filter. Additionally, every filter's enclosure has several interlinked resonators that are usually fixed to filter's base. Band selectivity (sharp band transitions) of the filters can be augmented by increasing the number of resonators. However, increasing the quantity of resonators also leads to higher insertion losses and increased size of the filter. A few of the industry-standard cavity filter variants are depicted in Fig. 1.1.

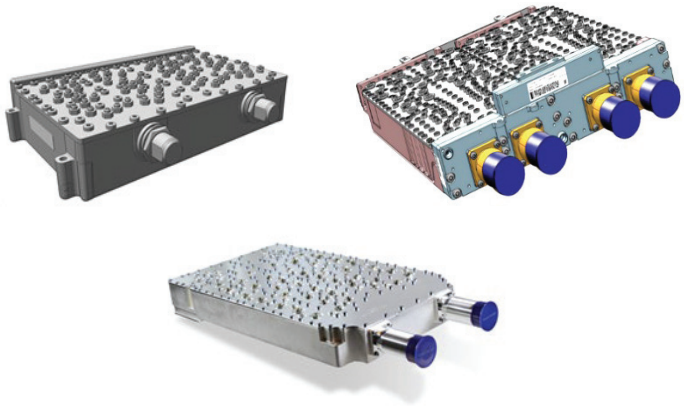

Figure 1.1. Samples of cavity filters used in the industry (Modelled in SolidWorks)

Higher-order filters with cross-coupled topology are commonplace in real-world applications as they satisfy the present-day sharp frequency requirements. This cross-coupling facilitates the creation of Transmission Zero (TZ) [1]. In addition to satisfying strict requirements for frequency selectivity, these TZs also help with design flexibility, achieving Chebyshev response, optimising in-band response, and reducing filter size. Thus, having TZs ensure reduced losses, swifter manufacturing, and decreased overall costs. The complex TZs synthesise to equalise the Group Delay (GD) and the real TZs eliminate the undesired interfering signals. In [2], the algorithm for determining the maximum realisable TZs for a given topology was introduced. The effectiveness of Frequency-Variant Couplings (FVCs) in fulfilling the stringent frequency constraints has been discussed in [3].

Due to reasons such as – inaccurate manufacturing tolerances, design mistakes, variations in properties of material, etc., the filters mar the anticipated frequency response. To compensate this, tuning the filter becomes inescapable [4]. A variety of approaches, from mechanical to electronic and magnetic systems, have been utilised for

tuning the filters. Various characteristics, such as tuning range, tuning quality, tuning speed, tuning complexity, power handling capacity, etc., are typically used to evaluate tuning methods. There are benefits and drawbacks to each technique, and none is unambiguously better than the others. The exact application and its constraints are the sole considerations that determine the tuning strategies and methods to use.

For post-fabrication filter tuning, elements such as varactors and screws are typically provided on the filter structure. The most prevalent type of tuning is mechanical tuning, in which tuning screws are affixed to the filter's surface. The "insertion depth" of tuning elements is the primary factor that determines variations in resonance frequencies, inter-resonator coupling between the cavities, and the filter's overall frequency response. The objective of tuning is to locate the tuning elements in the most optimal possible positions to meet the desired tuning criteria. It is safe to state that filter tuning is an optimisation problem by nature.

Filters can be classified according to:

a) type of components used – passive or active
b) filter response – low pass, high pass, band pass, band reject
c) frequency band – L-band, X-band, Xu-band, etc.
d) filter technology – coaxial, planar, dielectric filter, interdigital filters, waveguides, Substrate Integrated Waveguide (SIW) filters, Stepped Impedance Resonator (SIR) filter
e) ripple types – Butterworth, Elliptical, Chebyshev, Bessel, Gaussian, etc.

Given the wide range of filters available on the market, the tuning process cannot be generalised; that is, no one technique can be used to tune every kind of filter. A study conducted on combline filters showed that the overall response of those filters is impacted by the tuning structure [5] and the walls [6]. When tuning complex filters, that is, filters with higher-order and/or cross-coupled topologies, the amount of time required and the difficulty level increase exponentially (i.e., repeated adjustments are demanded). This is due to a highly non-linear relationship that exists between the tuning elements and the frequency response of the filter [7].

Because the tuning process is deterministic, skilled technicians are required. These human operators decide which tuning screw needs to be adjusted in which direction and to what extent by looking at the Scattering parameters (S-parameters) response of the filter, which are shown on a Vector Network Analyser (VNA). While there are some suggestions available [8] to support these technicians, extensive training is still mandated to achieve the requisite skill set. It's important to keep in mind that even if a technician is proficient at tuning one kind of filter, there's no guarantee that he or she will be able to do the same for other types or topologies of filters. Considering everything described above, filter tuning is now regarded as an "art" which requires experience, knowledge, and patience. Since it is difficult to locate new tuning technicians, the industry is also concerned about the sustainability of qualified and experienced tuning technicians. Additionally, because tuning involves heavy wrist motions, technicians frequently suffer wrist injuries, and the industries are responsible for paying for their medical bills. Therefore, the researchers in the sector are fighting to remove the manufacturing bottleneck by seeking automated ways to tune the assembled filters.

1.2 Research questions and objectives

This thesis aims to provide a complete automation solution to the filter tuning process that is apt for educational as well as industrial use. The suggested approach reduces human involvement to mounting the assembled filter in the holding fixture and initiating the tuning algorithm. This means there will be no need to train the technicians for the filter tuning process. The main objectives of this thesis can be summarized as:

1) To develop a simulating environment for reinforcement learning-based filter tuning algorithm(s) for testing the feasibility of proceeding in this direction and to decide the future strategy to solve the problem in hand.
2) To design and fabricate a universal test filter on which different automated filter tuning algorithms can be tested.
3) Building a customized experimental setup which can tune different kinds of filter using the automated filter tuning algorithm(s) by making only minor modifications.
4) To develop a vision-based system for distinguishing the tuning screws from the mounting screws and localising the tuning screws so that the positional coordinates can be used to send the tuning manipulator towards the tuning screws.
5) To develop and introduce a new fusion method(s) for tuning the MW filters which uses the theoretical knowledge of filtering theory, and combination of theoretical knowledge and Artificial Intelligence (AI) for tuning the filter. The sub-goals are:
    a) To generate dataset(s) which can be used by the Machine Learning (ML)-based algorithms while tuning the filter.
    b) Incorporating the speed-variation logic as per the difference between the current tuning state and the tuning target.
    c) To add feedback in the system for tracking the tuning error in real-time using ML-based methods to avoid the tuning errors.
6) To develop a real-time plotting module to kill the dependency on the VNA's commercial software which offers limited possibilities to make customized changes.

It is to be noted that optimising the tuning time has not been considered as an objective in this research work currently. Even if speed variation logic has been added into the system to reduce the overall tuning time, its optimisation has been suggested as the future scope. The design analysis of the designed experimental structure (i.e., stress analysis, strain analysis and vibration analysis etc.) has also been kept beyond the scope of this thesis due to enormous work. Also, the cost analysis has not been made yet as having a cost-effective automated tuning setup has not been the main objective of this research.

1.3 Novelties

This work has made the following contributions to meet the abovementioned objectives:

- Simulating the filter tuning process using reinforcement learning-based algorithms for deciding the tuning strategy. It is ensured that the key information is not lost when the pre-processing step is included for dimensionality reduction.
- Designing and fabricating a new test filter which allows the evaluation of automated tuning algorithms.
- Developing an automated setup based on a relative positioning system equipped with a customized tool-in-tool mechanism for complete tuning and locking of the filter's tuning screws. The experimental setup has been

designed in a way that it is suitable to tune different types of filters produced by the industry just by making minor modifications in the designed manipulator.

- Implementing vision-based approaches to differentiate the tuning screws from the mounting screws.
- Testing and comparing the novel fusion algorithms which use the theoretical knowledge and its combination with AI for automating the tuning process of cavity filters.
- Tracking the tuning error using Particle Filters (PF) so that the robotic manipulator is not following the instructions given to it blindly and the potential error can be recognized in its beginning phase.
- Removing the dependence on VNA's commercial software to get the information about the current tuning state of the filter by developing a customizable plotting module.

The novel filter tuning solution proposed in this thesis can be used as a standalone universal system for fully automated tuning of iris-coupled all-pole cavity filters equipped with quarter wavelength resonators. The proposed algorithms are evaluated on a test filter designed in this work. The proposed solution can also deal with similar systems by making slight modifications to software and/or hardware, but currently, they are kept beyond the scope of this thesis due to enormous work.

2 Literature Review on Filter Tuning

2.1 Chapter overview

Numerous researchers have put forth unique and distinctive approaches to decipher the problem of filter tuning. This chapter aims to comprehensively assess and consolidate the significant discoveries in filter tuning algorithms, while also acknowledging their constraints. In pursuit of automation objectives, the research community has introduced a range of appropriate mechanisms and diverse automated filter tuning solutions. This chapter discusses these contributions as well.

2.2 Scope of the literature review

The extensive literature review compiled in this chapter focuses exclusively on mechanical filter tuning (i.e., tuning with the help of screws) only. This thesis work is solely dedicated to passive filters, particularly cavity filters as they offer higher power handling capacity, stable operation in wide range of temperatures, and high-Q (quality factor).

The following have been kept beyond the scope of the literature review:

- Filters such as – active filters, microstrip filters, varactor-based filters, ferroelectric filters, superconducting filters.
- Theses – Master studies and doctorate studies
- Patents

2.3 Review of filter tuning techniques

The filter tuning methods proposed by the researchers can be categorized into seven major groups:

1) Filter Tuning in Time Domain
2) Sequential Filter Tuning Methods
3) Filter Tuning on the basis of Filter Diagnosis
4) Space Mapping based Filter Tuning
5) Sensitivity Analysis based Filter Tuning
6) Data-Driven Approaches for Tuning the Filters
7) Hybrid Methods

Fig. 2.1 illustrates the range of filter tuning techniques introduced by the research community in the past in which the groups as well as the sub-groups of the filter tuning techniques are presented.

2.4 Detailed comparison of tuning methods in literature

In [VIII], the author of the current investigation presented and discussed a detailed analysis of the available research related to filter tuning methods. The review which is solely dedicated to data-driven approaches is discussed in [VI]. This section aims to synthesize the key limitations of each type of technique. Table 2.1 presents the key limitations of the techniques proposed by the research community and the related publications published under each category.

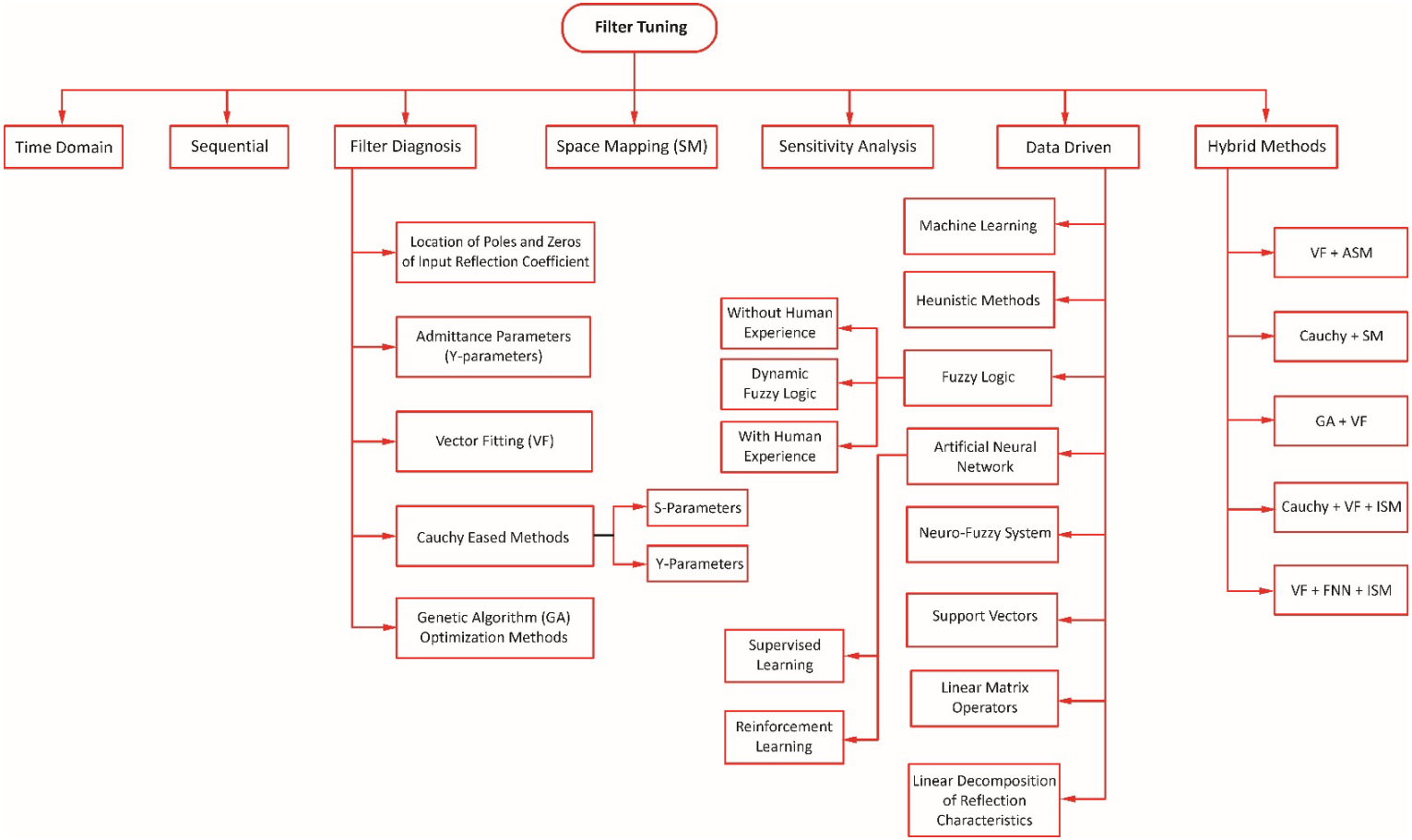

Figure 2.1. Various tuning techniques proposed in literature

Table 2.1. The key limitations of all the filter tuning techniques in literature

Techniques and Publications			Limitations	
Filter Tuning in Time Domain (TD) [9], [10], [11], [12], [13]			The TD methodology for filter tuning has limitations affecting its practicality. Challenges include difficulty in accurately determining coupling and resonant frequency values, reliance on an equivalent circuit model prone to inaccuracies, and the necessity of a reference "golden" filter for ideal responses, limiting adaptability. Additionally, fine-tuning adjustments are often required, requiring operator intervention and increasing complexity, the method is incapable of dealing with filters having asymmetrical frequency response (like multiplexers for satellite communications). Moreover, achieving the objective of adjusting each tuning screw only once is not possible. Multiple rotations to the screws are avoided as they can lead to Passive Inter-Modulation (PIM) effects and filter damage.	
Sequential Filter Tuning [14], [15], [16], [17], [18], [19], [20], [21], [22], [23], [9], [10], [11], [12], [24]			Sequential tuning techniques can help by splitting the filter tuning process into smaller sub-problems; however, the cumulative error propagation issue prevents the commercial application of this approach. Furthermore, segregating the resonators from the filter structure is challenging (particularly for dielectric resonator filters); shorting the resonators or removing the screws entirely from the filter surface is yet another problem while automating the filter tuning process. The authors of [21], [22] and [23] suggested strategies to solve the error propagation issue, but the final tuning state of the filter after implementing the aforementioned technique is not what is intended. This means that a laborious fine-tuning step becomes essential.	
FILTER	1	Location of Poles and Zeros of Input Reflection Coefficient [25], [26], [27], [28], [29]	Filter tuning methods that use the location of poles and zeros is a very iterative process. The accuracy of the locations identified for poles and zeros directly affects the correctness of the parameters extracted using this method. Errors are also introduced by adding more resonators, implying that higher-order filters cannot be tuned using this method. Additionally, the calibration processes used to define the reference plane for phase measurement are the primary determinant of the system's accuracy.	The primary drawbacks of all filter modeling-based techniques are that the mathematical models are typically simply approximations and not very accurate. It is either difficult or
	2	Y-Parameters [30], [31], [32], [33], [34], [35]	The phase loading effects must likewise be eliminated from Y-Parameters in order to retrieve the poles and residues, just like in the filter diagnosis based on widely utilised S-Parameters. Eliminating phase loading is a crucial step because, although phase loading is always present in a physical filter unit, it is not incorporated into the filter models based on Coupling Matrix (CM). Furthermore, the necessity for cautious manipulations makes this methodology unsuitable for use with an automated tuning solution.	

Techniques and Publications			Limitations		
DIAGNOSIS FILTER	3	Vector Fitting (VF) [36], [37]	Using the VF technique, further transformations such as the one suggested in [96] are required to extract an accurate CM. Alternatively, additional optimisation of the extracted CM is required. Furthermore, the VF approach is inappropriate for use with an automated tuning system since it only requires frequency samples defined in the positive direction.		occasionally impossible to find an accurate network model where all tuning elements are correctly represented. The fact that varying the location of a single tuning element typically impacts the performance of neighbouring elements as well is not considered by these approximations. In addition, the model-based methods cannot be generalised to other filter topologies. The fact that traditional CM ignores performance degradation brought on by
	Cauchy Methods	4a	S-Parameters based Cauchy Method [38], [39], [40], [41], [42], [43], [44], [45], [46], [47], [48], [34], [49]	The last step in any research study that employs the Cauchy method is to synthesise the CM using conventional methods detailed in references [97], [98], and [99]. The main problem with the Cauchy method (for diagnosing and tuning filters) is that it cannot handle higher-order systems because the Vandermonde matrix it uses becomes ill-conditioned and loses accuracy when the number of unknowns increases [100]. Although [101] discusses several helpful strategies to handle this issue, the accuracy of this approach is still insufficient to support the usage of this method to provide an automatic filter tuning solution. Another variation on the Cauchy method that may handle higher-order systems was introduced in [102], where the authors suggested preconditioning the system's main matrix using a suitable scaling technique. Matrix equilibration has been proposed in [103] and [104] as a key factor in increasing numerical computations. Thus, the approach suggested in [102] is time-consuming, computationally demanding, and underperforming at high detuning levels. Furthermore, the existence of second order effects generally results in a reduction of the accuracy of the Cauchy method.	
		4b	Y-Parameters based Cauchy Method [35]		
	5	Optimisation-based Filter Tuning [50], [51], [52], [53], [54], [55], [56], [21], [22], [17], [26]	All optimisation-based filter tuning techniques have the following general problems: they cannot handle highly detuned filters; they cannot accurately detect spurious and unwanted couplings between neighbouring elements; the process of locating the global minima is complex; and achieving the global minima primarily depends on the number and initial guess of the optimisation variables as well as the defined initial values. The method described in [105] is one way to overcome some of these issues. A technique for determining the parametric model was proposed in [105]. It combined the Differential Evolution Particle Swarm Optimisation (DESPO) algorithm with a Multiple Hidden Layered Extreme Learning Machine (MELM). The relationship between a change in screw length and an equivalent change in CM parameters could be demonstrated by this model.		

Techniques and Publications			Limitations	
DIAGNOSIS			Alternatively, a tuning model based on improved Back-Propagation Neural Network (BPNN) and Gauss Kernel Clustering presented in [106] can also be used where the use of the Shuffled Frog-Leaping algorithm can optimise the weights of the BPNN architecture. While these models may not be able completely resolve the issue, they can help with filter tuning to some extent.	practical uncertainty and material characteristic variations is another drawback of employing this methodology.
Space Mapping (SM) based Filter Tuning [57], [58], [59], [60]			When employing SM as a filter tuning solution, the fine model's information is crucial to the accuracy of the solution, or it requires a large number of pre-assigned parameters, which can lead to poor convergence or even algorithmic failure. Additionally, the quality of the mapping is greatly impacted by the chosen Parameter Extraction (PE) process. Briefly, PE is the process of matching and optimising the parameters of the coarse/surrogate model to the measurement result. Inaccurate results are the product of an erroneous PE process. Since the precise PE extraction procedure has not yet been disclosed, this technology cannot be applied commercially.	
Sensitivity Analysis based Filter Tuning [61], [25], [62], [51], [52], [53], [54], [33], [59]			Sensitivity analysis requires repeated measurements of sensitivity in order to be used for filter tuning. To obtain reliable results, sensitivity analysis is followed by an optimisation technique. The research discussed in this category did not take into account the practical aspects of tuning, such as the fact that a screw's turning affects the frequency and coupling of nearby screws. Instead, they were based solely on simulations. Moreover, the researchers' models were linear, which meant that they could only cover a certain range. In reality, though, the connection between the filter's input and output is non-linear. As a result, this process is time-consuming, limited to the "fine-tuning" stage, and unsuitable for tuning highly detuned filters.	
DATA	1	Machine Learning (ML) [63]	An enormous volume of precise training data is typically required for an ML system to operate well and consistently. Such data collection is costly in terms of money, computing power, and time. An additional significant issue with this method is the data's bias towards a specific kind of instrument (filter topology).	Every data-driven technique covered, including ANNs, SVMs, FL, ML, and heuristic

Techniques and Publications				Limitations	
DATA DRIVEN	2	Heuristic Methods (Derivative-free) [64]	Since the optimisation algorithms are lengthy and largely dependent on starting values, using the results of direct search optimisation routines is not the best method for filter tuning. Additionally, using heuristic approaches requires turning the screws multiple times. Automated tuning systems should avoid repetitive screw turnings as this might cause PIM issues within the filter.		approaches, learns its models from pre-recorded data. The quantity of accurate data that is accessible directly correlates with the accuracy of the data-driven models. The primary problems that negatively impact the effectiveness of data-driven strategies are incomplete, missing, dispersed, and lack of data, among other problems. Furthermore, the model's performance is impacted by the strong reliance on the techniques
	Fuzzy Logic	3a	Fuzzy Logic without using human experience [65], [66], [67]	Fuzzy-based methods for filter tuning have the following drawbacks: they are limited to in-line and lossless filters; they depend on the initial values of the Q-factor and CM elements; they are unable to provide information about the extent of deviation of the tuning element or the amount of adjustment required to bring the tuning screws to the desired tuning state; and they require a large number of linguistic rules to be defined in order to produce reliable results. Defining an excessive number of linguistic rules results in more complicated calculations and thus more delay. Furthermore, it is challenging to obtain a complex accurate model between the tuning screws and the CM elements.	
		3b	Fuzzy Logic with human experience [68], [69], [70]		
		3c	Dynamic Fuzzy		
	Artificial Neural Network (ANN)	4a	Supervised Learning [71], [72], [73], [24], [74], [75], [76]	ANN was used to tune MW devices and is still the most dependable multi-dimensional approximator. Nevertheless, the main problems with this approach are 1) it is unable to generalise; 2) a huge amount of training data is required. ANN models are data-driven and unaffected by filter structure, but they can only be used with filters of the same type once trained. Filters with different topologies will require a separate trained model; 3) if the current data fall outside the parameters of the data used to train the model, the optimal solution cannot be obtained; 4) real-time tuning model updates are not feasible; 5) the resulting training model may contain over-fitted data due to the conventional Back-Propagation method and the choice of the initial weights, and 6) using too many layers during the reinforcement learning process can result in an exponential rise in delay. Additionally, when using ANNs, it is also necessary to have a lengthy training period. There is now significant research being done to find an ANN-based fully automated filter tuning solution.	
		4b	Reinforcement Learning [77], [II], [78], [79], [III], [80]		

Techniques and Publications			Limitations	
DATA DRIVEN	5	Neuro-Fuzzy System [81]	When using Adaptive Neuro-Fuzzy Inference System (ANFIS), the data must be pre-processed, and the parameter convergence is poor. ANFIS models are also difficult to interpret.	employed, which frequently prevents generalisation to alternative topologies. Additionally, when a lot of training data is provided, the processing and calculation times grow substantially.
	6	Support Vectors [7], [82], [83], [84], [85]	The Support Vector models are not direct when it comes to filter tuning related research; that is, S-parameters are represented by a CM rather than in their original form taken from a VNA. The approximation of screw placements using the results of optimisation problem solutions is the other factor that contributed to inaccuracies. Furthermore, when human intelligence is not included in the modelling process and only filter structure is, the suggested approaches' generalisation capabilities suffer.	
	7	Linear Matrix Operator [86]	The quantity and quality of the data that is gathered greatly influences how well this methodology performs, even if it is not required to employ the training step when this methodology is implemented.	
	8	Linear Decomposition of Reflection Characteristics [87], [88]	The methodology avoided the requirement for a training phase by basing the system's response on the linear decomposition of the S-parameters. However, this process requires an optimisation step, which causes a delay in providing the final value.	
HYBRID	1	VF + ASM [89]	Getting the optimal tuning for the MW filters was the primary goal of employing hybrid filter tuning techniques. Even if there are advantages of utilising multiple techniques at once, this approach brings-in disadvantages of both approaches as well. The majority of combined techniques rely on imprecise filter modelling or PE processes.	
	2	Cauchy + SM-based [90], [91], [92]		
	3	GA + VF [93]		
	4	Cauchy + NN + ISM [94]		
	5	VF + FNN + ISM [95]		

2.5 Review of various automated filter tuning hardware

2.5.1 Single actuator

The equipment having a single actuator for tuning the screws sequentially tune the filters by rotating the screws one after the other. These types of systems are usually mounted on a Cartesian or SCARA (Selective Compliance Articulated Robot Arm).

Fig. 2.2 shows an automated setup introduced by COM DEV International Limited in 2003 [107]. This design has a single actuator which can rotate the screw as well as deal with the locking nut. This setup was used to tune the filters, diplexers as well as other multiplexers. It is mounted over a Cartesian bench. Fig. 2.3 shows 'Robby' robotic arm tuning a filter [108]. This robot uses Space Mapping optimisation technique for tuning the filter.

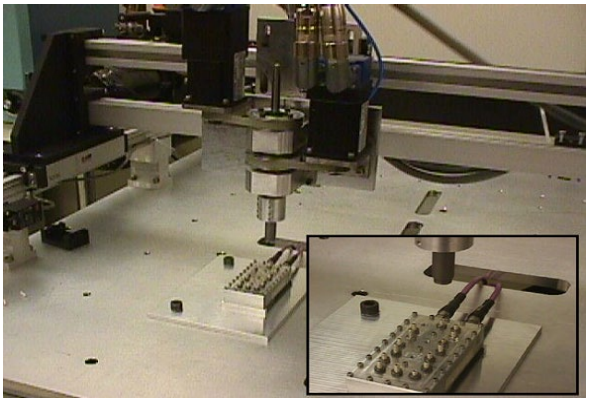

Figure 2.2. The cartesian robot by COM DEV tuning a cavity filter [107]

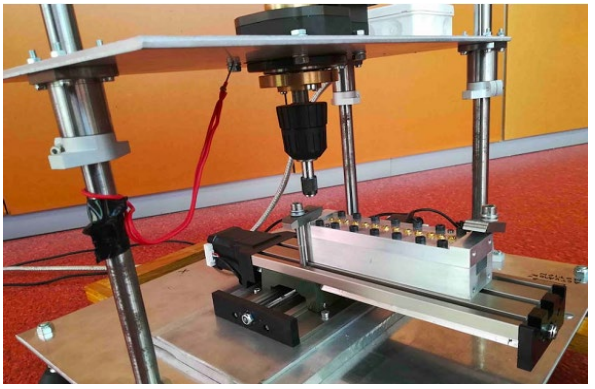

Figure 2.3. The 'Robby' robot tuning a cavity filter using ASM technique [108]

2.5.2 Multiple actuators

A multiple actuator setup allows many screws to be tuned simultaneously and hence can assist in parallel tuning. Such a setup can help in quick tuning. Fig. 2.4 shows a parallel tuning setup where flexible leads are used to transfer the stepper motor's motion to tuning screws of a waveguide filter using Fuzzy Logic (FL) technique [70] and scalar transmission technique [109].

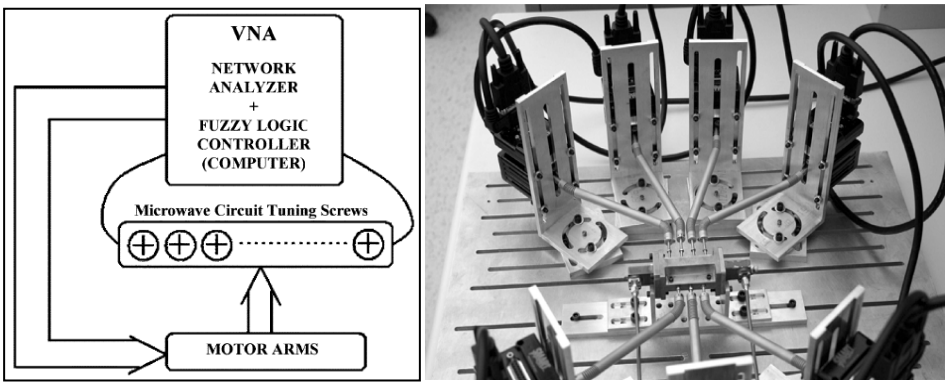

(a) (b)

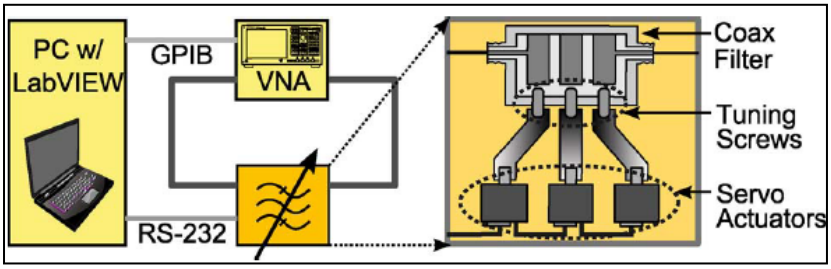

(c)

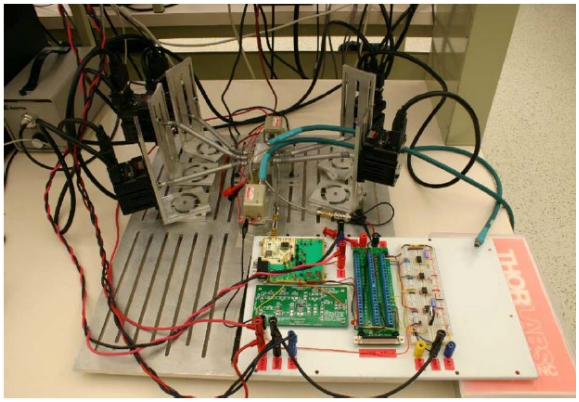

(d)

Figure 2.4. A multi-actuator robot – (a) and (b) block diagram of the tuning environment and tuning a waveguide filter using Fuzzy Logic [70]*; (c) and (d) block diagram and tuning environment and tuning a rectangular filter using scalar measurements-based algorithm* [109]

Fig. 2.5 presents a setup where 03 stepper motors are used for 03 stub matching of a WR-430 waveguide.

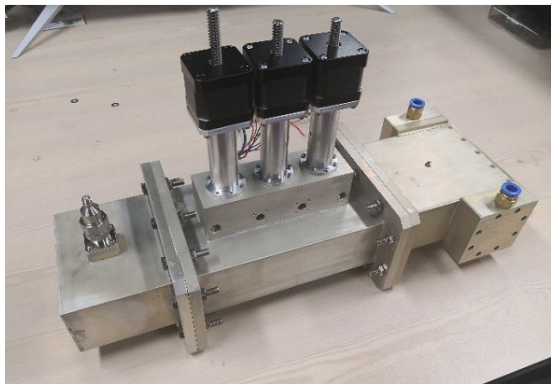

Figure 2.5. A parallel system of the 3-stub waveguide matching network [110]

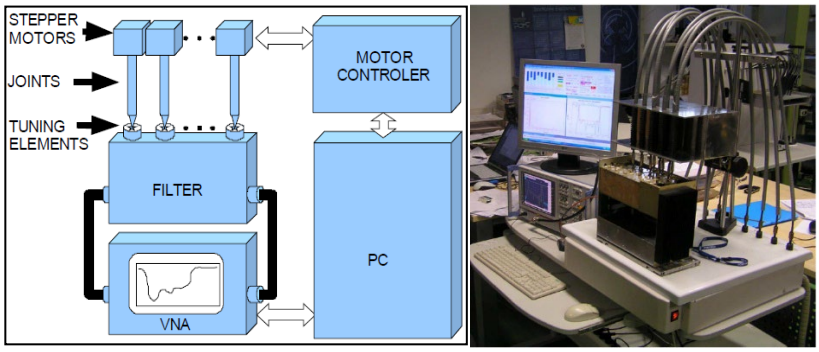

(a) (b)

Figure 2.6. IAFTT robot tuning the waveguide using DS + SA Algorithms – (a) block diagram; (b) filter tuning robot [64]

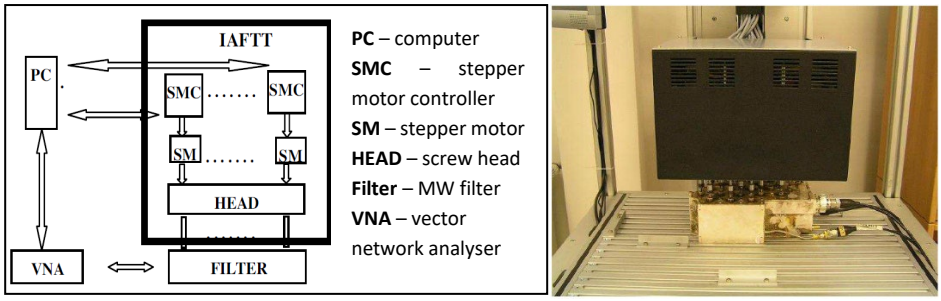

(a) (b)

Figure 2.7. A parallel filter tuning system with multiple actuators – (a) Block diagram of tuning environment [71]*; (b) Filter tuning robot* [111], [112]

2.6 Analysis of the literature review

2.6.1 Analysis related to tuning techniques

The decade-wise segregation of research publications in the field of filter tuning application has been compiled in Fig. 2.8. Scale of 1:1 on the y-axis of the Fig. 2.8 means that each coloured represents one publication of that category. The reader can even get

the information of the number of publications in each category (or each decade) by counting the number of blocks.

The main conclusions that can be drawn from the intensive literature review summarized in Fig. 2.8 are:

- Trends depicted in Fig. 2.8 show a downward trend in the research interest in tuning the filter based on – Time Domain (TD), Sensitivity Analysis, and Sequential Tuning techniques. One major reason contributing to this decline is that the filter tuning based on TD need special VNAs offering inverse Fourier transformations, and this method cannot be used to tune cross-coupled filters. Methods based on Sensitivity Analysis rely on equivalent filter models, demand for numerous measurements, and require various optimisation iterations, thus, making this technique suitable for the 'fine tuning' stage only. The Sequential Tuning methods proposed in the past suffer from cumulative error propagation issues.
- The techniques based on Space Mapping (SM) and Hybrid Methods have gathered the attention of researchers in recent times. The SM-based solutions are highly reliant on the accuracy of the fine model, and the Parameter Extraction (PE) process. However, an accurate PE process is not available yet.
- The rise in the data-driven approaches for tuning the MW filters in the last two decades can be witnessed in Fig. 2.8. This growth can be attributed to the fact that nowadays we have high computation capabilities provided by powerful CPUs and GPUs, as well as the availability of efficient algorithms. Thus, there is a potential to solve the overwhelming problems like the tuning of MW filters with the help of data-driven techniques.

2.6.2 Analysis related to filter tuning equipment

- The filter tuning equipment available in literature can be divided on the basis of number of actuator systems. Multiple-actuator systems allow a quick method of tuning the filters, but they need careful design of the tuning hardware. Such systems are designed according to a particular filter topology only i.e., they do not offer flexibility to deal with tuning of different kinds of filters available in the market.
- Single actuator-based tuning solutions are characterized by their larger tuning time, minimal need for intricate computations, and the ability to carry out parallel tuning operations. However, single actuator systems exhibit flexibility in handling different kinds of filters.
- Every filter tuning equipment developed by the research community operates in a strictly directive manner, meaning they do not rely on secondary feedback sources. The algorithm exclusively controls the stopping or restarting of the tuning process, a decision made only when the algorithm fails to achieve the desired tuning within the defined number of iterations.
- There is currently no filter tuning system capable of adjusting all types of cavity filters with minimal hardware and software changes, and possessing feedback source to detect the tuning error in the initial stages is yet not available.

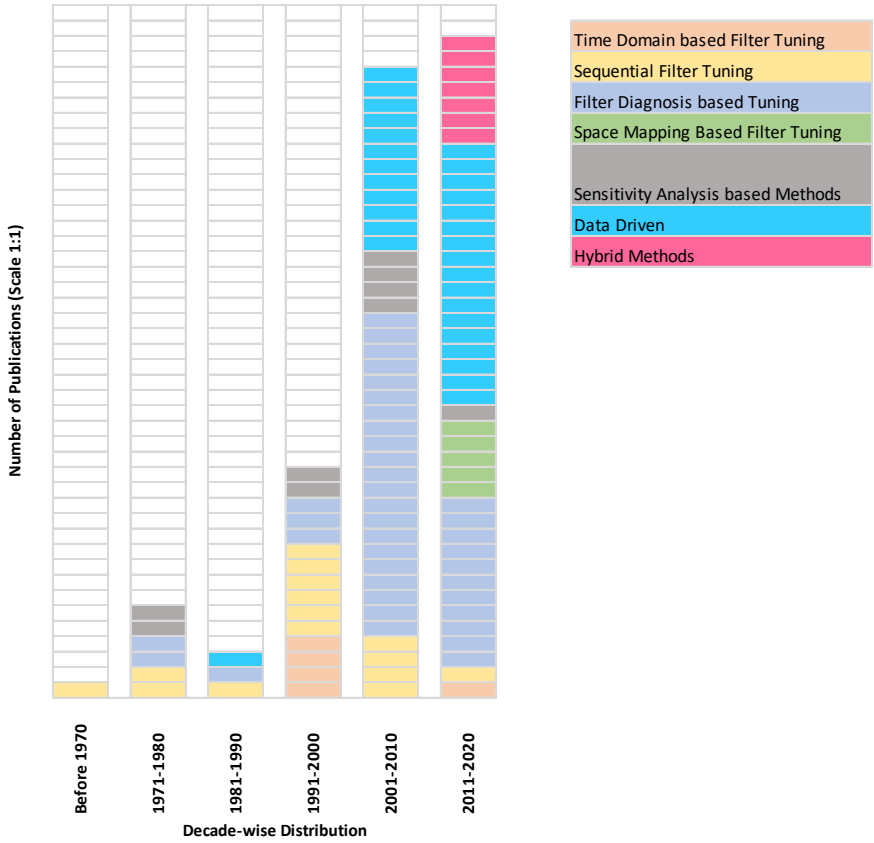

Figure 2.8. Decade-wise distribution of filter tuning techniques

2.7 Chapter summary

This chapter provided an extensive review related to various filter tuning techniques and various types of tuning equipment proposed in the literature. In light of the conclusions derived in section 2.5.1, the author of this thesis strongly advocates continued exploration of data-driven methods for post-production tuning of cavity filters.

The forthcoming chapter is specifically devoted to identifying the correct tuning algorithm using simulations. The suggested methods leverage reinforcement learning algorithms for meeting the desired frequency requirements.

3 Filter Tuning by Reinforcement Learning Simulations

3.1 Chapter overview

In Chapter 2 of the research, it was observed that none of the algorithms were able to fully grasp the intricate relationship between the position of the tuning screw and its corresponding S-parameters. One of the main challenges arises from the fact that there can be multiple combinations of screw positions that lead to the same S-parameter response. This lack of uniqueness complicates the tuning process and makes it highly dependent on the individual strategies of different technicians. Furthermore, it is important to note that the market offers a wide range of filters, each with its unique design parameters, so, generalisation of any kind is not possible. However, with the enhanced computational capabilities of modern computers and the introduction of several algorithms in recent years, it is feasible to explore intelligent methods to address the filter tuning problem.

Simulations are a good way to understand the present and potential problems occurring in the complex real-world tasks. Hence, the efforts presented in this chapter are dedicated to exploring reinforcement learning-based algorithms for tuning the filters. The basis of choosing reinforcement learning algorithms is the fact that they are inspired by learning process of living beings.

3.2 Overview of reinforcement learning and related algorithms

3.2.1 Reinforcement learning

Reinforcement learning is a class of ML that doesn't need any supervision rather it learns the patterns from the environment in which they are implemented. Reinforcement learning-based algorithms offer the solution to stochastic sequential decision-making problems where accurate mathematical modelling is not possible [113].

Reinforcement learning is based on Markovinan property i.e., the current position of an entity is independent of the steps taken in all previous timestamps. Markov Decision Process (MDP) provides a framework for mathematical modelling when outcomes are partly under the decision maker's control and partly random. Selecting the optimal action by the 'agent' from its current 'state' and aiming the maximum future 'reward' signal over time in the 'environment' is the goal of reinforcement learning. The notations in this context are:

- $s \in S$ – State of the considered system
- $a \in A$ – Action taken by the agent
- r – Reward Function
- π – Policy Function
- γ – Discount rate $\in (0,1]$ where a smaller value means we are emphasising more on the short-term rewards

In MDP terminology, the policy π is defined as a function which specifies the action to be taken corresponding to each state i.e. $\pi : S \rightarrow A$. At any instance the agent is in the state $s \in S$ when action $a \in A$ is taken to take it to the next state. This has been explained pictorially in Fig. 3.1 below.

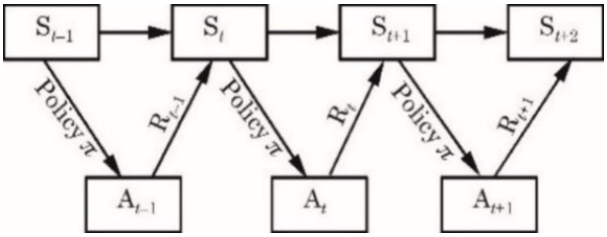

Figure 3.1. General sequence in reinforcement learning (also published in [II])

3.2.2 Q-Learning

Q-learning, a model-free reinforcement learning algorithm, is an off-policy method where an 'Agent' learns to take a good 'Action' while exploring the 'States'. In Q-learning, the quality i.e., Q-function (using Bellman's Equation) is given by Equation 3.1 below [114].

$$Q(s_{now},\ a_{now}) = \underbrace{r_{\text{now}}}_{\substack{\text{Immediate}\\ \text{reward}}} + \underbrace{\gamma \max_{a_{\text{future}}} Q(s_{\text{future}},\ a_{\text{future}})}_{\text{Discounted/Future Reward}} \tag{3.1}$$

The update rule is defined by equations 3.2 and 3.3 [114].

$$Q_{\text{est}}(s_{\text{now}},\ a_{\text{now}}) \longleftarrow Q_{\text{est}}(s_{\text{now}}, a_{\text{now}}) + \alpha\left[r_{\text{now}} + \gamma \max_{a_{\text{future}}} Q_{est}(s_{\text{future}},\ a_{\text{future}}) - Q_{\text{est}}(s_{\text{now}}, a_{\text{now}})\right] \tag{3.2}$$

$$s_{\text{now}} \longleftarrow s_{\text{future}} \text{ (Until termination)} \tag{3.3}$$

where: α = learning rate or step size (0,1].

3.2.3 Deep Q-Learning (DQN) and its application to filter tuning

Deep Q-Learning (DQN) algorithms came into existence by combining Q-learning with Neural Networks (NNs) as a result of advancements in Deep Learning [115]. Feed-forward NNs are used in this architecture for predicting the best possible Q-Values. Since DQN doesn't have initial data, the 'Agent' keeps past episodes – experiences pertaining to the state-action-reward-new state sequence – in a local memory. This local memory is called a data repository or experience replay. This information is then utilised as input to train the designed network architecture later on.

In reinforcement learning-based filter tuning, the filter is a "black box" and some requirements regarding the desired filter response are set for the filter to be considered as tuned. Rotating a screw correspondingly brings some change in the tuning state (the S-parameters would change). DQN was first applied to filter tuning process by Weng et al. in [77] however, the main limitations in that work were: a) the solution was often falling into local minima; and b) a Feed Forward (FF) structure was chosen. To solve the above-mentioned problems, the author of this thesis proposed an optimal Q-learning based algorithm as discussed in the next subchapter.

3.3 Optimal DQN algorithm applied to filter tuning

3.3.1 The novelty aspect

Considering the benefits of Reinforcement Learning; and the need of simulations to decide the future strategy in filter tuning process, the author implemented an optimal DQN algorithm. To overcome the limitations by Weng et. al in [77], the following changes were made by the author:

a) For increasing the accuracy, a CNN architecture was used.
b) A greedy policy was chosen for taking the 'actions' to explore the 'environment'.
c) Lagrangian Optimiser was used to find the global minima.

The results obtained in this work were published in [II]. The obtained results were better as compared to the ones obtained in [77]. The results are discussed in sub-section 3.3.3.

3.3.2 DQN algorithm and implementation

The reinforcement learning terminology mapped to filter tuning process can be described as:

- "Agent" (i.e., the learner) is the proposed algorithm.
- "Environment" (i.e., the Agent's world) is the simulated world.
- "States" (i.e., Agent's position) are various points considered on the S-parameter curve. Each state was represented by 501x1 vector, and the raw data was given to PCA algorithm to extract the features. Then, after PCA, the data was given to a 1-D CNN architecture.
- "Actions" (i.e., Agent's Input steps in Environment) are clockwise and counterclockwise turning angles of the screws.
- "Reward" (i.e., the Environment's feedback) is a numeric score.
- "Gamma" defined by the symbol "γ" (i.e., the discounted rate of reward) has been set as 0.95 in this work.
- "Policy" is the Agent's behaviour function (map from state to action).

The Q-Learning gradient is computed by Equation 3.4 [114]:

$$\frac{\partial \mathcal{L}(w)}{\partial w} = \mathbb{E}\left[\left(r_{\text{now}} + \gamma \underset{a_{\text{future}}}{max} Q_{\text{est}}(s_{\text{future}},\ a_{\text{future}},\ w) - Q_{\text{est}}(s_{\text{now}},\ a_{\text{now}}, w)\right) \frac{\partial Q_{est}(s_{now},\ a_{now}, w)}{\partial w}\right] \tag{3.4}$$

The proposed DQN algorithm implemented in this research work is presented in Fig. 3.2. To deal with non-exploration i.e., to update α (see Equation 3.2 for clarity), we used random exploration. At the stated probability of $\frac{1}{N}$ where N = number of trials i.e., number of times we have used "(s, a)-pairs", the programme took random action instead of optimal one and later, the probability of α was lowered automatically.

Algorithm parameters: step size $\alpha \in (0, 1)$, $\varepsilon > 0$
Initialize $Q(ss, aa)$, for all $ss \in S$, $aa \in A(s)$, randomly except that $Q(terminal, \cdot) = 0$
Loop for each episode:
Initialize ss
Loop for each step of episode:
Choose A from S using policy derived from Q (ε-greedy or random exploration)
Take action aa, observe rr, ss'
$Q(ss, aa) \leftarrow Q(ss, aa) + \alpha[rr + \gamma max_{aa} Q(ss', aa) - Q(ss, aa)]$
$ss \leftarrow ss'$
until ss is terminal
Optimise the loss function L using Lagrangian Optimiser
Equate $\frac{dL}{dx} = 0$ for finding the global optimum value using the constraint
Loss Function > Threshold Value

Figure 3.2. Proposed Q-learning Algorithm

3.3.3 Results obtained and conclusion

The results of the proposed algorithm are presented in Fig. 3.3. The condition for successful tuning is to have all the poles below the target return loss value. It was found that after training the network, the proposed algorithm could successfully drive the return loss curve below the –16 dB target value in 43 steps. Reaching the global minima was ensured using Lagrangian multiplier.

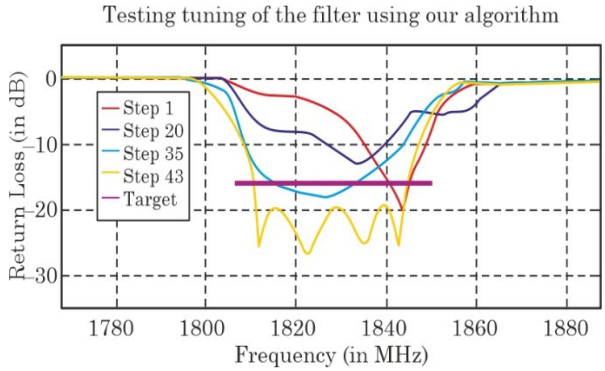

Figure 3.3. Results of implementing Optimal Q-Learning (also published in [II])

As compared to the algorithm presented by Weng et. al in [77] which took 48 steps, the algorithm proposed by the author could successfully tune the filter in 43 steps. Also, our algorithm ensured that it finds the global minima which was not the case with the technique presented in [77].

Even if the results of this proposed algorithm were better (i.e., lesser number of steps taken to reach the target value) as compared to the ones in [77], the major limitation of our research included the presence of "max" operator used in equation 3.2. The "max" component causes the algorithm to suffer the overestimation of Q-values for specific actions, resulting in biasness in the Agent learning. The action taken by the algorithm is beneficial for the near-term, but it ultimately results in a policy of lower quality

(i.e., smaller rewards later). Hasselt et. al in 2010 provided a solution to this "max" issue by introducing Double Q-Learning [116]. In 2016, the said author along with his co-authors demonstrated the overestimation bias in experiments conducted across multiple Atari Games Environments in [117] where DDQN was proposed. The core task of Double Q-Learning is to reduce the over-estimations in Q-value by decomposing the "max" operator into 'action selection' and 'action evaluation'. Hence, one network selects the action for the next state and another network provides the Q-value for that action. The 'selector' is "Q-Network", and the 'evaluator' is "Target-Network".

To overcome the limitations mentioned in the previous paragraph, the author of this thesis proposed and implemented a Double Deep Q-Learning (DDQN) algorithm to solve the problem in hand as discussed in the next sub-section.

3.4 Double Deep Q-Learning (DDQN) applied to filter tuning

3.4.1 The novelty aspect

As compared to our solution presented in [II] where DQN algorithm was proposed and implemented, the following changes were made by the author:

a) We have used DDQN with a CNN structure.
b) A dataset comprising of 998 states from a commercial filter to define the input "States". Each state had 501x1 vector (obtained from VNA's curve. The length could be varied by changing the sampling frequency if needed).
c) While performing dimension reduction, the Locally Linear Embedding (LLE) Technique [118] was used. LLE is better than PCA as the method ensures that we are not losing the feature information.

The results obtained in this research work were published by the author of this thesis in [III] which were better (i.e., lesser steps in tuning a higher filter order) as compared to the ones obtained in all the related publications. The results are discussed in details in sub-section 3.4.3 of this thesis.

3.4.2 DDQN algorithm and implementation

The Pseudo Code for the proposed solution used in this research is presented in Fig. 3.4.

Initialize main Q -network Q_θ, Target-network Q_θ, Memory buffer D, τ<<1
for each iteration **do**
  for each environment step **do**
    Observe ss and select $aa \sim \pi\,(aa, ss)$
    Execute aa and observe ss' and reward $rr = R(ss, aa)$
    Store (ss, aa, rr, ss') in memory D
  for each update step **do**
    sample $\boldsymbol{e_i} = (ss, aa, rr, ss') \sim D$
    Compute target Q-value:
    $$Q^*(ss, aa) \approx rr + \gamma Q_\theta\left(ss', \text{argmax}_{aa'} Q_\theta\,(ss', aa')\right)$$
    Perform gradient descent step on $(Q^*\,(ss, aa) - Q_\theta(\,ss, aa))^2$
    Update Target-network parameters:
    $\theta' \leftarrow \tau\theta + (1-\tau)\,\theta'$

Figure 3.4. Double Deep Q-learning Algorithm

DDQN algorithm used in this work aims to minimise the mean-square error between Q and Q* but Q′ is slowly copying the parameters of Q using Polyak Averaging as mentioned in equation 3.5 [119].

$$\theta' \leftarrow \tau\theta + (1-\tau)\theta' \tag{3.5}$$

where: θ: Primary Network Parameter

θ': Target Network Parameter

t : Rate of Averaging

In equation 3.5, following each run of the experience replay, the online network weights are reflected in the target network weights. In this work, t = 0.05 was used. Thus, the methodology used 95% of the old weights and updated 5% of the new weights.

Table 3.1. Attempted t-value analysis

S.No.	t-value	Result
1.	*t < 5%*	Slower convergence
2.	*t = 5%*	Optimal results
3.	*t > 5%*	Bigger errors

For reducing the dimensions yet keeping the features information intact, LLE technique [118] was implemented in this work. The analysis made regarding the choice of k-value i.e., the number of nearest neighbours for Dimensionality Reduction has been presented in Table 3.2 below.

Table 3.2. Attempted k-value analysis [III]

S.No.	k-value	Result
1.	*k < 5*	Disjointed curves, lost global properties
2.	*k = 5*	Optimal Result (and hence used in this work)
3.	*k > 5*	Smoothing of curve
4.	*k > 8*	Behaviour like traditional PCA approach

3.4.3 Results obtained

Fig 3.5 provides the results of our algorithm. The filter is considered to be tuned when the dips in the return loss are below the defined target line. After the network was trained, it emerged that the network could drive the curve below the –26 dB return loss target in just 23 steps.

The obtained results were compared with other publications in [77] and [II]. Table 3.3 is the presents the comparison. The effectiveness of the suggested DDQN algorithm is demonstrated by the fact that it is essentially more efficient in terms of the number of tuning steps and has the ability to learn superior strategies for tuning more complex filters than the ones that were previously employed.

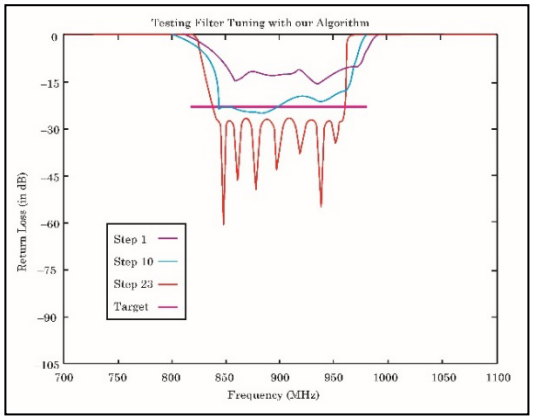

Figure 3.5. Results of implementing the DDQN algorithm (also published in [III])

The results of the simulated experiment found clear support for the proposed algorithm viz. DDQN algorithm as mentioned in Table 3.3. Overall, as compared to other methods, the proposed DDQN method was the one that obtained quite robust results (i.e., fewer tuning steps were needed to tune a higher ordered filter).

Table 3.3. Comparison with related research works

Reference Number	Dimension Reduction Algorithm	Tuning Algorithm	Filter Order	No. of Tuning Steps
[77] (Weng et al. results)	PCA	DQN	4	48
[II] (author's results)	PCA	Optimal DQN	4	43
[III] (author's results)	LLE	DDQN	9	23

3.5 Limitations

3.5.1 Limitations of the proposed methods

While working on implementation of reinforcement learning-based algorithms, the following conclusions were drawn:

a) Within the scope of this research work, simulating reinforcement learning-based algorithms in filter tuning was limited only to the reflection parameters (S_{11}) of bandpass filters.
b) The number of screws were also limited to a small number as only resonator screws were tuned.
c) Both the reinforcement learning-based algorithms proposed and implemented in this work stopped when the required specifications were met.
d) We limited the training of Q-networks to 150 epochs with maximum tuning steps being 1500. The hyperparameter tuning could be considered as a future work.
e) Q-learning-based methods tend to become ill-defined when we have continuous action space. In any on-policy method like Deep Deterministic Policy Gradient

(DDPG), the existing policy is improved. The next action is then taken from the improved policy i.e., it is not random. But this part was left for future research.

3.5.2 General limitations of reinforcement learning-based algorithms

a) High computation power is a prerequisite for implementing any reinforcement learning-based algorithm because the reinforcement learning 'agents' need an enormous amount (almost going towards infinity) of 'states' to accurately learn the correct strategies.
b) In all the reinforcement learning-based algorithms, some biasness is always induced when an 'agent' fails to fully explore the 'environment'.
c) The choice of reward function plays a big role in the final result. Since no set instructions are available to decide the rewards, this brings inaccuracies as well.

3.6 Chapter summary

In this chapter, the author introduced and implemented two reinforcement learning-based filter tuning algorithms within a simulated environment. The outcomes demonstrated that the algorithms devised in this study outperformed other comparable techniques in terms of efficiently tuning more intricate filters in fewer steps. However, in light of various constraints outlined in section 3.5, the author made the strategic choice to cease further exploration of reinforcement learning-based solutions for resolving the filter tuning problem. Instead, the decision was made to embark on investigating filter tuning algorithms that use theoretical knowledge and integration of both theoretical and AI-based approaches and apply them to physical filter units.

Since the commercial filters are designed according to a particular application, their design is unique which offer no or small variation in the tuning state. Therefore, it was decided that a new universal test filter will be designed which will allow us to investigate different tuning algorithms. The design of such a test filter design is presented in next chapter.

4 Development of New Test Filter

4.1 Chapter overview

Currently available commercial filters in the market are typically tailored for a specific application. They often come equipped with tuning screws, which serve the purpose of tuning the filter's frequency band and/or bandwidth, albeit within predefined limits. Achieving the desired frequency response involves altering the resonant frequency and inter-resonator coupling using these tuning screws. However, certain filter versions are deliberately designed without tuning screws, as their inherent design restricts their functionality to a specific frequency band. Consequently, a significant portion of commercial filters either does not facilitate the testing of new tuning algorithms or provides limited flexibility in parameter adjustments. Given this backdrop, the development of a new universal test filter, which can be used to evaluate and refine automated filter tuning algorithms, assumes paramount importance.

To test any new tuning methodology, a simpler filter topology with only the resonance adjusting screws is a good starting point. The inter-resonator coupling can be adjusted during the design phase where iris (horizontal or vertical or both) may be used. The size of iris opening determines the reactance magnitude of the filter. Designing an iris-coupled filter reduces the total number of screws over the filter's top plate. Also, a cavity filter with designed with solid resonators might serve various purposes like: a) preventing the screws from falling into the cavity; b) shorting the resonator if needed; c) helps in preventing the losses (increasing the screw penetration degrades the Q-value); and, d) helps in reducing the number of cases to be learnt by AI-based algorithms since there is a bottom limit for the screw penetrating inside the cavity. In case of a hollow resonator, the possible combinations of screw positions can grow exponentially high. The case of complete withdrawal of the screw from the filter's top plate can be controlled either by adding a special module in the computer programme or by using mechanical stoppers.

Considering all the factors mentioned in the previous paragraph, an all-pole L-band Chebyshev bandpass test filter having quarter-wavelength resonators was chosen to be designed. The test filter has been designed with solid resonators which ensures that the tuning screw will not fall into the cavity structure. The case of screw completely coming out of the filter plate was decided to be handled through the software part and has been discussed in Chapter 7. In this chapter, the author presents a newly designed universal filter, detailing its development process and performance assessment. This filter is intended to serve as a testing platform for evaluating the automated filter tuning algorithms.

4.2 Basic cavity filter

A cavity filter is a combination of various resonators coupled to each other. The property of resonator circuits which can be manipulated is capacitance. Tuning screws are usually mounted over the top surface of the cavity filters to change the capacitance externally. Some tuning screws are directly mounted over the cavities and are responsible for changing the resonance frequencies. Other screws include coupling and cross-coupling screws to alter the inter-resonator couplings.

Increasing the filter order (i.e., number of resonators) helps in achieving sharper band selectivity (which is a key characteristic of cavity filters) but it also increases the filter's Insertion Loss (IL) and filter's size. Optimisations are required for obtaining good filter performance while keeping the size of the filter small.

4.3 Filter design procedure

For designing a combline filter, the following steps are generally performed:

1. We start from choosing the correct filter type (Butterworth, Elliptic, Chebyshev etc.) according to the type of response expected from the filter.
2. The center frequency, BW, filter order, requirements for insertion loss and return loss are defined.
3. The structure of the filter is decided as per the constraints provided by the customers (if any).
4. The material and the geometry of the cavity, resonators, tuning screws are then decided. For simplicity, it is usually preferred to have the resonators of the same cross-section.

Historically, the engineers used various design tables and empirical formulas for designing the filters as presented in textbooks like [120]. With the advancement in computer technology these days, the designers are liberated to use filter designing software like ADS, CST, HFSS etc. However, to avoid the iterative 'hit-and-trial' in software-based filter designing, a combination of approaches is also sometimes used.

Within in allowed passband, the value of return loss must be minimized (it is expected to be <= -20 dB usually) whereas the insertion loss value should be maximized (expected to be close to 0 dB).

4.4 Design of 5-pole inline coaxial cavity test filter

4.4.1 Novelty aspect

The filter designed in this work is a universal test filter to test various algorithms as the commercial filters present either no or very limited possibilities to implement different algorithms. The choice of the filter order is determined based on introduced design requirements presented in section 4.3.2.

In this research work, the author designed a 5^{th} order all-pole inline coaxial cavity filter. The hollow cavity structure was machined within the aluminium enclosure. The extruded quarter-wavelength solid cylindrical posts within the conducting cavity walls act as resonators. The advantages of having solid resonators in the structure are already discussed in Section 4.1. To achieve the desired frequency response, tuning screws which are fixed within the cover plate and placed vertically above the individual resonators are provided. The cavity structure has not been plated from inside by any conducting material as commonly seen, however, the M4 sized tuning screws are plated with 3 µm layer of silver which assists in increasing the filter's overall performance. The inter-resonator coupling has been adjusted with the help of vertical iris as opposed to the commonly used coupling screws. The position, shape, orientation, and dimension of iris has been designed to achieve the desired frequency response. Adjusting the coupling between the resonators with the help of iris reduced the number of screws

mounted over the filter's top plate. Direct probe-touching method was used to achieve the desired I/O coupling and its distance (height) from the base is determined using the eigenmode solver of the considered design simulator.

4.4.2 Introduced design parameters

The basic design specifications from a filter to be realized are as under:

- Centre Frequency: 1,59 GHz (L-band)
- Bandwidth: 50 MHz
- Insertion loss: 0,5 – 0,9 dB
- Return loss: > 18 dB
- Number of resonators: 4 to 5
- Resonator length: Quarter wavelength
- Inter-resonator coupling adjustment mechanism: Iris
- Filter type: Cavity filter
- Filter topology: Coaxial
- Tuning Screws: Yes

4.4.3 Comparison with other similar designs

Two similar cavity filter designs are discussed in [121] and [122]. The approach for designing a MW cavity filter by researchers in [121] is different than the one presented in [122]. In [121], the filter is designed on the filter designing software, but the filter dimensions were mainly calculated using analytical formulas and g-value tables in [120]. The resonator length was calculated using λ/8 criteria. After deciding the cavity dimensions, the other dimensions like screw diameter, hole diameter, depth etc. are calculated using theoretical formulas. The approach in [122] used just a few analytical formulas but mainly relied on simulation solvers to obtain the filter dimensions. The final dimensions are found by Space Mapping (SM) optimisation technique using a combination of ADS software and HFSS software. ABCD parameters are also involved while optimisation. The author didn't fabricate the filter and didn't use tuning screws in their filter design.

The filter designed in this thesis work is a mix of [121] and [122] but also exhibits its uniqueness in some of the design aspects. The comparison of the designed test filter with other main filter design methodologies available in [121] and [122] is presented in Table 4.1. The main difference as compared to [122] is that the test filter designed in this research work is equipped with tuning screws as it was the case in [121]. The presence of tuning screws allows to achieve the desired frequency response.

It can be seen in Table 4.1 that the design of filter in this research work is a mix of design methodology presented in [121] and [122] in most of the criterion mentioned but possesses uniqueness in terms of the criteria for length determination. The input-output coupling method, resonator technology, and cavity material are common for all the designs discussed.

Table 4.1. The test filter design compared with other similar designs

Criteria	**Design in** [121]	**Design in** [122]	**In this work**
Frequency Band	S-band	**L-band**	**L-band**
Cavity Material	**Aluminium**	**Aluminium**	**Aluminium**
No. of Resonators	**5**	4	**5**
Resonator Material	Copper	**Aluminium**	**Aluminium**
Resonator Length Determination Criteria	λ/8	Eigen mode solver	~ λ/4
Resonator Size Variation	**No**	Yes	**No**
Resonator Shape	Hollow Cylinder	**Solid Cylinder**	**Solid Cylinder**
Resonator Technology	**Coaxial**	**Coaxial**	**Coaxial**
Resonator Mounting	Screws Drilled at the Bottom	**Cut within the Cavity**	**Cut within the Cavity**
Tuning Screws	**Yes**	No	**Yes**
Inter-resonator Coupling Adjustment Method	Screws	**Iris**	**Iris**
Filter Structure	**Cylindrical**	Square	**Cylindrical**
Input-Output coupling	**Direct Pin Contact**	**Direct Pin Contact**	**Direct Pin Contact**
Designing Software	**CST**	ADS + HFSS	**CST**
Design Optimisation	**No**	Yes (Space Mapping)	**No**
I/O Connectors	N-type	**SMA**	**SMA**
Filter Fabrication	**Yes**	No	**Yes**
Silver Plating of Cavity Walls	Yes	**No**	**No**

Note: The design similarities between different designs are depicted by the bold text

4.4.4 Choice of EM design software

In this work, CST Microwave Studio EM simulator by Dassault Systems (interchangeably used as CST software in this thesis) was used. CST software is based on Finite Integration Technique (FIT) which utilises integral form of the Maxwell's equations. For solving the EM-based problems, CST software has many kinds of solvers available which includes Time Domain Solver; Transient Solver, Eigenmode Solver, Frequency Domain Solver.

While designing the test filter, the Eigen-mode values of the design were checked in CST software. The design parameters were altered until the desired center frequency and Unloaded-Q of the resonators were obtained. This design was optimised i.e., the loop of changing the dimensions was repeated until the desired specifications were achieved.

4.4.5 Design of filter structure

A. Cavity Design

Key considerations: The shape and size of the cavity.

- For a cubical cavity – length, width, and height
- For a cylindrical cavity – the diameter and height

In this work, the author designed a cubical cavity which is connected to the test equipment and outer world with the help of SMA Connectors.

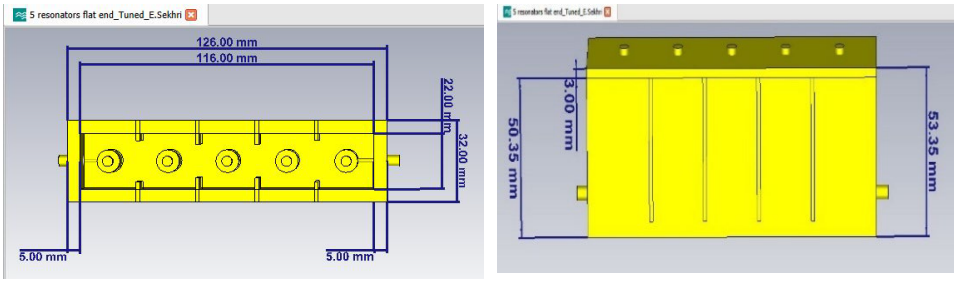

(a) (b)

Figure 4.1. Cubical cavity dimensions – (a) Length and Width; (b) Height

B. Resonator Design

Key considerations: The shape and size of the resonator. The resonator is usually kept at the center of the cavity structure but can be arranged in a zig-zag pattern or in straight line.

- **For a hollow resonator – outer diameter, inner diameter, and height**
- For a solid resonator – diameter and height

In this work, the author designed solid resonators with their length approximately equal to quarter-wavelength of the center frequency. So, for 1,59 GHz center frequency, λ = 188,55 mm (λ = c/f, where c = Speed of light). Correspondingly, the quarter-wavelength resonators i.e., λ/4 is 188,55/4 = 47,14 mm. Using Eigen-mode solver calculations in CST software and considering all the design and tuning requirements, the optimised resonator's length for the resonance frequency to be exactly as per the required center frequency of 1.59 GHz was found to be 40,35 mm for the designed 5th order filter. The main factor contributing to difference between these theoretical and optimised lengths is the capacitive load on the top end (open side) of the resonator.

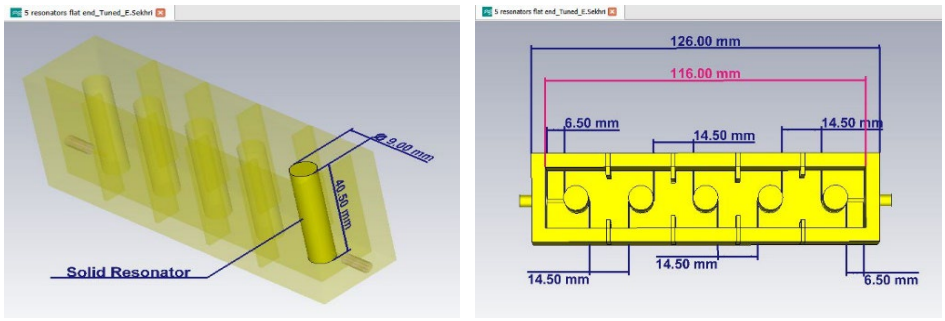

(a) (b)

Figure 4.2. Solid resonators – (a) isometric view; (b) top view

C. Tuning screws and their positions

Key considerations: The shape, size, positioning, material, and plating of the screws

- For screws without any tail-end disc – diameter of the screw, and the tail end towards the resonator)
- For screws with a tail-end disc attached – screw diameter, disc diameter, thickness of the disc, shape of the disc head (the end towards the resonator)

In this work, M4 screws plated with 3 µm silver plating without the disc have been used owing to being readily available. The screws used in this work are made of steel alloy and have Torx6 head on which screwdriver would be attached to tune the filter. The screws penetrate through the holes drilled in the filter's top plate and are placed exactly above the resonator posts.

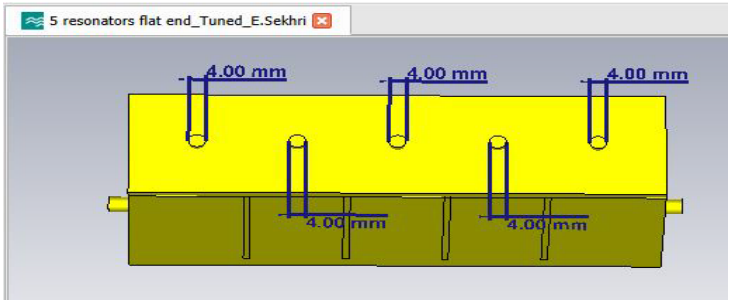

(a)

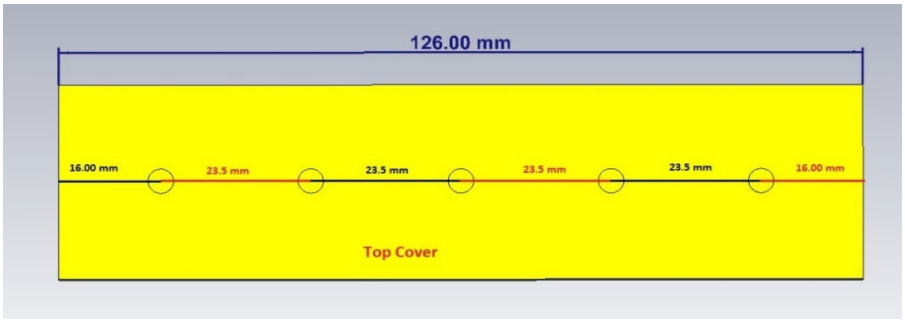

(b)

Figure 4.3. Tuning screws – (a) diameters; (b) tuning screws positions (shown over the top plate)

D. Inter-resonator coupling design

Key considerations: Shape, dimension, and the position in the cavity

- Horizontal iris – length, width, and height
- Vertical iris – width and height

For combline filters, capacitive coupling is achieved via probe (or wire) and the Inductive coupling is attained via iris. Not only probe/iris dimension but its position is also very important. Changing the iris gap brings change in both electric field distribution and magnetic field distribution within the cavity. This in turn changes the inter-resonator coupling strength. Generally, this gap is kept adjustable with the help of tuning elements. Iris can be horizontal or vertical. It has been observed that the horizontal iris is not suitable for the filters with large BW as they can't provide the required high values of coupling.

In this work, the iris gap is kept fixed by finalizing the iris dimensions while designing the test filter. This implies that the coupling value remains almost constant within the tuning range. In our case, we have vertical iris which are simpler in their design as compared to the horizontal ones.

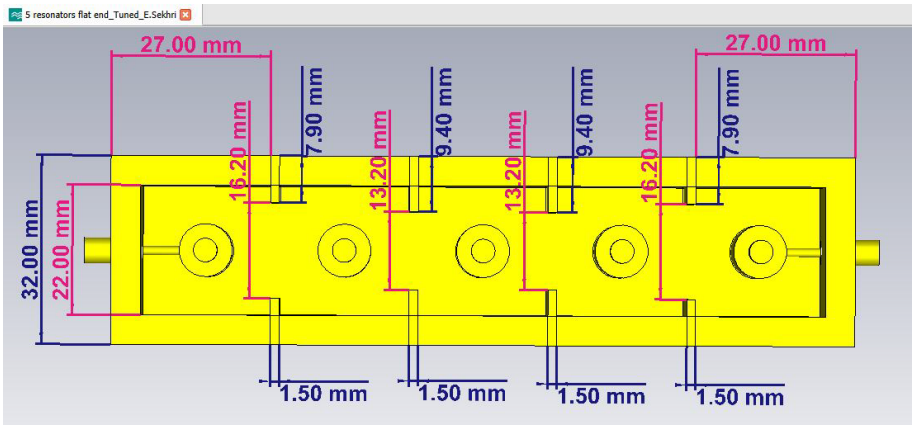

Figure 4.4. Vertical iris

E. I/O coupling design

Key considerations: Type of coupling, dimension, and its vertical positioning on the filter's wall

The Input/Output (I/O) ports can be connected by three possible ways:

a) Parallel coupling
b) Disc type coupling
c) Directly touching the connector pin to the I/O resonators

It was observed that the distance between feed line and resonator directly affects the electrical coupling. The smaller distance between them leads to stronger electrical coupling which correspondingly means lower external-Q value of the resonator.

In the designed test filter, the author used the direct touching method to achieve the desired frequency response. The position of the probe (its height from the base) is determined using the Eigen mode solver in CST Software.

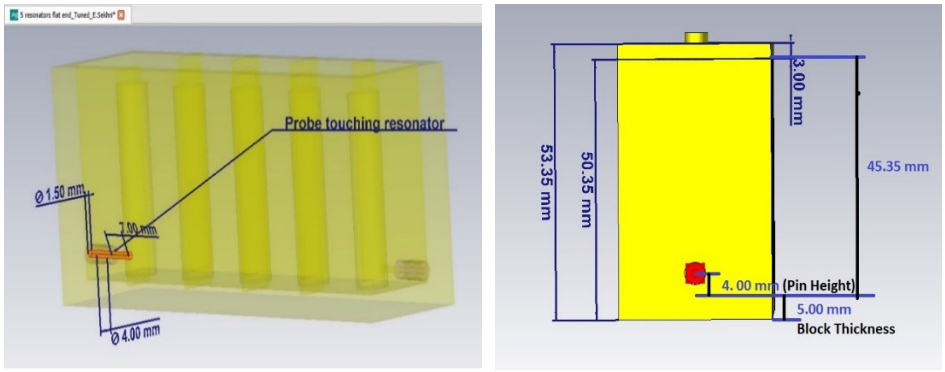

(a) (b)

Figure 4.5. Probe/pin – (a) Probe length (inside cavity) and diameter; (b) Probe position w.r.t to ground/base

The final dimensions of the various parts of the designed filter sent for manufacturing are given in Table 4.2. It should be noted that the gap between the cavity wall and the I/O resonators (also commonly known as 'end gap') cannot be determined empirically. In this design, we assumed it to be 6,5 mm. Only after having the value of end gap, we can find the overall length of the filter structure.

Table 4.2. Various dimensions of the designed test filter

Entity		Parameter	Dimension (in mm)
Cubical Cavity		Length	126
		Width	32
		Height	50,35
Solid Resonator		Height	40,35
		Diameter	9
Tuning Screw		Diameter	4
Iris	Iris 12 and Iris 45	Distance from outer wall	7,90
		Length	16,20
		Height	45,35
	Iris 23 and Iris 34	Distance from outer wall	9,40
		Length	13,20
		Height	45,35
Probe		Length (inside the cavity)	7
		Diameter	1,50
		Height (from the base)	9

4.5 Designed filter in CST software

The overall 3D filter structure designed in CST Software was simulated with Frequency Domain Solver feature. For dealing with the meshing used in the simulations, adaptive tetrahedral mesh was used. The complete structure of the designed filter is presented in Fig. 4.6. The S-parameter parameters were observed to check the accuracy of the design and are shown in Fig. 4.8 in Section 4.7. The design parameters and penetration depth of tuning screws are iteratively varied in the simulations until the desired frequency response was met.

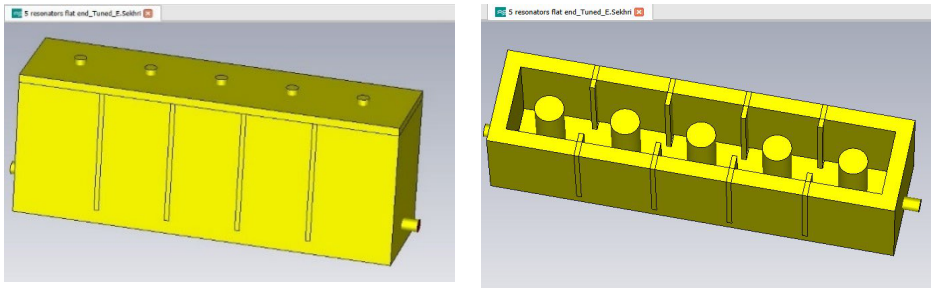

a) With top cover (toplet) b) Without toplet

Figure 4.6. Simulated 5-pole filter

4.6 Fabricated 5-pole filter

After finalizing the filter dimensions in CST Software, it was fabricated on a VMC (CNC) machine. Since the filter's cavity block has been manufactured as a single piece of aluminium with the resonator cylinders extruded from the base, the cutting speed of the tool was carefully chosen. The filter's top plate made from 3 mm thick aluminium sheet was cut separately. This top plate is firmly mounted over the cavity block to avoid the MW energy leakage. The commercially available M3-sized plate mounting screws made of normal alloy-steel don't bear any role other than holding the top plate. However, the M4 screws used for tuning are plated with 3 µm silver layer. The tuning screws are surrounded by nuts which ensure that the filter structure is airtight. Also, these nuts are locked tightly when the filters are tuned so that the tuning state of the filter won't change during its delivery phase.

Owing to their low cost and high frequency applications, SMA connectors were connected to the fabricated filter for sending and receiving the signals where the center pin touched the I/O resonators. Fig. 4.7 shows the assembled filter.

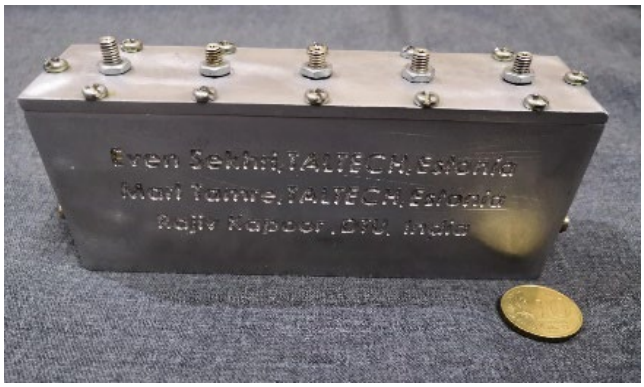

Figure 4.7. Fabricated 5-pole filter

Although the frequency of designed filter is centred around 1,60 GHz offering BW of 50 MHz, these values can be modified a bit with the help of tuning screws to make it suitable for a particular application requirement.

4.7 Comparing performance characteristics of simulated and fabricated filter

The following options are available for measuring the performance of MW Filters:

a) Vector Network Analyser (VNA)
    1) Scattering Parameters (S-parameters)
    2) Voltage Standing Wave Ratio (VSWR)
    3) Smith Chart
    4) Polar Plot
    5) Phase Plot
b) Spectrum Analyser
c) Special Waveguide Test Bench

In this work, we used the most common device among the ones mentioned above i.e., a VNA. To check the accuracy of the designed test filter, the S-parameters were chosen as an observation criterion. KEYSIGHT N9914A VNA [123] was used for testing the

performance of the filter. The fabricated filter was connected to a VNA, and its S-parameters were measured as shown in Fig. 4.8. Also, the simulated S-parameters captured from CST software while designing the filter are also shown in the same image. A good match between the S-parameters of a fabricated and simulated filter confirms the accuracy in the design. After tuning, the fabricated filter working as per the stated requirements. Fig. 4.8 shows that with-in the passband, the insertion loss of the filter is 0,7 dB and the value of return loss is found to be under -18 dB. The BW of the fabricated filter is also under the requirements set while designing the filter.

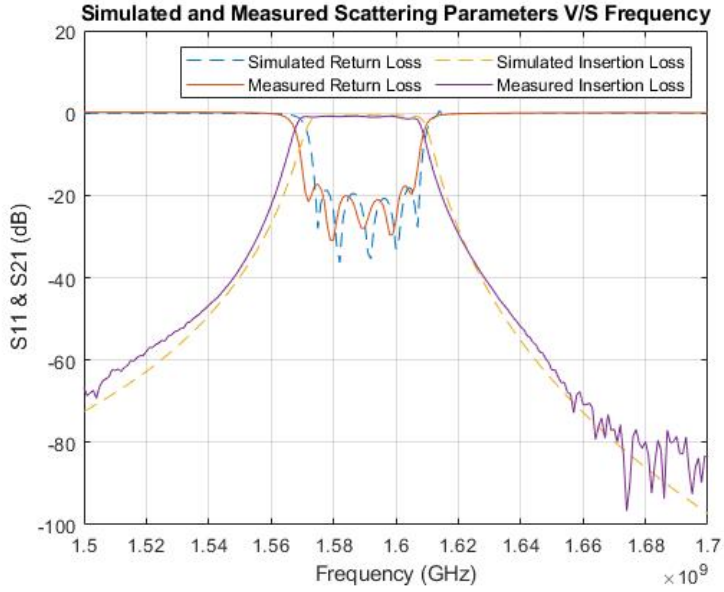

Figure 4.8. The difference between response of simulated and fabricated filters

4.8 Chapter summary

A new 5th order tuneable test filter having cubical cavity and quarter-wavelength long solid cylindrical resonators was designed to test the filter tuning algorithm(s). Varying the height of the tuning screws allowed us to vary the center frequency and BW. The I/O coupling has been realized using a touching pin and the inter-resonator coupling is adjusted with designed vertical iris as opposed to commonly used coupling adjustment screws. The choice was based on the fact that the designed iris reduced the total number of screws installed on the filter's top plate. The tuning screws were surrounded by nuts. These nuts serve two purposes: a) avoiding the RF energy leakage; and b) ensuring that the tuning state won't change when the tuned product is delivered to the customers. The designed test filter was then fabricated using an aluminium block. A good match was found between the response obtained from the simulated filter and the fabricated filter.

In order to assess the effectiveness of a novel algorithm designed for automating the filter tuning process, the development of an experimental setup is a requisite. To overcome the limitations of other filter tuning equipment available in the literature (presented in Chapter 2), coming up with a new experimental setup becomes inevitable. The ensuing chapter delineates the inception of this precise and versatile setup, distinguished by its precision and flexibility to fine-tune wide array of filters with minor modifications.

5 The Experimental Setup for Filter Tuning

5.1 Chapter overview

The tuning components in MW filters facilitate adjustments to achieve the specific frequency band required for a given application. Among these, tuning screws are the predominant choice for cavity filters. By altering the penetration depth of these screws, one can modify the resonance frequency and inter-resonator coupling values. To automate the filter tuning process, a robotic setup is needed. As discussed in Chapter 2, all the automatic filter tuning setups available in the literature exhibit certain limitations in terms of hardware and/or software which excludes the possibilities of incorporating them within the filter production lines. To have a generalised solution, a new experimental setup is needed which would allow its industrial usage and is apt for testing and comparing different filter tuning algorithms while being precise and resistant to environmental interference.

The new experimental setup should be designed so that it can tune not only the test filter designed in Chapter 4 but also should tune the other existing and upcoming commercial filters by making minor modifications. Having a flexible automated filter tuning system is also vital for increasing the volume of filter production in the industry. The main considerations while coming up with the new setup are full penetration and full withdrawal of tuning screws; simultaneously driving the screwdriver and outer nut; wider working range etc.

Taking all factors into account, this chapter introduces the design of a novel experimental configuration in which relative-positioning system has been used. This setup, as detailed within the chapter, offers adaptability for handling filters of various shapes, sizes, and topologies, requiring only minor modifications to accommodate them.

5.2 Principle block scheme of the new setup

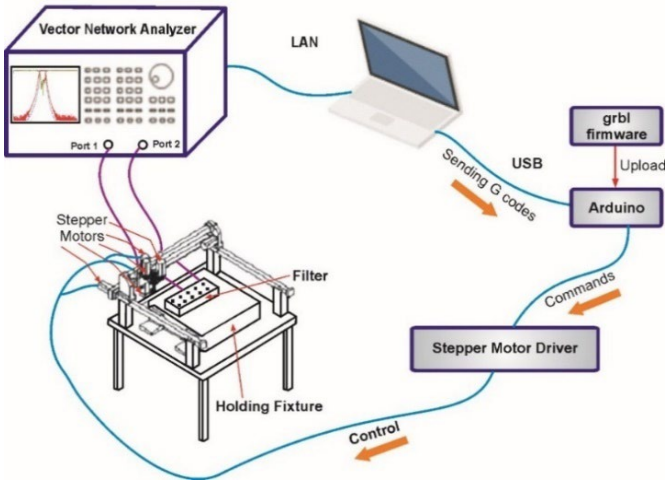

Figure 5.1. Principal block scheme

The main scheme of the new experimental setup is presented in Fig. 5.1. Once the required device drivers are installed, VNA is connected to that configured computer via LAN cable. The configured VNA is then connected to the test filter. The desired filter

characteristics are fetched into the computer. The connected computer sends G-codes via USB port to the microcontroller board (ATMEGA 328P) controlling the motors. Broadly, the whole setup can be seen as a combination of four different modules as following and are discussed in detail in the forthcoming sub-sections:

1. Mechanical module
2. Electronics module
3. Software module
4. Vision module

5.2.1 Mechanical module

5.2.1.1 Basic structure and configuration

The mechanical aspect of the experimental setup has been designed so that it can tune various types of commercial filters just by making small modifications. Most of the commercial filters have tuning screws and locking nuts around each of them to avoid – a) RF energy leakage, and b) detuning of the filter while transporting it to the customer. In case when the filter version is equipped with self-locking tuning screws, the nut driving motor can be easily disabled. Also, the design allows easy replacement of tuning screw head with the desired shape to tune different filter topologies.

After considering the design limits, the dimensions of the experimental setup were decided. The tuning screws were to be rotated using the torque provided by stepper motors. Due to presence of numerous screws (tuneable screws and plate mounting screws), there were spacing-related constraints. Considering space limitations and to avoid complex parallel computations, a single tuning actuator-based system was designed. The actuator approaches the tuning screws sequentially (one screw after the another). The sequential-tuning approach is slower, but it ensures high tuning accuracy as compared to parallel tuning approach in which many screws can be tuned simultaneously.

The author chose the cartesian configuration while designing the setup owing to its advantages such as – precision, wider working envelope (wide range of rectangular movement in X-, Y- and Z-direction) so that the higher ordered filters could also be tuned when needed, easy programming, high payload bearing capacity, and overhead grid offering bigger floor space. For the precise movement of the setup in X-, Y- and Z- direction, ball screw with small pitch size has been connected to stepper motors using the shaft couplers. The ‘home’ position of the machine is set using the limit switches. The relative-positioning system as used in [107][112] has been used in this work.

5.2.1.2 Tool-in-tool actuator

The tuning actuator designed in this work has a tool-in-tool arrangement where the inner tool is a screwdriver which is responsible for rotating the tuning screws and the outer tool deals with locking and unlocking the outer nut. This outer nut restricts the undesirable detuning of the filter while the other screws of the filter are being tuned or when the fully tuned filter is delivered to the customer. For tuning the filters without the locking nuts, the motor responsible for locking the nut can simply be disabled. The tool-in-tool manipulator is shown in Fig. 5.2.

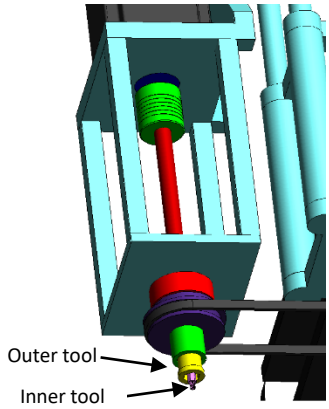

Figure 5.2. Basic structure of tool-in-tool actuator

The designed tool-in-tool actuator assembly allows the tuning of filters mounted with different kinds of screw heads just by replacing the screwdriver head, thus making the setup flexible. While tuning, the continuous contact between screwdriver and screw head is maintained with a spring-assisted sliding mechanism. This sliding mechanism allows the vertical movement of actuator as well as simultaneous movement of the tuning screw along its axis. The proposed actuating mechanism allows simultaneous and independent control of servomotor-based screwdriver as well as the lock-nut mechanism. Once the desired tuning state is achieved, the screwdriver is kept stable with the help of corresponding motor's holding torque while the other motor tightens the outer nut. This ensures that the current tuning state is retained, and repetitive rotations of tuning screws is avoided. The detailing of designed tool-in-tool is shown in Fig. 5.3.

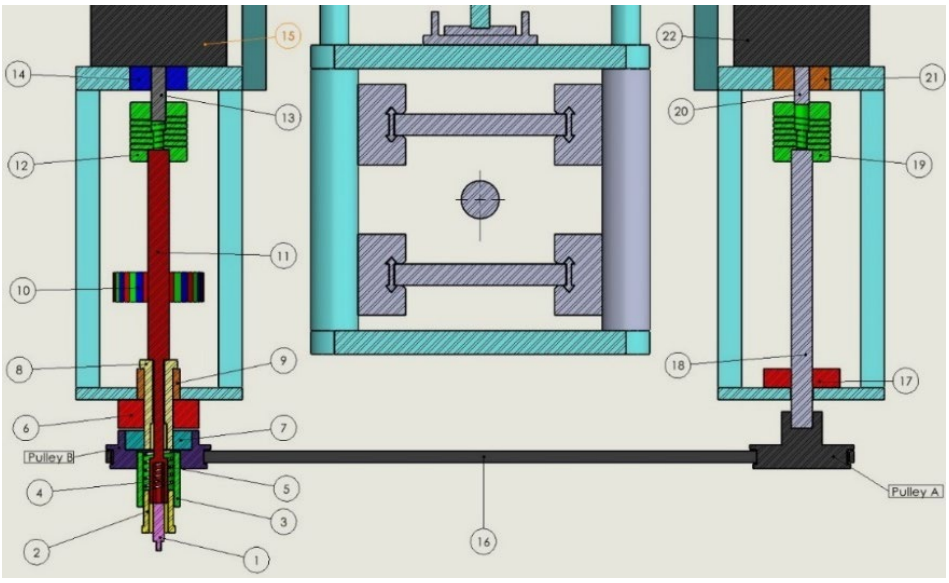

Figure 5.3. Designed tool-in-tool

The description of the various parts of the tool-in-tool mechanism has been explained in Table 5.1.

Table 5.1. Details of the parts of the tool-in-tool

Part Number	Description	Part Number	Description
1	Magnetic Screwdriver Head	12	Shaft Coupler
2	Magnetic Lock-nut Adapter	13	Motor Shaft
3	Adapter Coupling	14	Bush
4	Extension Shank Spring	15	Nema 23 Motor
5	Adapter Coupling Spring	16	Toothed Belt
6	Bush	17	Bush
7	Pulley Bearing	18	Drive Shaft (Pulley A)
8	Bearing Mounting Shaft	19	Shaft Coupler
9	Sleeve-type Bush	20	Motor Shaft
10	Auxiliary Coloured Disc	21	Bush
11	Drive Shaft (Screw Head)	22	Nema 23 Motor

To avoid a dense bunch of motors and wiring near the tool-in-tool structure, the servomotor responsible for driving the locking nut is placed at a distance from the axis of screwdriver motor. For transmitting the power from the unaligned stepper-motor to nut-driver, a belt-pulley system has been used. The use of timing belt over a spur gear minimizes the belt slippage when high torque is applied to lock/unlock the nut.

5.2.1.3 Auxiliary disc

The auxiliary disc shown as part number 10 in Fig. 5.3 is attached to the shaft which is rotating the screwdriver carrying out the actual tuning of the filter i.e., this disc rotates with the rotation motion provided by the stepper motor. A coloured strip has been pasted on this disc. The coloured strip is designed with a continuous pattern of Red-Green-BIue (R-G-B) coloured strips. This disc estimates the rotation angle as well as it determines the direction of screwdriver's rotation. The diameter of the disc on which the strip is pasted is chosen in a way that it meets the requirement of minimum angle resolution needed. The exact use of this auxiliary disc has been presented later in sections 7.6.3 and 7.6.4. For determining the direction of rotation, if the 'Green' colour strip is followed by a 'Blue' colour strip, it means the screwdriver is moving in counterclockwise (CCW) direction. However, if 'Green' colour strip is followed by a 'Red' coloured strip, the direction of rotation is clockwise (CW).

The outer diameter, D of this auxiliary disc is 38 mm and the thickness, T of the auxiliary disc is kept being 12,5 mm. The calculations related to this disc are given by equations 5.1 to 5.4:

Circumference of the auxiliary disc, C is given by:

$$C = 2\pi R \tag{5.1}$$

Substituting radius of the auxiliary disc, R = 19 mm gives:

$$C = 119{,}32\ mm \tag{5.2}$$

In order to have an angle resolution of 5°, the total coloured RGB strips (S) needed were:

$$S = \frac{360^\circ}{5^\circ} = 72 \tag{5.3}$$

The width of each strip (W) could be calculated using:

$$W = \frac{119{,}32}{72} = 1{,}65 \text{ mm} \tag{5.4}$$

The auxiliary disc is shown in Fig. 5.4.

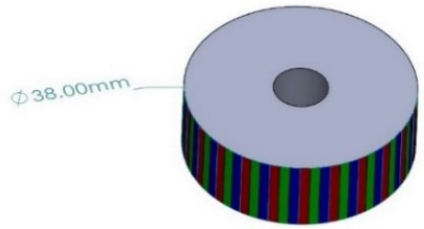

Figure 5.4. Auxiliary disc with continuous RGB pattern

5.2.2 Electronics module

By considering the flexibility related requirements in terms of torque and resolution (to allow the setup to tune wide variety of filters), NEMA 23 stepper-motors were selected. These motors offer high precision, provide the torque necessary to drive the setup, and offer sufficiently high holding torque. In our tuning setup design, 06 stepper motors have been used. Table 5.2 gives a small description of their use.

Table 5.2. Details of the usage of the motors in the experimental setup

S. No	Nomenclature Used	Position in the setup
1	M1	Controlling the X-axis (left side of setup)
2	M2	Controlling the X-axis (right side of setup)
3	M3	Controlling the Y-axis
4	M4	Controlling the Z-axis
5	M5	Controlling the Movement of Nut Fastener/Loosener
6	M6	Controlling the Tuning Screwdriver

Note: Motors M1 and M2 are wired together for smooth and precise motion of the setup in X-direction.

The motors are driven by a TB6600 stepper motor driver which gets control signals from the microcontroller.

5.2.3 Software module

From bird-eye view, Python programming language has been chosen to control the experimental setup as well as to test the new filter tuning algorithms on the designed experimental setup. With the increase in computation power, introduction of various AI-related libraries, it is possible to involve learning algorithms to the processes where an accurate mathematical model is not available (i.e., when the system can be considered as a 'blackbox'). The process of filter tuning falls under the same umbrella and hence there was a potential of finding a novel tuning solution.

After calibration, the VNA is connected to device under test (DUT) i.e., filter. The IP address of VNA allows real-time data transfer from VNA to computer through LAN cable. This data contains the information of current tuning state of the filter. The developed tuning algorithm compares the current state with the desired one and sends G-codes to

the microcontroller (Arduino). With the help of 'grbl' firmware, the microcontroller drives the specific stepper motor. The controller discussed in [124] has been used to control the speed of system as discussed later in detail in section 7.6.2.

The 'home' position has been defined to be one corner of the filter holding fixture which is made of wood. The presence of 06 limit switches assists in homing the machine. While tuning the filter with solid resonators, the tuning screw can't fall into the cavity. However, a special scenario where the screw may completely come out of the top plate is handled by measuring the pitch of the screw thread and monitoring the number of screw rotations through the developed program.

5.2.4 Vision module

A vision module has been added to the experimental setup to track the rotation angle as well as direction of rotation of screwdriver. A generic web-camera looks at the customized auxiliary disc as shown in Fig. 5.5.

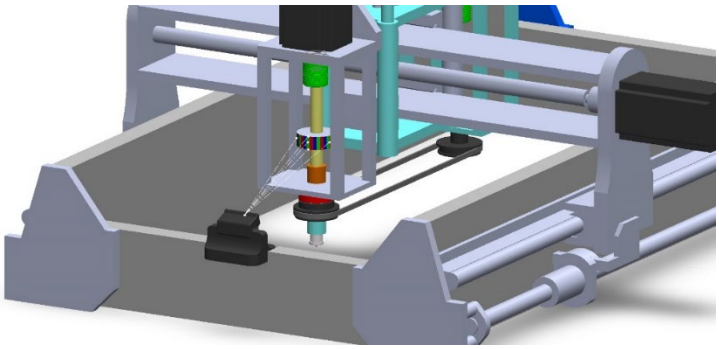

Figure 5.5. Camera looking at the auxiliary disc with coloured strip

5.3 The FAT robot

The experimental setup i.e., the FAT robot has been shown in Fig. 5.6.

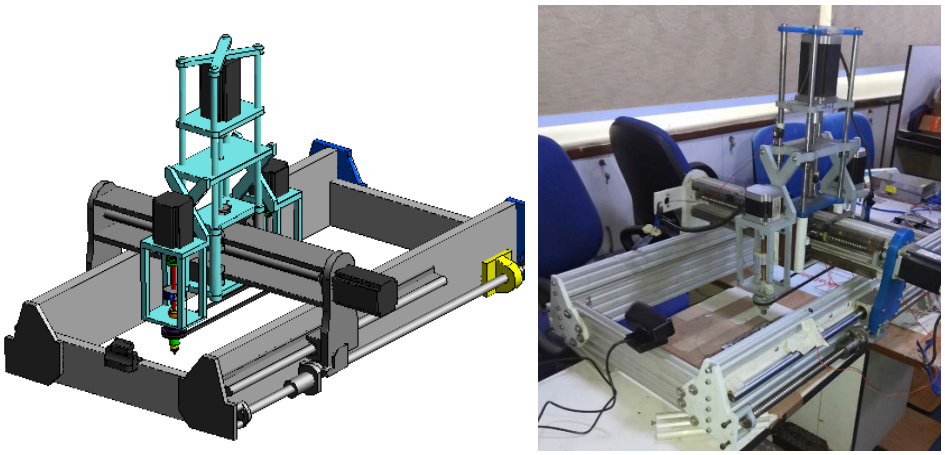

(a) (b)

Figure 5.6. Overall experimental setup – (a) SolidWorks Assembly; (b) Realized FAT Robot

5.4 Chapter summary

For implementing filter tuning algorithms, an experimental test setup was built. A customized tool-in-tool actuating mechanism was designed for finding the optimal positions of the tuning screws and then finalizing the locking of the nut of the test filter. To have bigger working envelop, cartesian configuration was selected. The details about the mechanical design and analysis of the structure are not discussed to stay aligned mainly with the topic of this thesis. As compared to other solutions proposed in the literature, the setup designed under this research work is flexible in terms of modifying the screw head to match various kinds of screw heads of the industrial filters and has a vision module dedicated to serve as an error detecting source so that the tuning error can be identified as soon as it occurs.

To deal with filters of different kinds, the stepper motors were chosen so that the torque and resolution requirements by various existing and upcoming industrial filters can be dealt. The movement of the designed Fully Automated Tuning (FAT) robot in 05 different axes have been controlled by 06 stepper motors (2 motors have been used for smooth movement in the X-direction). Each stepper motor is equipped with their dedicated motor driver which receives the control signal from the microcontroller. The whole system is mainly controlled by Python programming language and an HMI has been built to ease the movement of the robot. The homing process is assisted by the limit switches in all the linear translation axes.

Prior to applying any tuning algorithm to the filter, two essential preparatory steps must be completed:

1. Distinguishing the tuning screws from the plate mounting screws.
2. Manually configuring the tuning elements to their initial positions.

The subsequent chapter will expound on these essential tuning preliminaries.

6 Tuning Preliminaries

6.1 Chapter overview

The surface of the MW cavity filter, as depicted in Fig. 6.1, features an array of screws. Among these, some are tuning screws, which facilitate adjustments to the filter's tuning state. The remainder are mounting screws, primarily responsible for securing the top plate of the filter in place. Before commencing the automated tuning process, it is imperative for the algorithm to discern the position of each tuning screw on the filter. Achieving this necessitates the development of a method for distinguishing tuning and mounting screws. Once the tuning screws are identified, their position coordinates are sent to the algorithm to direct the tuning manipulator.

This chapter provides the insight to vision-based methods for detecting and localising the tuning screws of the filters. For testing the proposed methodologies, a used commercial filter shown in Fig. 6.1 was used.

(a) (b)

Figure 6.1. A commercial MW cavity filter – (a) top view; (b) perspective view

6.2 Differentiating the tuning screws using computer vision

6.2.1 Using Machine Learning

Before automating the filter tuning process, every screw fitted over the cavity filter must be efficiently classified either as a tuning screw or a mounting screw. To do this, a ML classifier may be used. The ML classifier based on supervised learning can build a model which would divide the given data into desired number of distinct classes. ANNs [125], Bayesian Networks [126], Decision Trees (DT) [127], K-Nearest Neighbours (KNNs) [128], Support Vector Machine (SVM) [129] are a few of the widely used classification techniques documented in the literature. The various steps to classify the screws using ML-based model are explained in the following sub-sections.

6.2.1.1 Setup used

For extracting the features of the screws correctly, a unique imaging setup was needed. The images used to generate the dataset for the ML-based classifier for localising the tuning screws were captured using a Logitech C525 HD 720p webcam. Since a powerful light source was necessary for proper illumination and for homogeneous reflection on the top plate (to create higher contrast), halogen lighting was used during the experiments. The overall setup is depicted in Fig. 6.2. The various parameters used in Fig. 6.2 were defined to be as following:

α = 45°
L_0 = 250 mm
W_0 = 350 mm
W_1 = 190 mm
L_1 = 240 mm
L_C = 38 mm

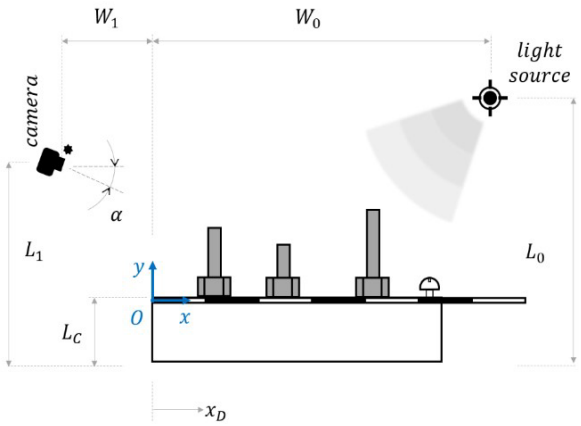

Figure 6.2. Imaging setup for ML-based screw differentiation (also published in [VI])

To prevent any screws being occluded i.e., the front screw covers the one(s) behind it, the camera mounting angle defined by α was chosen to be 45°.

6.2.1.2 Preprocessing

The procedure for preprocessing the acquired image processing is shown in Fig. 6.3. The acquired image i.e., RGB image of the commercial MW cavity filter is first converted into a binary image. The rusty mounting surface seen in Fig. 6.1 (we have considered a used MW filter in this chapter as stated earlier) was compensated by adjusting the brightness and contrast of the binary image. The 'value plane' was subsequently used to extract the grey image. The key reason for choosing this plane was that the tops of the screws were a little brighter than the rest of the filter assembly. Finally, the thresholding step assisted in separating all the screws (mounting screws as well as the tuning screws) from the filter's top surface. The resulting processed image was then used for further analysis.

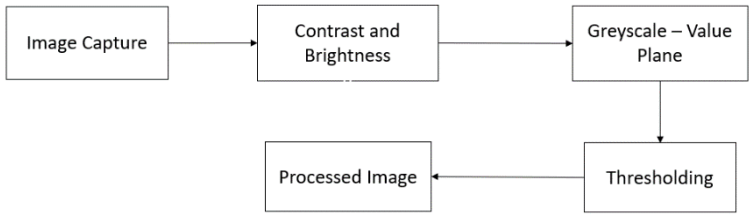

Figure 6.3. Image preprocessing steps (also published in [VI])

The original image and the corresponding processed image of the filter considered for testing the are displayed in Fig. 6.4 on the left and the right side respectively.

(a) (b)

Figure 6.4: The original image (left), and Processed image (right) (also published in [VI])

6.2.1.3 Screw classification

For classifying the screws correctly, features of all the screws must be extracted. To do this, Determinant of Hessian (DoH) method has been used. The Hessian matrix provides insights about the local variations and structures within the data. The determinant of this matrix leads to a matrix composed of second-order partial derivatives. For the image represented by f(x,y), the DoH is calculated as presented by equation 6.1.

$$\det \mathbf{H} = \begin{vmatrix} f_{xx} & f_{xy} \\ f_{yx} & f_{yy} \end{vmatrix} \tag{6.1}$$

In this work, when the processed image was given to the proposed solution, DoH method provided area as a feature vector. The screw dimensions were then manually measured and labeled as tuning screws or mounting screws depending on the area of the feature vector. Additionally, the classification of tuning and mounting screws was made easier by extracting the height parameter from the feature vectors obtained using DoH. Labeling took 92 minutes to complete. This linear SVM classifier, which was trained using the parameters presented in Table 6.1, used this labeled data for training the model. The SMO solver, which minimizes the one-norm problem by considering a series of 2-point minimizations, was used to implement the SVM algorithm.

Table 6.1. SVM algorithm parameters

Entity	Value
Lagrangian Multiplier	26 x 1 array
Bias Term for Hyperplane	-13.9878
Solver	SMO

After the model is trained using the labeled data, the screws in given image can be classified. The overall methodology for classifying the screws is presented in Fig. 6.5.

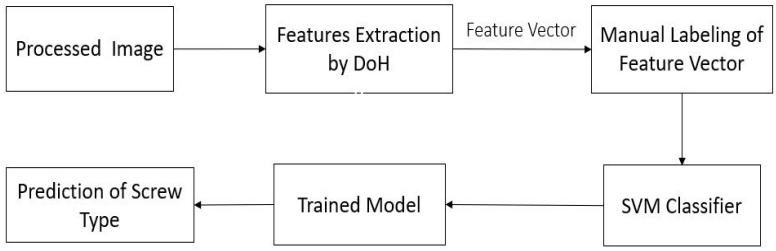

Figure 6.5. Screw classification methodology (also published in [VI])

The proposed methodology was tested on a commercial cavity filter shown in Fig. 6.1 on which a total of 144 screws are present. Out of these, 58 screws were the tuning screws and rest were the mounting screws. The goal of implementing the supervised learning algorithms on the processed image was to have a bounding box around the tuning screws.

6.2.1.4 Results and Discussions

Initially, the processed image and the feature vectors from DoH are given as an input to the trained SVM model and the resultant image with the predictions is shown in Fig. 6.6 where the bounding boxes are encapsulating the tuning screws. It can be seen in Fig. 6.6 that the proposed SVM model predicted a total of 60 tuning screws i.e., two false-positive results were predicted by the SVM algorithm.

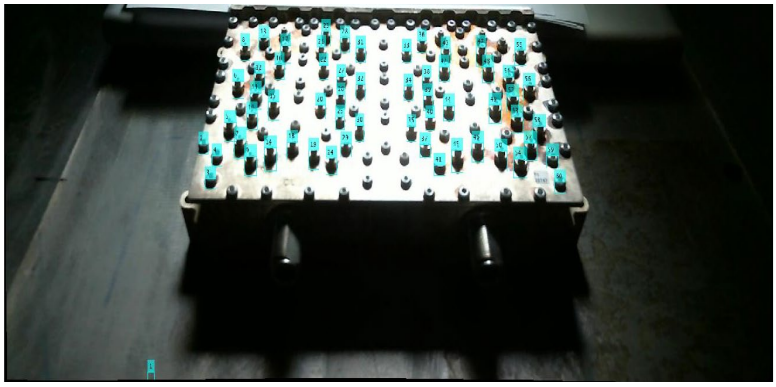

Figure 6.6. Tuning screws predicted by SVM model (also published in [VI])

The performance of the SVM algorithm was compared with the KNN and DT models. While implementing the KNN algorithm, the number of neighbours were defined to be 5 and the Euclidean distance between the nearest neighbours is used as a criterion. In the DT algorithm, the cross-validation was not considered. The predictor selection for DT was set to consider all the splits. The predictions made by KNN model and DT model are presented in Fig. 6.7 and Fig. 6.8 respectively.

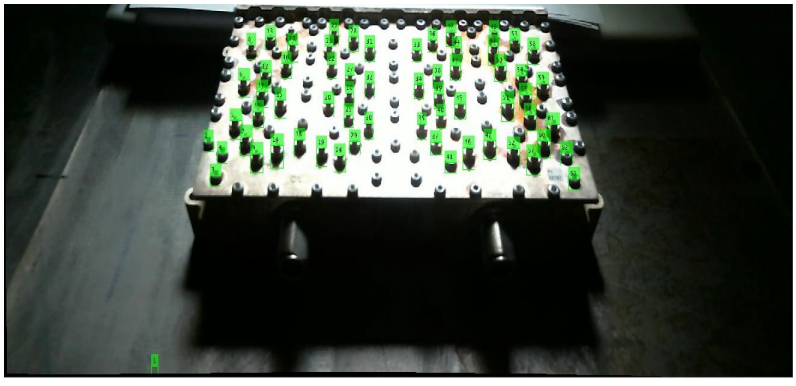

Figure 6.7. Tuning screws predicted by KNN model (also published in [VI])

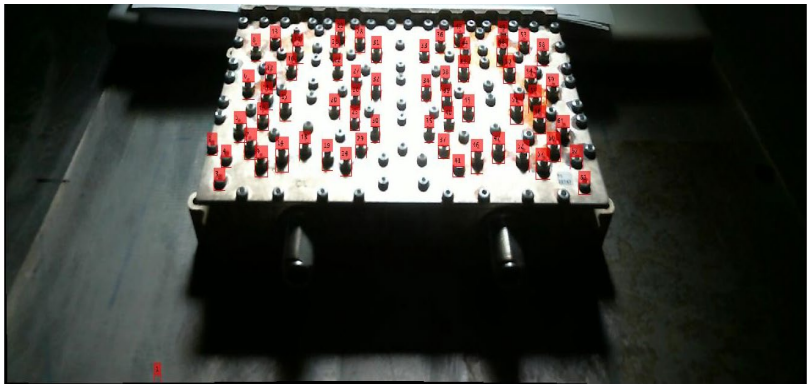

Figure 6.8. Tuning screws predicted by DT model (also published in [VI])

The results obtained by implementing KNN and DT algorithms on the processed image show the presence of 5 false-positive results i.e., a total of 63 tuning screws were predicted by both the algorithms.

The classification results for tuning screws obtained using different ML algorithms implemented are demonstrated in Table 6.2. Upon inspection, it becomes clear that the SVM model exhibited superior classification performance, with only 2 misclassified screws. In contrast, the other two state-of-the-art algorithms viz. KNN and DT which misclassified 5 screws each.

Table 6.2. Number of tuning screws obtained using the ML-based algorithms

ML Algorithm	Number of Screws Detected by the proposed classifier	Incorrectly Classified Screws (True Count = 58)
SVM	60	2
KNN	63	5
DT	63	5

Upon close examination of Figs. 6.6, 6.7, and 6.8, became evident that all three algorithms not only incorrectly classified some of the mounting screws as tuning screws, but also erroneously identified a similar shaped shadowed area as a tuning screw (as clear from the bottom portions of Fig. 6.6 to Fig. 6.8). Hence, a more robust and accurate method was required, one that does not hinge on the template matching or the trained ML model.

6.2.2 Using a novel band-subtraction method

Fig. 6.9 shows a magnified version of a small portion of the cavity filter that is the subject of this chapter (see to Fig. 6.1). The tuning screw is located on the top-right corner, and the mounting screw is located at the bottom-left corner.

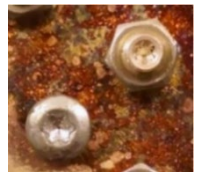

Figure 6.9. Different types of tuning screws on a cavity filter (also published in [IV])

Since the screws in Fig. 6.9 have distinct shapes, it may be possible to distinguish them using image processing techniques such as contour matching, shape detection, and pattern matching. It is not always the case, though, that mounting screws and tuning screws have different forms. Rather, commercial filters occasionally use the same screw head for every screw that is provided on the cavity filter. Therefore, a robust method is required to locate and categorise the screws that are attached to the filter structure.

To prevent losses, conductive materials are coated on tuning screws provided on the commercial filters. Because every material or compound has a unique reflectance to electromagnetic (EM) waves, these screws can be identified by their material properties. Thus, utilising the material composition, a novel vision-based technique may be applied to differentiate the tuning screws of a cavity filter from the mounting screws. As hyperspectral imaging can produce images in contiguous spectral bands, the materials can be characterized using their reflectance within certain spectral range of the EM spectrum. In this work, images from a hyperspectral camera were used to examine the characteristic image bands of screws from a commercial cavity filter. The datacube of a hyperspectral camera was used to extract information about relevant bands.

Spectroscopy and digital imaging are combined in hyperspectral imaging (HSI). By using this imaging approach, the scene is captured in discrete narrow bandwidths, allowing for the datacube to be processed further by selecting the appropriate image bands [130]. Different materials have distinct signatures across different wavelength bands due to their differing reflectance characteristics. Taking into account the scope of the current study activity, Fig. 6.10 shows the reflectance behaviour of carbon steel and silver (Ag) at wavelengths ranging from 0.2 µm (200 nm) to 20 µm (20000 nm). There are noticeable differences in the reflectance curves for the two metals. This spectral signature can be used to identify comparable materials.

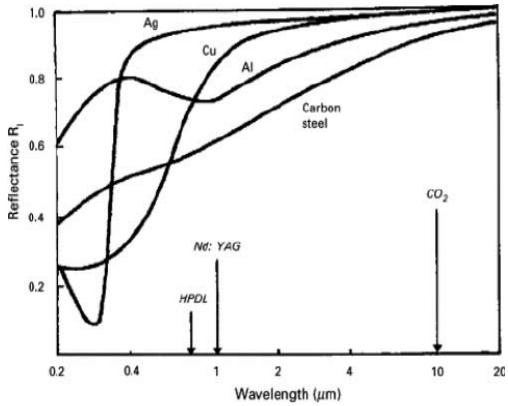

Figure 6.10. Reflectance curve for different metals [131]

As tuning screws used in industry are normally coated with a 3 µm silver layer (to enhance the conductivity) and mounting screws are usually composed of an alloy of steel, it is possible to distinguish between them using their reflectance signatures. The imaging setup utilised to carry out this task is shown in the following subsection.

6.2.2.1 Imaging setup

A Specim IQ Mobile Hyperspectral Camera [132] was used to differentiate the mounting screws and the tuning screws. This hyperspectral camera covers the 400–1000 nm wavelength range, has 204 picture bands (per pixel), and has a spectral resolution of 7 nm. The reflectance values for all the bands can be displayed in the spectral distribution of each pixel This camera was calibrated for white reference using a calibrated tile with 99% reflectance. On HSI images, no additional image processing procedures were carried out after the initial calibration. But unlike RGB, HSI cannot determine the objects' shape. Rather, only the necessary bands are selected and sent on for additional processing.

The entire setup that was used to capture the image from the hyperspectral camera has been shown in Fig. 6.11. The reference plate used for Specim IQ camera calibration is also shown in the same figure. Since in the EM spectrum, the wavelength of halogen light covers wider spectrum of wavelength spanning from the UV to the IR, two 400W halogen projectors were selected as the light source. The diffusing sheet was employed to guarantee homogeneous lighting.

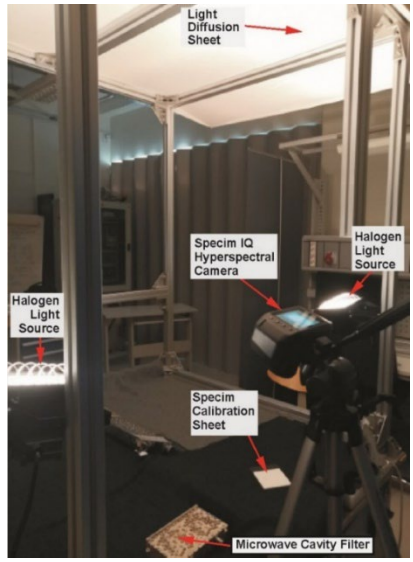

Figure 6.11. Setup for screw differentiation using hyperspectral imaging (also published in [IV])

6.2.2.2 Reflectance Trends

The material composition of a MW filter's mounting and tuning screws differs. Thus, different band options must be analysed in order to determine the effective spectral image bands. This allows the two types of screws to be distinguished from one another, as each material has unique spectral characteristics.

For fetching the reflectance information from the screws present on the filter considered, one screw of each category (tuning screw and mounting screw) was selected. Fig. 6.12(a) shows the locations of both the screws selected in one of the bands. The circle marked with blue colour presents a mounting screw and other orange coloured point is marked over a silver-plated tuning screw. The corresponding reflectance plots for both these screws are presented in Fig. 6.12(b) covering the wavelength ranging from 400 nm to 1000 nm.

A significant difference between reflectance value of both the screws can be seen in Fig. 6.12(b) within the pre-defined wavelength range. These results were obtained when

only one mounting screw, and one tuning screw were sampled which might not be sufficient to draw any conclusion. Thus, an average of 05 samples selected for each screw category was used to get more meaningful results. The locations and the corresponding bands of selected screws is reported in Fig. 6.13.

The goal was to use the mean reflectance value to precisely choose the right bands by considering numerous screws from each category. The locations of selected screws in one of the bands are displayed in Fig. 6.13(a). Figure 6.13(b) displays the relevant reflectance plots for each of these screws over the 400–1000 nm wavelength range. The average reflectance value was then used to choose the bands, as will be discussed in the following subsection.

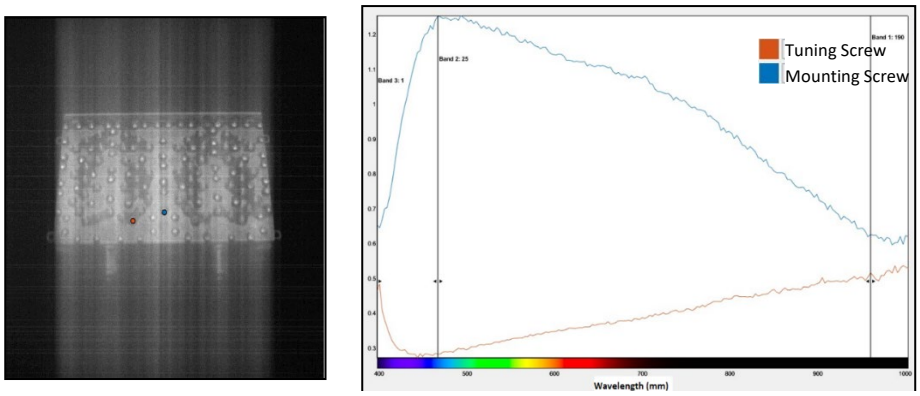

(a) (b)

Figure 6.12. Location and reflectance characteristics for 01 screw sampled from each type – (a) Screw Locations on a Band Image; (b) Reflectance-Wavelength Plots

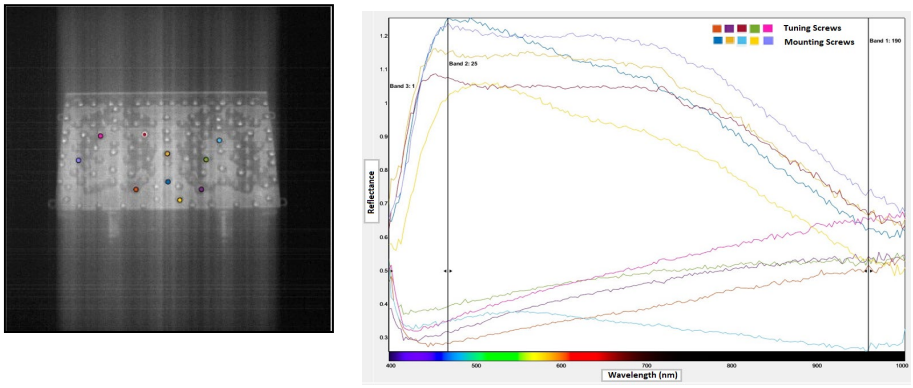

(a) (b)

Figure 6.13. Sampled 05 screws from each screw category and their reflectance response – (a) Screw Locations on a Band Image; (b) Reflectance-Wavelength Plots (also published in [IV])

6.2.2.3 Selection of bands

Hundreds of narrow bandwidth spectral bands make up HSI; most of them are correlated and produce redundant data. Processing a large amount of data decreases the computational efficiency [133] due to the Hughes phenomenon [134]. Therefore, selecting the spectral bands that offer unique characteristic information makes sense

[135]. In addition to increase in computation efficiency, the primary benefits of utilising a band selection strategy are the increase in classification accuracy [136] while ensuring preservation of the intrinsic information of the original pixel [137].

Band 25 and Band 190 were selected from the datacube by averaging the reflectance values of the selected tuning and mounting screws, as can be seen in Fig. 6.13. Due to the fact that Band 25 has the most distinguishing features that set it apart from the other screw type. This is shown in Figs. 6.12(b) and 6.13(b) where a notable difference in reflectance between the two screw groups can be seen. The wavelength of band 25 is roughly 467 nm. From the other end of the datacube, Band 190, having a wavelength of approximately 930 nm was selected. This is because Band 190 exhibits feature similarities between the two screws. This aspect can be observed from Figs. 6.12(b) and 6.13(b) where the reflectance characteristics show a slight variation in Band 190's reflectance properties.

It is noteworthy that the authors selected Band 190 even though the difference between the two curves was minimum around Band 197. The Band 190 was selected to exclude any potential spectral noise that could have been present in the last few bands near to the image's end. Images of Band 25 and Band 190 are shown in Figs. 6.14(a) and 6.14(b), respectively.

6.2.2.4 Band subtraction

It was discovered, empirically, that it was possible to distinguish between mounting screws and tuning screws by subtracting one band from the blue region (Band 25) and another band from the infrared (IR) region (Band 190) of the datacube could clearly differentiate tuning screws and mounting screws. As presented by equation 6.2, the image I_{result} was obtained when a 467 nm image (I_{467}) was subtracted from a 930 nm image (I_{930}).

$$I_{result} = I_{930} - I_{467} \tag{6.2}$$

When compared to the silver-plated tuning screws, the mounting screws seemed much darker, as seen in Figure 6.14(c), which is an image produced after implementing the band subtraction. Using this information, one may find the coordinates for the location of each tuning screw and this information can then be used to tune the filter autonomously.

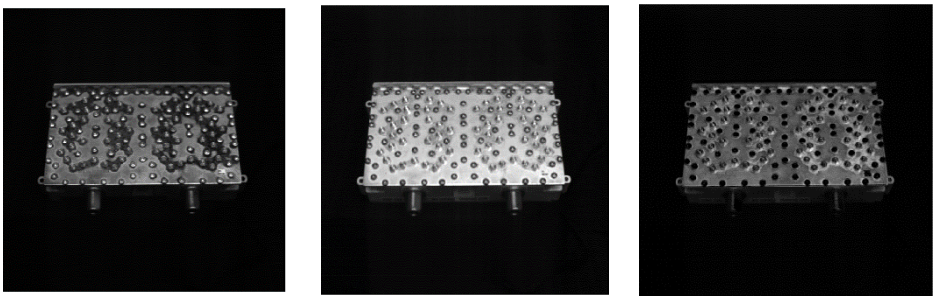

(a) (b) (c)

Figure 6.14. Band selection and band subtraction results – (a) Band 25 image; (b) Band 190 image; (c) Resultant Image after Band Subtraction (also published in [IV])

6.2.2.5 Experimentation results and analysis

Results of applying the band subtraction technique to the Specim hyperspectral camera image are shown in Fig. 6.15. For easy comparison, the RGB and the processed image – the outcome of band subtraction – are shown next to one another.

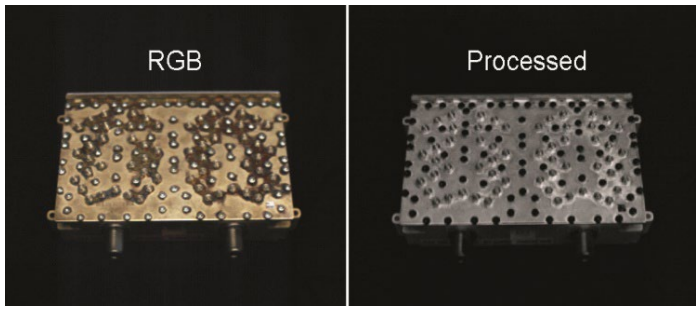

(a) (b)

Figure 6.15. Classification of screws using Specim hyperspectral camera – (a) RGB image; (b) final image (also published in [IV])

The suggested band-subtraction method led to encouraging findings as demonstrated in Fig. 6.15. Because they seem darker than the tuning screws, the mounting screws are easier to distinguish.

6.3 Comparison between different screw differentiating techniques

The classification accuracy of the various techniques implemented for distinguishing the tuning screws from the plate mounting screws are compared in Table 6.3.

Table 6.3. Screw classification accuracy of different algorithms implemented

Algorithm	Screw Classification Accuracy
SVM	96.66%
KNN	92.06%
DT	92.06%
Band-Subtraction	100%

The novel band-subtraction method demonstrated a remarkable 100% success rate in classification of the tuning screws as shown in Table 6.3. This breakthrough suggests that efforts to automate cavity filter tuning can greatly benefit from the adoption of this novel technique. With the tuning screws accurately identified, a robotic manipulator can then be instructed to tune the filter using the precise spatial coordinates of the tuning screws.

6.4 Setting the initial position of the tuning screws

Since an automatic screw feeding mechanism which will mount the screws on the filter's top plate is beyond the scope of this thesis, so the tuning screws are installed manually. Each screw is tightened until it touches the solid resonator below it, thus leading to shorting of the resonators. This has been decided to be the initial position of the tuning screws when the filter is assembled. Each tuning screw is then installed with a locking nut. The nuts are kept loose at this stage so that the tuning screws can rotate freely.

These nuts need to be tightened only when the resonator has been tuned. This ensures that, once the required filtering parameters have been achieved, the position of the tuning screw stays intact when the filter is delivered to the customer.

6.5 Chapter summary

This chapter presented the prerequisites which were needed before initiating the tuning process viz. – differentiate and localise the positional coordinates of all the tuning screws mounted on the filter using camera vision; and setting the initial state of the tuning screws. For differentiating the tuning screws from the plate mounting screws, various vision-based methodologies based on ML and band-subtraction method were implemented. The imaging setup and the image processing techniques were also discussed. The methodologies to localise the tuning screws have been validated on a commercial filter. It was found that the novel band-subtraction method proposed in this work led to 100% classification accuracy. The initial position of the tuning screws has been set in a way that each tuning screw touches (shorts) the resonator under it.

In the next chapter, a comprehensive overview of the automated filter tuning algorithms is provided. These algorithms are employed to fine-tune the filters utilising the FAT robot introduced in Chapter 5. The tuning process integrates theoretical knowledge and combination of theoretical principles with AI to tune the filter. Particle filtering has been used to dynamically track the tuning errors in real-time.

7 Automated Filter Tuning Algorithms

7.1 Chapter overview

While the filter tuning algorithms introduced by the research community have certainly contributed to the tuning process, they are often constrained by various limitations. These limitations include factors such as the need for human intervention during the filter tuning, the time-consuming nature of optimisation routines, and the iterative visitation and adjustment of screws. Continuous rotation of the tuning screws is also undesirable as it may result in undesirable Passive Inter-Modulation (PIM) effects. Moreover, many of these algorithms operate without any feedback from the system, essentially following the instructions blindly.

In light of these challenges, there arises a compelling need for a more universal solution. This solution should be capable of automatically tuning assembled filters, minimizing human involvement to the initiation of the tuning algorithm. It should also circumvent the need for repetitive screw adjustments. Additionally, an essential component of this solution is the inclusion of a feedback mechanism, enabling the early detection and rectification of potential tuning errors. Such a system not only streamlines the tuning process but also conserves time and valuable resources.

The solution presented in this work uses the information related to phase change of the input reflection coefficient is used for sequential tuning of the resonators of the all-pole filters. The proposed automated filter tuning solutions use either the Smith chart or the polar chart for tuning of the filters using the reflected signal (since shorting the resonators means no signal is getting transmitted). When moving from the input port to terminating port of the filter, all the resonators are brought to their resonance state successively with the help of the tuning screws. The proposed tuning algorithms use the theoretical knowledge in Polar chart based algorithm and the conjunction of theoretical knowledge and AI in Smith chart based algorithm to correctly tune the filter without visiting the screws iteratively. In both these algorithms, PFs-based algorithm ha been used to track the potential tuning errors in real-time using the developed vision module. Thus, the error can be detected and rectified during the early stages only. None of the previously published automated filter tuning solutions reported in the literature have used vision-based error compensation in real-time while tuning the filters based on Smith chart or polar chart.

7.2 Smith chart

One of the display modes to measure the filter's performance in terms of scattering coefficients is the Smith chart. This chart allows the calculation of transformation of a complex load impedance through any arbitrary length of the transmission line (TL). The Smith chart can be presented in terms of impedance (i.e., Z) or its reciprocal (admittance i.e. Y). Other than these charts, Immittance (YZ) Smith charts are also sometimes used in which both Y and Z entities are presented simultaneously.

It is common to find the normalized Smith charts for impedance, admittance and immittance. In this work, we restricted our discussion to impedance Smith charts only. The normalized impedance, z is expressed by equation 7.1 as:

$$z = \frac{Z}{Z_0} \tag{7.1}$$

where Z_0 = The characteristic impedance
Z = Impedance at any point on the Smith chart
z = Normalized impedance

One full rotation on the Smith chart presents an electrical line length of λ/2 or π radians on the phase scale. In impedance Smith chart, the upper half presents inductive reactance and corresponds to positive imaginary part of impedance. On the other hand, the lower half depicts capacitive reactance and corresponds to the negative imaginary part of impedance. A normalized impedance Smith chart is shown in Fig. 7.1. The right-most point on the impedance Smith chart presents an open circuit with impedance, z = infinity. Moving electrical length of λ/8 towards the load (moving anticlockwise) from open circuit point represents z = 0 + 1j i.e., inductive reactance. λ/4 anticlockwise movement from open circuit point represents a short circuit with z = 0 and 3λ/8 anticlockwise movement from the open circuit point represents z = 0 - 1j. Moving λ/2 anticlockwise from the starting point brings us back to the same point where z = infinity. The center point of Smith chart presents z = 1 + 0j i.e., matched impedance. The open circuit point, the short circuit point, and the matched load point are all located on the real axis which defines the purely resistive line.

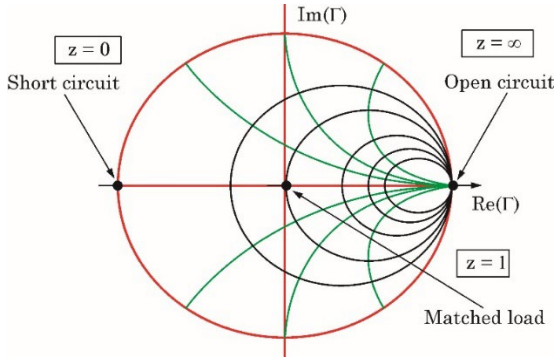

Figure 7.1. Impedance Smith chart

The green arcs in Fig. 7.1 represent the locus of constant reactance and the black circles are the locus of constant resistance.

7.3 Phase change of input reflection coefficient on Smith chart for tuning

For the all-pole filters designed with quarter-wavelength (λ/4) long resonators, like the one designed in Chapter 4, the quarter wavelength movement on the Smith chart can be used to tune the filters. This is because, as per the maximum power transfer theorem for complex network (a network consisting of real (resistive) and imaginary parts (reactive) from its components), the maximum power transfer occurs from source to load when the load impedance (Z_L) is equal to the complex conjugate of the source impedance (Z_S). Reaching the complex conjugate state by moving λ/4 on Smith chart signifies that the phase of the signal has been changed i.e., if the initial phase was capacitive, then, now we are in inductive zone and vice versa as briefly explained in section 7.2.

The input impedance of a Transmission Line (TL) is dependent on characteristic impedance, load impedance, length of the TL, and phase constant of the signal propagating through this TL. This relationship has been expressed by equation 7.2.

$$Z_{in} = Z_0 \left\{ \frac{Z_L + jZ_0 \tan \beta l}{Z_0 + jZ_L \tan \beta l} \right\} \quad (7.2)$$

where, Z_{in} = Input impedance

Z_0 = Characteristic impedance

Z_L = Load impedance

l = Length of TL

b = Phase Constant $= \frac{2\pi}{\lambda}$

For quarter-wavelength long resonators, the relation between wavelength scale and electrical length (bl) can be expressed as:

$$\beta l = \frac{2\pi}{\lambda} \times \frac{\lambda}{4} = \frac{\pi}{2} \text{ radians} \quad (7.3)$$

Now, rearranging and solving 7.2 and using equation 7.3 gives:

$$Z_{in} = Z_0 \frac{\tan \beta l}{\tan \beta l} \left\{ \frac{\frac{Z_0}{\tan \beta l} + jZ_0}{\frac{Z_0}{\tan \beta l} + jZ_L} \right\} \quad (7.4)$$

Now incorporating the fact that $tan\left(\frac{\pi}{2}\right) = \infty$ we get

$$Z_{in} = \frac{Z_0^2}{Z_L} \quad (7.5)$$

If we assume that the load impedance to be:

$$Z_L = A + Bj \quad (7.6)$$

Putting equation 7.6 into equation 7.5 gives:

$$Z_{in} = Z_0^2 \left[\frac{1}{A+Bj} \right] \quad (7.7)$$

$$Z_{in} = Z_0^2 \left[\frac{A-Bj}{(A+Bj)\ (A-Bj)} \right] \quad (7.8)$$

$$Z_{in} = Z_0^2 \left[\frac{A-Bj}{A^2+B^2} \right] \quad (7.9)$$

$$Z_{in} = Z_0^2 \left[\frac{A}{A^2+B^2} - \frac{Bj}{A^2+B^2} \right] \quad (7.10)$$

$$Z_{in} = \frac{Z_0^2}{A^2+B^2} (A - Bj) \quad (7.11)$$

$$Z_{in} = \text{A Constant Value} \times (A - Bj) \quad (7.12)$$

It is to be noted that Z_{in} in Equation 7.12 is a complex conjugate of the Z_L value assumed in equation 7.6 which is in conformity with the maximum power transfer theorem.

The λ/4 wavelength on electrical wavelength scale or π/2 radians on the phase scale represents half rotation on the Smith chart when reflection coefficients are considered. This λ/4 movement on the Smith chart is to be executed for all the resonators of an all-pole filters. While moving from input side to output side, the collective result after tuning all the resonators in this way is the matched impedance between the source and

the load. This implies that the return loss (RL) is small and insertion loss (IL) is closer to zero. This theoretical knowledge can be used to tune the iris-coupled all-pole quarter-wavelength filters.

Impedance can be expressed in terms of rectangular coordinate form i.e., $Z = R + Xj$ (as already discussed in section 7.2) or in terms of polar form as magnitude and phase angle i.e., $Z = |Z| \angle \vartheta$. This implies that the Smith chart as well as the polar chart are suitable to observe the impedance matching. The detailed discussion on polar chart is presented in the section 7.4 where the basic information of this chart as well as its similarities with Smith chart are highlighted.

7.4 Polar chart and its similarities with Smith chart

7.4.1 Polar chart

Concentric circles around the Smith chart's center point represents constant reflection factors. These circles are not presented on the Smith chart (refer Fig. 7.1). A chart which presents these circles is referred to as polar chart shown in Fig. 7.2 in which the radius of reflection circles is directly related to magnitude of reflection coefficient, Γ. The outermost circle presents Γ = 1 i.e., full reflection of the signal. A circle with Γ = 0,5 (although not shown) presents a 3-dB circle i.e., half of the entered signal is reflected. At the center point of the polar chart, no signal is getting reflected i.e., Γ = 0.

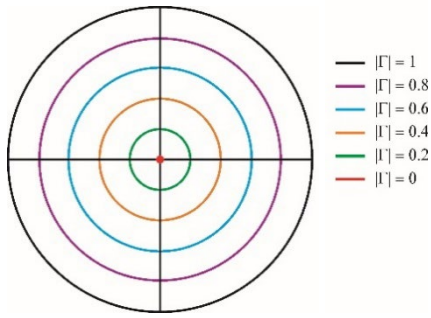

Figure 7.2. Polar chart

Theoretically, Γ is defined as ratio of reflected voltage to the input voltage at the load terminal. Thus, also known as voltage reflection coefficient. Mathematically, Γ is expressed as:

$$\Gamma = \frac{V_r}{V_i} \tag{7.13}$$

In terms of electric field strength, Γ is defined as the ratio of reflected wave's electric field strength to the electric field strength of the forward traveling wave.

$$\Gamma = \frac{\text{Electric Field Strength of a Reflected Wave}}{\text{Electric Field Strength of a Forward Wave}} \tag{7.14}$$

This quantity i.e., Γ plays its role when the line is unmatched i.e., it is terminated in a load Z_L which is not equal to the characteristic impedance Z_0, thus leading to reflections. In other words, the complex impedance encountered by the forward signal (incident wave) determines the reflections. Thus, the difference between Z_0 and Z_L defines the size of reflected wave. The expression defining Γ in terms of Z_0 and Z_L is given by:

$$\Gamma = \frac{Z_L - Z_0}{Z_L + Z_0} \tag{7.15}$$

Usually, it is a polar quantity and is expressed as:

$$\Gamma = |\Gamma| e^{j\theta} \tag{7.16}$$

In equation 7.15, the cases of open circuit, short circuit and matched load can be presented as:

- For open circuit, $Z_L = \infty$. Thus, $\Gamma = 1$. So, $|\Gamma| = 1$ and $\theta = 0$
- For close circuit, $Z_L = 0$. Thus, $\Gamma = -1$. So, $|\Gamma| = 1$ and $\theta = \pi$
- For matched load, $Z_L = Z_0$. Thus, $\Gamma = 0$

7.4.2 Similarities between Smith chart and polar chart

Although the output value provided by Smith chart and polar chart are considerably different, but both are similar in terms of the position of marker (angle as well as magnitude) at any instance. This can be seen in the images taken from Smith chart and polar chart of Keysight Fieldfox RF Analyser 9914A – 6,5 GHz [156] as shown in Fig. 7.3.

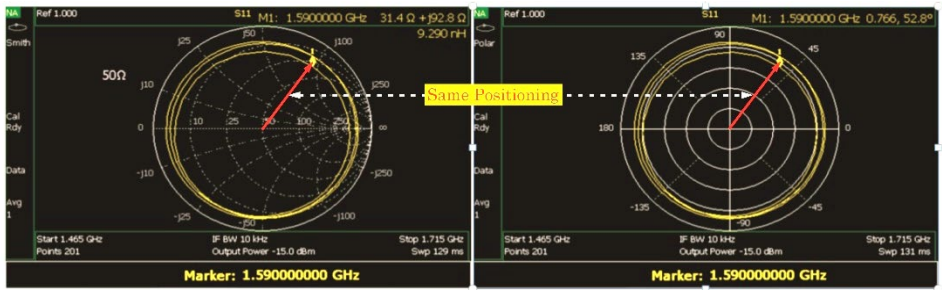

(a) (b)

Figure 7.3. Keysight 9914A VNA's Smith chart (left) and Polar display (right)

Knowing the fact that the scale to present resistance and reactance values on the Smith chart is exponential in nature; and that the Smith chart has infinity term involved which can be seen in Fig. 7.1 and Fig. 7.3, the information provided by the Smith chart cannot be directly used to automate the filter process. However, owing to the similarity in marker positioning in Smith chart and polar chart, the angle information from the polar chart of VNA can assist in automating the filter tuning process.

7.5 Particle filtering for rotation angle estimation

To estimate the rotation angle, colour-based particle filtering approach has been used in this work. The Particle Filters (PFs) track the colours on the RGB strip pasted on the auxiliary disc as discussed in section 5.2.1.

Particle filtering is based on Bayes theorem and can represent the posterior density function by random samples representing the i^{th} object's hypothetical state i.e., $s^{(i)}$ and its associated weight $w^{(i)}$ where i ranges from 1 to N (and N = No. of samples). The expected state X of the object estimated by the set of particles is presented by 7.17.

$$X = \sum_{i=1}^{N} s^{(i)} w^{(i)} \tag{7.17}$$

where, $$\sum_{i=1}^{N} w^{(i)} = 1$$

In this work, we are modelling the target by a rectangular box given by 7.18.

$$s = \{C^x, C^y, W^x, H^y\} \tag{7.18}$$

where, $C^x, C^y =$ x and y coordinates of centre position of the box

$W^x, H^y =$ Width and height of the rectangular box

The overall process of colour-based particle filtering used in this work estimates the posterior probability density function by using the cyclic process of Prediction – Update – Resampling. The implementation details of this have been discussed in the following sub-sections:

7.5.1 Prediction stage

The system model is used to predict each sample's distribution using the constant motion model given by equation 7.19 [138].

$$s_k = I \bullet s_{k-1} + v_{k-1} \tag{7.19}$$

where, $s_k =$ State at time k

$s_{k-1} =$ State at time k-1

$v_{k-1} =$ Zero mean Gaussian Noise with a constant variance-covariance matrix 'R' at time k-1

$I =$ Identity Matrix of size 4

7.5.2 Update stage

The measurements are used in update stage which modifies the prior density using importance sampling. Thus, new weights are computed and allocated to the corresponding samples. To achieve this, for the k^{th} sample $s_k^{(i)}$, the similarity D between the reference target model h_{ref} and sample target model $h_{s_k^{(i)}}$ of i^{th} particles is evaluated.

To be specific, the image region under the rectangular box for the state vector $s_k^{(i)}$ is used. For constructing the associate probability distribution *m*-colour histogram of the rectangular region is used. Thus, the similarity for bin *j* in the histogram of i^{th} particle and reference model is calculated using 7.20 [138].

$$D^2\left(h_{s_k^{(i)}},\ h_{ref}\right) = 1 - \sum_{j=1}^{N_{bin}} \sqrt{h_{s_k^{(i)}}(j).\ h_{ref}(j)} \tag{7.20}$$

If we call $D^2\left(h_{s_k^{(i)}},\ h_{ref}\right) = D^2$, the weights of the particles are extracted by equation 7.21 [138].

$$\omega^{(i)} = e^{-L \bullet D^2\left(h_{s_k^{(i)}},\ h_{ref}\right)} \tag{7.21}$$

The estimated state $\hat{S}_k$ is obtained by equation 7.22 [138].

$$\hat{S}_k \approx \sum_{i=1}^{N} \omega *_k^{(i)} s_k^{(i)} \tag{7.22}$$

where, $\omega^{*(i)} = \frac{\omega^{(i)}}{\sum_{i=1}^{N} \omega^{(i)}}$ = normalized weights

The choice of *L* controls the number of higher weight particles that can be generated. The analysis made on the choice of L-value is presented in Table 7.1.

Table 7.1. L-value analysis

S.No.	*l*-value	Result
1.	*High L*	More particles having weights closer to zero
2.	*Low L*	Almost equal weights of the particles
3.	*L = 1*	Optimal value which avoids under-fitting and over-fitting

7.5.3 Resampling stage

In this stage, the particles with small weights are discarded so that:

(a) The degeneracy problem can be avoided

(b) Computations are reduced

The resampling method comprises of three steps [138]:

(i) Generate N-ordered uniform random numbers for selecting the particles (*r* = 1 to N)

$$l_r = \frac{(r-1)+l}{N} \tag{7.23}$$

where l is a single random drawn from uniform distribution with the condition l Č $[0,1)$

(ii) For *r* = 1 to N, find an integer *j* such that

$$l_r \in \left[\sum_{i=1}^{j-1} \omega^{(i)}, \sum_{i=1}^{j} \omega^{(i)}\right] \tag{7.24}$$

Next, set *r (i) = j*.

(iii) For *i* = 1 to N, set new particles $s*_k^{(i)}$ such that $s_k^{r(i)} = s*_k^{(i)}$ and set new weights

$$\omega^{j(i)} = \frac{1}{N} \tag{7.25}$$

The angle is estimated based on the change in colour detection through the window of PF. The angle is a multiple of positive integer *I*, and the maximum offset between the colour change will persist 4.99°, thus is not accumulated with the progressive moments of the colour strip. The method of estimating the rotation angle using the coloured strip is depicted in Fig. 7.4.

Count = 1, Angle = 5°, Error = 0°

a) The rectangular box completely covering the red strip

Count = 1, Angle = 5°, Error = 2°

b) The rectangular box is between red and green strip

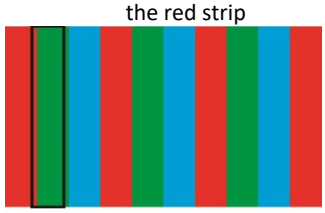

Count = 1, Angle = 5°, Error = 4°

c) The rectangular box is about to reach the green strip

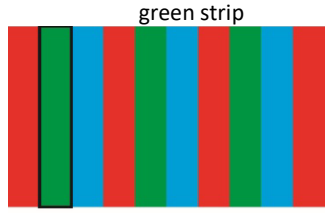

Count = 2, Angle = 10°, Error = 0°

d) The rectangular box covered the green strip completely

Figure 7.4. The estimating of rotation angle on the coloured strip

The pseudo code for the angle estimation based on strip count of the RGB pattern is shown in Fig. 7.5.

```
Initialize Count = 0
If color_change_detect == True
        Count = Count + 1
        E_PF = Count × 5
Else
        Count = Count
        E_PF = E_PF
```

Figure 7.5. Strip count based angle estimation

7.6 Modules developed for assisting automated filter tuning

To automate the filter tuning process and for ensuring the smooth and optimised performance of the tuning algorithms, a few modules were developed. These modules are:

1) Tuning screw localisation module
2) Speed variation module
3) Angle comparator module for error detection
4) Module for counting the screw turns
5) Nut locking module

7.6.1 Tuning screw localising module

As stated earlier in this chapter, before starting the implementation of any phase change-based filter tuning algorithm, the tuning screws must be differentiated from the plate mounting screws. The coordinates of the tuning screws are then used by the FAT robot so that the tuning manipulator can reach to the desired tuning screw and start

rotating it. Various methods for distinguishing the tuning screws from the mounting screws are discussed in Chapter 6 but owing to the 100% accuracy and reduced computation complexity, the band-subtraction technique has been used to detect and localise the tuning screws in this work.

7.6.2 Speed variation module

A strategy to optimise the tuning time was devised which was based on reducing the speed of the robot considering the difference between the current angle and the target angle value. The strategy was made so that the required 180° movement (λ/4 movement) was divided into 06 equal segments. During the beginning of the tuning, the speed value was set to be 6 and gradually decreasing by a unit (i.e., by 1) with progression to every next segment. Table 7.2 presents the summary of the logic used in this work.

Table 7.2. Variation of actuator speed as per the phase angle

Segment Number	Phase Angle Movement Range	Speed Value
1	0° to 30°	6 (Starting Speed)
2	31° to 60°	5
3	61° to 90°	4
4	91° to 120°	3
5	121° to 150°	2
6	151° to 180°	1
-	Above 180°	0 (Stop tuning)

Note: The speed levels can further be optimised as needed. However, the only factor to consider while deciding the speed levels is the fact that setting the faster speeds might present the case where the rotation angle crosses (i.e., jumps) the target value of 180°. This error is accumulated and ultimately leads to inaccurate tuning results at the end of tuning process.

7.6.3 Angle comparator module for error detection

In automated filter tuning solution without any feedback, the designed system will rely solely on the machine code instructions. This means that even if there is an error/fault, the machine will keep following the instructions blindly and would lead to inaccurate tuning results at the end. Therefore, feedback is important to detect the error to reduce the wastage of time and resources. Also, the error detection would eliminate the need of having a manual supervision while tuning.

As discussed in section 7.3 that the information about phase change is to be used by the FAT robot, the angle information from polar chart or Smith chart is the primary factor that drives the whole tuning system. To ensure that this angle information is correct, real-time feedback from the system must be used so that the tuning error can be detected as soon as it occurs.

In this work, PFs are used as a feedback source to detect the error in the rotation angle as no dataset is needed; support non-linearity easy implementation; are parallelizable which allow faster computation; and are independent of size of the system. The implementation details of PF have been explained in section 7.5. The vision module

discussed in section 5.2.4 estimates the rotation angle using the colour strip pasted on the auxiliary disc shown in Fig 5.4. The estimated angle is compared with the updated rotation angle provided by VNA when the tuning screws rotate and accordingly, the control signal is sent to the FAT robot as shown in Fig. 7.6.

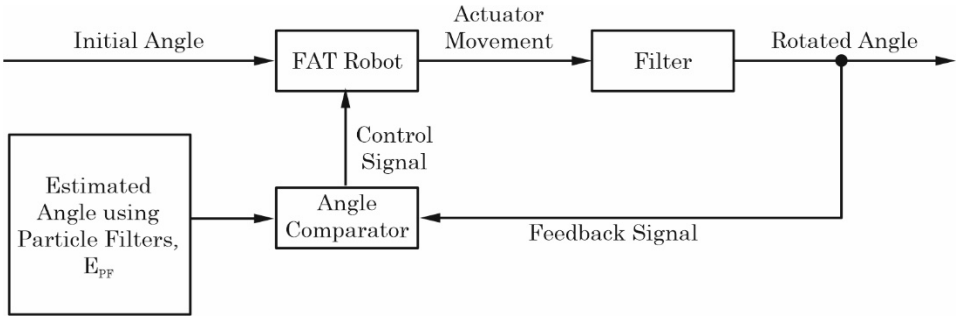

Figure 7.6. Angle comparison to detect the tuning error

7.6.4 Module for counting the screw turns

Once the tuning screws are localised, the tuning screws are made to touch the solid resonator beneath them i.e., the resonators are shorted. To avoid the case that the tuning screw comes off the filter surface while tuning, the number of turns made by the tuning screws are counted. The rotation of tuning screw is caused by the rotation of the screwdriver. Thus, PF-based colour tracking of the rotations of the same auxiliary disc attached on the screwdriver (which was used to compare the rotation angle in previous sub-section 7.5.3 using the vision module 5.2.4) was used to count the turns of tuning screw. The permissible turns of the screws were defined to be 07 turns (can be changed easily as per the need) which ensure that the screw is not coming-off the filter surface. This has actually been tracked using the rotation angle where the limiting angle is 2520° (7 full rotations = 7 X 360° = 2520°). The algorithm has been made so that if the number of turns made by a screw exceeds the defined value, the tuning is aborted immediately after displaying an error message - “Tuning is aborted as screw turns exceed the defined limit” on the computer screen. In such a case, the filter structure must be inspected for the root cause. Once the fault is rectified, the screws are shorted again, and the tuning process must restart.

7.6.5 Nut locking module

Locking the nuts ensures the product consistency i.e., the tuning state remains unchanged when the filter is under its delivery stage to the customer as well as during its use phase. When the last resonator is tuned to the state that the desired band specifications are met, the nut locking process which is to be executed by motor M5 in this work is initiated.

When the last tuning screw is brought to its optimal position and the correct tuned state of filter is achieved, the FAT robot doesn’t move towards its set initial position or towards its defined home position. Rather, FAT robot starts moving vertically downwards (i.e., towards the filter’s top plate). The tuned position of that tuning screw is retained using the holding torque of screwdriver motor (motor M6 in this work). The FAT robot continues to move downwards until the nut-tightener part i.e., outer tool of the designed tool-in-tool mechanism touches the thin metallic plate installed on the top plate of the

filter as shown in Fig. 7.7. When an electrical contact is made between nut tightener tool and the thin metal sheet on the filter base, the nut is tightened by motor M5.

Figure 7.7. A thin metallic sheet on the filter's top plate to implement the nut locking strategy.

The nut-locking strategy used in this work has been implemented in a way that once the filter meets the desired tuning state, the nuts are locked starting from the last screw and then sequentially locking the previous nuts all the way to the first screw i.e., from the output side of the filter to the input port side. The reasons for this choice are:

- The correctness of filter's final tuning state can only be verified once the last resonator is un-shorted, and the tuning screw is brought to its optimal state (as all the resonators are shorted initially). Thus, the unnecessary tightening of nuts can be avoided if the filter is not tuned to its desired state at the end due to fault in the filter structure e.g., soldering mistakes; RF energy leakage due to fault in connectors; insufficient shorting of the resonators in the beginning state; loose mounting of the filter's top plate etc.
- The FAT robot is already positioned above the last tuning screw (the one towards the output port of the filter) and thus it can start tightening nuts starting from that screw.
- When all the nuts are tightened from output port towards the input port, the FAT robot would be tightening the nut around the first tuning screw (the one towards the input port of the filter). Since the tuning of next filter unit starts from the first screw of the shorted filter, the FAT robot would already be close to its defined home position which would be closer to first tuning screw of the filter.

The above-mentioned modules are common for both of the automated filter tuning algorithms proposed in this work. The exact implementation of both these modules is described in the proposed algorithms themselves. Other than these common modules, some algorithm specific modules are also developed which are explained in detail in those corresponding sub-chapters.

7.7 Polar chart based automated filter tuning algorithm

7.7.1 VNA's polar angle fetching

In this work, Keysight Fieldfox RF Analyser 9914A – 6,5 GHz [156] has been used which is a Vector Network Analyser (VNA). This considered VNA is a 2-port device which allows the measurement of S-parameters in Logarithmic Magnitude (Log-Mag) scale, Linear magnitude scale, Group Delay (GD), Phase Response, Voltage Standing Wave Ratio etc.

The polar chart of the considered VNA shows the angles in a way that the bottom of the chart depicts negative angle values between 0° and 180° and positive angle values between 0° and 180° for values on the top half of the chart as presented in Fig. 7.8. The point presenting 180° in Fig 7.8 actually represents ±180°.

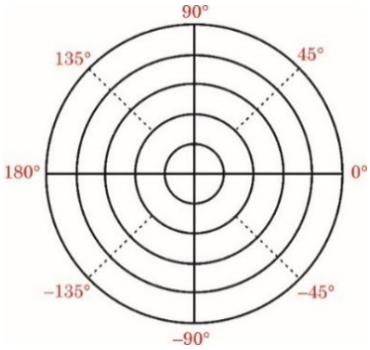

Figure 7.8. Angle distribution of the considered VNA

As mentioned in Section 7.3, we are interested in determining the phase change of the input reflection coefficient when traveling λ/4 (180°) on the polar chart from the starting position of the VNA's centre frequency marker. This position is an arbitrary point on the polar chart when the filter with shorted resonators is connected to the VNA. So, for accurately fetching the rotation angle information from the considered VNA, the logic presented in Fig. 7.9 has been used.

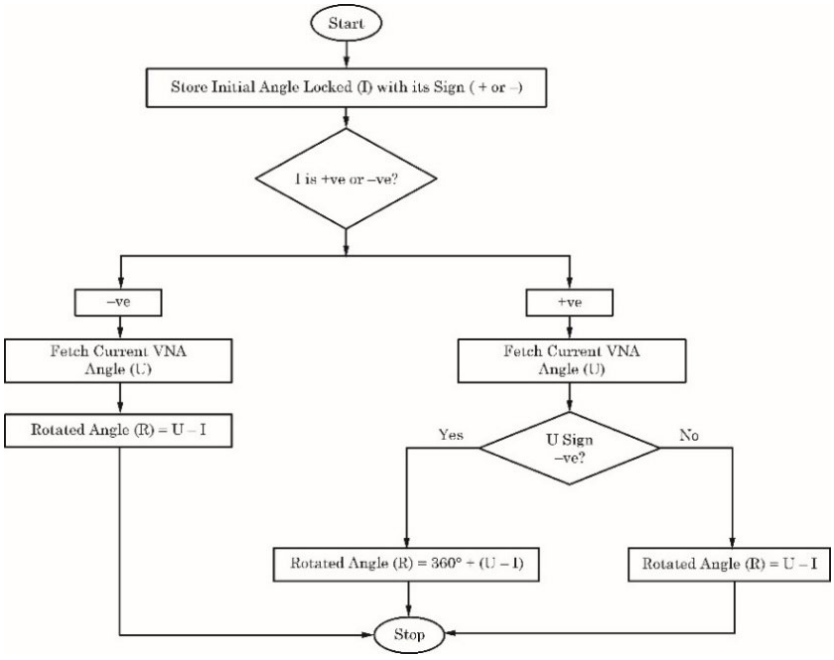

Figure 7.9. Rotation angle determination for tuning

In the beginning, when the filter with all the resonators shorted is connected to the filter, the angle information of the centre frequency marker position is stored as the initial angle (I). When the tuning screws of the filter are rotated, the marker position on the polar plot changes. The updated angle (U) and the initial angle are used to find the amount by which the screw has been rotated already. The sign of this initial angle is then used to determine the correct rotation angle. When I is negative or when the sign of both I and U is positive after the rotation, the rotation angle, R is obtained using equation 7.26.

$$R = U - I \tag{7.26}$$

However, for the case when I is positive, but U gets a negative value, then the rotation angle is calculated by equation 7.27 i.e.:

$$R = 360° + (U - I) \tag{7.27}$$

Thus, when I is +174° and U is -174°, equation 7.27 gives the correct rotation angle value of 12°.

7.7.2 Automated filter tuning algorithm using polar chart

The proposed algorithm for automated tuning of the all-pole filters using the polar chart of the VNA is presented in Fig. 7.10. The working of the proposed algorithm can be divided into following 03 different stages:

1) Performing tuning preliminaries and initializing
2) Filter tuning
3) Locking the screw nuts

These stages are now explained in the following sub-sections.

7.7.2.1 Tuning preliminaries and setting-up the FAT Robot and VNA

Initially, the tuning screws of the assembled filter are localised, and number of tuning screws mounted on the filter are stored in the variable N_s. Then, all the resonators of the filter to be tuned are shorted (the tuning screws are made to touch the top surface of solid resonators under them). The hexagonal screw nuts are not tightened at this stage so that the tuning screws can rotate easily. Once this process finishes, the FAT robot (which will conduct the actual tuning of the filter) is unlocked and brought to its defined 'home' position. The calibrated VNA is then connected to the filter via RF connectors and the connection between VNA and the PC is made using a LAN cable. The algorithm sets the VNA display format to the polar chart. Then, the VNA screen is set to display the parameters related to the filter to be tuned i.e.: start frequency (f_{start}), stop frequency (f_{stop}), centre frequency (f_0), the bandpass filter's lower cut-off frequency (f_1) and upper cut-off frequency (f_2). The number of plotting points (N_{points}) displaying the filter's tuning state are then defined. The frequency marker is initialized at the centre frequency of the filter. Then, the screw number (i), machine's speed when moving upwards (MUS), machine's speed when moving downwards (MDS), screwdriver's speed when moving upwards (SUS), screwdriver's speed when moving downwards (SDS), nut's locking speed (NLS), nut's unlocking speed (NUS), pre-defined value (P) to detect the start of rotation, and limiting angle difference value (L) specifying the maximum allowable difference between estimated angle and updated VNA angle are initialized as per the values defined in Table T-1 in Fig 7.10.

7.7.2.2 Filter tuning stage

Once the filter, the VNA, and the FAT robot are ready, the tuning process is initiated. The particles to estimate the rotation angle (E_{PF}) of the screwdriver are initiated to detect the tuning error and to count the numbers of screw turns as explained in previous subsections. The FAT robot is then positioned above screw number 1 and threshold angle (Th) responsible for varying the speed of tuning is set to 30°. Additionally, the rotated angle (R) and E_{PF} are both set to 0° at this stage. The initial angle depicted by the current position of the VNA's frequency marker is stored as I. Then, the tool-in-tool assembly is lowered with MDS so that the screwdriver mates within the tuning screw's head. While moving vertically downwards, the screwdriver is made to continuously rotate in counterclockwise (CCW) direction with the defined SDS value for unscrewing/un-shorting the resonator. As rotation of tuning screw would change the angle on the VNA, the new VNA angle (N) is continuously fetched. As per the implemented strategy, the whole actuator mechanism will continue moving downwards until the difference between N and I is less than P. Once the difference between N and I is greater than or equal to P, the FAT robot will reverse its direction (i.e., it will start moving in upward direction) to un-short the resonator with the defined upward motion speeds for machine (MUS) and screwdriver (SUS). The rotation of tuning screws changes the VNA's angle, and the PFs start estimating the rotation angle. This updated rotation angle is stored as (U). Particle filtering is used to estimate the angle (E_{PF}) as explained in section 7.5. If E_{PF} exceeds the value of 2520°, the tuning stops with an error message mentioning that the maximum permissible turns of the tuning screw have been exceeded is displayed on the PC screen. If E_{PF} is less than 2520°, the difference between the PF-estimated values of current angle $(E_{PF})_{now}$ and the previous angle $(E_{PF})_{previous}$ is calculated to determine the rotation angle ΔE_{PF}. The rotated angle (R) is calculated using the VNA's polar chart angle calculation logic explained in section 7.7.1. It is to be noted that the rotation angle determination logic presented in Fig. 7.9 has been depicted in a more detailed way in Fig. 7.10 for the clear understanding of the reader. The rotated angle calculation formulas given in both figures (Fig. 7.9 and Fig. 7.10) will bring us to the same value of rotation angle R.

The speed of the filter tuning is also varied on the basis of angle R as stated in section 7.6.2. The difference between the values of R and ΔE_{PF} is checked if it is less than the defined L value. This L value is taken according to the resolution provided by the RGB strip pasted on the auxiliary disc. This acts as the secondary source to verify the correctness of the angle provided by the VNA. If the difference is greater than L, an error message mentioning the discrepancy between both the angles is displayed and the tuning process stops. However, if the difference between the angles R and ΔE_{PF} is found to be less than L, the tuning process continues. The algorithm checks for angle R and keeps varying the speed of the FAT robot according to logic explained in 7.6.2. Once the complex conjugate value ±0,5° is approached (180° rotation with a tolerance limit of ±0,5° is completed), the FAT robot goes to the next screw and threshold value (Th) is again set to 30° and the angles R and ΔE_{PF} are set to 0°. The tuning continues until the last screw is brought to the complex conjugate of the previous resonator.

7.7.2.3 Locking the nuts of tuning screws

Once all the tuning screws are tuned, the outer nuts of the tuning screws are locked with defined nut locking speed (NLS) defined in Table T-1 as per the strategy mentioned in 7.6.5. The screwdriver sits into the tuning screwhead groove and holds the tuning screw position using the motor's holding torque while the nuts are tightened. Once all the nuts are locked, the filter tuning process is terminated.

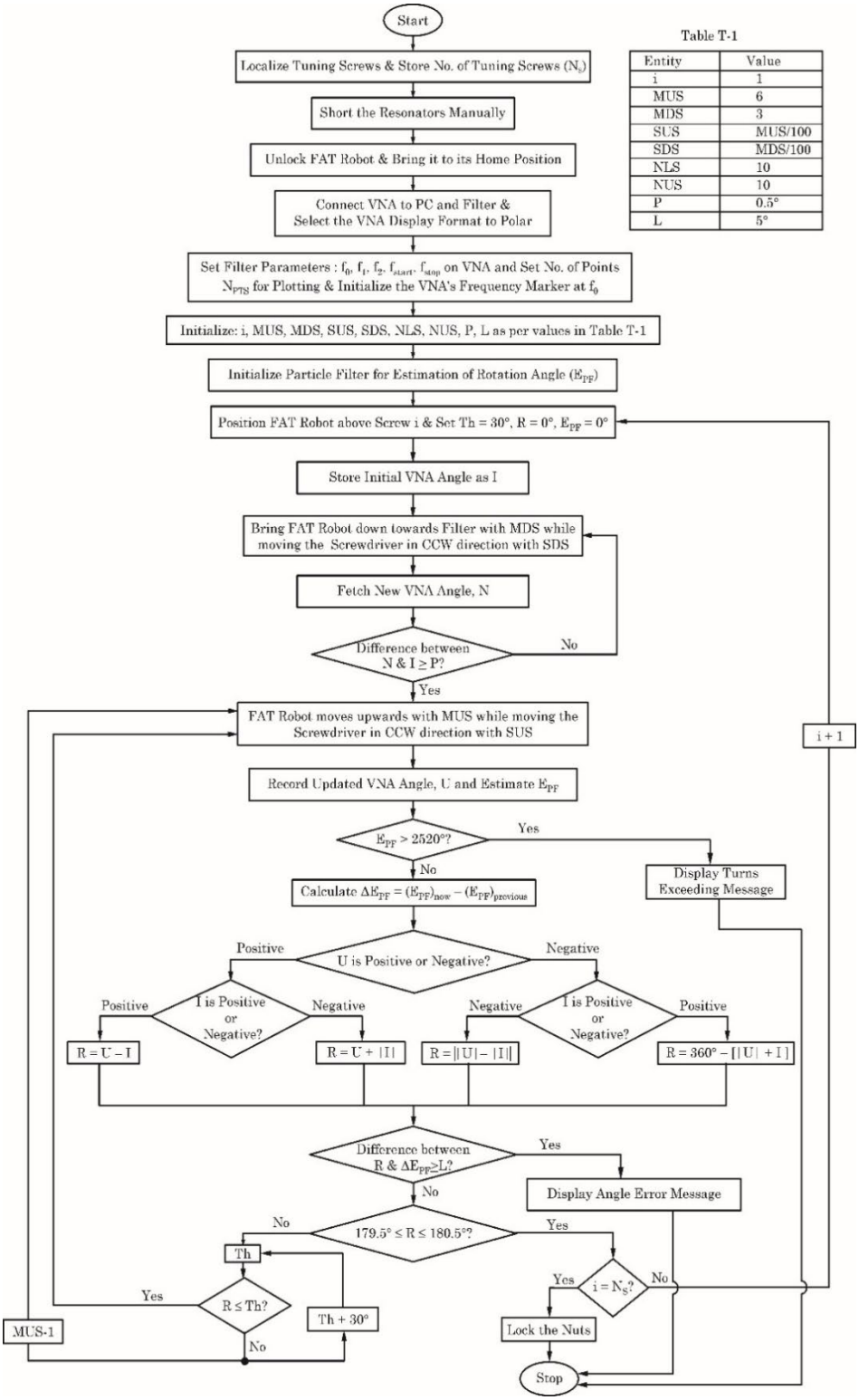

Table T-1

Entity	Value
i	1
MUS	6
MDS	3
SUS	MUS/100
SDS	MDS/100
NLS	10
NUS	10
P	0.5°
L	5°

Figure 7.10. Proposed automated filter tuning using polar chart

7.8 Smith chart-based filter tuning using YOLOv5

7.8.1 YOLOv5 dataset generation

As already stated in section 7.4 that due to complexity involved in dealing with the exponential scale as well as the infinity term of the Smith chart, the information provided by the Smith chart cannot be directly used. Thus, there is a need to have parametric tracking approach to come-up with an automated filter tuning algorithm based on Smith chart.

Owing to its high tracking accuracy, YOLOv5 model was used to track the tuning parameters represented by frequency marker on the Smith chart. The frequency marker is set at the centre frequency for tuning the filter. This frequency marker is shown within the bounding box in Fig 7.11.

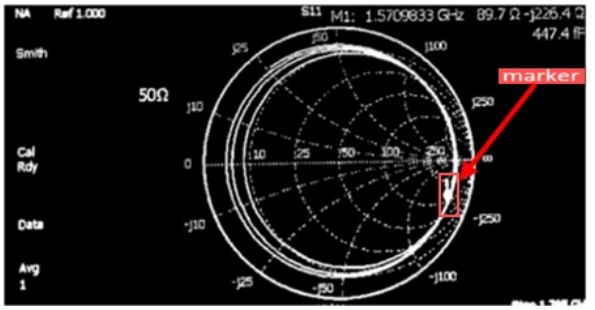

Figure 7.11. The frequency marker shown within the boundary box (also published in [V])

A labelled marker dataset was created in order to tune the filter using the frequency marker movement. While the cavity filter was being manually tuned, the dataset images were captured. The images were labelled once they had been acquired. Fig. 7.12 shows the process for obtaining images for the dataset where the smartphone camera is placed to capture the VNA's Smith chart when the filter is being manually tuned. The dataset is available publicly[1].

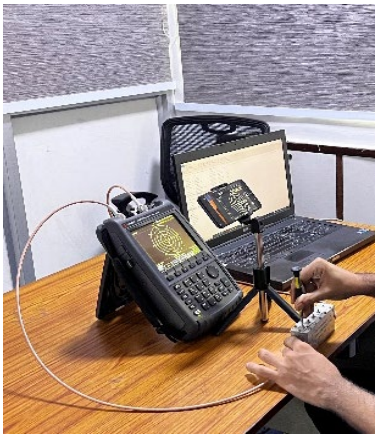

Figure 7.12. Generation of dataset while filter is being tuned manually

[1]https://ieee-dataport.org/documents/labelled-marker-dataset-smith-chart-image-processing-based-intelligent-tuning-microwave

Total dataset comprises of 4967 labelled images and the bifurcation of the dataset is presented in Table 7.3.

Table 7.3. YOLOv5 dataset (also published in [IV])

Category	Number	Split
Training Dataset	3475	70%
Validation Dataset	992	20%
Testing Dataset	500	10%
Total	4967	100%

7.8.2 Training the deep network

Before training the network, the labelled images without implementing any pre-processing were used and without using cross-validation stages. The details of hardware and software of the system used for implementing the proposed Smith-chart based automated filter tuning solution are presented in Table 7.4. The hyperparameters for deep network training are presented in Appendix 3.

Table 7.4. PC specifications

	Entity	Version
Hardware	RAM	16 GB
	Processor	Ryzen-9 5800 HS
	GPU	RTX 3060 – 6 GB
Software	System	Linux – Ubuntu 20
	CUDA Core	3840
	Programming	Python 3.8

In a batch size of 16, images with the size of 640 x 640 were used to train the model for 100 epochs. In regard to this, 1 epoch meant that both Feed Forward Neural Network (FFNN) and Back Propagation Neural Network (BPNN) have finished for the entire dataset for training. The Stochastic Gradient Descent (SGD) optimiser with a decaying factor of 0,005 and learning rate of 0.01 was used in model training process. With these parameters it took 1 h 37 min to train the YOLOv5 model. The curves depicting the effectiveness of the model training are illustrated in Appendix 2.

7.8.3 Smith chart-based tuning

The proposed algorithm for automated tuning of all-pole filters using the parametric tracking of the VNA's Smith chart is presented in Fig. 7.13. The working of the proposed algorithm has been divided into following 04 different stages:

1) Tuning preliminaries and initializing stage
2) Visual data acquisition and image processing stage
3) Filter tuning stage
4) Nuts locking stage

These stages are discussed in detail in the following subsections:

7.8.3.1 Tuning preliminaries and Initialization FAT robot and VNA

The algorithm starts with localisation of tuning screws using the band-subtraction method discussed in Chapter 6 and storing number of tuning screws as N_s. Initially all the tuning screws are made to touch the solid resonators (shorting process is executed). The nuts of the tuning screws are not tightened so that the tuning screws can be rotated

easily. The FAT robot is then unlocked and brought to its defined 'home' state. The VNA is then connected to PC via LAN cable and the VNA is connected to the filter through RF connectors and cables. The VNA's display is then set to Smith chart. The VNA display is set according to the following filter parameters: start frequency (f_{start}), stop frequency (f_{stop}), centre frequency (f_0), the bandpass filter's lower cut-off frequency (f_1) and upper cut-off frequency (f_2), and number of plotting points (N_{points}) to display the tuning state. Once VNA parameters are initialized, the frequency marker of VNA is initialized at f_0.

Then, the screw number (i), machine's upward moving speed (MUS), machine's downward moving speed (MDS), screwdriver's speed when the machine is moving upwards (SUS), screwdriver's speed when the machine is moving downwards (SDS), nut's locking speed (NLS), nut's unlocking speed (NUS), pre-defined value (P) to detect the start of screw rotation, and limiting angle value (L) specifying the maximum allowable difference between estimated angle by YOLO-based marker tracking (E_{YOLO}) and estimated angle by PF (E_{PF}) are initialized as per the values defined in Table T-2 in Fig 7.12. To estimate the rotation angle using particle filtering, the particles are then initialized.

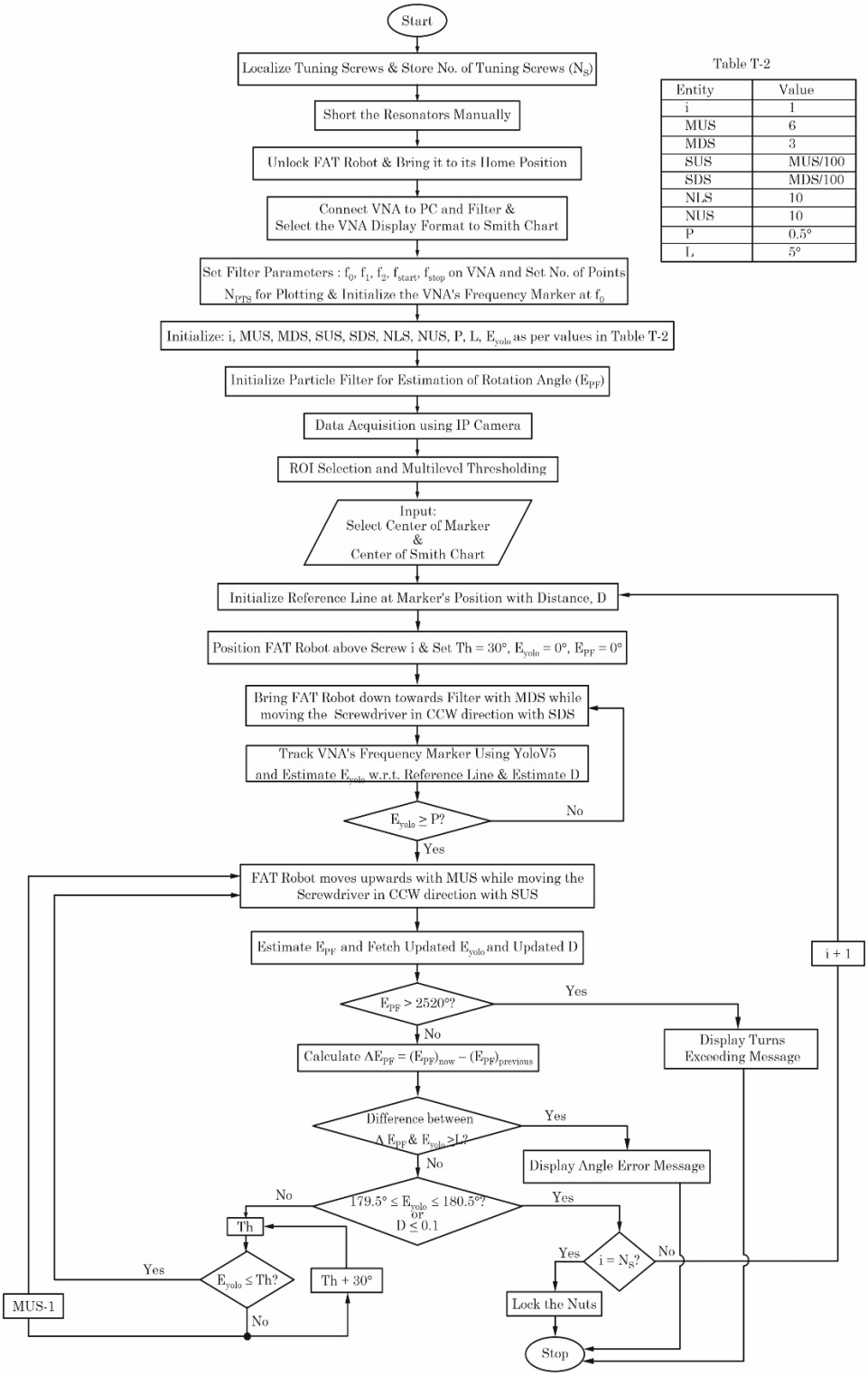

Table T-2

Entity	Value
i	1
MUS	6
MDS	3
SUS	MUS/100
SDS	MDS/100
NLS	10
NUS	10
P	0.5°
L	5°

Figure 7.13. Proposed Smith chart-based filter tuning algorithm

7.8.3.2 Visual data acquisition and its image processing

A smartphone is setup in a way that its camera acquires the real-time video of the VNA's screen depicting the Smith chart. This camera works as an IP camera. Thus, adding vision into the system allows the system to work without the need of modifying the VNA's internal software. This setup is shown in Fig. 7.14.

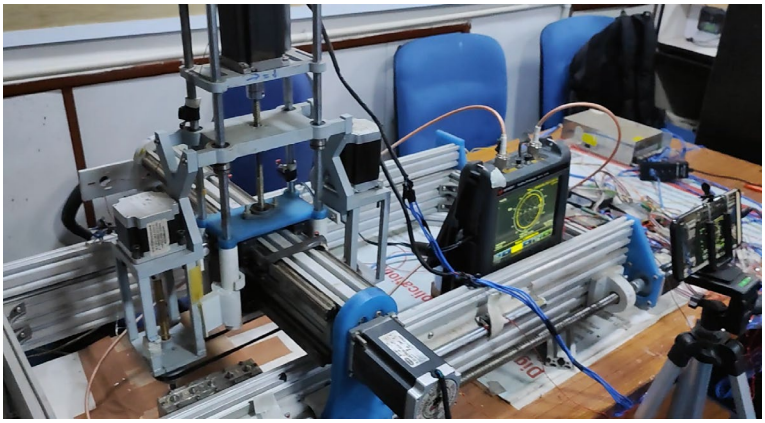

Figure 7.14. Smartphone camera looking at VNA's Smith chart

The YOLOv5 dataset created (presented in section 7.8.1) for automating the filter tuning process was trained on the raw images captured for dataset generation. However, to increase the accuracy of the results and to remove the noise, a Region of Interest (ROI) was selected. To remove the inaccurate classification of the marker, a 2nd pre-processing step i.e., a multi-level thresholding step (a segmenting approach) was added to the system. This 2nd step allowed the accurate tracking of the frequency marker even when the marker is obscured by several circles appearing on the VNA screen while the filter is being tuned. The results before and after the ROI selection and multilevel thresholding steps are presented in Fig. 7.15. Thus, everything required to tune the filter is set by this stage. A video showing the tracking of VNA marker on the Smith chart in real-time is made publicly available[2]. The robustness of this approach was also tested on the polar chart of the VNA even if the dataset related to polar chart was not created. The test results for polar chart are also made available in public domain[3] where even the ROI was also not selected proving the tracking robustness.

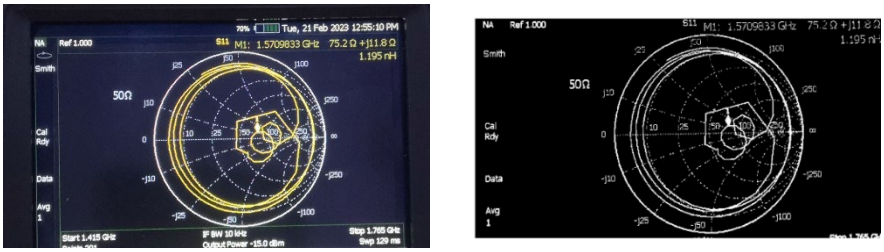

Figure 7.15. Original image (left) and Results of ROI selection and multilevel thresholding (right)

[2] https://drive.google.com/file/d/1wzAYKqaHbO9KfMKuJodRXBITJSt6x7-n/view?usp=sharing

[3] https://drive.google.com/file/d/1G8V77oR8zpIWrSALvRlRqjUMv4sJ4gzw/view?usp=sharing

7.8.3.3 Filter tuning stage with angle change and reference line switching logic

The tuning starts by selecting two points on the Smith chart by computer mouse – a) the centre of the marker, and b) centre of Smith chart (matched load point on the Smith chart). This step helps in accelerating the image processing operation speed and avoiding time wastage in searching for the centres. Selecting these two points initialize the reference line having the distance (D) between marker's centre and Smith chart's centre. This reference line is used to track the rotated angle as well as the distance D. It must be noted that D is directly proportional to the amount of signal reflected by the filter. As more and more resonators are tuned, the marker converges towards the matching point i.e., center of the Smith chart thus simultaneously reducing the D value.

Then, the FAT robot is positioned above screw number 1 and the threshold angle (Th) responsible for speed variation is set to 30°. At this stage the angle estimated by YOLO-based marker tracking (E_{YOLO}) and the angle estimated by PF (E_{PF}) is set as 0°. The FAT robot is then brought down towards the filter surface with MDS while the screwdriver is moving in CCW direction with SDS. The marker of the VNA is tracked in real-time using the trained YOLOv5 model which estimates the angle E_{YOLO} w.r.t to reference line and estimates the value of D. The algorithm checks if angle estimated by YOLO, E_{YOLO} is greater than or equal to pre-defined value (P). If angle E_{YOLO} is less than P, the FAT robot will continue moving downwards with MDS and SDS. Once the value of E_{YOLO} is greater than or equal to P, it symbolizes that the screwdriver is in contact with the tuning screw's head. Thus, the FAT robot will reverse its direction (i.e., it will start moving in upward direction) to un-short and tune the resonator with the defined upward motion speeds for machine (MUS) and screwdriver (SUS).

While rotating the tuning screw, the updated values of angle E_{YOLO} and D are fetched and the angle E_{PF} is also estimated. The value of E_{PF} is used to track the rotated angle which is to be used to detect the rotation angle error as well as the number of turns made by the screw. This E_{PF} value has the limiting value of 2520° which symbolizes the 07 full turns of the tuning screw. If E_{PF} exceeds this value, an error message mentioning the turns exceeding message is displayed and the tuning algorithm stops. Else, if this value is less than 2520°, the value of estimated rotated angle by PF (ΔE_{PF}) is calculated using the current value $(E_{PF})_{now}$ and the previous value $(E_{PF})_{previous.}$ If the difference between E_{YOLO} and ΔE_{PF} is greater than the limiting angle value L (defined by minimum angle resolution provided by the RGD strip attached to the auxiliary disc), the tuning stops after displaying the angle error message. However, if the difference between both the estimated angles E_{YOLO} and E_{PF} is lesser than L, condition of reaching the complex conjugate value (180°) is checked with the set tolerance of ±0,5° or if the distance D of the reference line is under the pre-set value of 0.1 (i.e., the marker is quite close to the matching point of the centre line). The 2nd condition defined here i.e., checking if the distance D is below a pre-set value provides robustness to the tuning system. If any of the conditions is not met, the FAT robot continues to tune the resonator using the speed variation logic presented in 7.6.2. Once any of these conditions is met, the resonator is tuned, and the reference line switches itself from the previous point to its complex conjugate point on the Smith chart with new distance D. The FAT robot then continues to tune the rest of the resonators by setting the Th to 30°, and the angles E_{YOLO} and E_{PF} are set to 0°.

7.8.3.4 Locking the outer nuts of tuning screws

When all the tuning screws are successfully tuned using the complex conjugate point, the nut surrounding each of the tuning screw is locked with the defined speed of NLS which ensures that the required amount of torque is provided to lock the nuts tightly. These nuts are locked as per the nut-locking strategy discussed in 7.6.5. The tuning algorithm stops once all the nuts are tightened.

7.9 Chapter summary

In this chapter, automated algorithms to sequentially tune the all-pole filters on the basis of phase change of the input reflection coefficient (S_{11}) were presented. Before tuning the filter, all the resonators were shorted. By sequentially tuning the resonators from the input side of the filter to the output side, the filter can be tuned without visiting the tuning screws iteratively. Two different automated filter tuning algorithms have been presented. The polar chart-based algorithm uses the angle information from VNA as a primary factor for tuning. For implementing the Smith chart-based algorithm, YOLOv5 dataset was generated to train the deep network. The VNA's frequency marker (set at the centre frequency of the filter) has been tracked in real-time using an IP camera to estimate the rotation angle. Both these algorithms compare the angle rotation information provided by them with the rotation angle estimated by PFs so that the tuning error can be detected at the early stage. Some other common modules – for differentiating the tuning screws from mounting screws; for varying the tuning speed as per the targeted rotation angle; for comparing the correctness of rotated angle; for counting the turns made by the tuning screws; and, for locking the position of tuning screws using the nuts have been developed to assist the filter tuning process by both proposed algorithms.

The next chapter presents the results obtained from tuning the test filter designed in Chapter 4 using the FAT robot presented in Chapter 5, thus validating the accuracy and efficiency of the proposed tuning methods and the developed FAT robot.

8 Results and Discussions

8.1 Filter used for testing the proposed algorithms

The automated filter tuning algorithms proposed in this work can be implemented to any all-pole filter with quarter wavelength long solid resonators which are iris-coupled. The solid resonators allow the shorting of resonators before initiating the tuning algorithm and setting the inter-resonator couplings through vertical iris reduces the number of tuning screws.

To test the proposed automated filter tuning algorithms, the 5^{th} order all-pole filter designed and fabricated in Chapter 4 has been used. The tuning process is performed by the robotic system designed and discussed in Chapter 5.

8.2 Results of polar chart-based automated filter tuning

8.2.1 Tuning results of the VNA's commercial software

As shorting the resonators is the first step while testing the proposed algorithms, Fig 8.1(a) presents the case when the all the resonators are brought to their shorted state. The VNA is not fully calibrated and hence the initial state of marker is not appearing at the outermost circle of the polar chart). For tuning the filter, the resonators are tuned sequentially from the input side of the filter to its output side. While considering the phase-change of the input reflection coefficient viz S_{11}, resonator number 1 is considered to be tuned when we rotate the centre frequency marker by an electrical length of $\lambda/4$ i.e., 180° rotation on the polar chart. Fig. 8.1(b) shows the case when the resonator number 1 of the test filter is tuned. At this stage, resonators 2, 3, 4, and 5 are shorted (or strongly detuned). Fig. 8.1(c) presents the case when resonators 1 and 2 are tuned while all the next resonators are still in highly detuned state. Next, Fig. 8.1(d) and 8.1(e) show the state when resonators 3 and 4 are tuned in the sequential manner while maintaining the tuned state of all the screws previously tuned as it is. While tuning the last resonator, the curve converges to the centre point of the chart which is a point showing the state where the reflection coefficient is close to zero i.e., most of the signal is getting transmitted. In Fig. 8.1(f), the converged state of input reflection coefficient towards the centre of the polar chart shows the case when the filter is tuned.

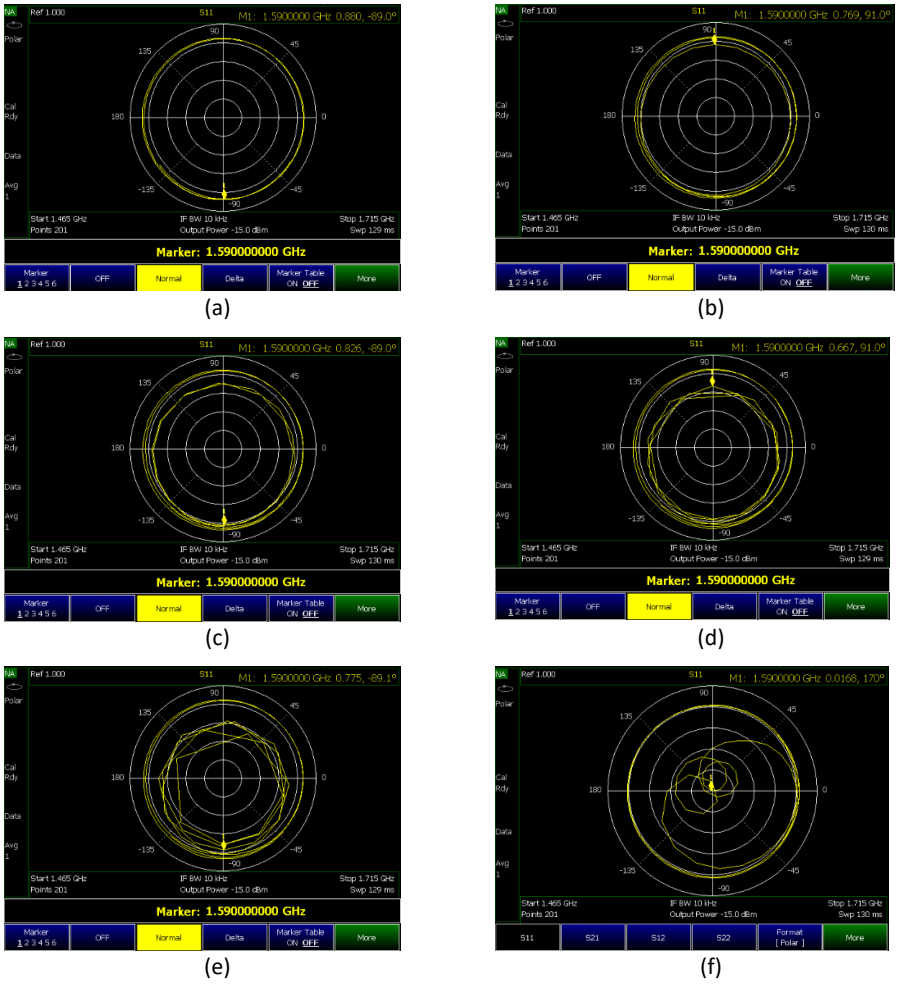

Figure 8.1. Results of automated tuning of a 5th order all pole filter on polar chart – (a) all resonators shorted; (b) after tuning resonator 1; (c) after tuning resonator 1 and 2; (d) after tuning resonator 1, 2 and 3; (e) after tuning resonator 1, 2, 3, and 4; (f) after tuning resonator 1, 2, 3, 4, and 5

The introduced design parameter presented in section 4.3.2 defined the limits for magnitude of RL to be > 18 dB and permissible IL range to be between the range of 0,5 to 0,9 dB. The results of RL and IL are presented in Fig. 8.2(a) and (b) respectively.

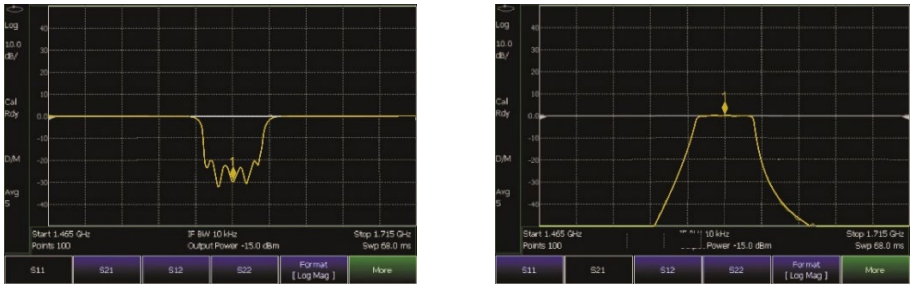

Figure 8.2. VNA's curves of return loss and insertion loss after the tuning – (a) Return Loss (S_{11}); (b) Insertion Loss (S_{21})

8.2.2 Tuning results on the developed plotting module

The commercial VNA's software for plotting the tuning results, a customized plotting module was developed under the scope of this work. This allows to possibility to add more features if needed later. Fig 8.3 shows the tuning results on a polar chart developed by the author. The details of Fig 8.3(a) to 8.3(f) are same as discussed in section 8.2.1. Before starting the tuning process on the FAT robot, all the resonators are shorted as shown in Fig. 8.3(a). Then all the resonators are tuned sequentially starting from the first resonator till the last one. When a resonator is getting tuned, all the other next resonators are kept in the shorted state. Once a resonator is tuned, all the previously tuned resonators are kept in the same tuned state. No fine-tuning is needed in this case for any of the resonators.

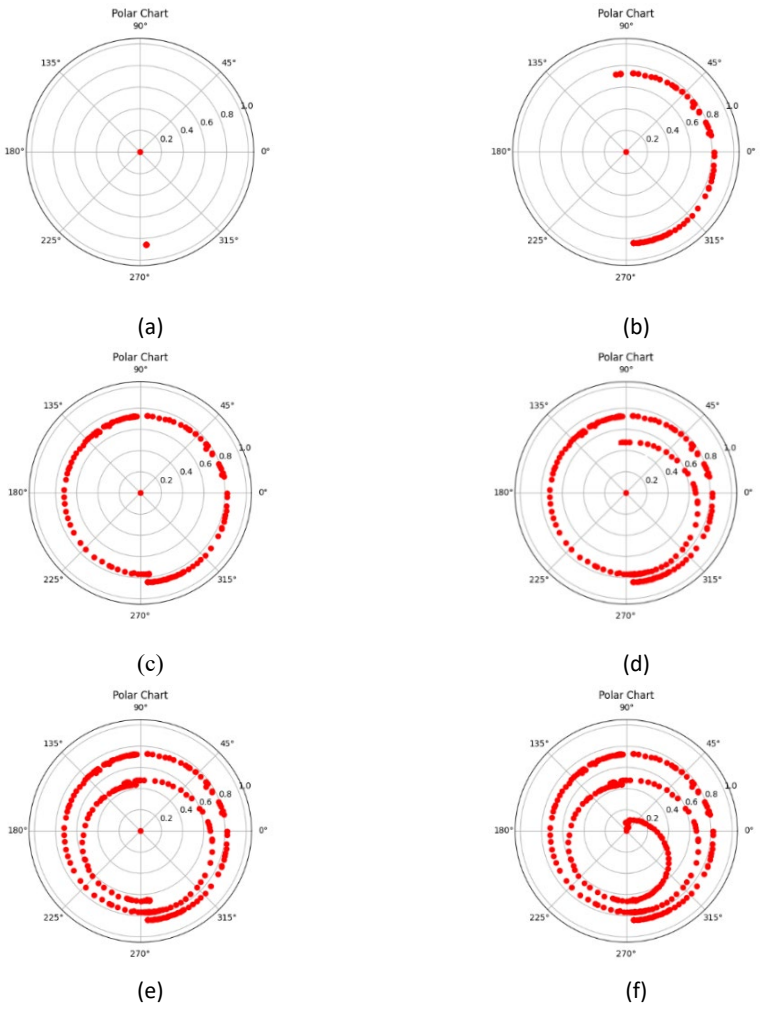

Figure 8.3. Tuning results on a developed module for plotting the polar plot – (a) all resonators shorted; (b) after tuning resonator 1; (c) after tuning resonator 1 and 2; (d) after tuning resonator 1, 2 and 3; (e) after tuning resonator 1, 2, 3, and 4; (f) after tuning resonator 1, 2, 3, 4, and 5

The results of RL and IL are also plotted using the custom developed module as presented in Fig. 8.4(a) and (b) respectively. Meeting the IL and RL tuning requirements stated in section 4.3.2 confirms that the filter has been tuned.

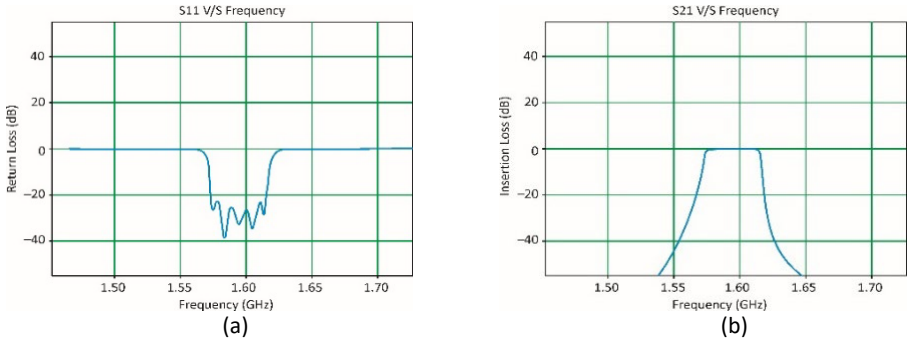

Figure 8.4. Curves depicting the return loss and insertion loss after tuning using the developed plotting module – (a) Return Loss (S_{11}); (b) Insertion Loss (S_{21})

8.3 Tuning results for Smith-chart based tuning

As already stated, before initiating the filter tuning process, the resonators of the filter are shorted first. The filters are tuned based on angle information fetched by the movement of marker over the Smith chart of the VNA. The marker is tracked by the trained YOLOv5 model using IP camera. The angle between the initial position of the marker and the moving marker is estimated in real-time and the reference line switching logic was implemented as shown in Fig. 8.5.

Figure 8.5. Results of automated tuning of a 5th order all pole filter on Smith chart – (a) all resonators shorted; (b) after tuning resonator 1; (c) after tuning resonator 1 and 2; (d) after tuning resonator 1, 2 and 3; (e) after tuning resonator 1, 2, 3, and 4; (f) after tuning resonator 1, 2, 3, 4, and 5

8.4 Total tuning time elapsed by algorithms

The total tuning time taken by the proposed automated filter tuning algorithms on the designed FAT robot when a filter with shorted resonators is placed for tuning was noted. While testing this, the readings of the proposed algorithm with as well as without the speed variation logic were noted. The total time taken by the proposed algorithms in both the cases is presented in Table 8.1.

Table 8.1. Time taken for tuning a 5th order filter using the proposed algorithms

	Time Without Speed Variation	**Time With Speed Variation**
Polar chart-based tuning	17 minutes 49 seconds	9 minutes 32 seconds
Smith chart-based tuning	17 minutes 10 seconds	9 minutes 38 seconds

8.5 Discussions

With successive tuning of the resonators, a spiral shape converging towards inside can be observed. This inward convergence is because of the fact that the since more resonators are involved so the amount of reflected signal reduces. Since the radius of constant reflection circles is directly proportional to amount of reflected signal, so, less reflections are depicted by the inward trend.

The tuning times can also be optimised further as per the need of the task while assuring that the final rotated angle is not exceeding the target angle beyond the defined tolerance. A higher speed of rotation may bring us the case where the final rotated angle jumped the target angle before the robot stops, thus leading to error accumulation.

8.6 Chapter Conclusion

The results of automated filter tuning algorithms proposed in this work are evaluated on the test filter designed and fabricated in Chapter 4 using the FAT robot presented in Chapter 5. The proposed algorithms can be used to tune the all-pole filters with quarter wavelength long solid resonators in which the inter-resonator coupling between the resonators was adjusted with the help of designed iris.

The tuning times for both the algorithms are compared with and without the speed variation logic implementation. The reliance on commercial VNA's software is eliminated by introducing a real-time plotting module for polar plot.

9 Conclusion, Limitations and Future Work

9.1 Conclusion

MW bandpass filters play a sterling role in Radio Base Stations (RBS) and radar systems by effectively isolating desired signals from the crowded electromagnetic spectrum. With the rapid expansion of cellular communication networks in recent years, there is an increased need for filters that meet specified frequency criteria. As a result, there is a pressing need in the industry to efficiently manufacture a substantial quantity of precisely calibrated filters at competitive prices. Subsequent to production, these filters must undergo tuning to address any discrepancies stemming from their design, manufacturing process, and material properties.

Various types of filters exist in the market. The main characteristics desired from a MW filter are - a) Sharp Out-of-band Selectivity (sharp rejection beyond the passband limits); b) High-Q-value (low loss value); and c) Compact size (small form factor). Among the common filter structures available, the cavity filters are most widely used in terrestrial communication industry owing to their robust behaviour; capability of handling high power; high Q-value (high quality); and temperature stability. At MW frequencies, the cavity filter structures are often used because at high frequencies the values of inductors (L) and capacitors (C) becomes impractical. While designing a cavity filter, the main considerations related to size of the filters are – the size of the filter becomes very large at the low frequencies; at high frequency, the size becomes very small and leads to appearance of higher modes.

Following an extensive review of the literature, it became evident that over the past two decades, the research community has gravitated towards data-driven approaches for filter tuning. This shift can be attributed to the enhanced computational capabilities provided by modern, powerful CPUs and GPUs, as well as the emergence of new algorithms capable of tackling intricate problems. Therefore, to test the possibility of using reinforcement learning in tuning the cavity filters, two reinforcement learning-based filter tuning algorithms i.e., Optimal Deep Q-Learning (DQN) and Double-Deep Q-Learning (DDQN) were proposed by the author. When implemented, the results of both these algorithms outperformed the related works presented by other researchers. Given the constraints identified within reinforcement learning-based tuning algorithms, the author opted to cease further exploration of this approach for resolving the filter tuning challenge. Instead, the decision was made to assess various filter tuning algorithms on physical filter units.

Commercial filters are meticulously crafted for specific applications, resulting in unique designs that provide little to no flexibility in terms of tuning adjustments. Therefore, a new 5^{th} order tuneable test filter having solid resonators of the size of quarter-wavelength was designed in CST software to test the automated filter tuning algorithms. Varying the height of the tuning screws allowed to vary the center frequency and BW of the filter. The inter-resonator coupling was adjusted with the designed vertical iris which reduced the total number of screws installed on the filter's top plate. The tuning screws were surrounded by hex-nuts to avoid the RF energy leakage and to ensure the product consistency during its transportation and during the use phase. The designed test filter was fabricated using an aluminium block cut by a CNC machine as per the designed dimensions. A good match was found between the response obtained from the simulated filter and the fabricated filter.

To test any new algorithm for automating the filter tuning process, an experimental setup is needed. Since all of the filter tuning equipment in the literature follow the instructions blindly i.e., no feedback system was introduced; and most of these solutions were designed to tune a particular filter topology; so, the need of having a new experimental setup becomes inevitable. Thus, an automated filter tuning robot (FAT robot) was built. To have bigger working envelop, cartesian configuration was selected. The use of limit switches provided the safety as well as assistance in 'homing' the robot. To deal with filters of different kinds, the stepper motors are chosen so that the torque and resolution requirements by various industrial filters can be dealt. The stepper motors are equipped with their dedicated motor driver which receives the control signal from the microcontroller. The whole system is mainly controlled by Python programming language. A customized tool-in-tool actuating mechanism was designed for bringing the tuning screws to their optimal positions followed by locking the outer nut (hex nut) of each tuning screw. The designed system allows accurate tuning of the filters. The detailed analysis of the mechanical design is not considered in this research work. As compared to other solutions proposed in the literature, the setup designed under this research work tracked the screw driver's angle rotation in real-time using the customized vision-module added to the system; and offers flexibility to tune different kinds of industrial filters by making minor adjustments.

Before even initiating filter the tuning process, the two obligatory steps are needed viz. – a) to differentiate the tuning screws of the filter from the plate mounting screws and storing the positional coordinates of all the tuning screws; and b) setting the tuning screws to their initial state. The detection and localising of tuning screws were performed using the introduced vision-based methods, where-in, the imaging setup and the image processing techniques were also discussed. The state-of-the-art ML algorithms and a novel band-subtraction method were tested to differentiate and localise the tuning screws. Both these methodologies of localising the tuning screws have been validated on a commercial filter. The initial position of the tuning screws has been set to be the one in which each tuning screw touches (shorts) the resonator under it.

Once the tuning pre-requisites were met, two automated algorithms were proposed. These tuning algorithms incorporated theoretical knowledge while tuning the filters using polar chart, and combination of theoretical knowledge and AI to tune the filters based on change in phase of the input reflection coefficient (S_{11}) on polar chart and Smith chart. The polar chart-based algorithm uses the angle information from VNA connected to the filter as a primary factor for tuning. For implementing the Smith chart-based algorithm, YOLOv5 dataset is generated to train a deep network. The VNA's frequency marker (set at the center frequency of the filter) was tracked in real-time to estimate the rotation angle using an IP camera in Smith-chart based tuning algorithm. Both these algorithms compared the rotated angle provided by them with the rotation angle estimated by PFs so that the tuning error can be detected at the early stage. Some other common modules i.e. – for differentiating the tuning screws from mounting screws; for varying the tuning speed as per the targeted rotation angle; for comparing the correctness of rotated angle; for counting the turns made by the tuning screws; and, for locking the position of tuning screws using the nuts have been developed to assist the filter tuning process by both proposed algorithms. The proposed algorithms can be used to tune the all-pole filters equipped with quarter wavelength long solid resonators in which the inter-resonator coupling between the resonators is adjusted with the help of designed iris.

The results of automated filter tuning algorithms proposed in this work are evaluated on the test filter designed and fabricated in Chapter 4 using the FAT robot presented in Chapter 5. By sequentially tuning the resonators from the input side of the filter to the output side, the filter is tuned without visiting the tuning screws iteratively. The tuning times for different algorithms are compared for the cases when the speed variation logic is not implemented as well as for the case when the speed is varied as per the amount of angle a tuning screw has been rotated. The reliance on commercial VNA's software is eliminated by introducing a real-time plotting module for polar plot.

Thus, the following objectives were achieved:

- Two reinforcement learning-based algorithms for filter tuning i.e., DQN and DDQN were simulated to decide the strategy of moving further.
- A new universal test filter to evaluate the automated filter tuning algorithm was fabricated.
- An experimental setup i.e., FAT robot equipped with customizable actuator mechanism was developed.
- Vision-based methods to distinguish the tuning screws and mounting screws and obtaining the positional coordinates of tuning screws were developed.
- Novel automated filter tuning algorithms with a provision of varying the tuning speed as per the target angle were tested and compared. The algorithms use the theoretical knowledge and its conjunction of AI to tune the filters.
- Particle filtering was used to track the tuning error in real-time.
- A customizable real-time plotting module was developed to fetch the current tuning state of the filter without relying on the VNA's commercial software.

Thus, this thesis offered a complete solution to automate filter tuning, useful in both educational and industrial settings. The proposed solutions limit human involvement to mounting the filter and initiating the automated tuning algorithm, thereby obviating the necessity for technician training in the filter tuning process.

9.2 Limitations

Every research endeavour carries inherent limitations, serving as stepping stones for future exploration and refinement. The main limitations of this research are:

- One of the major limitations of the current work is that the process of shorting the resonators is performed manually.
- The proposed algorithm lacks the capability to effectively tune cross-coupled filters.
- Another limitation of the current setup is that the tuning speed is not optimised, resulting in extended tuning times.
- Another noteworthy limitation is that a comprehensive mechanical analysis of the experimental setup has not been conducted, which means important structural considerations have not been thoroughly explored.
- Additionally, an in-depth cost analysis has not been performed, leaving the financial implications of automated filter tuning process unexplored and unexamined.

9.3 Future Scope

Research is the bridge to the future, and its scope knows no bounds. With every discovery, we unlock new doors of possibility paving the way for innovations and breakthroughs that will shape tomorrow. This final section of the thesis elucidates the forthcoming potential. The avenues for further exploration within the research domain are:

- For tuning more complex filters, Coupling Matrix (CM) approach can be used.
- A potential avenue for improvement lies in fine-tuning the speed variation logic to align with the specific requirements of each filter unit, potentially yielding even greater efficiency gains.
- A comprehensive analysis of the experimental setup can be conducted to thoroughly explore the important structural considerations.
- Cost-analysis can be made to come-up with a cost-effective automated tuning setup.
- An upgrade to servo motors, controlled by PLC, holds promise for achieving heightened precision compared to the current use of stepper motors. Also, this advancement could lead to more accurate and reliable tuning processes.
- Vision system can be used to make the system more robust so that the FAT robot can calibrate itself according to the orientation angle of the filter. Currently we have a wooden fixture for holding the filter at its desired place and the positional coordinates obtained using the proposed vision-based methods take the tuning manipulator towards the tuning screws. Also, incorporating the camera to determine the rotation angle and height of tuning screws can make system more adaptable.
- For production lines, with exceptionally high demand, implementing a multiple-actuator system could enable simultaneous tuning of screws leading to significant reduction in the tuning time.
- A screw feeding mechanism can be introduced to the system. This system will place the tuning screws over the filter's top plate.
- Currently, the feedback has been taken via particle filtering. An encoder may be added to the designed system for receiving the primary feedback and PFs can serve as the secondary feedback source.
- Smith-chart based tuning needs the centres of the Smith chart as well as the center of the frequency marker set at the center frequency f_0. This step can be automated by a proper vision setup so that the offset introduced by the VNA's Smith chart display can be compensated.
- Bigger dataset maybe generated for tracking the marker. This will increase the confidence level of the marker and can deal with the cases where the marker disappears momentarily.
- The manual shorting of the screws can be replaced by shorting them with the help of a computer programme. The algorithm could automatically set the initial position of the tuning screws either by turning them a set number of times, or by ensuring the deflection change stays within a certain range.

List of Figures

List of Tables

References

[1] J. Brian Thomas, “Cross-Coupling In Coaxial Cavity Filters - A Tutorial Overview,” *IEEE Trans Microw Theory Tech*, vol. 51, no. 4, pp. 1368–1376, 2003, doi: 10.1109/TMTT.2003.809180.

[2] S. Amari and J. Bornemann, “Maximum Number of Finite Transmission Zeros of Coupled Resonator Filters with Source/Load-Multiresonator Coupling and a given Topology,” in *Asia-Pacific Microwave Conference Proceedings, APMC 2000, Sydney, NSW, Australia*, Sydney, Australia, 2000, pp. 1175–1177. doi: 10.1109/apmc.2000.926040.

[3] Y. L. Zhang, “Improved Matrix Synthesis for Inline Filters with Transmission Zeros Generated by FVC,” *Progress In Electromagnetics Research M*, vol. 76, pp. 9–17, 2018, doi: 10.2528/PIERM18101502.

[4] J. A. Ruiz-Cruz, C. Wang, and K. A. Zaki, “Advances in Microwave Filter Design Techniques,” *Microwave Journal, 51*, pp. 26–44, 2008.

[5] H. W. Yao, C. Wang, and K. A. Zaki, “Effects of Tuning Structures on Combline Filters,” in *1996 26th European Microwave Conference (EuMC 1996), Prague, Czech Republic*, Prague, Czech Republic, 1996, pp. 427–430. doi: 10.1109/EUMA.1996.337605.

[6] J. M. Chuma and D. Mirshekar-Syahkal, “Effects of Walls on Coupling Between Coupled Combline Resonators,” *IEE Proceedings: Microwaves, Antennas and Propagation*, vol. 149, no. 1, pp. 53–56, 2002, doi: 10.1049/ip-map:20020180.

[7] L. Han, K. Wu, X.-P. Chen, and F. He, “Influence and Tuning of Tunable Screws for Microwave Filters Using Least Squares Support Vector Regression,” *International Journal of RF and Microwave Computer-Aided Engineering*, vol. 20, no. 4, pp. 422–429, 2010, doi: 10.1002/mmce.

[8] A. Lindner, E. Biebl, and A. Strasse, “A Manual Tuning Method for Coupled Cavity Filters,” in *Proceedings of 36th European Microwave Conference, Manchester, UK*, 2006, pp. 1340–1342. doi: 10.1109/EUMC.2006.281264.

[9] J. Dunsmore, “Tuning Band Pass Filters in the Time Domain,” in *1999 IEEE MTT-S International Microwave Symposium Digest, Anaheim, CA, USA*, 1999, pp. 1351–1354. doi: 10.1109/MWSYM.1999.779638.

[10] “Simplified Filter Tuning Using Time Domain, Application Note, AN 1287-8, 1999, (Republished in 2000 by Agilent as 5968-5328E).”

[11] J. Dunsmore, “Advanced Filter Tuning using Time Domain Transforms,” in *29th European Microwave Conference, EuMC 1999, Munich Germany*, 1999, pp. 72–75. doi: 10.1109/EUMA.1999.338412.

[12] “Network Analysis Solutions Advanced Filter Tuning Using Time Domain Transforms, Application Note 5980-2785EN, 1999 (Republished by Keysight in 2017).”

[13] S. Burger and M. Hoeft, “Improved Filter Tuning in the Time Domain,” in *1st Australian Microwave Symposium, ASM 2014, Melbourne, VIC, Australia*, Melbourne, VIC, Australia: IEEE, 2014, pp. 27–28. doi: 10.1109/AUSMS.2014.7017349.

[14] M. Dishal, “Alignment and Adjustment of Synchronously Tuned Multiple-Resonant-Circuit Filters,” *Proceedings of the IRE*, vol. 39, no. 11, pp. 1448–1455, 1951, doi: 10.1109/JRPROC.1951.273611.

[15] A. E. Atia and A. E. Williams, “Measurements of Intercavity Couplings,” *IEEE Trans Microw Theory Tech*, vol. 23, no. 6, pp. 519–522, 1975, doi: 10.1109/TMTT.1975.1128614.

[16] M. H. Chen, “Short-Circuit Tuning Method for Singly Terminated Filters,” *IEEE Trans Microw Theory Tech*, vol. 25, no. 12, pp. 1032–1036, 1977, doi: 10.1109/TMTT.1977.1129269.

[17] L. Accatino, “Computer-Aided Tuning of Microwave Filters,” in *1986 IEEE MTT-S International Microwave Symposium Digest, Baltimore, MD, USA*, 1986, pp. 249–252. doi: 10.1109/MWSYM.1986.1132161.

[18] J. B. Ness, “A Unified Approach to the Design, Measurement and Tuning of Coupled-Resonator Filters,” *IEEE Trans Microw Theory Tech*, vol. 46, no. 4, pp. 343–351, 1998, doi: 10.1109/22.664135.

[19] J. B. Ness, “Alignment of Cross-Coupled Resonator Filter using the Group Delay Technique,” *Microw Opt Technol Lett*, vol. 18, no. 3, pp. 174–179, 1998, doi: Ness, J. B. (1998). Alignment of cross-coupled resonator filters using the group delay technique. Microwave and Optical Technology Letters, 18(3), 174–179. doi:10.1002/(sici)1098-2760(19980620)18:3<174::aid-mop5>3.0.co;2-c.

[20] N. Zahirovic and R. R. Mansour, “Sequential Tuning of Coupled Resonator Filters using Hilbert Transform Derived Relative Group Delay,” in *2008 IEEE MTT-S International Microwave Symposium Digest, Atlanta, GA, USA*, 2008, pp. 739–742. doi: 10.1109/MWSYM.2008.4632938.

[21] G. Pepe, F. Gortz, and H. Chaloupka, “Computer-Aided Tuning and Diagnosis of Microwave Filters using Sequential Parameter Extraction,” in *2004 IEEE MTT-S International Microwave Symposium Digest, Fort Worth, TX, USA*, 2004, pp. 1373–1376. doi: 10.1109/MWSYM.2004.1338824.

[22] G. Pepe, F. J. Görtz, and H. Chaloupka, “Sequential Tuning of Microwave Filters using Adaptive Models and Parameter Extraction,” *IEEE Trans Microw Theory Tech*, vol. 53, no. 1, pp. 22–31, 2005, doi: 10.1109/TMTT.2004.839342.

[23] A. Lindner, H. Kugler, and E. Biebl, “Manual Filter Tuning by Cloning Frequency Domain Data,” in *European Microwave Conference, EUMC 2007, Munich Germany*, 2007, pp. 329–331. doi: 10.1109/EUMC.2007.4405193.

[24] J. J. Michalski, “Inverse Modeling in Application for Sequential Filter Tuning,” *Progress In Electromagnetics Research*, vol. 115, pp. 113–129, 2011, doi: 10.2528/PIER11021103.

[25] J. Marquardt and G. Muller, “Computer-Aided Tuning of Microwave Circuits,” in *IEEE MTT-S International Microwave Symposium Digest, San Diego, CA, USA*, San Diego, CA, USA, USA, 1977, pp. 147–150. doi: 10.1109/MWSYM.1977.1124388.

[26] A. E. Atia and H. Yao, “Tuning & Measurements of Couplings and Resonant Frequencies for Cascaded Resonators,” in *2000 IEEE MTT-S International Microwave Symposium Digest, Boston, MA, USA*, 2000, pp. 1637–1640. doi: 10.1109/MWSYM.2000.862291.

[27] H. T. Hsu, H. Yao, K. A. Zaki, and A. E. Atia, “Computer-Aided Diagnosis and Tuning of Cascaded Coupled Resonators Filters,” *IEEE Trans Microw Theory Tech*, vol. 50, no. 4, pp. 1137–1145, 2002.

[28] H. T. Hsu, Z. Zhang, K. A. Zaki, and A. E. Atia, “Parameter Extraction for Symmetric Coupled-Resonator Filters,” *IEEE Trans Microw Theory Tech*, vol. 50, no. 12, pp. 2971–2978, 2002, doi: 10.1109/TMTT.2002.805283.

[29] A. Ghadiya and S. Soni, “Sequential Parameter Extraction of Direct-Coupled Resonator Filter,” in *2014 Fourth International Conference on Communication Systems and Network Technologies, Bhopal, India*, IEEE, 2014, pp. 25–29. doi: 10.1109/CSNT.2014.14.

[30] W. Meng and K. L. Wu, “Analytical Diagnosis and Tuning of Narrowband Multicoupled Resonator Filters,” *IEEE Trans Microw Theory Tech*, vol. 54, no. 10, pp. 3765–3771, 2006, doi: 10.1109/TMTT.2006.881623.

[31] H. Kabir, Y. Wang, M. Yu, and Q. J. Zhang, “High-Dimensional Neural-Network Technique and Applications to Microwave Filter Modeling,” *IEEE Trans Microw Theory Tech*, vol. 58, no. 1, pp. 145–156, 2010, doi: 10.1109/TMTT.2009.2036412.

[32] M. Meng and K. L. Wu, “An Analytical Approach of Extracting Coupling Matrix and Unloaded Q of a Bandpass Filter,” in *IEEE MTT-S International Microwave Symposium Digest, Boston, MA, USA*, 2009, pp. 1345–1348. doi: 10.1109/MWSYM.2009.5165954.

[33] M. Meng and K. L. Wu, “An Analytical Approach to Computer-Aided Diagnosis and Tuning of Lossy Microwave Coupled Resonator Filters,” *IEEE Trans Microw Theory Tech*, vol. 57, no. 12, pp. 3188–3195, 2009, doi: 10.1109/TMTT.2009.2033868.

[34] R. Wang, L. Z. Li, and L. Peng, “Diagnosis of Lossy Resonator Filters with Source-Load Coupling using Y-parameters,” *International Journal of RF and Microwave Computer-Aided Engineering*, vol. 24, no. 6, pp. 713–717, 2014, doi: 10.1002/mmce.20816.

[35] R. Wang, L.-Z. Li, and L. Peng, “Improved Diagnosis of Lossy Resonator Bandpass Filters using Y-parameters,” *International Journal of RF and Microwave Computer-Aided Engineering*, vol. 25, no. 9, pp. 807–814, 2015, doi: 10.1002/mmce.20919.

[36] C. K. Liao, C. Y. Chang, and J. Lin, “A Vector-Fitting Formulation for Parameter Extraction of Lossy Microwave Filters,” *IEEE Microwave and Wireless Components Letters*, vol. 17, no. 4, pp. 277–279, 2007, doi: 10.1109/LMWC.2007.892970.

[37] H. Hu and K. L. Wu, “A Generalized Coupling Matrix Extraction Technique for Bandpass Filters with Uneven-Qs,” *IEEE Trans Microw Theory Tech*, vol. 62, no. 2, pp. 244–251, 2014, doi: 10.1109/TMTT.2013.2296744.

[38] A. G. Lamperez, T. K. Sarkar, and M. S. Palma, “Filter Model Generation from Scattering Parameters using Cauchy Method,” in *2002 32nd European Microwave Conference, Milan, Italy*, 2002, pp. 1–4. doi: 10.1109/EUMA.2002.339310.

[39] A. García-Lampérez, S. Llorente-Romano, M. Salazar-Palma, and T. K. Sarkar, “Efficient Electromagnetic Optimization of Microwave Filters and Multiplexers Using Rational Models,” *IEEE Trans Microw Theory Tech*, vol. 52, no. 2, pp. 508–521, 2004, doi: 10.1109/TMTT.2003.822021.

[40] A. G. Lampérez, T. K. Sarkar, and M. S. Palma, “Generation of Accurate Rational Models of Lossy Systems using the Cauchy Method,” *IEEE Microwave and Wireless Components Letters*, vol. 14, no. 10, pp. 490–492, 2004, doi: 10.1109/LMWC.2004.834576.

[41] G. Macchiarella and D. Traina, “A Formulation of the Cauchy Method Suitable for the Synthesis of Lossless Circuit Models of Microwave Filters from Lossy Measurements,” *IEEE Microwave and Wireless Components Letters*, vol. 16, no. 5, pp. 243–245, 2006, doi: 10.1109/LMWC.2006.873583.

[42] D. Traina, G. Macchiarella, and J. Bertelli, “Computer-Aided Tuning of GSM Base-Station Filters-Experimental Results,” in *2006 IEEE Radio and Wireless Symposium, San Diego, CA, USA*, 2006, pp. 587–590. doi: 10.1109/RWS.2006.1615225.

[43] M. Esmaeili and A. Borji, “Diagnosis and Tuning of Multiple Coupled Resonator Filters,” in *2010 18th Iranian Conference on Electrical Engineering, ICEE 2010, Isfahan, Iran*, IEEE, 2010, pp. 124–129. doi: 10.1109/IRANIANCEE.2010.5507088.

[44] G. Macchiarella, “Extraction of Unloaded Q and Coupling Matrix from Measurements on Filters with Large Losses,” *IEEE Microwave and Wireless Components Letters*, vol. 20, no. 6, pp. 307–309, 2010, doi: 10.1109/LMWC.2010.2047455.

[45] R. Wang and J. Xu, “Computer-Aided Diagnosis of Lossy Microwave Coupled Resonators Filters,” *International Journal of RF and Microwave Computer-Aided Engineering*, vol. 21, no. 5, pp. 519–525, 2011, doi: 10.1002/mmce.20537.

[46] R. Wang and J. Xu, “Extracting Coupling Matrix and Unloaded Q from Scattering Parameters of Lossy Filters,” *Progress In Electromagnetics Research*, vol. 115, pp. 303–315, 2011, doi: 10.2528/PIER11021604.

[47] R. Wang, J. Xu, C. L. Wei, M. Y. Wang, and X. C. Zhang, “Improved Extraction of Coupling Matrix and Unloaded Q from S-Parameters of Lossy Resonator Filters,” *Progress in Electromagnetics Research*, vol. 120, pp. 67–81, 2011, doi: 10.2528/PIER11072804.

[48] W. H. Cao, C. Liu, Y. Yuan, and M. Wu, “Extracting Coupling Matrix From Lossy Filters With Uneven-Qs Using Differential Evolution Optimization Technique,” *International Journal of RF and Microwave Computer-Aided Engineering*, vol. 28, no. 6, pp. 1–10, 2018, doi: 10.1002/mmce.21269.

[49] P. Zhao and K. L. Wu, “A New Computer-Aided Tuning Scheme for General Lossy Coupled-Resonator Bandpass Filters Based on the Cauchy Method,” *HKIE Transactions Hong Kong Institution of Engineers*, vol. 23, no. 1, pp. 52–62, 2016, doi: 10.1080/1023697X.2015.1129292.

[50] H. L. Thal, “Computer-Aided Filter Alignment and Diagnosis,” *IEEE Trans Microw Theory Tech*, vol. 26, no. 12, pp. 958–963, 1978, doi: 10.1109/TMTT.1978.1129528.

[51] P. Harscher, J. Hofmann, R. Vahldieck, and B. Ludwig, “Automatic Computer-Controlled Tuning System for Microwave Filters,” in *2000 30th European Microwave Conference (EuMC), Paris, France*, 2000, pp. 1–4. doi: 10.1109/EUMA.2000.338639.

[52] P. Harscher and R. Vahldieck, “Automated Computer-Controlled Tuning of Waveguide Filters using Adaptive Network Models,” *IEEE Trans Microw Theory Tech*, vol. 49, no. 11, pp. 2125–2130, 2001, doi: 10.1109/22.963147.

[53] P. Harscher, R. Vahldieck, and S. Amari, “Automated Test and Tuning System for Microwave Filters,” in *IEEE MTT-S International Microwave Symposium Digest (Cat. No.01CH37157), Phoenix, AZ, USA*, 2001, pp. 1543–1546. doi: 10.1109/MWSYM.2001.967197.

[54] P. Harscher, R. Vahldieck, and S. Amari, “Automated Filter Tuning Using Generalized Low-Pass Prototype Networks and Gradient-Based Parameter Extraction,” *IEEE Trans Microw Theory Tech*, vol. 49, no. 12, pp. 2532–2538, 2001, doi: 10.1109/22.971646.

[55] M. Kahrizi, S. Safavi-naeini, and S. K. Chaudhuri, “Computer Diagnosis and Tuning of Filters Using Model-Based Parameter Estimation and Multi-Level Optimization,” in *2000 IEEE MTT-S International Microwave Symposium Digest (Cat. No.00CH37017), Boston, MA, USA*, 2000, pp. 1641–1644. doi: 10.1109/MWSYM.2000.862292.

[56] M. Kahrizi, S. Safavi-naeini, S. K. Chaudhuri, and R. Sabry, “Computer Diagnosis and Tuning of RF and Microwave Filters Using Model-Based Parameter Extraction,” *IEEE Transactions on Circuits and Systems - I: Fundamental Theory and Applications*, vol. 49, no. 9, pp. 1263–1270, 2002, doi: 10.1109/TCSI.2002.802363.

[57] A. Rodriguez *et al.*, “Robust Optimization and Tuning of Microwave Filters and Artificial Transmission Lines using Aggressive Space Mapping Techniques,” in *2017 IEEE MTT-S International Microwave Symposium (IMS 2017), Honololu, HI, USA*, 2017, pp. 1501–1504. doi: 10.1109/MWSYM.2017.8058909.

[58] D. Miek and M. Höft, “Compensation of Cross-Dependencies in Computer Aided Tuning of Microwave Filters by Simplified Space Mapping Approach,” in *2018 IEEE MTT-S International Conference on Numerical Electromagnetic and Multiphysics Modeling and Optimization (NEMO 2018), Reykjavik, Iceland*, 2018, pp. 1–4. doi: 10.1109/NEMO.2018.8503481.

[59] S. Li, X. Fan, P. D. Laforge, and Q. S. Cheng, “A Post-fabrication Tuning Method using Space Mapping and Surrogate Modeling Techniques,” in *49th European Microwave Conference (EuMC 2019), Paris, France*, European Microwave Association (EuMA), 2019, pp. 392–395. doi: 10.23919/EuMC.2019.8910767.

[60] S. Li, X. Fan, P. D. Laforge, and Q. S. Cheng, “Surrogate Model-Based Space Mapping in Postfabrication Bandpass Filters’ Tuning,” *IEEE Trans Microw Theory Tech*, vol. 68, no. 6, pp. 2172–2182, 2020, doi: 10.1109/TMTT.2020.2977022.

[61] J. F. Pinel, “Computer-Aided Network Tuning,” *IEEE Transactions on Circuit Theory*, vol. 18, no. 1, pp. 192–194, 1971, doi: 10.1109/TCT.1971.1083228.

[62] P. M. Marshall and P. Tissi, “A New Algorithm for the Accurate Alignment of Microwave Networks,” *IEEE Trans Microw Theory Tech*, vol. 39, no. 10, pp. 1754–1758, 1991, doi: 10.1109/22.88547.

[63] A. R. Mirzai, C. F. N. Cowan, and T. M. Crawford, “Intelligent Alignment of Waveguide Filters using a Machine Learning Approach,” *IEEE Trans Microw Theory Tech*, vol. 37, no. 1, pp. 166–173, 1989.

[64] T. Cegielski and J. Michalski, “Heuristic Methods for Automated Microwave Filter Tuning,” in *2008 17th International Conference on Microwaves, Radar and Wireless Communications (MIKON 2008), Wroclaw, Poland*, 2008, pp. 1–4. doi: N/A.

[65] V. Miraftab and R. R. Mansour, “Computer-Aided Tuning of Microwave Filters using Fuzzy Logic,” in *2002 IEEE MTT-S International Microwave Symposium Digest, Seattle, WA, USA*, 2002, pp. 1117–1120. doi: 10.1109/TMTT.2002.805291.

[66] V. Miraftab and R. R. Mansour, “Computer-Aided Tuning of Microwave Filters using Fuzzy Logic,” *IEEE Trans Microw Theory Tech*, vol. 50, no. 12, pp. 2781–2788, 2002, doi: 10.1109/TMTT.2002.805291.

[67] V. Miraftab and R. R. Mansour, “A Robust Fuzzy-Logic Technique for Computer-Aided Diagnosis of Microwave Filters,” *IEEE Trans Microw Theory Tech*, vol. 52, no. 1, pp. 450–456, 2004, doi: 10.1109/TMTT.2003.820895.

[68] V. Miraftab and R. R. Mansour, “Tuning of Microwave Filters by Extracting Human Experience using Fuzzy Logic,” in *2005 IEEE MTT-S International Microwave Symposium Digest, Long Beach, CA, USA*, Long Beach, CA, USA: IEEE, 2005, pp. 1605–1608. doi: 10.1109/MWSYM.2005.1517011.

[69] V. Miraftab and R. R. Mansour, “Automated Microwave Filter Tuning by Extracting Human Experience in terms of Linguistic Rules using Fuzzy Controllers,” in *2006 IEEE MTT-S International Microwave Symposium Digest, San Francisco, CA, USA*, 2006, pp. 1439–1442. doi: 10.1109/MWSYM.2006.249541.

[70] V. Miraftab and R. R. Mansour, “Fully Automated RF/Microwave Filter Tuning by Extracting Human Experience using Fuzzy Controllers,” *IEEE Transactions on Circuits and Systems - I : Regular Papers*, vol. 55, no. 5, pp. 1357–1367, 2008, doi: 10.1109/TCSI.2008.916614.

[71] J. J. Michalski, “Artificial Neural Networks Approach in Microwave Filter Tuning,” *Progress In Electromagnetics Research M*, vol. 13, pp. 173–188, 2010, doi: 10.2528/PIERM10053105.

[72] J. J. Michalski, “Artificial Neural Network Algorithm for Automated Filter Tuning with Improved Efficiency by Usage of Many Golden Filters,” in *2010 18th International Conference on Microwave Radar and Wireless Communications (MIKON 2010), Vilnius, Lithuania*, 2010, pp. 1–3. doi: N/A.

[73] J. J. Michalski, T. Kacmajor, J. Gulgowski, and M. Mazur, “Consideration on Artificial Neural Network Architecture in Application for Microwave Filter Tuning,” *Piers Online*, vol. 7, no. 3, pp. 271–275, 2011, doi: N/A.

[74] T. Kacmajor and J. J. Michalski, “Principal Component Analysis in Application for Filter Tuning Algorithms,” in *2011 IEEE MTT-S International Microwave Workshop- Series on Millimeter Wave Integration Technologies, Sitges, Spain*, Sitges, Spain, 2011, pp. 121–123. doi: 10.1109/IMWS3.2011.6061853.

[75] J. J. Michalski and T. Kacmajor, “Filter Tuning Algorithm with Compressed Reflection Characteristic by Daubechies D4 Wavelet Transform,” in *2011 41st European Microwave Conference (EuMC 2011), Manchester, UK*, 2011, pp. 778–781. doi: 10.23919/EuMC.2011.6101931.

[76] T. Kacmajor, P. Kant, and J. J. Michalski, “Microwave Filter Tuning for Different Center Frequencies based on Artificial Neural Network and Phase Compensation,” in *2014 20th International Conference on Microwaves, Radar and Wireless Communications (MIKON 2014), Gydnia, Poland*, 2014, pp. 1–4. doi: 10.1109/MIKON.2014.6899833.

[77] Z. Wang, J. Yang, J. Hu, W. Feng, and Y. Ou, “Reinforcement Learning Approach to Learning Human Experience in Tuning Cavity Filters,” in *2015 IEEE International Conference on Robotics and Biomimetics (ROBIO 2015), Zhuhai, China*, 2015, pp. 2145–2150. doi: 10.1109/ROBIO.2015.7419091.

[78] Z. Wang, Y. Ou, X. Wu, and W. Feng, “Continuous Reinforcement Learning With Knowledge-Inspired Reward Shaping for Autonomous Cavity Filter Tuning,” in *2018 IEEE International Conference on Cyborg and Bionic Systems (CBS 2018), Shenzhen, China*, 2018, pp. 53–58. doi: 10.1109/CBS.2018.8612197.

[79] Z. Wang, S. Jin, J. Yang, X. Wu, and Y. Ou, “Real-Time Tuning of Cavity Filters by Learning from Human Experience: A Vector Field Approach,” in *2016 12th World Congress on Intelligent Control and Automation (WCICA 2016), Guilin, China*, 2016, pp. 1931–1936. doi: 10.1109/WCICA.2016.7578618.

[80] S. Lindstah and X. Lan, “Reinforcement Learning with Imitation for Cavity Filter Tuning,” in *2020 IEEE/ASME International Conference on Advanced Intelligent Mechatronics (AIM-2020), Boston, USA*, 2020, pp. 1335–1340. doi: 10.1109/AIM43001.2020.9158839.

[81] T. Kacmajor and J. J. Michalski, “Neuro-Fuzzy Approach In Microwave Filter Tuning,” in *IEEE MTT-S International Microwave Symposium Digest, Baltimore, MD, USA*, 2011, pp. 1–4. doi: 10.1109/MWSYM.2011.5972771.

[82] J. Zhou and J. Huang, “Intelligent Tuning for Microwave Filters Based on Multi-Kernal Machine Learning Model,” in *2013 5th IEEE International Symposium on Microwave, Antenna, Propagation and EMC Technologies for Wireless Communications, Chengdu, China*, Chengdu, China, 2013, pp. 259–266. doi: 10.1109/MAPE.2013.6689881.

[83] J. Zhou, B. Duan, and J. Huang, “Support-Vector Modeling of Electromechanical Coupling for Microwave Filter Tuning,” *International Journal of RF and Microwave Computer-Aided Engineering*, vol. 23, no. 1, pp. 127–139, 2013, doi: 10.1002/mmce.20683.

[84] J. Zhou, J. Huang, P. Li, and N. Li, “Hybrid Modeling of Microwave Devices using Multi-Kernel Support Vector Regression with Prior Knowledge,” *International Journal of RF and Microwave Computer-Aided Engineering*, vol. 25, no. 3, pp. 219–228, 2015, doi: 10.1002/mmce.20852.

[85] W. H. Cao, C. Liu, Y. Yuan, M. Wu, and S. B. Wu, “Parametric Modeling of Microwave Filter using Combined MLS-SVR and Pole-Residue-Based Transfer Functions,” *International Journal of RF and Microwave Computer-Aided Engineering*, vol. 28, no. 5, pp. 1–10, 2018, doi: 10.1002/mmce.21246.

[86] J. J. Michalski, “On Linear Mapping of Filter Characteristic to Position of Tuning Elements in Filter Tuning Algorithm,” *Progress In Electromagnetics Research*, vol. 123, pp. 279–298, 2012, doi: 10.2528/PIER11101009.

[87] Kacmajor Tomasz; Michalski Jerzy Julian, “Approximation of Filter Characteristic to Tuning Element Positions Using Coarse Set,” in *2012 19th International Conf. on Microwaves, Radar and Wireless Communications, Warsaw, Poland*, Warsaw, Poland, 2012, pp. 684–687. doi: 10.1109/MIKON.2012.6233555.

[88] T. Kacmajor and J. J. Michalski, “Filter Tuning Based on Linear Decomposition of Scattering Characteristics,” *Progress in Electromagnetics Research*, vol. 135, pp. 451–464, 2013, doi: 10.2528/PIER12112603.

[89] Y.-L. Zhang, T. Su, Z.-P. Li, and C.-H. Liang, “A Fast Tuning Method for Microwave Filter Using VF-ASM Technology,” *Progress In Electromagnetics Research M*, vol. 30, pp. 25–37, 2013, doi: 10.2528/PIERM13012201.

[90] Y.-L. Zhang, T. Su, Z.-P. Li, and C.-H. Liang, “A Hybrid Computer-Aided Tuning Method for Microwave Filters,” *Progress In Electromagnetics Research*, vol. 139, pp. 559–575, 2013, doi: 10.2528/PIER13032903.

[91] Y. L. Zhang and J. X. Yan, “A Hybrid Computer-Aided Tuning Method for Microwave Filters with Asymmetrical Phase Shift Effects,” in *2015 Asia-Pacific Microwave Conference (APMC 2015), Nanjing, China*, 2015, pp. 1–3. doi: 10.1109/APMC.2015.7412944.

[92] S. Wu, C. Liu, W. Cao, and M. Wu, “A New Method for Hybrid Diagnosis and Tuning of Coaxial Cavity Filter,” in *2017 36th Chinese Control Conference (CCC 2017), Dalian, China*, 2017, pp. 9692–9696. doi: 10.23919/ChiCC.2017.8028902.

[93] R. Wang, L.-Z. Li, L. Peng, X.-Q. Tu, and X.-X. Zhong, “Diagnosis of Coupled Resonator Bandpass Filters Using VF and Optimization Method,” *Progress In Electromagnetics Research M*, vol. 51, pp. 195–203, 2016, doi: 10.2528/PIERM16083001.

[94] S. Wu, W. Cao, M. Wu, and C. Liu, “A Tuning Method for Microwave Filter via Complex Neural Network and Improved Space Mapping,” *World Academy of Science, Engineering and Technology: International Journal of Electronics and Communication Engineering*, vol. 12, no. 3, pp. 222–228, 2018, doi: 10.5281/zenodo.1316311.

[95] S. Wu, W. Cao, C. Liu, and M. Wu, “A Computer-Aided Tuning Method for Microwave Filters by Combing T-S Fuzzy Neural Networks and Improved Space Mapping,” *Computer Modeling in Engineering and Sciences*, vol. 116, no. 3, pp. 433–453, 2018, doi: 10.31614/cmes.2018.03309.

[96] P. Kozakowski, A. Lamecki, P. Sypek, and M. Mrozowski, “Eigenvalue Approach to Synthesis of Prototype Filters with Source/Load Coupling,” *IEEE Microwave and Wireless Components Letters*, vol. 15, no. 2, pp. 98–100, 2005, doi: 10.1109/LMWC.2004.842838.

[97] R. J. Cameron, “General Coupling Matrix Synthesis Methods for Chebyshev Filtering Functions,” *IEEE Trans Microw Theory Tech*, vol. 47, no. 4, pp. 433–442, 1999, doi: 10.1109/22.754877.

[98] R. J. Cameron, “Advanced Coupling Matrix Synthesis Techniques for Microwave Filters,” *IEEE Trans Microw Theory Tech*, vol. 51, no. 1, pp. 1–10, 2003.

[99] R. J. Cameron, A. C. M. Kudsia, and R. R. Mansour, *Microwave Filters for Communication Systems - Fundamentals, Design and Applications*, Second Edi. USA: John Wiley & Sons Inc., 2007. doi: 10.1002/9781119292371.

[100] G. H. Golub and C. F. Van Loan, “Matrix Computations 3rd Edition.” The Johns Hopkins University Press, Baltimore, Maryland, USA, 1996.

[101] D. Traina, G. Macchiarella, and T. K. Sarkar, “Robust Formulations of the Cauchy Method Suitable for Microwave Duplexers Modeling,” *IEEE Trans Microw Theory Tech*, vol. 55, no. 5, pp. 974–982, 2007, doi: 10.1109/TMTT.2007.895394.

[102] D. Traina and G. Macchiarella, “New General Formulation of the Cauchy Method for the Accurate Model Extraction of Higher Order Microwave Systems,” *Microw Opt Technol Lett*, vol. 49, no. 8, pp. 1957–1961, 2007, doi: 10.1002/mop.

[103] J. H. Wilkinson, “Error Analysis of Direct Methods of Matrix Inversion,” *Journal of ACM (JACM)*, vol. 8, no. 3, pp. 281–330, 1961, doi: 10.1145/321075.321076.

[104] F. L. Bauer, “Optimally Scaled Matrices,” in *Numerische Mathematik 5*, 1963, pp. 73–87.

[105] S. Wu and W. Cao, “Parametric Model for Microwave Filter by using Multiple Hidden Layer Output Matrix Extreme Learning Machine,” *IET Microwaves, Antennas and Propagation*, vol. 13, no. 11, pp. 1889–1896, 2019, doi: 10.1049/iet-map.2018.5823.

[106] S. B. Wu and W. H. Cao, “Tuning Model for Microwave Filter by using Improved Back-Propagation Neural Network based on Gauss Kernel Clustering,” *International Journal of RF and Microwave Computer-Aided Engineering*, vol. 29, no. 8, pp. 1–10, 2019, doi: 10.1002/mmce.21787.

[107] M. Yu, “A Fully Automated Filter Tuning Robot for Wireless Base Station Diplexers - Presentation,” in *IEEE International Microwave Symposium - Workshop: Computer Aided Filter Tuning, (IMS 2003), Philadelphia, Pennsylvania*, 2003. doi: 10.13140/2.1.4648.1923.

[108] J. C. Melgarejo, J. Ossorio, S. Cogollos, M. Guglielmi, V. E. Boria, and J. W. Bandler, "On Space Mapping Techniques for Microwave Filter Tuning," *IEEE Trans Microw Theory Tech*, vol. 67, no. 12, pp. 4860–4870, 2019, doi: 10.1109/TMTT.2019.2944361.

[109] N. Zahirovic, R. R. Mansour, and M. Yu, "Scalar Measurement-based Algorithm for Automated Filter Tuning of Integrated Chebyshev Tunable Filters," *IEEE Trans Microw Theory Tech*, vol. 58, no. 12, pp. 3749–3759, Dec. 2010, doi: 10.1109/TMTT.2010.2085791.

[110] A. Muller, P. Soto, and V. E. Boria, "Design Procedure for Coaxial Combline Filters based on Segmentation and Space Mapping Strategies," in *2017 IEEE MTT-S International Conference on Numerical Electromagnetic and Multiphysics Modeling and Optimization for RF, Microwave, and Terahertz Applications (NEMO 2017), Seville, Spain*, 2017, pp. 13–15. doi: 10.1109/NEMO.2017.7964171.

[111] "Intelligent Automatic Filter Tuning Tool (IAFTT): European Patent Application No. P382895 assigned by Polish National Patent Office," 2007

[112] SpaceForest Innovative Solutions, "IAFTT Robot," Automated Tuning.

[113] R. S. Sutton and A. G. Barto, *Reinforcement Learning: An Introduction*. Cambridge, MA, USA: MIT Press, 1998. doi: 10.1179/175622708X282910.

[114] C. J. C. H. Watkins, "Learning from Delayed Rewards," Ph.D Thesis, King's College, Cambridge University, UK, 1989.

[115] V. Mnih *et al.*, "Playing Atari with Deep Reinforcement Learning," *NIPS Deep Learning Workshop*. pp. 1–9, 2013. doi: 10.48550/arXiv.1312.5602.

[116] H. Van Hasselt, "Double Q-learning," *Advances in Neural Information Processing Systems 23: 24th Annual Conference on Neural Information Processing Systems 2010, NIPS 2010*, pp. 1–9, 2010.

[117] H. Van Hasselt, A. Guez, and D. Silver, "Deep Reinforcement Learning with Double Q-Learning," in *30th AAAI Conference on Artificial Intelligence (AAAI 2016)*, 2016, pp. 2094–2100. doi: 10.1609/aaai.v30i1.10295.

[118] S. Roweis and L. Saul, "Nonlinear Dimensionality Reduction by Locally Linear Embedding," *Science v.290*, vol. 290, no. 5500, pp. 2323–2326, 2000, doi: 10.1126/science.290.5500.2323.

[119] B. T. Polyak and A. B. Juditsky, "Acceleration of Stochastic Approximation by Averaging," *SIAM J Control Optim*, vol. 30, no. 4, pp. 838–855, 1992, doi: 10.1137/0330046.

[120] G. L. Matthaei, L. Young, and E. M. T. Jones, *Microwave Filters, Impedance-Matching Networks, and Coupling Structures*. Norwood, MA, 02062: Artech House, 1964.

[121] M. S. Anwar and H. R. Dhanyal, "Design of S-band Combline Coaxial Cavity Bandpass Filter," in *15th International Bhurban Conference on Applied Sciences and Technology, (IBCAST 2018), Bhurban, Pakistan*, 2018, pp. 866–869. doi: 10.1109/IBCAST.2018.8312328.

[122] B. Gowrish and S. K. Koul, "Designing RF and Microwave Band Pass Filters Using Coupled Resonators," *IETE Journal of Education*, vol. 62, no. 1, pp. 6–11, 2021, doi: 10.1080/09747338.2021.1909503.

[123] Keysight, "N9914A FieldFox Handheld RF Analyzer, 6.5 GHz," Official Documentation.

[124] V. T. Minh, M. Tamre, and E. Sekhri, “Modeling and Robust Control Algorithms for a Linear Belt Driven System,” *Open Computer Science*, vol. 8, no. 1, 2018, doi: 10.1515/comp-2018-0010.

[125] C. C. Aggarwal, *Neural Networks and Deep Learning*. Springer International Publishing, 2018. doi: 10.1007/978-3-319-94463-0.

[126] B. G. Marcot and T. D. Penman, “Advances in Bayesian Network Modelling: Integration of Modelling Technologies,” *Environmental Modelling and Software*, vol. 111, pp. 386–393, Jan. 2019, doi: 10.1016/j.envsoft.2018.09.016.

[127] A. Trabelsi, Z. Elouedi, and E. Lefevre, “Decision Tree Classifiers for Evidential Attribute Values and Class Labels,” *Fuzzy Sets Syst*, vol. 366, pp. 46–62, Jul. 2019, doi: 10.1016/j.fss.2018.11.006.

[128] Y. Zhang, G. Cao, B. Wang, and X. Li, “A Novel Ensemble Method for K-Nearest Neighbor,” *Pattern Recognit*, vol. 85, pp. 13–25, Jan. 2019, doi: 10.1016/j.patcog.2018.08.003.

[129] J. Cervantes, F. Garcia-Lamont, L. Rodríguez-Mazahua, and A. Lopez, “A Comprehensive Survey on Support Vector Machine Classification: Applications, Challenges and Trends,” *Neurocomputing*, vol. 408, pp. 189–215, Sep. 2020, doi: 10.1016/j.neucom.2019.10.118.

[130] S. Jia, L. Shen, J. Zhu, and Q. Li, “A 3-D Gabor Phase-based Coding and Matching Framework for Hyperspectral Imagery Classification,” *IEEE Trans Cybern*, vol. 48, no. 4, pp. 1176–1188, Apr. 2018, doi: 10.1109/TCYB.2017.2682846.

[131] M. M. Quazi, M. A. Fazal, A. S. M. A. Haseeb, F. Yusof, H. H. Masjuki, and A. Arslan, “Laser-based Surface Modifications of Aluminum and its Alloys,” *Critical Reviews in Solid State and Materials Sciences*, vol. 41, no. 2, pp. 106–131, Mar. 2016, doi: 10.1080/10408436.2015.1076716.

[132] Specim Spectral Imaging Ltd, “Specim IQ Technical Specifications.” Accessed: Apr. 10, 2023. [Online]. Available: https://www.specim.com/iq/tech-specs/

[133] F. Luo, B. Du, L. Zhang, L. Zhang, and D. Tao, “Feature Learning using Spatial-Spectral Hypergraph Discriminant Analysis for Hyperspectral Image,” *IEEE Trans Cybern*, vol. 49, no. 7, pp. 2406–2419, Jul. 2019, doi: 10.1109/TCYB.2018.2810806.

[134] G. F. Hughes, “On the Mean Accuracy of Statistical Pattern Recognizers,” *IEEE Trans Inf Theory*, vol. IT-14, no. 1, pp. 55–63, 1968, doi: 10.1109/TIT.1968.1054102.

[135] W. Sun and Q. Du, “Hyperspectral Band Selection: A Review,” *IEEE Geoscience and Remote Sensing Magazine*, vol. 7, no. 2, Institute of Electrical and Electronics Engineers Inc., pp. 118–139, Jun. 01, 2019. doi: 10.1109/MGRS.2019.2911100.

[136] Q. Wang, F. Zhang, and X. Li, “Optimal Clustering Framework for Hyperspectral Band Selection,” *IEEE Transactions on Geoscience and Remote Sensing*, vol. 56, no. 10, pp. 5910–5922, Oct. 2018, doi: 10.1109/TGRS.2018.2828161.

[137] Y. Zhan, D. Hu, H. Xing, and X. Yu, “Hyperspectral Band Selection Based on Deep Convolutional Neural Network and Distance Density,” *IEEE Geoscience and Remote Sensing Letters*, vol. 14, no. 12, pp. 2365–2369, Dec. 2017, doi: 10.1109/LGRS.2017.2765339.

[138] J. Xiao and M. Oussalah, “Robust Model Adaption for Colour-based Particle Filter Tracking with Contextual Information,” *J Vis Commun Image Represent*, vol. 79, pp. 103270(1)-103270(11), 2021.

Acknowledgements

The cup of my gratitude overflows…

Undertaking the PhD has been a truly awe-inspiring experience for me, which would not have been possible without the love, support, and guidance that I received from n number of people. Through this tiny little space in the thesis, I would like to express my sincere gratitude to all who have contributed to the completion of this research endeavour in one way or the other.

It cannot be argued with that the most influential person in my research career has been my supervisor, Prof. Mart Tamre, Emeritus Department of Electrical Power Engineering and Mechatronics, Tallinn University of Technology, Estonia. His cooperation, discipline and encouragement allowed me to grow not only as a researcher but also as a person. I sincerely appreciate all his contributions of time, scholarly inputs, consistent encouragement, and all that he did for me professionally as well as personally.

I am thankful to my Ph.D. supervisors Prof. Rajiv Kapoor, Department of Electronics and Communication, Delhi Technological University, India and Prof. Anton Rassõlkin, Department of Electrical Power Engineering and Mechatronics, Tallinn University of Technology, Estonia not only for their guidance and cooperation in research facilities but also for their love, affection, cooperation and support.

I would also like to extend my gratitude and appreciations to all the teachers and staff in the Department Prof. Ivo Palu, Prof. Toomas Vaimann, Dr Dhanushka, Ms. Merle, Ms. Svetlana and all others for their never-ending support whenever I knocked their doors.

I greatly appreciate the support I received from Dr Robert Hudjakov and all the experts who helped me in reviewing and finalizing the tools prepared for the research. In all seriousness, all the members have been very kind and cordial with their input, time, ideas and recommendations. Thank you so much!

My deep appreciation goes out to the support that I received from DTU family. I am especially grateful to Mr. Deepak Sharma, Mr. Rahul Kumar, Mr. Nikhil who infused new ideas and zeal in me. I gained a lot from them; their scholarly interactions and suggestions at various points made this thesis come true. I am truly and heartily indebted.

No research is possible without the funding support. I take this opportunity to express my gratitude to Government of Estonia, Archimedes Foundation, and DoRa for their services and cooperation. Also, I extend a big thanks to my department at TalTech who supported me during my study period.

Finally, all thanks to the people who shaped me into who I am – my parents. I owe everything to my parents who, first breathed life to the idea of pursuing a PhD; raised me with a desire to work hard in achieving my dreams; supported me in all pursuits of my life; and who longed to see this achievement come true. Maa Papa your prayers for me was what sustained me this far. I would not have been here if you hadn't provided your unconditional love and care. Without your optimism and support, the seed that turned into a young plant might have withered away.

My siblings Dr Esha Sekhri and Ashish Kapoor have been my best friends and I thank them for all their advice and support. I doubt I will ever be able to convey my appreciation and regard fully, but I owe my eternal gratitude. I love you both!

My study was made less obstacle ridden because of the presence of my friends Md. Tahzeeb Khan, Ajay Sharma, Simranjot Singh, Sarvesh Srivastava, Nikhil Kamboj.

Finally, I thank God for letting me through all hardships and difficulties. I could sense your presence everywhere and every day. Thank you for granting me the wisdom, health and strength to undertake this research and enabling me to complete it. Your blessings had made my dream come true. I will trust you for my future. Thank you, God!

Abstract

Fully Automated Tuning of Microwave Coaxial Cavity Filter

The present day's increased connectivity requirements have led to rapid production of the components related to communication. Microwave (MW) cavity filters are widely used in Wireless Base Stations (WBS) and radar systems to segregate the desired frequency from the crowded electromagnetic (EM) spectrum. To meet the evolving communication requirements, a huge variety and copious amount of filters are produced by the companies.

To compensate the design flaws and manufacturing tolerances, the assembled filters are tuned to meet the stated frequency requirements. Filters are usually equipped with tuning elements to vary the frequency response. Among various tuning elements, silver-coated screws are most widely used. Adjusting the vertical height of these tuning screws varies the resonant frequency as well as the inter-resonator coupling between the resonators. Being stochastic in nature, the filter tuning process is performed manually by the trained technicians. To acquire the required skillset, an intensive training is provided to these technicians. However, completing the training does not guarantee the proficiency of technicians in tuning the filters, and sustaining the competent technicians is also a major concern for the industry. Additionally, the wrists are heavily loaded while tuning the filters which often leads to injuries, and hence, a financial burden on the industries to bear the surgery expenses. Thus, automating the filter tuning process is a buzzword in the research community actively working in the field of MW filters.

After conducting an extensive literature review it was found that the existing filter tuning techniques were limited either to a particular filter topology, or they required numerous complex computations and/or optimisations on equivalent mathematical models. Additionally, the filters are tuned using the programmed insructions only without any feedback from the system. In terms of hardware, the automated filter tuning solutions developed by research community were not flexible to tune different topologies of filters. Also, an important aspect in automating the filter tuning process i.e., distinguishing the tuning screws from the plate mounting screws yet remained explored.

This research work aimed to provide complete solution to automate the filter tuning process. To differentiate between the different kinds of screws installed on the filter's top plate, a novel vision-based method was developed. In this work, two novel automated filter tuning fusion algorithms were presented in which the theoretical knowledge and its conjunction with AI were combined to tune the filter on the basis of change in phase of the filter's input reflection coefficient. The use of Smith chart and polar chart for automating the filter tuning process have been presented for the first time. Customized dataset has been curated to track the variation of tuning parameters on the Smith chart in real-time. The FAT robot designed in this work offers flexibility in tuning different kinds of filters by attaching the required tool in the magnetic socket of the manipulator. The use of colour-based particle filtering has been used to detect the tuning error in the initial stage of its occurance with the help of customized vision module. This vision module also counts the screw turns using the rotation angle information of the screwdriver, thus avoiding the condition where the tuning screw comes out of the filter's top plate. A dedicated plotting module has also been developed to eliminate the dependence on commercial VNA's software offering limited capabilities.

The developed algorithms have been evaluated on a 5^{th} order all-pole test filter fabricated under the scope of this work. The test filter is equipped with quarter-wavelength long solid resonators (having solid resonators ensured that the screws will not fall inside the cavity filter). The proposed algorithms could sequentially tune the resonators of the filters without iteratively visiting the tuning screws autonomously. Although optimising the tuning time has not been considred as the primary objective, a logic to vary the tuning speed on the basis of target angle was implemented. The tuning times of the algorithms with and without speed variation have been compared.

The automated filter tuning solution presented in this work eliminated the need of training the technicians to tune the filters. The human involvement was restricted to mounting the filter and starting the algorithm. This solution presented in this work can be used for educational as well as industrial purposes.

Lühikokkuvõte

Mikrolaine-koaksiaalfiltrite täisautomaatne häälestamine

Tänapäeva kasvanud ühenduvusnõuded on viinud sidetehnikaga seotud komponentide tootmise kiire kasvuni. Mikrolaine-koaksiaalfiltreid kasutatakse laialdaselt traadita süsteemide tugijaamades ja radarisüsteemides, et eraldada soovitud sagedus täistuubitud elektromagnetilisest spektrist. Ettevõtted toodavad tohutuid variatsioone ja suures koguses filtreid, et vastata arenevatele sidenõuetele.

Projekteerimisvigade ja tootmistolerantside kompenseerimiseks häälestatakse kooostatud filtrid vastama kindlaks määratud sagedusnõuetele. Filtrid on tavaliselt varustatud häälestuselementidega sageduskarakteristiku muutmiseks. Erinevatest häälestuselementidest kasutatakse enim hõbedaga kaetud häälestuskruvisid. Nende häälestuskruvide vertikaalse kõrguse reguleerimine muudab nii resonantssagedust kui ka resonaatoritevahelist koostööd. Olles oma olemuselt stohhastiline, viivad filtri häälestamise protsessi läbi koolitatud tehnikud käsitsi. Vajalike oskuste omandamiseks korraldatakse neile tehnikutele intensiivne koolitus. Koolituse läbimine ei taga aga tehnikute vilumust filtrite häälestamisel ning ka kompetentsete tehnikute ülalpidamine on tööstuse jaoks suur murekoht. Lisaks on häälestajate randmed filtrite häälestamise ajal tugevalt koormatud, mis põhjustab sageli kutsehaigusi ja vigastusi ning on seega tööstusharule täiendav rahaline koormus. Seega on filtrite häälestamise protsessi automatiseerimine mikrolaine-koaksiaalfiltrite valdkonnas oluline ülesanne aktiivselt tegutsevatele teadlastele. Ulatuslikku kirjanduse ülevaate baasil leiti antd töös, et olemasolevad filtri häälestamise tehnoloogiad olid piiratud kas konkreetse filtri topoloogiaga või nõudsid arvukalt keerulisi arvutusi ja/või optimeerimisi samaväärsete matemaatiliste mudelite puhul. Lisaks häälestatakse filtreid ainult eelkoostatud instruktsioonide abil ilma süsteemi tagasisideta. Riistvara osas ei olnud seni teadlaste poolt välja töötatud automatiseeritud filtrite häälestamise lahendused paindlikud erinevate filtrite topoloogiate häälestamiseks. Samuti on jäänud veel lahendamata oluline aspekt filtri häälestamise protsessi automatiseerimisel, st häälestuskruvide eristamine plaadi kinnituskruvidest.

Selle uurimistöö eesmärk oli pakkuda täielikku lahendust filtri häälestamise protsessi automatiseerimiseks. Filtri pealmisel plaadil asuvate erinevat tüüpi kruvide eristamiseks töötati välja uudne masinnägemise põhine meetod.

Selles töös on pakutud välja kaks uudset automatiseeritud filtri häälestamise hübriidalgoritmi, milles kombineeriti AI teoreetilised teadmised ja elemendid, et häälestada filtrit tema sisendpeegeldusteguri faasimuutuse alusel. Smithi diagrammi ja polaardiagrammi kasutamist filtri häälestamise protsessi automatiseerimiseks on kasutatud esmakordselt. Kasutatakse kohandatud andmestikku, et jälgida Smithi diagrammi häälestusparameetrite muutumist reaalajas. Selles töös välja töötatud täisautomaatne häälestusrobot, kus vajalik tööriist kinnitatakse manipulaatori magnetpesasse, tagab paindlikkuse erinevate filtrite häälestamisel. Häälestusvea tuvastamiseks selle esinemise algfaasis on kasutatud värvipõhist osakeste filtreerimist kohandatud masinnägemise mooduli abil. See masinnägemise moodul loendab ka kruvi pöördeid, kasutades kruvikeeraja pöördenurga infot, vältides nii olukorda, kus häälestuskruvi väljub filtri ülemisest plaadist. Samuti on välja töötatud spetsiaalne graafikamoodul, et kõrvaldada sõltuvus kaubanduslikust vektor- võrguanalüsaatori piiratud võimalusi pakkuvast tarkvarast. Väljatöötatud algoritme on hinnatud käesoleva töö raames valmistatud 5. järku täis-pooluste testfiltril. Testfilter on varustatud

veerandlainepikkusega pikkade monoliit-resonaatoritega (monoliit-resonaatorite olemasolu tagab, et kruvid ei kukuks filtri sisse). Kavandatud algoritmid võivad häälestada järjestikku filtrite resonaatoreid ilma iteratiivselt ja sõltumatult häälestuskruvide asukohti külastamata. Kuigi häälestusaja optimeerimist ei ole selles töös peetud esmaseks eesmärgiks, rakendati loogikat häälestuskiiruse muutmiseks sihtnurga alusel. Samuti võrreldi töös algoritmide häälestusaegu kiiruse variatsiooniga ja ilma.

Käesolevas töös esitatud uus automatiseeritud filtrite häälestamise lahendus välistab vajaduse koolitada tehnikuid filtrite häälestamiseks. Inimese osalus piirdub filtri paigaldamise ja algoritmi käivitamisega. Antud töös toodud lahendust saab kasutada nii hariduslikel kui ka tööstuslikel eesmärkidel filtreid tootvates ettevõtetes.

Appendix 1

Publication I

M. Vu, M. Tamre and **E. Sekhri**, “Modeling and Robust Control Algorithm for a Linear Belt Driven System,” *Open Computer Science,* vol. 8, pp. 142–153, 2018, doi: 10.1515/comp-2018-0010.

Research Article Open Access

Vu Trieu Minh*, Mart Tamre, and Even Sekhri

Modeling and robust control algorithms for a linear belt driven system

https://doi.org/10.1515/comp-2018-0010
Received October 13, 2017; accepted June 13, 2018

Abstract: This paper proposes the mathematical modeling and robust control algorithms for linear belt system with the help of sliding mode control approach. Due to the elasticity of the belt, the presence of frictions, and the un-modeled dynamics, conventional controllers cannot provide precise position control of carriage. Dealing with this kind of system, a robust controller is needed and the chattering-free sliding mode control (SMC) approach is used to design the robust controller. A belt stretching estimator is also incorporated into the control law. Simulations show that the system is free from chattering and robust to disturbances. The reference tracking position is performed with the minimal errors to an extent that can be considered negligible. The time for reaching the reference tracking position is very fast. The system is safe for all mechanical and electrical devices.

Keywords: robust controller, linear belt, sliding mode control, chattering free, un-modeled dynamics, friction model, equivalent control

1 Introduction

Usage of belt drives has gathered significant attention and become the most common method of power transmission used in most common systems/devices. Another significant sphere where the belt drives are exhaustively used includes industrial transportation systems where they are often called conveyor belts. Belt drives are better and more popular than other power transmission mechanisms such as the chains or the gears because they have a number of advantages including low cost, simple, low maintenance, smooth operation, fast and flexible installation, noise-free, cleanliness, no lubrication needed, can absorb sudden shocks, wide speed ratio range operations, easy to visualize the failure, etc. in [1].

Presently, toothed belts (also called as timing belts) are a leading edge in industrial applications for power transmission with precise position tracking and rapidly changing dynamics (such as in 3D printers). The main advantages of toothed belts are high efficiency, long travel length, suitability to high speed applications and low cost. However, the main disadvantages of the belt drives are high tracking errors, uncertain dynamics and vibrations. The motion equations and the mathematic modellings of such a linear belt driven system is discussed in [2].

The controllers for belt drives are considered like PIDs by re-designing to cope-up higher-order-node in [3]. However, these controllers become unstable with high resonant frequencies. Further, they are not sufficient enough to deal with the tracking errors. Some additional methods such as signal processing and noise filtering are used to improve the belt drive performances in [4], but they are not sufficient for mechanical vibrations, plant variations, load-torque disturbances and uncertain dynamics. A number of other approaches like linear quadratic regulator (LQR), composite non-linear feedback (CNF), adaptive control and sliding mode control (SMC) have provided better control performances.

Every controller has its advantages and disadvantages. SMC has also a major drawback of discontinuous switching action so as to keep the system stable and to operate in accordance to the desired expectations. This means that the control must switch with infinite frequency to provide the total rejection to the uncertainties present in the system. This discontinuous mode leads to a phenomenon called “chattering” in [5], which is dangerous for mechanical systems and may lead to wear and tear of the parts involved and in extreme cases may even lead to the failure of the whole system.

In this research, a chattering-free SMC is considered to control the belt drive. Belt- stretch and its control are important to achieve the vibration-free performance in [6]. Thus, paramount importance is given to the belt-stretch

*Corresponding Author: Vu Trieu Minh: Department of Electrical Power Engineering and Mechatronics Tallinn University of Technology, 19086 Tallinn, Estonia, E-mail: trieu.vu@ttu.ee
Mart Tamre, Even Sekhri: Department of Electrical Power Engineering and Mechatronics Tallinn University of Technology, 19086 Tallinn, Estonia, E-mail: mart.tamre@ttu.ee, even.sekhri@ttu.ee

in the present research endeavor. The control law is derived by the combination of the Lyapunov function and the SMC theory. The use of Lyapunov function allows stabilizing the system upon any uncertainties and disturbances. Therefore, the Lyapunov applications in [7] and in [8] are used to design the SMC.

Owing to its simplicity and robustness, SMC approach has attracted significant attention from researchers since 1980s. The achievements include almost all kinds of systems such as the SMC for the non-linear systems in [9], SMC for discrete systems in [10], SMC for time-delay systems in [11], and SMC for large systems in [12]. To address the problems of chattering and unknown bound of the uncertainties present, various methods such as the higher order SMC in [13], the adaptive SMC in [14], and the adaptive fuzzy SMC which combine the advantages of both SMC and fuzzy logic controllers are discussed in [15] and in [16].

The objective of this research is to design a robust controller for a linear belt driven system based on SMC to control the position and velocity of a carriage on with the ship model tagged. This is from a real project in Kuressaare, Estonia, to build a water cannel to test the ship navigational and hydrodynamic properties, such as the ship behavior/friction in the waves. The carriage is driven by two toothed belts and two motors as seen in Figure 1. The motive is to make the system robust enough to deal with the unknown parameters and disturbances whilst keeping the tracking position and velocity errors as low as possible. Advanced robust, adaptive control designs are referred to in [17], [18] and [19].

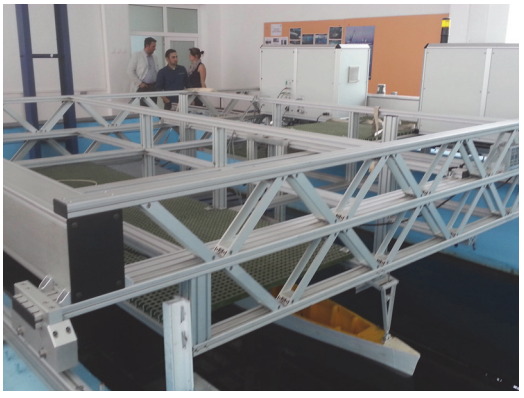

Figure 1: Real linear belt driven system in Kurresaare, Estonia.

The contents of this paper are as follows: Section 2 develops the mathematical model formulation of the system; Section 3 presents the SMC controller design; Section 4 presents the results of simulation; Section 5 draws the conclusions and recommendations.

2 Mathematical model

The considered system consists of a DC motor which provides the main motive force to the system, two pulleys with same dimensions that stretch the belt where the one which is connected to the motor and is the driving pulley, and the other is the driven pulley; a carriage (which is considered as the load-side of the system) whose tracking position and velocity errors are to be minimized ultimately; and the belt for force transmission from the driven pulley to the load carriage. The arrangement represents a complex-cum-nonlinear distributed parameter system.

The following assumptions are made for the system: gear reduction ratio has its value equal to unity in the simulated system; the motor has negligible delay in providing high-dynamic torque response; the system is free from backlash of belt drives due to pre-tensioning; the link between motor shaft and belt drive's driving pulley is rigid; the belt elasticity is equivalent to a mass-less spring; the unknown disturbances/noises consist of friction present between DC motor and the driving pulley and carriage guiding rail transmission guiding channels. Figure 2 shows the diagrammatic representation of the equivalent spring-mass system in lieu of these underlying assumptions.

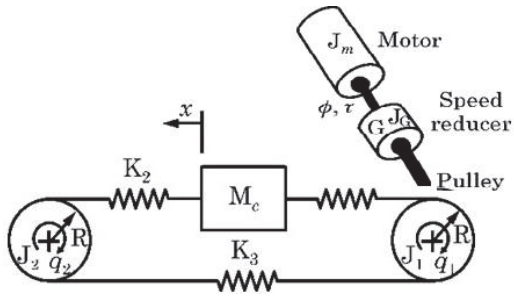

Figure 2: Equivalent spring-mass system.

Using modal analysis, the sixth-order dynamic equations for the system are depicted in equations (1), (2), and (3) in [2]. For generating these equations the detailed anal-

ysis is made in [6].

$$(J_1 + G^2(J_G + J_m))\ddot{q}_1 + \tau_{f1} = G(-R[K_1(x)(Rq_1 - x) - K_3(Rq_2 - Rq_1)], \quad (1)$$

$$J_{2\ddot{q}_2} + \tau_{f2} = R[K_2(x)(x - Rq_2) - K_3(Rq_2 - Rq_1)], \quad (2)$$

$$M_c\ddot{x} + f_f = K_1(x)(Rq_1 - x) - K_2(x)(x - Rq_2), \quad (3)$$

where, J_G, J_m – Moment of Inertia of the speed reducer and the motor, respectively; J_1, J_2 – Moment of Inertia of driving and the driven pulley, respectively; M_c – Carriage mass; G – Speed reducer gear ratio; R – Radius of the pulleys; K_1, K_2, K_3 – Position dependent belt elasticity coefficients; q_1, q_2, ϕ – Angular position of the driving pulley, driven pulley, and the motor, respectively; x – Position of carriage; τ – Torque developed by the motor; τ_{f1}, τ_{f2} – Friction torque which affects the pulleys; f_f – Friction force on the carriage.

The 6th order model discussed above is a three-mass model and it is a highly-coupled and non-linear system with external disturbances which enter both in the driving-side, i.e., motor-side and also on the load-side of the system. An important point to be considered is that the inertias at the load-side and the motor-side are high as compared to those at the driving and driven pulleys [6]. So, the 6th order model is reduced to 4th order model (two-mass model) as described in equations (4), (5), and (6). The two-mass model includes only the first resonance.

$$J\ddot{\varphi} + \tau_f = \tau - LKw, \quad (4)$$

$$M\ddot{x} + f_f = Kw, \quad (5)$$

$$w = L\varphi - x, \quad (6)$$

where: J – Motor inertia; M – Mass on the load side (approx. to the Cart Mass); τ_f – Motor Side friction torque that perturb the system ; f_f – Force of friction in the system; K – Coefficient of Elasticity of the belt; w – Belt-stretch; L – Transmission constant of the linear belt-drive = R/G;

Belt-stretch is an important consideration. The model can hence be modified according to the vibration analysis. It is to be noted that to simplify the calculations, the parameter "L", i.e., transmission coefficient is assumed to be unity while finding the new set of equations for the modified model. The modified model can be written as:

$$J\ddot{w} + K_w w = \tau - \tau_{wf}, \quad (7)$$

$$M\ddot{x} + f_f = K, \quad (8)$$

where: $\tau_{wf} = \tau_f - \kappa f_f$, $K_w = K(1+\kappa)$, $\kappa = J/M$ (inertia ratio).

The resonance frequency of the elastic belt-drive system is given by Equation (9):

$$\omega_0 = \sqrt{\frac{K}{J}(1 + \kappa)}. \quad (9)$$

The control model for the modified system where belt-stretch is considered is shown in Figure 3. The system has a control input signal τ. It has two parts where the first one is for the Belt-Stretch Dynamics and the second one is for the Load Side Dynamics. Both these parts are described by their independent nominal and linear 2nd order dynamics. The disturbance torque perturbs the belt-stretch side and the friction force perturbs the load side.

In real life, the main problems in such a system arise from many factors some of which include: Elasticity of the belt; Load-position dependent friction; Non-linearity of induced belt forces; Large friction effects; etc. The prime interest is to generate the control scheme for the system mentioned in Figure 3 so that the position tracking can be simulated and the position error of the cart position can be minimized. Also, from the simulation, results of various other parameters can also be fetched.

3 Free chattering SMC design

The design of SMC is two-stepped process: Defining the switching hyperplane or switching surface or sliding surface; and Designing the control law. First, the switching hyperplane often designated by "σ" is defined which is basically dependent on the desired dynamical behavior of the system. This σ actually provides a measure of the distance of the state-trajectory from the sliding surface located at $\sigma = 0$. Secondly, a control law is designed to drive the states onto the pre-defined sliding surface. Also, it makes sure that they remain there and slide along the sliding surface or in the bounded vicinity of that sliding surface. The control is continuous in all the segmented regions but it alters the structure when the dynamics of the state-trajectory crosses the boundary defined by the sliding surface, i.e., sliding manifold.

The ultimate goal is to find the control input which takes the system towards the sliding surface manifold and then restricts it there despite of the perturbations present in the system which basically include all the uncertainties of the system.

Let a Single Input-Single Output (SISO) non-linear considered mechanical system in the state-space be defined as:

$$\dot{z}_i = z_{i+1}, \quad (10)$$

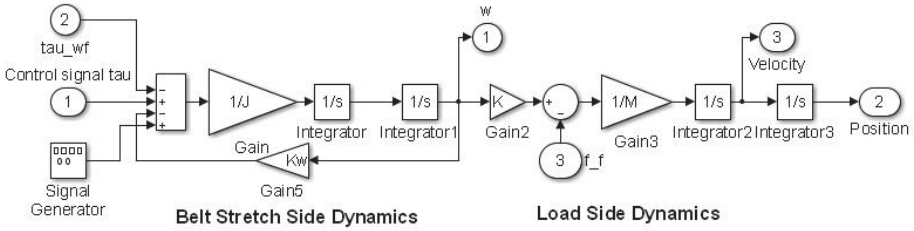

Figure 3: Simulink scheme of linear belt-driven system.

$$\dot{z}_n = f(z) + b(z)u + d(t), \tag{11}$$

where: $i = 1, \ldots, n–1$; $z^T = [z_1 \ldots, z_n]$ is a system state vector; u – scalar input; $f(z)$ – the bounded non-linear driving term of system-state vector; $b(z)$ – the bounded non-linear control gain of the system-state vector; $d(t)$ – the bounded scalar disturbances.

Now, the prime goal is to determine control signal "u" that restricts the motion of the system-states z to the pre-defined sliding surface $\sigma(z,t) = 0$ even in the presence of $f(z)$, $b(z)$ and $d(t)$. The convergence (of system states) to the sliding surface is called the reaching phase. The motion within the sliding manifold is called the sliding phase.

The control with discontinuities on sliding manifold is working on the following defined principles (termed as switching function):

$$u = \begin{cases} u^+, & \sigma(z,\ t) > 0, \\ u^-, & \sigma(z,\ t) < 0. \end{cases} \tag{12}$$

Here, u^+ and u^- are selected such that the Lyapunov function candidate has its derivative to be negative-definite. But, the discontinuous control in many applications leads to failure of VSS which further leads to "chattering" which is an important issue while dealing with the system under consideration. Hence, the chattering-free SMC is to be used in this task. For this purpose, another additional state of the system is needed as introduced in [7] and also discussed in [9] to eliminate the discontinuities on the control signal. So, it yields,

$$\dot{z}_i = z_{i+1}, \tag{13}$$

$$z_{n+1} = g(z,\ u) + b(z)\dot{u} + \dot{d}(t), \tag{14}$$

where $g(z, u) = \dot{f}(z) + \dot{b}(z)u$, $i = 1, \ldots, n$.

The condition which is to be fulfilled so that the system states start moving towards; and finally reach the sliding surface is called the reaching condition. The solution given by $\sigma = 0$ will have at least asymptotic stability if the control satisfies the condition that the derivate of any assumed Lyapunov's candidate function will be semi-negative definite. To meet this criterion, considering the Lyapunov candidate of the form:

$$V(\sigma) = \sigma^2/2. \tag{15}$$

The squared distance to the surface (as measured with term σ^2) decreases along the system trajectory. Hence, it will constrain the trajectories to actually point towards the pre-defined sliding surface. Once the system reaches the surface, the system trajectories will then be on the surface.

The reachability condition can be proved when the condition $\sigma, \dot{\sigma} < 0$ is fulfilled. The robust law is chosen with proportional rate given by $\dot{\sigma} = -D\sigma,\ \ D > 0$ where D is the damping coefficient arbitrarily chosen to achieve a required rate of robustness of the closed-loop system. The value of D determines the disturbance rejection and ideally the value of gain D should be as high as possible. But, it is not possible in the practical applications. The value of D is limited by various factors including: un-modeled dynamics of electro-magnetic torque; noise levels; discrete control algorithm implementation.

The derivative of Lyapunov's candidate function V as stated by Equation (15) will thus have the form:

$$\dot{V} = -D\sigma^2,\ D > 0. \tag{16}$$

Now, from the condition $\dot{V} = \sigma\dot{\sigma} = -D\sigma^2$ and by application of the knowledge regarding the equivalent control method in which the equivalent control signal u_{eq} is not the control action applied to the nominal plant. It can be imagined as representing (at an average) the same effect as shown by the applied discontinuous control and can hold the system on the sliding surface:

$$\dot{u} = \dot{u}_{eq} + D\sigma. \tag{17}$$

The obtained equivalent control u_{eq} is actually the solution of $\dot{\sigma}|_{\sigma=0} = 0$.

The control law u can be obtained as:

$$u = \int_0^t \dot{u} dt. \tag{18}$$

This control assures invariant motion of the system in the sliding mode if the value of the disturbance $d(t)$ complies to matching conditions. The control will be achieved when the derivative of Lyapunov candidate is negative, i.e.,

$$\dot{V} = \sigma\dot{\sigma} = -D\sigma^2 < 0. \tag{19}$$

The task of designing the sliding surface or sliding manifold is an important step which is constructed in a system state-space. Thus, σ combines system's state-variables in such a way that the system's motion in the sliding manifold is asymptotically stable. The definition of the system states is in accordance to the adopted system model. In case of higher-order sliding mode approach, the original system states can be extended so as to achieve the smooth control.

For the system considered, the conventional SMC design approach involves switching function of first order which could be taken as:

$$\sigma = \Delta\dot{x} - c\Delta x, \tag{20}$$

where: Δx – the error signal = $r(t) - x$, i.e., reference position – actual position; c – our design variable.

The SMC which is free from chattering for the linear belt-driven system must have a switching function of second-order in the motion control. Hence, taking the switching function to be:

$$\sigma = \Delta\ddot{x} + K_v\Delta\dot{x} + K_p\Delta x, \tag{21}$$

where: Δx – corrected position; $\Delta\dot{x}$ – corrected velocity; $\Delta\ddot{x}$ – corrected acceleration; K_v and K_p – positive control gain values to shape the second-order dynamic behavior of the error in desired position.

But for elastic systems, the switching function is given by:

$$\sigma = \Delta\ddot{x} + K_v\Delta\dot{x} + K_p\Delta x + \gamma(\ddot{w} + \alpha\dot{w}), \tag{22}$$

where α and γ – arbitrarily chosen positive control gains in order to reduce the vibrations due to belt compliance and elasticity so as to shape asymptotically stable motion dynamics on the sliding manifold.

The portion of belt-stretch dynamics is added to switching function definition ($\dot{w} + \alpha w$). It basically aims at coping with resonant frequency ω_0 and also to achieve asymptotically stable dynamics of motion.

A little consideration to equation (22) says that if the belt is stiff then both $\ddot{w}$ and $\dot{w} = 0$ and we will reach equation (21).

For the controller implementation, the only signals we require are position and the velocity of the system. The other required model parameters are the equivalent mass, i.e., $J + M$, the moment of inertia of the motor, i.e., J and lastly the resonance frequency, i.e., ω_0 of the system. And then the other control parameters, i.e., K_v, K_p, α, γ are designed.

The Simulink description of the belt-stretch consideration being implemented and the calculation of the control law for the system is as shown in Figure 4.

The constructed sliding manifold as described in Equation (22) allows the steady state position error to reach the zero value assuring the operation to be vibration-free. In order to give a little more explanation about choice of the switching function, σ has been opted such that it complies with the order of the system. Also, it involves position tracking error and its order up to the 2nd order along with the dynamics of vibration suppression, i.e., $\dot{w}$ and $\ddot{w}$.

It is to be noted here that higher order derivatives of position error are simply not available in the practice. All the variables involved in σ are then available in the implemented control law which actually requires the integral of σ.

Considering control engineer's perspective, σ is a measure for a distance to sliding manifold. The sliding manifold is constructed so as to bring the driving position error to zero while operating at vibration-free mode. In practice, the ultimate convergence is hard to guarantee, especially, in the case of simplified version of the control law. However, by the high-gain approach, it can asymptotically converge to a vicinity of the sliding manifold at a fair robustness.

In practical scenarios, it is difficult to observe belt-stretch's first and second order derivatives. So, Equation (8) belt-stretch is computed as:

$$w = \frac{M}{K}\ddot{x} + \frac{1}{K}f_f. \tag{23}$$

The first and second order derivatives are hence calculated by differentiating "w". In MATLAB Simulation, it can be done by using the "Derivative" blocks from Simulink library (in Figure 4).

Now, as discussed earlier that the control law needs the derivative of switching function σ. So, differentiating Equation (22),

$$\dot{\sigma} = \Delta\dddot{x} + K_v\Delta\ddot{x} + K_p\Delta\dot{x} + \gamma(\dddot{w} + \alpha\ddot{w}). \tag{24}$$

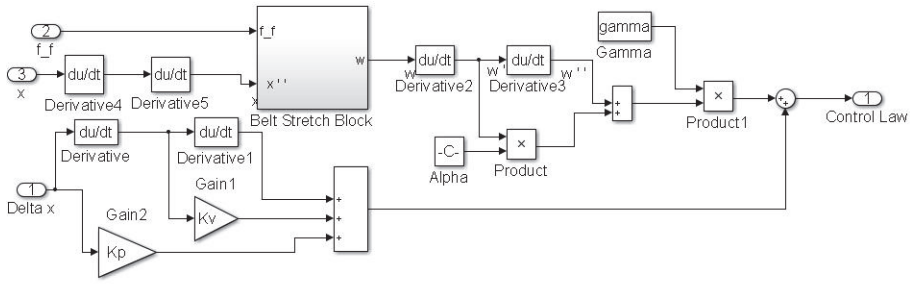

Figure 4: Control law including the belt-stretch.

Here, $\dot{w}$ is obtained by rearranging the terms involved in Equation (7) as:

$$\dot{w} = -\omega_0^2 w + \frac{\tau - \tau_{wf}}{J}. \tag{25}$$

$\ddot{w}$ is calculated by differentiating the Equation (25), i.e., calculating $d\dot{w}/dt$.

So,

$$\dot{\sigma} = \Delta\dddot{x} + K_v\Delta\ddot{x} + K_p\Delta\dot{x} + \gamma\left(-\omega_0^2\dot{w} + \frac{\dot{\tau} - \tau_{wf}}{J} + \alpha\ddot{w}\right). \tag{26}$$

Now, from condition $\dot{\sigma} = 0$ where $\dot{\tau}$ becomes $\dot{\tau}_{eq}$:

$$0 = \Delta\dddot{x} + K_v\Delta\ddot{x} + K_p\Delta\dot{x} + \gamma\left(-\omega_0^2\dot{w} + \frac{\dot{\tau}_{eq} - \tau_{wf}}{J} + \alpha\ddot{w}\right). \tag{27}$$

Re-arranging the terms leads to:

$$\gamma\dot{\tau}_{eq} = -J\left[\Delta\dddot{x} + K_v\Delta\ddot{x} + K_p\Delta\dot{x}\right] + J\gamma\omega_0^2\dot{w} - J\gamma\alpha\ddot{w} + \gamma\dot{\tau}_{wf}. \tag{28}$$

Further rearrangement of terms yields:

$$\dot{\tau}_{eq} = -\frac{J}{\gamma}\left[\Delta\dddot{x} + K_v\Delta\ddot{x} + K_p\Delta\dot{x}\right] + J\left[\omega_0^2\dot{w} - \alpha\ddot{w}\right] + \dot{\tau}_{wf}. \tag{29}$$

Using the knowledge of resonance frequency (from Equation 29) we can deduce that,

$$\omega_0^2 = \frac{K}{J}\frac{(M+J)}{M}. \tag{30}$$

Rearranging the terms in Equation 21 above gives the following:

$$\frac{M}{K} = \frac{(M+J)}{J}\cdot\frac{1}{\omega_0^2}. \tag{31}$$

Multiplying and dividing the equation of $\dot{\tau}_{eq}$ by $\frac{K}{M}$ we get:

$$\dot{\tau}_{eq} = -\frac{M}{K}J\beta\left[\Delta\dddot{x} + K_v\Delta\ddot{x} + K_p\Delta\dot{x}\right] + J\left[\omega_0^2\dot{w} - \alpha\ddot{w}\right] + \tau_{wf} \tag{32}$$

where $\beta = K/M\gamma = A$ gain value.

High value of β can extend the robust bandwidth of the operation but it is always limited in the real life. For example, in belt-drives, it is normal to have force-transmission delay which may lead to unstable belt response. Hence, β value is actually a result of design compromise. Also, $\beta = \gamma^{-1}K/M > 0$ is the design parameter which shapes the dynamics of the system motion when $\sigma = 0$.

Substituting $\frac{M}{K}$ from Equation (31) to Equation (32):

$$\dot{\tau}_{eq} = -\frac{\beta}{\omega_0^2}(M+J)\left[\Delta\dddot{x} + K_v\Delta\ddot{x} + K_p\Delta\dot{x}\right] + J\left[\omega_0^2\dot{w} - \alpha\ddot{w}\right] + \tau_{wf}. \tag{33}$$

Now, equivalent control torque signal can be obtained by integrating the $\dot{\tau}_{eq}$ over the time limit 0 to t, i.e.

$$\tau_{eq} = \int_0^t \dot{\tau}_{eq}dt. \tag{34}$$

So, integrating Equation (33),

$$\tau_{eq} = -\frac{\beta}{\omega_0^2}(M+J)\left[\Delta\ddot{x} + K_v\Delta\dot{x} + K_p\Delta x\right] + J\left[\omega_0^2 w - \alpha\dot{w}\right] + \tau_{wf}. \tag{35}$$

Here, in Equation (35), we can see that we need acceleration signal which is generally not available. We have only position and velocity sensors installed with-in the system.

So, to find $\ddot{x}$ we have to use Equation 28 where rearranging the terms provides:

$$\Delta\ddot{x} = \frac{Kw - f_f}{M}. \tag{36}$$

Hence,

$$\tau_{eq} = -\frac{\beta}{\omega_0^2}(M+J)\left[K_v\Delta\dot{x} + K_p\Delta x\right] - \frac{\beta}{\omega_0^2}(M+J)\left(\frac{Kw - f_f}{M}\right) + J\left[\omega_0^2 w - \alpha\dot{w}\right] + \tau_{wf}, \tag{37}$$

$$\tau_{eq} = -\frac{\beta}{\omega_0^2}(M+J)\left[K_v\Delta\dot{x} + K_p\Delta x\right] - \frac{\beta}{\omega_0^2}(Kw - f_f) + \frac{\beta}{\omega_0^2}\frac{J}{M}(Kw - f_f) + J\left[\omega_0^2 w - \alpha\dot{w}\right] + \tau_{wf}, \quad (38)$$

$$\tau_{eq} = -\frac{\beta}{\omega_0^2}(M+J)\left[K_v\Delta\dot{x} + K_p\Delta x\right] - \frac{\beta}{\omega_0^2}Kw + \frac{\beta}{\omega_0^2}f_f - \frac{\beta}{\omega_0^2}\frac{J}{M}Kw + \frac{\beta}{\omega_0^2}\frac{J}{M}f_f + J\left[\omega_0^2 w - \alpha\dot{w}\right] + \tau_{wf}. \quad (39)$$

Now, substituting the value of τ_{wf} in Equation (39) we get:

$$\tau_{eq} = -\frac{\beta}{\omega_0^2}(M+J)\left[K_v\Delta\dot{x} + K_p\Delta x\right] - \frac{\beta}{\omega_0^2}Kw + \frac{\beta}{\omega_0^2}f_f - \frac{\beta}{\omega_0^2}\frac{J}{M}Kw + \frac{\beta}{\omega_0^2}\frac{J}{M}f_f + J\left[\omega_0^2 w - \alpha\dot{w}\right] + \tau_f - \kappa f_f. \quad (40)$$

After re-arranging the terms we get:

$$\tau_{eq} = -\frac{\beta}{\omega_0^2}(M+J)\left[K_v\Delta\dot{x} + K_p\Delta x\right] - \frac{\beta}{\omega_0^2}Kw - \frac{\beta}{\omega_0^2}\frac{J}{M}Kw + J\omega_0^2 w - J\alpha\dot{w} + \tau_f + \left[\frac{\beta}{\omega_0^2} + \frac{\beta}{\omega_0^2}\kappa - \kappa\right] f_f, \quad (41)$$

$$\tau_{eq} = -\frac{\beta}{\omega_0^2}(M+J)\left[K_v\Delta\dot{x} + K_p\Delta x\right] - J\left[\alpha\dot{w} + \left(\frac{\beta}{\omega_0^2}\frac{K}{J} + \frac{\beta}{\omega_0^2}\frac{K}{M} - \omega_0^2\right)w\right] + \tau_f + \xi f_f, \quad (42)$$

where $\xi = \kappa\left(\frac{\beta}{\omega_0^2} - 1\right) + \frac{\beta}{\omega_0^2}$.

Solving the Equation (42) and substituting $\omega_0^2 = \frac{K}{J}\left[\frac{M+J}{M}\right]$ we get:

$$\tau_{eq} = -\frac{\beta}{\omega_0^2}(M+J)\left[K_v\Delta\dot{x} + K_p\Delta x\right] - J\left[\alpha\dot{w} + (\beta - \omega_0^2)w\right] + \tau^{dist}, \quad (43)$$

where $\tau^{dist} = \tau_f + \xi f_f$ – the system disturbance signal.

It is to be noted that ξ is related to both the plant-model parameters and enforced belt-stretch dynamics parameters.

In order to obtain a continuous control of the signal σ, the control law applies the condition $\dot{\sigma} = -D\sigma$ in order to obtain control signal of the form $u = u_{eq} + D\sigma$ as explained earlier.

But we do not have the perfect knowledge about the whole system and in reality, τ^{dist} is not a measurable entity so, τ_{eq} is replaced with the estimated value $\hat{\tau}_{eq}$. The estimate $\hat{\tau}_{eq}$ does not assure the convergence to the sliding surface hence the discontinuous term is also added to it as described in Equation (44).

$$\tau = \hat{\tau}_{eq} + \frac{\beta}{\omega_0^2}(J+M)D\sigma. \quad (44)$$

Performance of robust controller as obtained from Equation (44) plays an important role in desensitizing the system from the disturbances. This also allows for implementation of the rapid vibration-free belt response which can further aid in rejecting the load side equation.

Equivalent control estimation is determined by:

$$\hat{\tau}_{eq} = \frac{\beta}{\omega_0^2}(J+M)a^c - J(\alpha\dot{\omega} + (\beta - \omega_0^2)w), \quad (45)$$

where $a^c = K_v\Delta\dot{x} + K_p\Delta x$.

Now, the control torque signal is given by Equation (46) as:

$$\tau = \int_0^t \dot{\tau}dt = \hat{\tau}_{eq} + \int_0^t \dot{\tau}_{SMC}dt. \quad (46)$$

The Equation (46) has 2 components: estimation of equivalent control; and estimation of disturbance and convergence to pre-defined sliding manifold.

Using Equations (44) to (46), the system motion projection on σ-space is governed by:

$$\dot{\sigma} + D\sigma = \frac{\omega_0^2}{\beta}\frac{\dot{\tau}^{dist}}{J+M}. \quad (47)$$

Equation (47) in combination with the condition $\sigma\dot{\sigma} = -D\sigma^2$; $D > 0$, proves the system's asymptotically stable reaching phase. The convergence is dictated by the right side of Equation (47).

Having a stable solution where $\sigma = 0$ can be guaranteed if $\dot{\tau}^{dist} = 0$, i.e., it should be constant. Also, then the derivative of considered Lyapunov's function candidate is negative definite, i.e.,

$$\dot{V} = -D\sigma^2, \quad D > 0.$$

In systems with fast sampling rate, the fast convergence rate can be achieved. If the rate of change of disturbance is low, i.e., $\dot{\tau}^{dist} = 0$ then the control law will keep the system states in the vicinity of the pre-defined sliding manifold.

4 Simulation results

The system considered in the research being simulated in MATLAB-Simulink is depicted in Figure 5.

The control and simulation system as shown in Figure 5 consisted of four main blocks: The nominal plant (I)

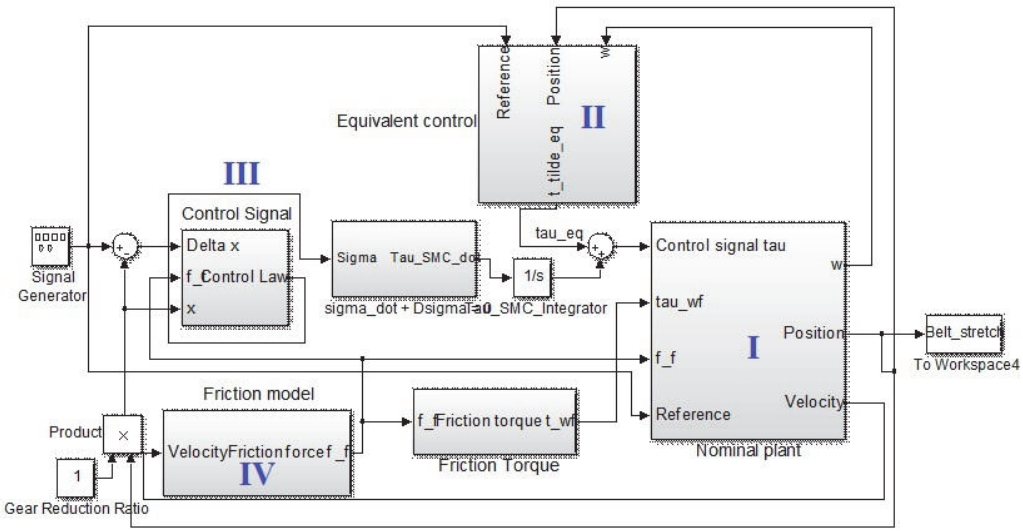

Figure 5: The control and simulation system.

in Figure 6; Equivalent control block for eliminating the chattering (II) in Figure 7; Control creation signal (III): and Friction model (IV) in Figure 8.

In the nominal plant (Figure 5), a noise/disturbance signal with a magnitude of 1 and frequency of 0.5 rad/sec was added to check the robustness and the chattering free for the control system.

The Belt stretch; Friction torque; and the Control torque to the nominal plant is shown in Figure 9. It can be seen that the Belt stretching block in Figure 8 helps to estimate and minimize the belt stretching to very low value from 3e-03 m and then later it oscillates around the magnitude of 1e-03 m in correspondence to the varying reference input signal. The control torque, thus, is calculated to minimize the position errors. At the starting point, the torque magnitude is quite high with the approximate magnitude of 985 Nm, and later stays within the range of +200 to −200 Nm.

Now, to check the robustness of this system, a phaseship of pi/2, i.e., 90° is induced to the reference signal as shown in Figure 10.

In Figure 10, it can be seen that the system is robust enough to deal with the initial offset. It took 1.6 secs to track the reference path and the tracking results are free from chattering.

The system is now tested further with the square tracking. Fiction torque is estimated in the friction mode and used to calculate the friction torque and the control torque. Figure 11 shows the results of belt stretch, friction torque and the control torque for tracking a square reference.

Figure 12 shows the system output performance when it tracks a square reference. Similarly to Figure 10 at the starting point, a high different jump took place because of the initial offset. The output rapidly tracks the reference line. And at time line in 6 s, the reference suddenly is falling and the output follows with a small offset error. But in 13 s and 19 s, this error is eliminated. The overshooting values are kept at small levels.

Finally, the system is tested tracking on a saw reference with the same magnitude and frequency as the sinuous and square signals. Results in belt stretch, friction torque and the control torque show that the system performs better than previous tracking references. The input torque to keep the belt tracking to the reference is also smaller as shown in Figure 13.

Figure 14 shows the saw tracing performance. At starting point and at 13 s, the tracking overshoots are high due to the big sudden fall of the reference line. However the output very fast tracks to the reference without error.

The above simulations show that the controller has provided chattering-free input in the control torque. The

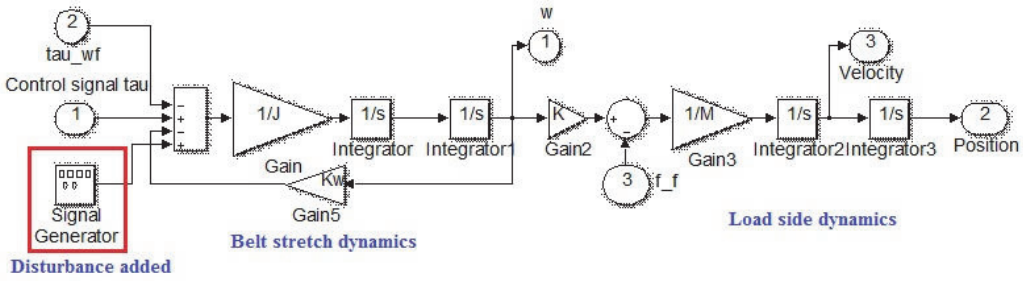

Figure 6: Nominal plant added with disturbance.

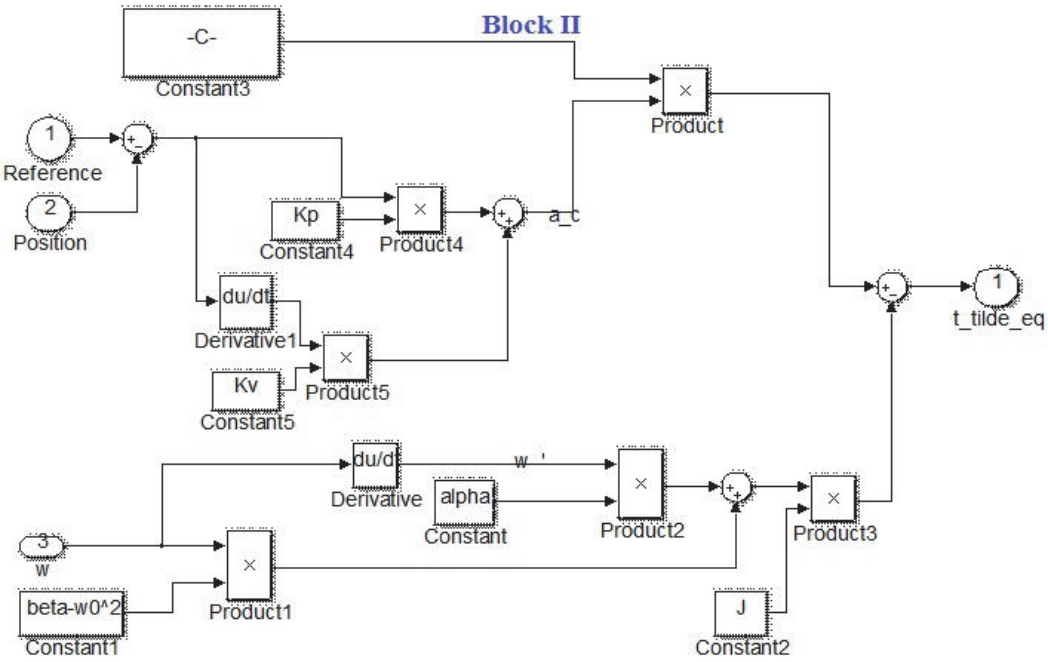

Figure 7: Equivalent control.

tracking errors are small and the system can detect the reference switching and generate the control torque correspondingly. The tracking overshoots become smaller since the system has adapted to those changes.

5 Conclusion

This study has included the use of chattering free SMC as in equivalent controller and the belt stretching estimation as in internal friction model into the control law. This SMC provides free chattering and then, the system is safe for all mechanical and electrical devices. The tracking errors are very small. The reference tracking position is achieved at

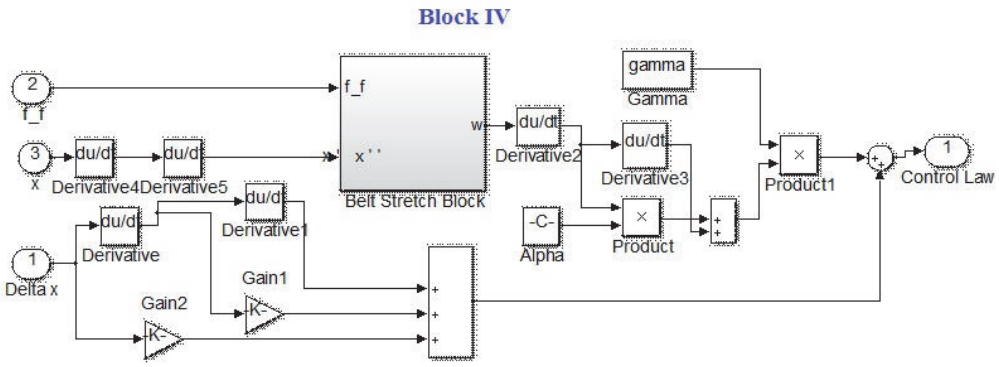

Figure 8: Friction model.

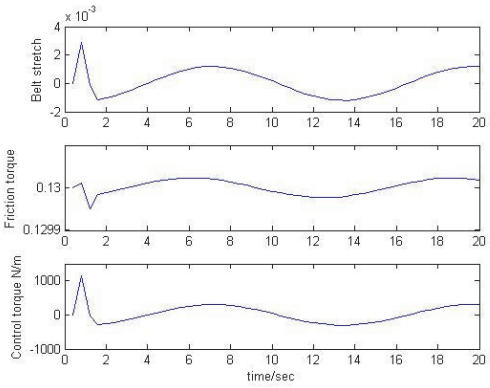

Figure 9: Friction model with sinuous reference.

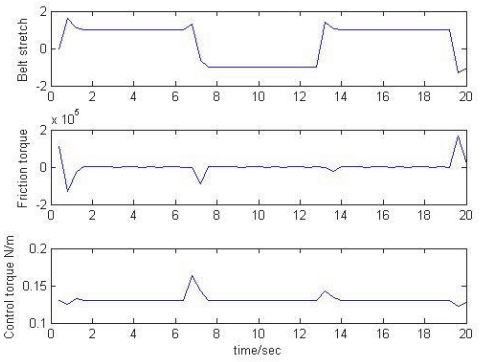

Figure 11: Friction model with square reference.

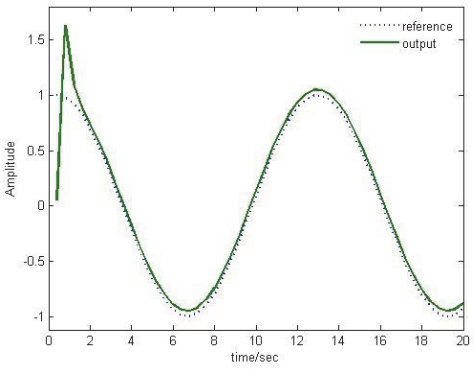

Figure 10: Robust sinuous referenced tracking.

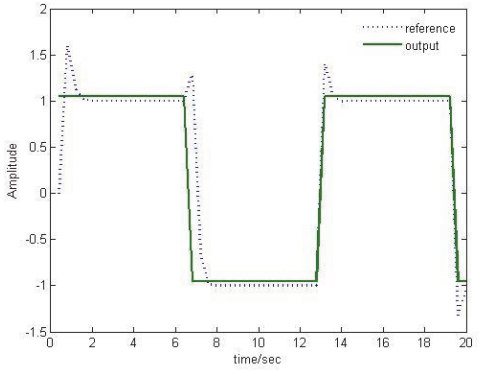

Figure 12: Robust square referenced tracking.

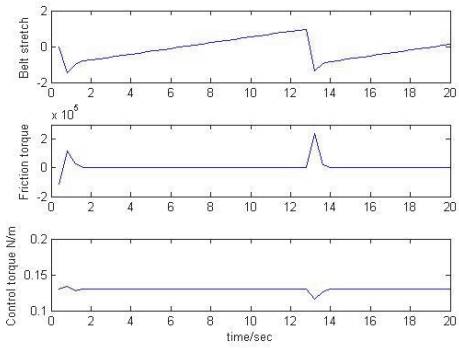

Figure 13: Friction model with saw reference.

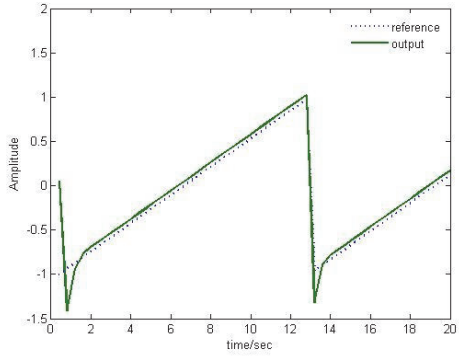

Figure 14: Robust saw referenced tracking.

quite a fast pace and the controller can be able to eliminate any disturbances entering into the system. The magnitude of belt stretching is considerably reduced after the belt stretch control estimator is incorporated into the control law. Experiments are also conducted to test the robustness of the system by changing the initial positions at the starting point. The system swiftly detected and consequently responded to those changes.

In future research, a combination of chattering free SMC and a disturbance observer can be used together to reduce the tracking errors and to deal with the problem of friction as well as disturbance dynamics. Further comparative study of the time delay control in the sliding mode (TDC-SMC) and other control methods can be applied and analyzed to select a better chattering free SMC solution.

Acknowledgement: The authors would like to thank the Department of Electrical Power Engineering and Mechatronics, Tallinn University of Technology (TTU) for supporting this research project.

Conflict of interests

The authors declare that this article is our own research property and there is no conflict of interests regarding the publication of this paper.

References

[1] Cepon G., Boltezar M., Dynamics of a belt-drive system using a linear complimentarity problem for the belt-pulley contact description, Journal of Sound and Vibration, 2009, 319(3-5), 1019-1035

[2] Hace A., Jezernik K., Sabanovic A., SMC with disturbance observer for a linear belt drive, IEEE Transactions on Industrial Electronics, 2007, 54(6), 3402-3412

[3] Zhang G., Furusho J., Speed control of two-inertia system by PI/PID control, IEEE Transactions on Industrial Electronics, 2000, 47(3), 603-609

[4] Ellis G., Lorenz R. D., Resonant load control methods for industrial servo drives, In: Proceedings of Annual Meeting of IEEE Industry Applications Society, Rome, Italia, 2000

[5] Levant A., Chattering analysis, IEEE Transactions on Automatic Control, 2010, 55(6), 1380-1389

[6] Sabanovic A., Sozbilir O., Goktug G., Sabanovic N., Sliding mode control of timing-belt servo system, In: Proceedings of IEEE International Conference on Electrical Drives and Power Electronics, Rio de Janeiro, Brazil, 2003

[7] Gurbani C., Kumar V., Designing robust control by sliding mode control technique, AEEE Research Publications, 2013, 3(2), 137-144

[8] Chifi-alauhi A., Messaoud H., Chaabane M., Sliding mode control, with integrator, for a class of non-linear systems, Scientific Research Engineering, 2011, 3, 435-444

[9] Lesniewski P., Bartoszewicz A., Hyperbolic tangent based switching reaching law for discrete time sliding mode control of dynamical systems, In: Proceedings of Recent Advances in Sliding Modes, Istanbul, Turkey, 2015

[10] Kochetkov S., Utkin V., Invariance in systems with un-matched perturbations, Journal of Automation and Remote Control, 2013, 74(7), 1097-1127

[11] Shtessel Y., Edwards C., Fridman L., Levant A., Sliding mode control and observation, In: Birkhauser, 2014, ISBN 978-0-8176-4893-0

[12] Bandyopadhyay B., Thakar V. K., Discrete time output feedback sliding mode control for nonlinear MIMO systems: A step motor case, International Journal of Systems Science, 2008, 39(1), 89-104

[13] Zeinali M., Adaptive Chattering-free sliding mode control design using fuzzy model of the system and estimated uncertainties and its application to robot manipulators, In: Proceedings of Recent Advances in Sliding Modes, Istanbul, Turkey, 2015

[14] Zeinali M., Notash L., Adaptive Sliding mode control with uncertainty estimator for robot manipulators, Journal of Mechanism and Machine Theory, 2010, 45(1), 80-90

[15] Minh V. T., Abdul Rani A. M., Modeling and control of distillation column in a petroleum process, Mathematical Problems in Engineering, Open Access, 2009, art. ID 404702
[16] Wanga B., Shic P., Karimi H., Fuzzy sliding mode control design for a class of disturbed systems, Journal of Franklin Institute, 2014, 351, 3593-3609
[17] Minh V. T., Hashim B., Awang M., Development of a real-time clutch transition strategy for parallel hybrid electric vehicle, Journal of Systems and Control Engineering, 2012, 226(2), 188-203
[18] Minh V. T., Afzulpukar N., Muhamad W., Fault detection model based controller for process system, Asian Journal of Control, 2011, 13(3), 382-397
[19] Minh V. T., Pumwa J., Fuzzy logic and slip controller of clutch and vibration for hybrid vehicle, International Journal of Control, Automation and Systems, 2013, 11(3), 526-532

Publication II

E. Sekhri, M. Tamre and R. Kapoor, "Optimal Q-Learning Approach for Tuning the Cavity Filters," *2019 20th International Conference on Research and Education in Mechatronics (REM), Wels, Austria*, 2019, pp. 1–5, doi: 10.1109/REM.2019.8744118.

2019 20th International Conference on Research and Education in Mechatronics (REM)
May 23-24, 2019, Wels, Austria

Optimal Q-Learning Approach for Tuning the Cavity Filters

Even Sekhri
Department of Electrical Power Engineering and Mechatronics
Tallinn University of Technology
Tallinn, Estonia
even.sekhri@taltech.ee

Mart Tamre
Department of Electrical Power Engineering and Mechatronics
Tallinn University of Technology
Tallinn, Estonia
mart.tamre@taltech.ee

Rajiv Kapoor
Department of Electronics and Communication
Delhi Technological University
New Delhi, India
rajivkapoor.dtu@gmail.com

***Abstract*—The current research paper elucidates the optimal approach for tuning the Microwave Cavity Filters. The proposed solution uses Q-learning approach which is a special case of Temporal Difference used in Reinforcement Learning. The results are optimized using Lagrangian Multiplier. The proposed algorithm is tested on a commercially used filter. In this research work, only four screws were used for training the algorithm and for testing it. The algorithm could understand the strategies and could tune the reflection characteristics of the considered filter in 43 steps which proves the effectiveness of the algorithm to assist in the tuning process.**

Keywords— Q-Learning, Microwave Cavity Filter Tuning, Lagrangian Multiplier, Optimization

I. INTRODUCTION

Due to the recent rise in cellular communication, the network providers are motivated to install new Radio Base Stations (RBS) to manage the data traffic and to provide better connectivity. The spectrum is crowded now, and the need to filter out the desired frequency is high. Microwave (MW)/Radio frequency (RF) cavity filter is one of the major components in the RBS because of its High-Q factor, stability against environmental effects, reliable operation and robustness. To meet the connectivity requirements, raised by the substancial increase in the number of users, numbers of installed filter units have increased exponentially. As a consequence, the need for having high volume production of these filters is all-time high.

After the production, filters are assembled and pre-tuned. Due to various imperfections in the design, filter tolerances and material's dielectric constants, the filter needs to be properly tuned. Currently, tuning is done manually by the trained technicians and is a highly iterative, time-consuming and monotonous process. This process may vary from 15 minutes to a few hours by studying the scattering parameters (also called as S-parameters) response of the filter [1]. Attaining ample proficiency is also equally time-consuming even if some guiding documents are available in [2]. While rotating the screws, the technicians observe the S-parameters response of the filter on the Vector Network Analyzer (VNA) with the aim of tuning the filter in the well-defined frequency limits. Lot many filter topologies, with different frequencies and bandwidth, are available in the market which makes generalization next to impossible.

At times, even after being trained for a few months, some trainees remain inefficient in performing the task. The sustainability of the tuners also poses a big concern especially because finding new tuners is not a cakewalk. The major reason why tuning is difficult is because there is a complex correlation between the tuning elements and the filter response [3]. The beforementioned paragraphs suggest that tuning is a cumbersome task. Hence, searching automated means of doing this process is the bone of contention of the researchers in the field to remove the bottleneck of production.

The next section discusses all the potent efforts made by the researchers for the advancement in the field.

II. LITERATURE SURVEY

Automating the cavity filter tuning by using Machine Learning (ML) has been studied quite exhaustively by the researchers for decades. The concept of using ML Algorithm for finding the solution to this tuning problem was first presented in 1989 [4], in which the researchers did not use any Mathematical Modeling or Coupling Matrix Extraction procedure. They used waveguide filter and presented an algorithm that could only assist the human operator to fast tune but could not tune the filter automatically. The major drawback of their time was the assumption that the coupling screws are already correctly pre-adjusted. Continued researches in the area many other techniques were proposed. These included algorithms based on Adaptive Models [5] which was based on the approximate network models that were derived using the prototype network. This is not feasible to implement in real life. Fuzzy Logic was also implemented in this area [6]–[10] which although gave more flexibility, but no consideration was given to human experience in [6] and [7]. The usage of inevitable human experience came only in [8][9] and [10] which could assist in the accurate tuning. The major issue with the methods used by these researchers was that they were based on coupling matrix extraction from the mathematical model. However, the accurate mathematical model for the cavity filter is not reported into the literature yet. Another major issue with these researches was related to having an insufficient amount of linguistic rules. Both these factors limited this method to

978-1-5386-9257-8/19/$31.00 ©2019 European Union

be used in real life. Artificial Neural Networks (ANN) was used to get the inverse model of the filter [11]–[14]. This method was also not without its shortcomings as it required huge amount of training data, which further led to increased time in the filter tuning. Later, a hybrid approach of combining two or more techniques was proposed in [15]. In recent times, researchers are resorting to Reinforcement Learning (RL) [16] in which they had used only two screws for training their model. Selection of the reward cost was their key concern. The same authors also tried a vector field approach [17] but the algorithm was not at all intelligent. Later in [18] the authors combined the techniques in [16] and [17] and used DDPG framework to have continuous RL but used a simple filter model. They turned only four screws that too in a limited range, with the curve that chaged only on the vertical side.

The above overview indicates the amount of efforts put forth by the researchers for the advancement in the area. However, the findings of these numerous analytical and practical approaches were either incomplete or deficient or nonviable; as none of the researches were able to find the solution that could tune the complex filters automatically. The reason why most of the methods proposed by researchers cannot be implemented in real life is that they modelled the filters only but did not focus on the role of human intelligence. The role of an experienced tuner is inevitable. The data from the human experience can exponentially increase the performance of the system. This approach has been discussed in recent times in [10] and [16] but, yet, it needs to be explored further to achieve Automated Filter Tuning.

Developing a meaningful algorithm can reduce the time and fabrication costs significantly. Computerized Automatic Tuning (CAT) of MW filters is challenging but it indeed will meet the demands of rapidly increasing market [19][20][21]. It will have the potential of not only tuning the filter automatically and reduce human dependency but, it also can open the path for understanding the patterns behind this process. The ideal automated CAT must not have any human involvement; mathematical filter modeling should be avoided; and finally, the filter must reach its optimum state of tuning. Considering all these requirements, and understanding the fact that the humans train their Natural Neural Network while they learn and try to tune the filter makes the usage of ANN the basis of this research work. Reinforcement Learning (RL) does not need any supervision rather it learn the patterns from the environment in which they are implemented. In this research work, RL has been used and the Reflection Curve (S_{11}) is considered. Q-Learning is used in this research work and the Loss function is optimized using Lagrangian Multiplier to obtain the Global Minima. The subsequent section illustrates the Q-Learning approch and discusses the Learning Model used in this current research work which is then optimized.

III. Q-Learning Algorithm Based Tuning

A. Preliminaries

The Device Under Test (DUT) is a cavity filter which is connected to Vector Network Analyzer (VNA) using input/output ports. VNA is the device which provides input to the filter and then also depicts the current frequency response of the filter in the form of S-parameters curves. The data can be extracted in terms of Insertion Loss (the useful energy dissipated as heat), Return Loss (the signal reflected back towards the source), Passband Signal (the absolute value should be as close to 0 dB as possible) and the Band-Reject Signal (with or without Transmission Zeros). In this research work, we considered only Return Loss Curve (S_{11}) as the state. The goal of the tuning is only to minimize the absolute value of the Return Loss and to ensure it is below the target value of -16dB in the passband zone.

B. Formulation

Markov Decision Process (MDP) provides a framework for mathematical modeling when outcomes are partly under the decision maker's control and partly random. In [16], researchers used Q-Learning in the field of Filter Tuning which was based on Stochastic Gradient Descent (SGD) Algorithm. The filter model used by them was very simple and often faced the problem of trapping into local minima. In this work, authors decided to use Q-learning approach considering Convolutional Neural Network (CNN) architecture so as to reach towards the Global Minima of the defined Cost Function using Lagrangian Multiplier. In MDP, the Learner and the Decision-Maker is named as "Agent" and it interacts with the "Environment". MDP is basically defined by *s,a,r,p* and γ where:

$s \in S$ – the State of the considered system

$a \in A$ – the Action taken by the agent

$r : S \times A \rightarrow R$ – the Reward Function

$p(s_{future} \mid s_{now}, a_{now})$ – the state transition (probability) function or system dynamics

γ – the discount factor $\in (0,1]$

In MDP (and RL), the policy π is defined as a function which specifies the action to be taken corresponding to each state i.e. $\pi : S \rightarrow A$. At any instance the agent is in the state $s \in S$, action $a \in A$ and then its future state is s_{future}. This has been explained pictorically in Fig. 1 below.

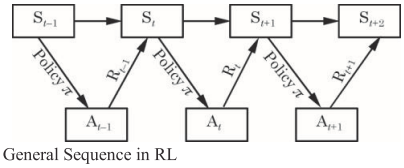

Fig. 1: General Sequence in RL

In our case, agent is the designed algorithm; states are the points considered on S-parameter curve; actions are clockwise and anti-clockwise turning angles of the screws; the discount factor γ is set to 0.95 in this research. The target of the Q-Algorithm is to maximize the future rewards after learning the policy $\pi(s_{now}) \rightarrow a_{\text{now}}$. In this research work, the target of the Q-algorithm is to ensure that the return loss i.e. S_{11} parameters of the filter is below the target value which is -16 dB in our case. The s-parameters of the DUT are obtained and are compared with the target value in the passband zone. In case, the S_{11} parameters of DUT are already below the target line, then, the distance is defined to be zero. But, in alternate case, the distance d is recorded by taking the absolute value of the difference between the two curves. If this d value is getting smaller, the system receives a reward point of 1 else it gets a zero as its reward. When the system is presented with a state, the system takes an action against it and receives the corresponding reward and reaches the next (future) state and saves this sequence. After this, a mini-batch of the saved sequence is extracted to train the designed network. Further, the future action a_{future} which actually maximizes the Q-value of state s_{future} is selected for the future cycle.

C. The Q-Learning Model

The quality i.e. Q-function (using Bellman's Equation) is given by (1) below.

$$\mathrm{Q}(s_{now}, a_{now}) = \underbrace{r_{\text{now}}}_{\substack{\text{Immediate}\\ \text{reward}}} + \underbrace{\gamma \max_{a_{\text{future}}} \mathrm{Q}(s_{\text{future}}, a_{\text{future}})}_{\text{Discounted/Future Reward}} \tag{1}$$

Keeping optimal value V* (stated in (3)) then an optimal policy is to decide deterministically, and the optimal action is given by (2).

$$a^*(s_{\text{now}}) = \arg\max_{a_{\text{now}}} \mathrm{Q}^*(s_{\text{now}}, a_{\text{now}}) \tag{2}$$

(where a^* is the optimal action and Q^* is the optimal Q-value)

i.e. $$\mathrm{V}^*(s_{\text{now}}) = \max_{a_{\text{now}}} \mathrm{Q}^*(s_{\text{now}}, a_{\text{now}}) \tag{3}$$

The Q-Algorithm used is drawn in Fig. 2. The update rule is defined by (4) and (5).

$$\mathrm{Q}_{\text{est}}(s_{\text{now}}, a_{\text{now}}) \leftarrow \mathrm{Q}_{\text{est}}(s_{\text{now}}, a_{\text{now}}) + \alpha\left[r_{\text{now}} + \gamma \max_{a_{\text{future}}} Q_{est}(s_{\text{future}}, a_{\text{future}}) - \mathrm{Q}_{\text{est}}(s_{\text{now}}, a_{\text{now}}\right] \tag{4}$$

& $$s_{\text{now}} \leftarrow s_{\text{future}} \text{ until termination} \tag{5}$$

where: α = learning rate or step size (0,1].

To deal with non-exploration i.e. to update α, we used random exploration. At the stated probability of $\frac{1}{N}$ where N = number of trials i.e. number of times we have used "(s, a)-pairs", the program took random action instead of optimal one and later, the probability of α was lowered automatically.

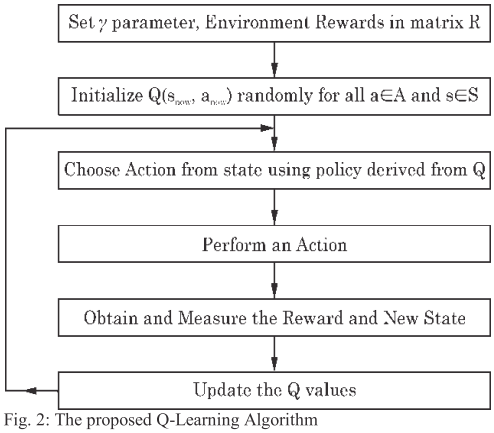

Fig. 2: The proposed Q-Learning Algorithm

The loss function is defined by (6) as:

$$\mathcal{L}(w) = \mathbb{E}\left[\left\{\underbrace{r_{\text{now}} + \gamma \max_{a_{\text{future}}} \mathrm{Q}_{\text{est}}(s_{\text{future}}, a_{\text{future}}, w)}_{\text{target}} - \underbrace{\mathrm{Q}_{\text{est}}(s_{\text{now}}, a_{\text{now}}, w)}_{\text{estimated}}\right\}^2\right] \tag{6}$$

Then, the Q-Learning gradient is computed by (7) as:

$$\frac{\partial \mathcal{L}(w)}{\partial w} = \mathbb{E}\left[\left\{r_{\text{now}} + \gamma \max_{a_{\text{future}}} \mathrm{Q}_{\text{est}}(s_{\text{future}}, a_{\text{future}}, w) - \mathrm{Q}_{\text{est}}(s_{\text{now}}, a_{\text{now}}, w)\right\}\frac{\partial \mathrm{Q}_{est}(s_{now}, a_{now}, w}{\partial w}\right\} \tag{7}$$

To remove correlation, we built the data set from agent's own experience and we took the following action:

1. Taking action a_{now} using greedy policy
2. Store the transition $T\ (s_{now}, a_{now}, r_{future}, s_{future})$ in replay memory $\mathcal{D}$.
3. Taking sample random mini-batch from the stored transition
4. Optimizing MSE between Q-network and Q-learning targets given by (8)

$$\mathcal{L}(w) = \mathbb{E}_{s_{\text{now}}, a_{\text{now}}, r_{\text{now}}, s_{\text{future}} \sim \mathcal{D}}\left[\left\{\underbrace{r_{\text{now}} + \gamma \max_{a_{\text{future}}} \mathrm{Q}_{\text{est}}(s_{\text{future}}, a_{\text{future}}, w)}_{\text{target}} - \underbrace{\mathrm{Q}_{\text{est}}(s_{\text{now}}, a_{\text{now}}, w)}_{\text{estimated}}\right\}^2\right] \tag{8}$$

The loss function is optimized end-to-end by Lagrangian optimization mentioned in (9) i.e.

$$\mathcal{L}(f, \gamma, x) = f(t, y) + \gamma . x(t, y) \tag{9}$$

and, later we equated $\frac{d\mathcal{L}}{dx} = 0$ to find the global optimum value with the constraint given in (10) i.e. :

Loss Function > Threshold Value (10)

The next section of this research paper is dedicated to the experimentation methodology used and the results obtained henceforth. A detailed discussion of the results is also presented.

IV. Experimentation

A. General Implementation Details

In this research work, the DUT is a version of Huawei Cavity Filter with two channels. We used only one channel i.e Receiver Side (RX Side) and four resonator screw of RX Side for performing the actions. Hence, we had eight actions to be performed (rotation angles of all the four screws in both directions by one full rotation i.e. 360°). The environment used in this research work is simulated, where we generated training samples by randomly inserting the screws one by one manually.

As a function approximator, we used CNN Architecture where the input is the passband section of the S-parameters. The input of Q-network was set at 25 artificial neurons and the output layer consisted of eight neurons indicating the eight valid actions for the Q-values.

For training the network, we randomly drew 35 sequences from the collected database $\mathcal{D}$. A greedy policy was used so as to obtain the biggest estimated Q-value.

B. Results

We trained the defined network for 150 epochs each with 1000 tuning steps as the maximum value. After training the network, it was tested with 50 random states. After 100 training epochs, the algorithm was tested with 100 random states.

Fig. 3 provides the results of our algorithm. It was found that after training the network it could successfully drive the curve below –16 dB return loss target and just after 43 steps the filter was successfully tuned. Global Minima was ensured by the use of Lagrangian Multiplier.

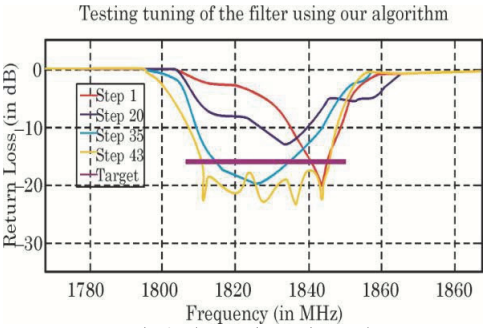

Fig. 3: The experimentation results

C. Discussion of the Results

The current research proved the effectiveness of Q-learning, the proposed algorithm could successfully find the correct screw position and global optimum. The major limitations and hence, further implications of our research include:

a) In this present research, only reflection characteristics are considered without considering the forward insertion loss.

b) Further, only the distance between the current reflection characteristics and the target value within the passband was used. The limit lines on the sides (for sharper transition between stopband and passband), however, were unobserved.

c) Our reward policy considers only the distance between current and target values, the penalty for complete removal or insertion of the tuning screw, however, is not considered. This is a major consideration in real scenarios and hence must be given a heavy penalty. In addition, no reward was assigned to successfully tuning the filter.

V. Conclusion

The current research highlighted the difficulties of manual tuning of cavity filters which led to the need of tuning the filters by autonomated means. A Q-learning algorithm was propsed as a viable solution. The designed algorithm could learn the tuning strategies and updated the estimated Q-values iteratively. The effectivess of the algorithm was ensured by experiments. The designed algorithm could successfully tune the raw filter (using only four resonator screws) after 43 steps.

References

[1] T. Kacmajor, P. Kant, and J. J. Michalski, “Microwave filter tuning for different center frequencies based on Artificial Neural Network and phase compensation,” *2014 20th Int. Conf. Microwaves, Radar Wirel. Commun. MIKON 2014*, 2014.

[2] A. Lindner, E. Biebl, and A. Strasse, “A Manual Tuning Method for Coupled Cavity Filters,” in *Proceedings of 36th European Microwave Conference*, pp. 1340–1342.

[3] L. Han, K. Wu, X.-P. Chen, and F. He, “Influence and Tuning of Tunable Screws for Microwave Filters Using Least Squares Support Vector Regression,” *Int. J. RF Microw. Comput. Eng.*, vol. 20, no. 4, pp. 422–429, 2010.

[4] A. R. Mirzai, C. F. N. Cowan, and T. M. Crawford, “Intelligent alignment of waveguide filters using a machine learning approach,” *Microw. Theory Tech. IEEE Trans.*, 1989.

[5] P. Harscher, J. Hofmann, R. Vahldieck, and B. Ludwig, “Automatic Computer-Controlled Tuning System for Microwave Filters,” in *30th European Microwave Conference*, 2000, pp. 1–4.

[6] V. Miraftab, S. Member, and R. R. Mansour, “Computer-Aided Tuning of Microwave Filters using Fuzzy Logic,” in *Miraftab, Vahid Mansour, Raafat R*, 2002, vol. 50, no. 12, pp. 2781–2788.

[7] V. Miraftab and R. R. Mansour, “A robust fuzzy-logic technique for computer-aided diagnosis of microwave filters,” *IEEE Trans. Microw. Theory Tech.*, vol. 52, no. 1 II, pp. 450–456, 2004.

[8] V. Miraftab and R. R. Mansour, “Tuning of microwave filters by extracting human experience using Fuzzy Logic,” *IEEE MTT-S Int. Microw. Symp. Dig.*, vol. 2005, no. C, pp. 1605–1608, 2005.

[9] V. Miraftab and R. R. Mansour, “Automated microwave filter tuning by extracting human experience in terms of linguistic rules using fuzzy controllers,” *IEEE MTT-S Int. Microw. Symp. Dig.*, pp. 1439–1442, 2006.

[10] V. Miraftab and R. R. Mansour, “Fully automated RF/microwave filter tuning by extracting human experience using fuzzy controllers,” *IEEE Trans. Circuits Syst. I Regul. Pap.*, vol. 55, no. 5, pp. 1357–1367, 2008.

[11] J. J. Michalski, “Artificial Neural Networks Approach in Microwave Filter Tuning,” *Prog. Electromagn. Res. M*, vol. 13, pp. 173–188, 2010.

[12] J. J. Michalski, T. Kacmajor, J. Gulgowski, and M. Mazur, “Consideration on Artificial Neural Network Architecture in Application for Microwave Filter Tuning,” *Piers Online*, vol. 7, no. 3, pp. 271–275, 2011.

[13] J. Gulgowski and J. J. Michalski, “The analytic Extraction of The Complex-Valued Coupling Matrix and its Applcation in the Microwave Filter Modeling,” in *Progress In Electromagnetics Research*, 2012, vol. 130, no. July, pp. 131–151.

[14] J. J. Michalski, “Inverse Modeling in Application for Sequential 0Filter Tuning,” in *Progress In Electromagnetics Research*, 2011, vol. 115, no. February, pp. 113–129.

[15] T. Kacmajor and J. J. Michalski, “Neuro-fuzzy approach in microwave filter tuning,” *IEEE MTT-S Int. Microw. Symp. Dig.*, pp. 2–5, 2011.

[16] Z. Wang, J. Yang, J. Hu, W. Feng, and Y. Ou, “Reinforcement learning approach to learning human experience in tuning cavity filters,” *2015 IEEE Int. Conf. Robot. Biomimetics, IEEE-ROBIO 2015*, pp. 2145–2150, 2015.

[17] Z. Wang, S. Jin, J. Yang, X. Wu, and Y. Ou, “Real-time tuning of cavity filters by learning from human experience: A vector field approach,” *Proc. World Congr. Intell. Control Autom.*, vol. 2016–Septe, pp. 1931–1936, 2016.

[18] Z. Wang, Y. Ou, X. Wu, and W. Feng, “Continuous Reinforcement Learning With Knowledge-Inspired Reward Shaping for Autonomous Cavity Filter Tuning Continuous Reinforcement Learning With Knowledge-Inspired Reward Shaping for Autonomous Cavity Filter Tuning*,” in *Proceedings of 2018 IEEE International Conference on Cyborg and Bionic Systems*, 2018, no. December, pp. 53–58.

[19] H. Hsu, S. Member, H. Yao, S. Member, and K. A. Zaki, “Computer-Aided Diagnosis and Tuning of Cascaded Coupled Resonator Filters,” in *IEEE Transactions on Microwave Theory and Techniques*, 2002, vol. 50, no. 4, pp. 1137–1145.

[20] J. B. Ness, “A unified approach to the design, measurement, and tuning of coupled-resonator filters,” *IEEE Trans. Microw. Theory Tech.*, vol. 46, no. 4, pp. 343–351, 1998.

[21] G. Pepe, F. Gortz, and H. Chaloupka, “Computer-aided tuning and diagnosis of microwave filters using sequential parameter extraction,” *Microw. Symp. Dig. 2004 IEEE MTT-S Int.*, vol. 3, p. 1373–1376 Vol.3, 2004.

Publication III

E. Sekhri, R. Kapoor and M. Tamre, "Double Deep Q-Learning Approach for Tuning Microwave Cavity Filters using Locally Linear Embedding Technique," *2020 International Conference on Mechatronic Systems and Materials (MSM), Bialystok, Poland*, 2020, pp. 1–6, doi: 10.1109/MSM49833.2020.9202393.

Double Deep Q-Learning Approach for Tuning Microwave Cavity Filters using Locally Linear Embedding Technique

Even Sekhri*
Department of Electrical Power Engineering and Mechatronics
Tallinn University of Technology
Tallinn, Estonia
even.sekhri@taltech.ee

Rajiv Kapoor
Department of Electronics and Communication
Delhi Technological University
New Delhi, India
rajivkapoor.dtu@gmail.com

Mart Tamre
Department of Electrical Power Engineering and Mechatronics
Tallinn University of Technology
Tallinn, Estonia
mart.tamre@taltech.ee

***Abstract* — From past two decades, Microwave Cavity Filter is the buzzword in communication arena. They are highly valued owing to their high-Q factor and robustness. Once assembled, the filter needs to be properly tuned to compensate for various design imperfections and manufacturing tolerances, which till date is carried out manually. To overcome these limitations a Computer-Aided Tuning (CAT) method has been proposed using Double Deep Q-Learning (DDQN) Algorithm to fine tune Microwave Cavity Filters. Owing to copious data obtained using a commercial filter, the researchers have used Locally-Linear Embedding (LLE) approach for dimension reduction. The algorithm has been tested via simulation of a 9th order filter. Furthermore, four screws were used for training and testing the algorithm. The proposed algorithm could tune the considered filter in 23 steps only. The quick tuning, received towards the end of the research, proves that the algorithm is effective in facilitating the tuning process.**

Keywords— Microwave Cavity Filter Tuning, LLE, DDQN, RL, Computer-Aided Tuning, Q-Learning, Deep Learning (DL).

I. INTRODUCTION

Microwave Cavity Filters are widely used in satellite and wireless communication owing to its High-Q, reliability and stable operation under various kinds of environment situations. Even if filter theory is already well established, still, the output falls short of the expected standard results. Various factors including, but not limited to, design imperfections, manufacturing tolerances and influence of material characteristics, inculpate the achievement of desired results. Hence, paramount importance has been given to post-production filter tuning [1]. Filter Tuning is an expensive, boring and time-consuming activity and trained technicians are needed for it. To meet the stringent frequency selection requirements, enhanced communication quality and to avoid signal cross-talk, more and more-higher order filters (means more tuning screws) are installed these days. Also, to meet these strict requirements, there are restrictions on both sides of the passband too which are realized using cross-couplings [2]. These cross-couplings make the tuning task even more difficult and tedious.

In most cases, the tuning is done using mechanical screws in the circuit package which allows the variation of center-frequency of the resonator and sometimes also the coupling between them. Presently, tuning is done manually by the trained technicians where they inspect the filter response i.e. scattering parameters on Vector Network Analyzer (VNA). The goal is to meet the desired output response. This highly iterative process relies solely on the experience a technician has.

The complex correlation between the tuning screws and filter output makes the tuning a difficult task. Also, due to various applications and hence various filter topologies, generalization is not possible. The sustainability of technicians and finding new tuning technicians is a major concern for the industry. To overcome the above mentioned problems and in favor of having fully automated filter production, a Computer-Aided Tuning (CAT) is highly desired.

The current paper advocated the usage of DDQN Algorithm for tuning the filters, and rest of the paper is structured as follows - the second section gives a detailed overview of the related literature; the third section presents the data collection and Q-learning algorithms; the methodology used is outlined in the fourth section wherein LLE technique for dimension reduction and the used DDQN Algorithm are discussed; presentation of the results and conclusions are drawn in final section of the paper.

II. LITERATURE SURVEY

A lot of tuning algorithms were developed by the researchers in last 03 decades. Majority of the efforts were made in the field of Frequency Domain (discussed in next paragraph). However, Dunsmore made a few efforts in Time Domain (TD) approach where the research works were published under the category of band-pass filter design [3] as well as regarding their tuning methods [4], [5]. However, this TD method is not efficient for filters having various cross-couplings. In majority of real world applications, filters with cross-couplings are employed.

Various techniques based on Frequency Domain were proposed by researchers in the past. Many researchers used coupling matrix (CM) extraction (filter diagnosis) to determine the detuning elements and the needed adjustment amounts. This is done by comparing theoretical CM with untuned filter's CM. The major contribution in extracting

978-1-7281-6956-9/20/$31.00 ©2020 IEEE

CM was proposed by in [6] where source and load coupling elements were not considered which was later modified and the advanced version is presented in [7]. But both these methods were applicable to lossless filters. Some other diagnosis methods are discussed in [8][9] but were applicable to lossless filters only too whereas most commercial filters are lossy. A technique for tuning lossy microwave filters (with uneven Qs) was proposed recently [10] and a CM extraction technique to assist in tuning of highly lossy microwave filters was proposed in 2018 [11] but the magnitude of loss considered in both the researches is less than real life filters.

Automating the cavity filter tuning by using Artificial Intelligence (AI) has been reported in the related literature. The first Machine Learning (ML) Algorithm for finding the solution to this tuning problem of waveguide filters was presented in 1989 [12]. But, the coupling screws were pre-adjusted and the influence of coupling screws was not considered. Tuning using Fuzzy Logic was also implemented in [13]–[17] which although provided solution, but these techniques couldn't map the strategies implemented by technicians into linguistic rules. Rather, all these solutions were just a qualitative analysis. Another limitation of this approach was to use approximate mathematical models which lead to poor tuning accuracy. Artificial Neural Network (ANN) was used to get the inverse model of the filter [18]–[21]. Therein, discrete filter characteristics were the inputs and corresponding screw positions were the network outputs. But, the need of a large amount of training data makes the technique computationally expensive. Later, Neuro-Fuzzy approach was proposed in [22] which although reduced the learning vector data but it was not sufficient to bring the strongly detuned filter to tuned state. Recently, a CAT method by combing TS-Fuzzy Neural Networks and Improved Space Mapping was presented in [23] which had a fast convergence speed of the optimization algorithm but the radius of confidence and the need of pre-adjustment of initial value restricted the usage of this method in industry.

Reinforcement Learning (RL) for tuning the filters was initially proposed in [24] in which authors had used only two screws for training their model. Reward selection was not so well dealt there and the algorithm was trapping into local minima. Later, same authors combined the techniques in [24] and [25] and presented a DDPG framework for continuous RL. The key concern was the fact that they had used a simple filter model and turned four screws but in a limited range. An optimal Q-learning technique (using DQN) was presented by us in [26] where we used 04 screws and Lagrangian Multiplier to ensure the global minima. But the reward for reaching the tuning target and punishment for complete removal/full insertion of tuning screws was missing.

All the aforementioned studies indicate that seminal contributions have been made by the researchers to take the one notch above his/her predecessor. However, previous studies cannot be considered as conclusive as the researchers were unable to find the solution that could tune the raw complex filter automatically. The major shortcoming of previous researches, according to authors of current paper, is its under-emphasis to human intelligence. Previous researches, however, can only be considered as the first step towards a more profound understanding of achieving Automated Filter Tuning.

The first step to meet the desired goal is the development of a robust algorithm that is not only time-efficient but also cuts the fabrication cost significantly. The current research work is the continuation of work presented in [26]. In this research, the authors propose the usage of DDQN algorithm for filter tuning. DDQN falls under the category of ANN based Reinforcement Learning (RL). We have considered only the filter's reflection character (S_{11}) to come-up with a robust algorithm which minimizes the Loss function.

This algorithm is expected to tune the filter automatically, will have less reliance on humans and enables future researches to understand the patterns behind this complex tuning process.

The next section is dedicated to data collection; relating the Q-Learning terminology as per the current task; and understanding the Q-Learning approach via various Q-learning algorithms.

III. Data Collection and Q-Learning Framework

A. Data Collection

2000 samples of scattering parameters were extracted from a 9th order commercial filter with 02 cross-couplings (i.e. 9p2z filter) by randomly inserting the screws on various positions. We used Planar 304/1 VNA for fetching the data related to the chosen filter where we extracted the information related to Return Loss of a two-port filter i.e. S_{11} parameter only. The commercial filter has 900 MHz as its centre frequency. For testing the proposed DDQN Algorithm, a 9th order filter was simulated.

B. Q-Learning Terminology Used

Q-Learning which is categorized under Reinforcement Learning becomes an obvious choice when decision making is sequential and we have long term goal. In RL terminology and as shown in Figure 1:

- "Agent" (i.e. the learner) is the proposed DDQN Algorithm.
- "Environment" (i.e. the Agent's world) is the simulated world.
- "States" (i.e. Agent's position) are various points considered on S-parameter curve.
- "Actions" (i.e. Agent's Input steps in Environment) are clockwise and counter-clockwise turning angles of the screws.

- "Reward" (i.e. the Environment's feedback) is a numeric score.
- "Gamma" defined by symbol "γ" (i.e. the discounted rate of reward) has been set as 0.95 in this work.
- "Policy" is the Agent's behavior function (map from state to action).

The goal of Reinforcement Learning is to choose the optimal action by the Agent from its current State while targeting the maximum future Reward in the Environment. The notation, in this context, which is used in this research work, is:

$ss \in S$ – State of the considered system
$aa \in A$ – Action taken by the agent
rr – Reward Function
$'$ – Transition at $t+1$
π – Policy Function
γ – Discount rate $\in (0,1]$

The target of the proposed algorithm is to ensure that the S_{11} value is less than -26 dB by learning the optimal Policy.

As compared to our solution proposed in [26] we have used DDQN with CNN structure rather than 2-layered DQN structure. In addition, we have a bigger dataset from a commercial filter to define the input "States". While performing dimension reduction, Locally Linear Embedding (LLE) Technique [27] has been used in this paper to ensure that we are not loosing features information.

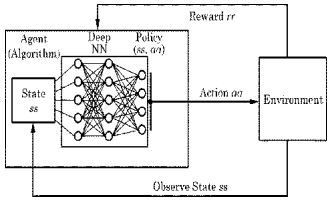

Figure 1: Agent-Environment Interaction

In our current algorithm, collected and dimensionally reduced S_{11} parameters are compared with the set target with-in the passband zone. If S_{11} parameters are already below the target line, then, the distance d obtains the zero value. But if current scattering parameters are above the target line then the d is taken as an absolute value of the difference between the current and target line. Using l_2 norm of all these d values, the distance of whole S_{11} curve is fetched. For rewarding the Agent, if d value gets smaller, the Agent receives a reward point of +10 else it gets a zero. Also, if the screw turning was over 720° (which mimics the full insertion or complete removal of the screw) then a reward of -2 (a penalty) was given to the Agent to discourage such actions.

C. Q-Learning and Deep Q-Learning (DQN)

The Q-function defined using Bellman's Equation is mentioned by Equation (1). The equation reveals that the maximum future reward an Agent will receive is the reward for entering the current state ss plus the maximum future reward for ss' i.e. for next state.

$$Q(ss, aa) = \underbrace{rr}_{\text{Immediate reward}} + \underbrace{\gamma \max_{aa'} Q(ss', aa')}_{\text{Discounted Future Reward}} \quad (1)$$

The update rule is defined by (2).

$$Q(ss, aa) \longleftarrow Q(ss, aa) + \alpha\left[rr + \gamma \max_{aa'} Q(ss', aa') - Q(ss, aa)\right] \quad (2)$$

where: α = learning rate $(0,1]$

The rule i.e. (2) terminates when: $ss \longleftarrow ss'$

The Pseudo Code for generic Q-Algorithm is presented in Algorithm 1 below.

Algorithm 1: Original Q-learning (Pseudo Code)

Algorithm parameters: step size $\alpha \in (0, 1]$, $\varepsilon > 0$
Initialize $Q(ss, aa)$, for all $ss \in S$, $aa \in A(s)$, randomly except that $Q(terminal, \cdot) = 0$
Loop for each episode:
  Initialize ss
  Loop for each step of episode:
    Choose A from S using policy derived from Q (ε-greedy or random exploration)
    Take action aa, observe rr, ss'
    $Q(ss, aa) \leftarrow Q(ss, aa) + \alpha[rr + \gamma \max_{aa'} Q(ss', aa') - Q(ss, aa)]$
    $ss \leftarrow ss'$
  until ss is terminal

It is to be noted that Q-Learning is associated with updating Q-Tables. The Q-table is initialized randomly and later, with experience, this Q-Table is updated.

With the advancement in the area of Deep Learning, Q-Learning was inter-mixed with Neural Networks which brought Deep Q-Learning (DQN) Algorithms into existence. This architecture has feed-forward neural networks to predict best possible Q-Values. DQN doesn't have any initial data hence Agent stores previous episodes (experiences related to the sequence of state-action-reward-new state) in a local memory called as data repository or experience replay. Later, this information is utilized as an Input Data and to train the designed network.

But, Q-Learning often performs poor in stochastic environments. The "max" operator used in Equation (2) is the problematic factor. The same problem applies to DQN. Because of this "max" factor, the algorithm suffers overestimation of Q-values for certain actions i.e. there is a bias in the Agent learning. Algorithm takes such an action which is good for short-term but ultimately leading to lower quality policy (i.e. lower rewards later).

The solution to this bias problem is to use Double Q-Learning introduced in 2010 by Hasselt [28]. In 2016, the overestimation bias was illustrated in experiments across various Atari Games Environments by the same author with his co-authors [29]. The core task of Double Q-Learning is to reduce the over-estimations in Q-value. This is achieved by

having one network to select the action for the next state and other network to provide the Q-value for that action. The 'selector' is "Q-Network" and 'evaluator' is "Target-Network".

The next section deals with methodology used in this research wherein LLE and DDQN are discussed in detail.

IV. METHODOLOGY

A. Locally Linear Embedding (LLE)

LLE is a method involving non-linearity for dimensionality reduction. Given enough data points in high dimensions, LLE projects the data to lower dimensions. It is assumed that the data point and its neighbors lie 'on' or 'very close' to a locally linear patch. Hence the data point is assumed to be approximated as a linear weighted combination of its neighbors. The basic idea states that this linear combination is invariant to the transformation and remains unchanged when unfolded (to lower space). Two constrained least-squared optimization problems are solved for having low dimensioned configuration.

There are three main steps in LLE Algorithm. Firstly, k-neighbors are identified for every data point $\vec{X}_i$ (mostly Euclidean Distance is used). Secondly, weights W_{ij} are computed to reconstruct $\vec{X}_i$ from its neighbors using equation (3).

$$E(W) = \sum_i \left| \vec{X}_i - \sum_j W_{ij} \vec{X}_j \right|^2 \tag{3}$$

This weight matrix W is found by minimizing the residual sum-of-squares for reconstructing each $\vec{X}_i$ data point.

In the third step, $\vec{X}_i$ is mapped to low dimensional vector i.e. Y_i to preserve the geometry of high-dimensional neighborhood. The cost function presented by equation (4) is minimized using constraints.

$$\Phi(Y) = \sum_i \left| \vec{Y}_i - \sum_j W_{ij} \vec{Y}_j \right|^2 \tag{4}$$

The coordinates of Y are found by using the same weights for minimizing the reconstruction errors.

The most important step in LLE Algorithm is to define the k number of nearest neighbors. Selection of 'k' has direct influence in the transformations i.e. scaling, rotation and translation. It depends mainly on the data features like sampling density and geometry of the curve. In our research problem, different values of k were visually tested on various values to find the optimal number of nearest neighbors. The optimal k was found to be *5* and it was hence used in this research.

B. Double Deep Q-Learning (DDQN) Algorithm Used

In the original Double Q-Learning Algorithm introduced in 2010 [28], Q-Network is calculating $Q(ss,aa)$ while the Target-Network is calculating $Q(ss',aa)$.

In this research work, we have rather used Modified Deep Double Q-learning (DDQN) Algorithm. We have a model Q for evaluation and a target model Q' for action selection. Q^* is the optimal Q model (refer equation (5)).

$$Q^*(ss, aa) \approx rr + \gamma Q(ss', \arg\max_{aa'} Q'(ss, aa)) \tag{5}$$

In equation (5), Q network is used for selecting the actions based on current state of the environment. Q' network is retrieving the Q values.

The Pseudo Code for the proposed solution used in this research is presented in Algorithm 2 below.

Algorithm 2: Double Deep Q-learning Algorithm

Initialize main Q-network Q_θ, Target-network $Q_{\theta'}$, memory buffer D, τ<<1
for each iteration **do**
  for each environment step **do**
    Observe ss and select $aa \sim \pi(aa, ss)$
    Execute aa and observe ss' and reward $rr = R(ss, aa)$
    Store (ss, aa, rr, ss') in memory D
  for each update step **do**
    sample $e_i = (ss, aa, rr, ss') \sim D$
    Compute target Q-value:
      $Q^*(ss, aa) \approx rr + \gamma\, Q_{\theta'}(ss', \text{argmax}_{aa'} Q_{\theta'}(ss', aa'))$
    Perform gradient descent step on $(Q^*(ss, aa) - Q_\theta(ss, aa))^2$
    Update Target-network parameters:
      $\theta' \leftarrow \tau\theta + (1-\tau)\theta'$

The Algorithm 2 presented above is trying to minimize the mean-square error between Q and Q^* but Q' is slowly copying the parameters of Q using Polyak Averaging as mentioned in equation (6) below.

$$\theta' \leftarrow \tau\theta + (1-\tau)\theta' \tag{6}$$

In equation (6), the target network weights are reflecting the online network weights after every run of the experience replay. θ is Primary Network Parameter and θ' is Target Network Parameter. τ is the Rate of averaging.

We have used τ = 0.05. This means that we are updating 5% of new weights and using 95% of the old weights.

The information flow in the tuning process used in this research work has been described in Figure 2 pictorially.

The next section i.e. Section V focuses on research design and results obtained henceforth. A detailed discussion of results and comparison with other closely related research works is also presented thereafter.

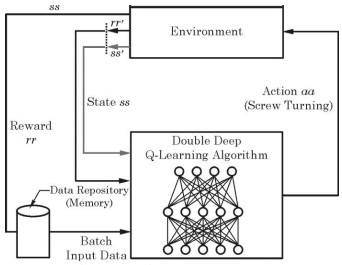

Figure 2: Information flow in proposed DDQN Algorithm

V. EXPERIMENTATION

A. General Implementation Details

For testing the algorithm, a 9th order filter was simulated. For performing the actions, four resonator screws were used which means eight actions (rotation of screws) to be performed. The screws were allowed to have two full rotations on each side i.e. clockwise and counter-clockwise rotations. The environment used in this research work is simulated, but the training data was fetched from a commercial cavity filters by randomly inserting the resonant screws one by one manually for 2000 times.

The analysis made regarding the choice of k-value i.e. number of nearest neighbors for Dimensionality Reduction has been presented in Table 1 below.

Table 1: Attempted k-value analysis

S.No	k-value	Result
1.	$k < 5$	Disjointed curves, lost global properties
2.	$k = 5$	Optimal Result (and hence used in this work)
3.	$k > 5$	Smoothing of curve
4.	$k > 8$	Behavior like traditional PCA approach

As a function approximator, we used CNN Architecture where the input is the dimensionally reduced S_{11} parameters in the pass-band. The input of Double Deep Q-network was set as 30 artificial neurons and the output layer consisted of eight neurons indicating the eight valid actions for the Q-values.

For training the network, we randomly drew 40 sequences from the repository. A random exploration policy was used so as to obtain the biggest estimated Q-value.

B. Results

We trained the defined network for 200 epochs each with 1500 tuning steps as the maximum value. After training the network, it was tested with 250 random states.

Figure 3 provides the results of our algorithm. It was found that after training the network, it could successfully drive the curve below –26 dB return loss target in just 23 steps.

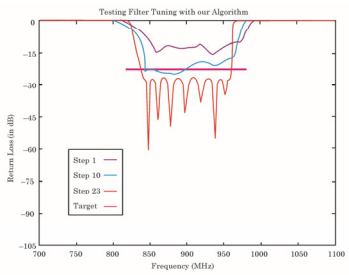

Figure 3: The experimentation results

C. Comparison of Results with Other Similar Researches

This section deals with comparison of obtained results with other similar results. The comparison has been compiled into Table 2. The proposed tuning algorithm is essentially more efficient in terms of number of tuning steps and is able to learn better strategy for tuning a more complex filter than the ones used previously which proves the effectiveness of the proposed algorithm.

Table 2: Comparison with related research works

Reference Number	Dimension Reduction Algorithm	Tuning Algorithm	Filter Order	No. of Tuning Steps
[24]	PCA	DQN	4	48
[26]	PCA	Optimal DQN	4	43
This paper	LLE	DDQN	9	23

D. Discussion of the Results

The results of the simulated experiment found clear support for the proposed algorithm viz. DDQN algorithm. Overall, our method was the one that obtained quite robust results. The major limitations which may further be used as prescriptions for future work include, but are not limited to:

a) The current research focused only on S_{11} characteristics (reflection parameter) without giving due consideration to filter's insertion losses.

b) Distance between the current S_{11} parameters and the target value within the passband was used without considering the side limit lines for sharper transition between stopband and passband.

VI. CONCLUSION

The current research highlighted the difficulties of manual tuning of cavity filters which led to the need of tuning the filters by automated means. Double Deep Q-learning algorithm was proposed as a viable solution. The designed algorithm could learn the tuning strategies. The effectiveness of the algorithm was ensured by experiments. The designed algorithm could successfully tune the simulated raw filter (using only four resonator screws) after only 23 steps.

References

[1] W. H. Cao, C. Liu, Y. Yuan, and M. Wu, "Extracting Coupling Matrix From Lossy Filters With Uneven-Qs Using Differential Evolution Optimization Technique," *Int. J. RF Microw. Comput. Eng.*, vol. 28, no. 6, pp. 1–10, 2018.

[2] J. Brian Thomas, "Cross-coupling in coaxial cavity filters - A tutorial overview," *IEEE Trans. Microw. Theory Tech.*, vol. 51, no. 4 II, pp. 1368–1376, 2003.

[3] J. Dunsmore, "Novel filter design method using time domain transforms ms," *1999 29th Eur. Microw. Conf. EuMC 1999*, vol. 3, pp. 211–214, 1999.

[4] J. Dunsmore, "Tuning Band Pass Filters in the Time Domain," *IEEE MTT-S Int. Microw. Symp. Dig.*, pp. 1351–1354, 1999.

[5] J. Dunsmore, "Advanced filter tuning using time domain transforms," *1999 29th Eur. Microw. Conf. EuMC 1999*, vol. 2, pp. 72–75, 1999.

[6] R. J. Cameron, "General Coupling Matrix Synthesis Methods for Chebyshev Filtering Functions," *IEEE Trans. Microw. Theory Tech.*, vol. 47, no. 4, pp. 433–442, 1999.

[7] R. J. Cameron, "Advanced Coupling Matrix Synthesis Techniques for Microwave Filters," *IEEE Trans. Microw. Theory Tech.*, vol. 51, no. 1, pp. 1–10, 2003.

[8] P. Harscher, R. Vahldieck, and S. Amari, "Automated filter tuning using generalized low-pass prototype networks and gradient-based parameter extraction," *IEEE Trans. Microw. Theory Tech.*, vol. 49, no. 12, pp. 2532–2538, 2001.

[9] H. T. Hsu, Z. Zhang, K. A. Zaki, and A. E. Atia, "Parameter extraction for symmetric coupled-resonator filters," *IEEE Trans. Microw. Theory Tech.*, vol. 50, no. 12, pp. 2971–2978, 2002.

[10] R. Das, Q. Zhang, A. Kandwal, and H. Liu, "Coupling Matrix Extraction Technique for Auto Tuning of Highly Lossy Filters," in *IEEE MTT-S International Microwave Symposium Digest*, 2018, vol. 2018-June, pp. 697–700.

[11] R. Das, Q. Zhang, A. Kandwal, and H. Liu, "Coupling Matrix Extraction Technique for Auto Tuning of Highly Lossy Filters," *IEEE MTT-S Int. Microw. Symp. Dig.*, vol. 2018-June, pp. 697–700, 2018.

[12] A. R. Mirzai, C. F. N. Cowan, and T. M. Crawford, "Intelligent alignment of waveguide filters using a machine learning approach," *Microw. Theory Tech. IEEE Trans.*, 1989.

[13] V. Miraftab, S. Member, and R. R. Mansour, "Computer-Aided Tuning of Microwave Filters using Fuzzy Logic," in *Miraftab, Vahid Mansour, Raafat R*, 2002, vol. 50, no. 12, pp. 2781–2788.

[14] V. Miraftab and R. R. Mansour, "A robust fuzzy-logic technique for computer-aided diagnosis of microwave filters," *IEEE Trans. Microw. Theory Tech.*, vol. 52, no. 1 II, pp. 450–456, 2004.

[15] V. Miraftab and R. R. Mansour, "Tuning of microwave filters by extracting human experience using Fuzzy Logic," *IEEE MTT-S Int. Microw. Symp. Dig.*, vol. 2005, no. C, pp. 1605–1608, 2005.

[16] V. Miraftab and R. R. Mansour, "Automated microwave filter tuning by extracting human experience in terms of linguistic rules using fuzzy controllers," *IEEE MTT-S Int. Microw. Symp. Dig.*, pp. 1439–1442, 2006.

[17] V. Miraftab and R. R. Mansour, "Fully automated RF/microwave filter tuning by extracting human experience using fuzzy controllers," *IEEE Trans. Circuits Syst. I Regul. Pap.*, vol. 55, no. 5, pp. 1357–1367, 2008.

[18] J. J. Michalski, "Artificial Neural Networks Approach in Microwave Filter Tuning," *Prog. Electromagn. Res. M*, vol. 13, pp. 173–188, 2010.

[19] J. J. Michalski, T. Kacmajor, J. Gulgowski, and M. Mazur, "Consideration on Artificial Neural Network Architecture in Application for Microwave Filter Tuning," *Piers Online*, vol. 7, no. 3, pp. 271–275, 2011.

[20] J. Gulgowski and J. J. Michalski, "The analytic Extraction of The Complex-Valued Coupling Matrix and its Applcation in the Microwave Filter Modeling," in *Progress In Electromagnetics Research*, 2012, vol. 130, no. July, pp. 131–151.

[21] J. J. Michalski, "Inverse Modeling in Application for Sequential Filter Tuning," in *Progress In Electromagnetics Research*, 2011, vol. 115, no. February, pp. 113–129.

[22] T. Kacmajor and J. J. Michalski, "Neuro-fuzzy approach in microwave filter tuning," *IEEE MTT-S Int. Microw. Symp. Dig.*, pp. 2–5, 2011.

[23] S. Wu, W. Cao, M. Wu, and C. Liu, "A Tuning Method for Microwave Filter via Complex Neural Network and Improved Space Mapping," *Int. J. Electron. Commun. Eng.*, vol. 12, no. 3, pp. 218–224, 2018.

[24] Z. Wang, J. Yang, J. Hu, W. Feng, and Y. Ou, "Reinforcement learning approach to learning human experience in tuning cavity filters," *2015 IEEE Int. Conf. Robot. Biomimetics, IEEE-ROBIO 2015*, pp. 2145–2150, 2015.

[25] Z. Wang, S. Jin, J. Yang, X. Wu, and Y. Ou, "Real-time tuning of cavity filters by learning from human experience: A vector field approach," *Proc. World Congr. Intell. Control Autom.*, vol. 2016-Septe, pp. 1931–1936, 2016.

[26] E. Sekhri, M. Tamre and R. Kapoor, "Optimal Q-Learning Approach for Tuning the Cavity Filters," 2019 20th International Conference on Research and Education in Mechatronics (REM), Wels, Austria, 2019, pp. 1-5, doi: 10.1109/REM.2019.8744118.

[27] S. Roweis and L. Saul, "Nonlinear dimensionality reduction by locally linear embedding," *Sci. v.290*, vol. 290, no. 5500, pp. 2323–2326, 2000.

[28] H. Van Hasselt, "Double Q-learning," *Adv. Neural Inf. Process. Syst. 23 24th Annu. Conf. Neural Inf. Process. Syst. 2010, NIPS 2010*, pp. 1–9, 2010.

[29] H. Van Hasselt, A. Guez, and D. Silver, "Deep reinforcement learning with double Q-Learning," in *30th AAAI Conference on Artificial Intelligence, AAAI 2016*, 2016, pp. 2094–2100.

Publication IV

E. Sekhri, M. Tamre, R. Kapoor and D. C. Liyanage, “Novel Band-Subtraction Technique to Differentiate Screws for Microwave Cavity Filter Tuning,” *2023 3rd International Conference on Electrical, Computer, Communications and Mechatronics Engineering (ICECCME)*, Tenerife, Canary Islands, Spain, 2023, pp. 1–6, doi: 10.1109/ICECCME57830.2023.10253048.

Proc. of the International Conference on Electrical, Computer, Communications and Mechatronics Engineering (ICECCME 2023)
19-21 July 2023, Tenerife, Canary Islands, Spain

2023 3rd International Conference on Electrical, Computer, Communications and Mechatronics Engineering (ICECCME) | 979-8-3503-2297-2/23/$31.00 ©2023 IEEE | DOI: 10.1109/ICECCME57830.2023.10253048

Novel Band-Subtraction Technique to Differentiate Screws for Microwave Cavity Filter Tuning

Even Sekhri*
Department of Electrical Power Engineering and Mechatrocnics
Tallinn University of Technology
Tallinn, Estonia
ORCID: 0000-0002-2578-1910

Mart Tamre
Department of Electrical Power Engineering and Mechatrocnics
Tallinn University of Technology
Tallinn, Estonia
ORCID: 0000-0002-7489-9683

Rajiv Kapoor
Department of Electronics and Communication
Delhi Technological University
New Delhi, India
ORCID: 0000-0003-3020-1455

Dhanushka Chamara Liyanage
School of Engineering – Smallcraft Competence Center
Tallinn University of Technology
Tallinn, Estonia
ORCID: 0000-0003-4526-0837

***Abstract*— Frequency response of a Microwave (MW) cavity filter is changed by rotating the tuning screws installed on the filter surface. Numerous screws are present on the surface of the filter, not all of which contribute to the alteration of tuning state as some of the screws are just the plate mounting screws. This paper presents a vision-based method for distinguishing the tuning screws of a cavity filter from the mounting screws. The tuning screws used in industry are coated with a conducting material to avoid losses. In this work, through hyperspectral imaging, characteristic image bands of screws of a commercial cavity filter were analyzed. From this analysis, the tuning screws were identified using their material properties since every material or compound has its own reflectance to Electromagnetic (EM) waves. The novel band subtraction technique proposed in this work distinguished all the tuning screws from the mounting screws. This proposed technique was then validated using a monochrome industrial camera attached with suitable optical bandpass filters. Achieving the classification accuracy of 100% with a monochrome camera proved the effectiveness of the proposed method. The results obtained can be used to identify and locate the tuning screws especially for the case when the technical drawing of the filter is not available. These extracted positional coordinates of tuning screws can assist in Fully Automated Tuning (FAT) of the cavity filters.**

Keywords*— *Bandpass filters, Band Subtraction, Cavity Filter, Feature Extraction, Filter Tuning, Hyperspectral Imaging, Microwave filter, Monochrome camera, Screw Detection.

I. INTRODUCTION

Microwave (MW) cavity filters are used in Radio Base Stations (RBS) for separating the desired frequencies from tensed communication spectrum. To compensate for the mistakes like manufacturing defects, design errors, variations in material properties, mechanical tolerances etc., the assembled filters require tuning. Mechanical tuning, that uses tuning screws, is the most common way to tune the cavity filters. The frequency response of the filter is determined by the depth at which the tuning elements are inserted within the cavity. Now since, the filter tuning process is stochastic in nature, it is time consuming, laborious and requires skilled technicians to tune the filter to the desired frequency range [1].

A cavity filter is usually made up of a metallic block with screws on its top plate. Fig. 1 shows ta commonly used cavity filter. One can observe the presence of several screws on the assembled filter. Among these, the 'mounting screws' serve the purpose of holding the top metallic plate over the whole structure. The remaining screws are the 'tuning screws' which are used to alter the performance of the filter. The present research focuses on the filter type shown in Fig. 1

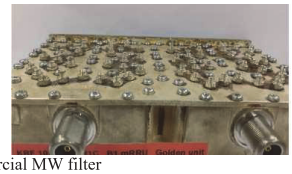

Fig. 1. A commercial MW filter

Fig. 2 presents the magnified portion of a small region of the cavity filter presented in Fig. 1. Noticeably the screws shown in Fig. 2 have different shapes (a mounting screw on bottom left corner and a tuning screw on the top right corner).

Fig. 2. Different types of screws of a cavity filter

The screws shown in Fig. 2 have different shapes and hence image processing techniques like shape detection/pattern matching/contour matching etc. could be used to differentiate them. However, the difference between the shapes of tuning screws and mounting screws is not guaranteed. Rather, commercial filters sometimes have same screw head for all the screws (tuning screws as well as mounting screws). Hence, a robust technique is needed to identify and classify the screws present on the filter structure.

This research work presents a novel band-subtraction technique for distinguishing the tuning screws and mounting

979-8-3503-2120-3/23/$31.00 ©2023 IEEE

screws of a MW cavity filter. The information about relevant bands was extracted using the datacube of a hyperspectral camera. The suggested methodology can assist in discriminating the screws on the basis of their material composition. The methodology plays crucial role for the case when no technical information about the filter and its screws is available. An in-depth analysis of the existing research reveals that no such methodology has been used or presented in the literature yet.

The remainder of the paper is structured in five sections. Section II presents the literature review of various screw detection techniques; Section III presents hyperspectral imaging (HSI) along with its application in metal detection. In section IV authors discuss the novel band-subtraction methodology for differentiating the screws. Experimentation results and their analysis is discussed in Section V. Section VI concludes the paper and provides future recommendations.

II. Literature Review: Screw Detection

In [2], authors used Canny operator-based edge detection technique to extract the contours and then template matching step was used to classify the screws. [3] presents a multi-template matching algorithm for the detection of screws and their semi-autonomous removal from the ceiling panel. The technique didn't hold firm grounds because of the following reasons – any change in color or illumination yielded inaccurate results; there was always a reliance on a fixed template and; every application would require a new template which is both tedious and time consuming. Hence, the major drawback of this technique was its lack of generalizability.

A combination of grayscale, color depth and HSV characteristics were used to achieve high accuracy in screw detection [4]. The algorithm was invariant to scale, translation and rotation but relied on Harris corner detection and HSV analysis, both getting influenced by the lighting conditions. Also, RGB depth sensor (Kinect) was needed to remove holes which demanded extra computations.

In 2018, a screw detection technique utilizing Hough circle detection was introduced [5]. However, its effectiveness was limited when dealing with multiple circular components. The commercial application of this method was further constrained due to the requirement of adjusting multiple parameters such as the camera's brightness settings. In [6], a fusion technique which combined the features extracted from Hough transform, and from Deep Learning (DL)-based classifier was presented. The work in [6] was then extended where the algorithm could additionally do the classification of 12 different types of screwheads [7]. While this work successfully eliminated the need for a depth sensor, the detection setup requirements were unsuitable for the production lines.

Some researchers used CNN-based techniques for screw detection applications. A combination of Faster R-CNN and RES (Rotation Edge Similarity) was used for classifying the screws [8] but the technique's commercialization was hindered by its paltry computational speed. Another Faster-RCNN-based model used general screw features for detecting the screws [9] using a DSLR camera. The authors combined image pre-processing and object detection steps with visual reasoning to achieve accurate results. The model's performance was enhanced by retraining it with true-negative results. Nevertheless, the image processing steps executed in this study had a substantial impact on the proposed model's performance.

The work presented in [10] is closely related to the one discussed in the current research. The authors of [10] used basic image processing techniques for detecting the tuning screws on the basis of its geometry. However, their work was reliant on a particular type of screw.

The dependencies of various screw detection techniques discussed above are listed in Table I. Each technique is constrained by one or more of these specific issues.

TABLE I. Dependencies of Screw Detection Techniques Available in Literature

Specification	Related Example
Device Specific	Electric motor screws, battery screws, etc.
Screw Specific	Shape and/or size of its head
Environment Specific	Illumination state, shadows, shiny objects
Methodology Specific	Stickers or other round objects detected as screws, damaged screws are not detected etc.

From Table I, it can be inferred that all the aforementioned methods of detecting the screws lack generalizability. Therefore, a more robust screw detection technique is needed to differentiate between the tuning and mounting screws.

Since the tuning screws are plated with silver and mounting screws are made of steel alloy, analyzing their reflectance characteristics by HSI can help in differentiating them. To date, this approach of tuning screw detection has not been reported in scholarly research. In the next section authors discuss research in the field of HSI and its application in detecting the coatings, metals and compounds.

III. Hyperspectral Imaging-Based Detection

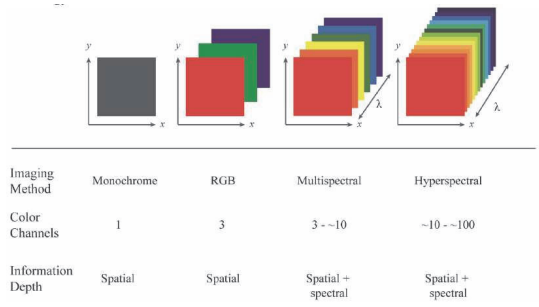

Fig. 3. Different image methods and their characteristics [11]

Fig. 3 displays various imaging techniques and their features. A monochrome camera considers the whole visible spectrum and only measures its integral intensity. Only the visible portion of EM spectrum (400-700 nm) is covered by RGB, which primarily contains spatial information. The RGB band is not appropriate for all applications, hence multispectral or hyperspectral cameras are employed instead. Multispectral

images are a collection of images captured in a continuous spectrum at several wavelength bands that form a datacube. Datacube is a 3D representation of spatial data (x and y coordinates) and spectral data (in the z-axis). A hyperspectral image is a multispectral image with hundreds of bands [12] that contains the entire wavelength spectrum for each pixel. Additionally, the wavelength range of hyperspectral images encompasses the ultraviolet to mid-infrared spectrum in addition to visible range. HSI combines spectroscopy and digital imaging. With this imaging technique, the scene is captured in narrow bandwidths, and necessary image bands can be selected from the datacube for further processing [13].

The reflectance characteristics of different materials produce a unique signature at different wavelength bands. Considering the scope of the current research work, the reflectance behavior of Silver (Ag) and Carbon Steel from 0.2 µm (200 nm) to 20 µm (20000 nm) wavelength can be seen in Fig. 4. Significant variations between the reflectance curves for two metals are visible. On the basis of this spectral signature, similar materials can be identified.

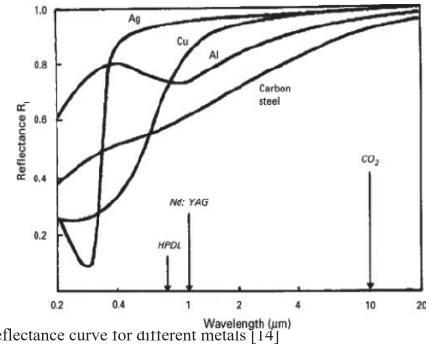

Fig. 4. Reflectance curve for different metals [14]

Since HSI contains hundreds of narrow bandwidth spectral bands, the majority of them are correlated and provide redundant information. Processing a large amount of data decreases the computational efficiency [15] due to the Hughes phenomenon [16]. Hence, it makes sense to choose the spectral bands that provide distinct characteristic information [17]. The main advantages of utilizing a band selection technique are the increase in classification accuracy [18] while preserving the intrinsic information of the original pixel [19], in addition to increase in computation efficiency.

In related literature, band selection technique has been used in determining the aluminium oxide thickness [20]. Several research groups have employed the HSI technique for detection of corrosion. Using HSI, corrosion on carbon steel samples [21][22], mild steel used in the aeronautical industry [23], copper [24] etc. has been detected. Researchers have also provided an SVM classifier-based Metal Object Detection (MOD) approach for identifying ferromagnetic, non-ferromagnetic, and non-metallic items [25].

A hypothesis that the tuning and mounting screws of a cavity filter can be differentiated using HSI was developed after reviewing the research into HSI-based methods for detecting the metals, metal coatings, and alloys. Since mounting screws are typically made of an alloy of steel and tuning screws used in industry are usually coated with a 3 µm silver layer (to increase the conductivity), their reflectance signature can be utilized to differentiate them from each other.

IV. Methodology

A. Imaging Setup

The initial attempts to detect the tuning screws were made using a Specim IQ Mobile Hyperspectral Camera [26]. In total, this hyperspectral camera has 204 image bands (for each pixel), a spectral resolution of 7 nm, and operates in the 400–1000 nm wavelength range. The reflectance values for all the bands can be displayed in the spectral distribution of each pixel. Using a calibrated tile with 99% reflectance, this camera is calibrated for white reference. After initial calibration, no further image processing steps are performed on HSI images. However, unlike RGB, HSI is unable to detect the geometry of the objects. Instead, the required bands are selected and forwarded to be processed further.

The overall configuration utilized to capture the image from the hyperspectral camera is shown in Fig. 5. A reference plate used for calibrating the Specim IQ camera can also be seen in Fig. 5. Two 400W halogen projectors were used for lighting, along with a light diffusing sheet. The halogen projectors were chosen as the light source since they cover a wider spectrum of wavelengths. The wavelength covered by halogen light spans from the UV region to the IR region in the EM spectrum. To ensure homogeneous lighting, the diffusing sheet was used.

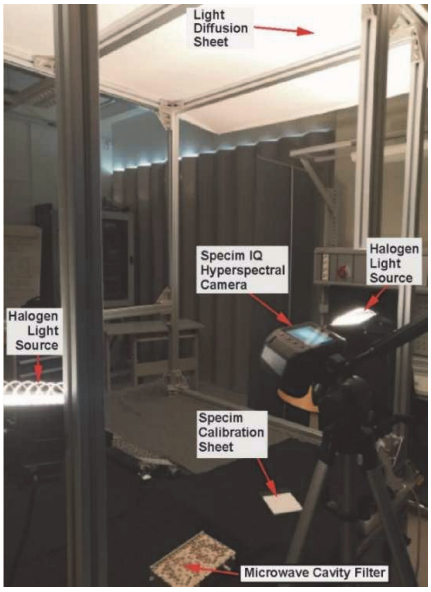

Fig. 5. Image acquisition setup

Even though a built-in RBG camera exists in the Specim IQ hyperspectral camera, the RGB image it produces has a different spatial resolution. Additionally, there can be misalignments between the RGB image and hyperspectral image in the vertical and/or horizontal direction. The RGB

scene of an image taken with a hyperspectral camera is displayed in Fig. 6, but only the marked area was used for HSI processing, as is the case with all only the marked area was used as shown in all other images in the following sections of this paper.

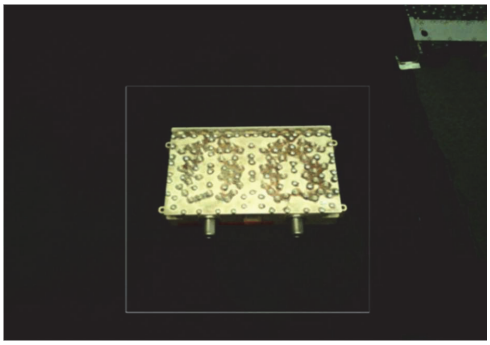

Fig. 6. RGB scene captured by a hyperspectral camera

B. Reflectance Trends

Tuning screws and mounting screws of a MW filter have different material composition. Since each material has its unique spectral characteristics, different band alternatives have to be tested in order to identify the effective spectral image bands to distinguish between the two types of screw.

Five screws from each category (05 tuning screws and 05 mounting screws) were chosen in order to retrieve the reflectance data from the screws that were installed on the filter under consideration. The purpose of considering many screws from each category was to precisely choose the appropriate bands using the mean reflectance value. Fig. 7a shows the locations of selected screws in one of the bands. The corresponding reflectance plots for all these screws are presented in Fig. 7b for the wavelength range of 400 nm to 1000 nm. The choice of bands was then made using the average reflectance value, as is covered in the next subsection.

C. Selection of Bands

After averaging the reflectance values of the chosen tuning and mounting screws were averaged, band 25 and band 190 were selected from the datacube. Band 25 has been chosen because it has the most distinguishing features for both types of screws (see a significant variation in reflectance between the two categories of screws in Fig. 7b). Band 25 has an approximate wavelength of 467 nm. Band 190, having wavelength of roughly 930 nm, was chosen from the opposite end of the datacube because it exhibits some similarities in features between the two screws (see Fig. 7b for a modest variation in reflectance characteristics in this band). It is significant to note that the authors chose band number 190 even though the difference between the two curves was minimal around band 197. This band was chosen in order to get rid of any spectral noise that might have been present in the last few bands near the end of the image. Images of bands 25 and 190 are shown in Figs. 8a and 8b, respectively.

D. Band Subtraction

Empirically, it was found that subtracting one band from the blue region (band number 25) and another band from the infrared (IR) region (band number 190) of the datacube could clearly differentiate tuning screws and mounting screws. As presented by (1), I_{result} image was obtained when a 467 nm image (I_{467}) was subtracted from a 930 nm image (I_{930}).

$$I_{result} = I_{930} - I_{467} \qquad (1)$$

Figure 8c, which shows the image produced adhering to band subtraction, makes it evident that the mounting screws looked noticeably darker when compared to the silver-plated tuning screws. With the aid of this knowledge, one can determine the coordinates for each tuning screw's location and tune a filter autonomously.

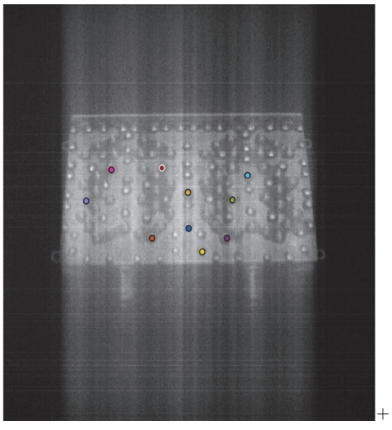

7 (a): Screw Locations on a Band Image

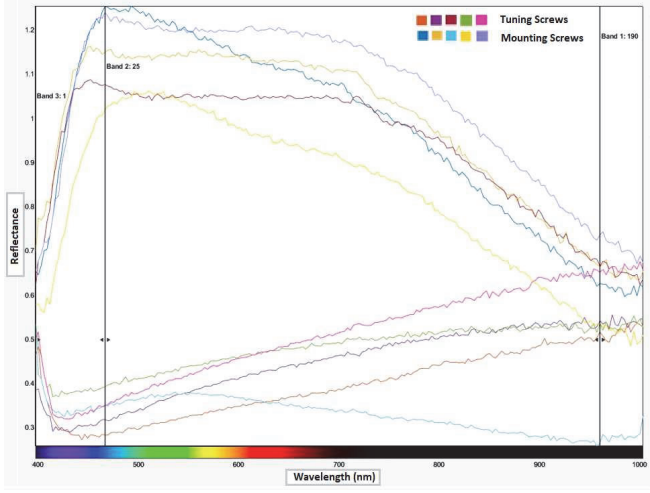

7 (b): Reflectance-Wavelength Plots

Fig. 7. Sampled 05 screws from each screw category and their reflectance response

8 (a). Band 25 Image

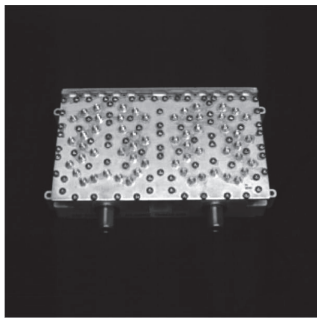

8 (b). Band 190 Image

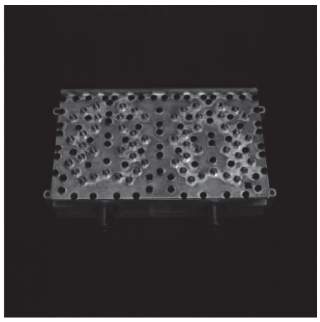

8 (c). Resultant Image after Band Subtraction

Fig. 8. Band selection and band subtraction results

V. Experimentation Results and Analysis

A. Specim Hyperspectral Camera

Fig. 9 displays the outcome of the band subtraction method applied to the image captured with the Specim hyperspectral camera. Both the RGB and the processed image, which is the result of band subtraction, are displayed next to each other for convenience.

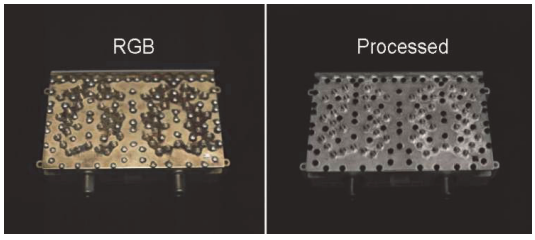

Fig. 9. Classification of screws using Specim hyperspectral camera

Fig. 9 demonstrates that using the suggested methods led to encouraging findings. The mounting screws stand out from the tuning screws owing to their darker appearance. As detailed in the following subsection, the efficiency of the postulated band subtraction methodology was then assessed on an industrial monochrome camera.

B. Besler Monochrome Camera

The analysis done on the hyperspectral images showed that the most effective spectral bands for the application considered in this work are band 25 and band 190, and they must be subtracted. This methodology was tested on the images acquired by an industrial monochrome camera.

To apply the suggested band subtraction process, the Basler camera with a progressive scan CCD-sensor for capturing VGA-640 x 480 images was used. The camera's connection with a compatible PC was made via an IEEE 1394 firewire interface. Two optical bandpass filters i.e., blue bandpass filter (associated to band 25) and IR bandpass filter (corresponding to band 190), were attached to the camera. Fig. 10 shows a Basler monochrome camera used in this work on which the light (optical) filters were mounted.

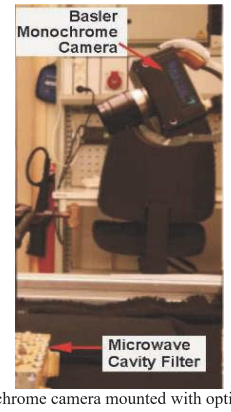

Fig. 10. Basler monochrome camera mounted with optical bandpass filters

It is evident from the findings displayed in Fig. 11 that the classification accuracy of 100% was reached by using the light bandpass filters (decided by our suggested methods) with a monochrome camera. As shown in Fig. 11, the mounting screws appear to be darker than the tuning screws.

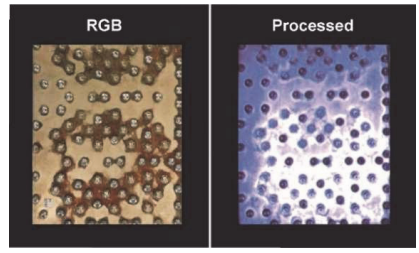

Fig 11. The results screws classified by the Besler monochrome camera

A monochrome camera, which is significantly less expensive and computationally efficient than a hyperspectral camera, can attain the same classification accuracy as a hyperspectral camera, as shown in Figures 10 and 11. The technique of automating cavity filter tuning can benefit from this study's conclusions. Once the tuning screws have been differentiated, a robotic manipulator can be instructed to tune a filter based on their spatial coordinates.

VI. Conclusion

In this research, the tuning screws, that are used to tune a MW cavity filter, were distinguished using a novel band selection method. The analysis made on the images acquired from a hyperspectral camera helped in selecting the most efficient spectral bands from the hyperspectral datacube. Empirically, it was found that the suggested band subtraction methodology could distinguish between the screws according to their material composition. The process was subsequently tested on an industrial monochrome camera fitted with the appropriate optical bandpass filters. The conclusions were validated by the results, which showed that a monochrome camera—which is less expensive and computationally more effective than a hyperspectral camera—was able to detect and classify screws with 100% accuracy. Based on a comprehensive analysis, it can be concluded that the methodology utilized in this study is highly effective in distinguishing and categorizing various types of screws. The proposed methodology plays a pivotal role for the case when the technical drawings of the filter is not available. The camera can be set in perspective view or can be mounted overhead. The position coordinates of tuning screws thus determined can be utilized in a FAT system for MW filters.

References

[1] R. V. Snyder, "Practical aspects of microwave filter development," *IEEE Microwave Magazine 8*, no. April, pp. 42–54, 2007.

[2] P. Gil, J. Pomares, S. V. T. Puente, C. Diaz, F. Candelas, and F. Torres, "Flexible multi-sensorial system for automatic disassembly using cooperative robots," *Int J Comput Integr Manuf*, vol. 20, no. 8, pp. 757–772, Dec. 2007, doi: 10.1080/09511920601143169.

[3] S. R. Cruz-Ramirez, Y. Mae, T. Takubo, and T. Arai, "Detection of screws on metal-ceiling structures for dismantling tasks in buildings," in *IEEE/RSJ International Conference on Intelligent Robots and Systems, Nice - France*, 2008.

[4] M. Bdiwi, A. Rashid, and M. Putz, "Autonomous disassembly of electric vehicle motors based on robot cognition," in *IEEE International Conference on Robotics and Automation, Stockholm - Sweden*, 2016.

[5] N. M. Difilippo and M. K. Jouaneh, "A system Combining Force and Vision Sensing for Automated Screw Removal on Laptops," *IEEE Transactions on Automation Science and Engineering*, vol. 15, no. 2, pp. 887–895, Apr. 2018, doi: 10.1109/TASE.2017.2679720.

[6] E. Yildiz and F. Worgotter, "DCNN-Based screw detection for automated disassembly processes," in *Proceedings - 15th International Conference on Signal Image Technology and Internet Based Systems, SISITS 2019*, Institute of Electrical and Electronics Engineers Inc., Nov. 2019, pp. 187–192. doi: 10.1109/SITIS.2019.00040.

[7] E. Yildiz and F. Wörgötter, "DCNN-based screw classification in automated disassembly processes," in *ROBOVIS 2020 - Proceedings of the International Conference on Robotics, Computer Vision and Intelligent Systems*, SciTePress, 2020, pp. 61–68. doi: 10.5220/0009979900610068.

[8] X. Li *et al.*, "Accurate screw detection method based on faster R-CNN and rotation edge similarity for automatic screw disassembly," *Int J Comput Integr Manuf*, vol. 34, no. 11, pp. 1177–1195, 2021, doi: 10.1080/0951192X.2021.1963476.

[9] G. Foo, S. Kara, and M. Pagnucco, "Screw detection for disassembly of electronic waste using reasoning and re-training of a deep learning model," in *Procedia CIRP*, Elsevier B.V., 2021, pp. 666–671. doi: 10.1016/j.procir.2021.01.172.

[10] C. Yao, Y. Yuan, J. Li, and L. Bi, "High Precision Tuning Device of Microwave Cavity Filter based on Hand-Eye Coordination," *Chinese Control Conference, CCC*, vol. 2019-July, pp. 7063–7068, 2019, doi: 10.23919/ChiCC.2019.8866244.

[11] D. C. Liyanage, M. Tamre, and R. Hudjakov, "Hyperspectral/Multispectral Imaging Methods for Quality Control," in *Handbook of Research on New Investigations in Artificial Life, AI, and Machine Learning*, M. K. Habib, Ed., Hershey, PA, USA: IGI Global, 2022, pp. 438–461. doi: 10.4018/978-1-7998-8686-0.ch017.

[12] J. M. Amigo, "Hyperspectral and multispectral imaging: setting the scene," in *Data Handling in Science and Technology*, Elsevier Ltd, 2020, pp. 3–16. doi: 10.1016/B978-0-444-63977-6.00001-8.

[13] S. Jia, L. Shen, J. Zhu, and Q. Li, "A 3-D gabor phase-based coding and matching framework for hyperspectral imagery classification," *IEEE Trans Cybern*, vol. 48, no. 4, pp. 1176–1188, Apr. 2018, doi: 10.1109/TCYB.2017.2682846.

[14] M. M. Quazi, M. A. Fazal, A. S. M. A. Haseeb, F. Yusof, H. H. Masjuki, and A. Arslan, "Laser-based surface modifications of aluminum and its alloys," *Critical Reviews in Solid State and Materials Sciences*, vol. 41, no. 2, pp. 106–131, Mar. 2016, doi: 10.1080/10408436.2015.1076716.

[15] F. Luo, B. Du, L. Zhang, L. Zhang, and D. Tao, "Feature learning using spatial-spectral hypergraph discriminant analysis for hyperspectral image," *IEEE Trans Cybern*, vol. 49, no. 7, pp. 2406–2419, Jul. 2019, doi: 10.1109/TCYB.2018.2810806.

[16] G. F. Hughes, "On the mean accuracy of statistical pattern recognizers," *IEEE Trans Inf Theory*, vol. IT-14, no. 1, pp. 55–63, 1968.

[17] W. Sun and Q. Du, "Hyperspectral band selection: A review," *IEEE Geoscience and Remote Sensing Magazine*, vol. 7, no. 2, Institute of Electrical and Electronics Engineers Inc., pp. 118–139, Jun. 01, 2019. doi: 10.1109/MGRS.2019.2911100.

[18] Q. Wang, F. Zhang, and X. Li, "Optimal clustering framework for hyperspectral band selection," *IEEE Transactions on Geoscience and Remote Sensing*, vol. 56, no. 10, pp. 5910–5922, Oct. 2018, doi: 10.1109/TGRS.2018.2828161.

[19] Y. Zhan, D. Hu, H. Xing, and X. Yu, "Hyperspectral band selection based on deep convolutional neural network and distance density," *IEEE Geoscience and Remote Sensing Letters*, vol. 14, no. 12, pp. 2365–2369, Dec. 2017, doi: 10.1109/LGRS.2017.2765339.

[20] F. Gruber, P. Wollmann, B. Schumm, W. Grählert, and S. Kaskel, "Quality control of slot-die coated aluminum oxide layers for battery applications using hyperspectral imaging," *J Imaging*, vol. 2, no. 2, Jun. 2016, doi: 10.3390/jimaging2020012.

[21] T. De Kerf, G. Pipintakos, Z. Zahiri, S. Vanlanduit, and P. Scheunders, "Identification of corrosion minerals using shortwave infrared hyperspectral imaging," *Sensors*, vol. 22, no. 1, Jan. 2022, doi: 10.3390/s22010407.

[22] T. De Kerf, A. Gestels, K. Janssens, P. Scheunders, G. Steenackers, and S. Vanlanduit, "Quantitative detection of corrosion minerals in carbon steel using shortwave infrared hyperspectral imaging," *RSC Adv*, vol. 12, no. 50, pp. 32775–32783, Nov. 2022, doi: 10.1039/d2ra05267a.

[23] M. M. Antony, C. S. S. Sandeep, and M. V. Matham, "High resolution probe for corrosion monitoring using hyper spectral imaging," in *AIP Conference Proceedings*, American Institute of Physics Inc., Feb. 2021. doi: 10.1063/5.0036100.

[24] M. Al Ktash *et al.*, "UV hyperspectral imaging as process analytical tool for the characterization of oxide layers and copper states on direct bonded copper," *Sensors*, vol. 21, no. 21, Nov. 2021, doi: 10.3390/s21217332.

[25] Y. Tian *et al.*, "Metal object detection for electric vehicle inductive power transfer systems based on hyperspectral imaging," *Measurement (Lond)*, vol. 168, Jan. 2021, doi: 10.1016/j.measurement.2020.108493.

[26] Specim Spectral Imaging Ltd, "Specim IQ Technical Specifications," Apr. 14, 2019. https://www.specim.com/iq/tech-specs/ (accessed Apr. 10, 2023).

Publication V

E. Sekhri, M. Tamre, R. Kapoor and R. Kumar, "A Novel Real-time Parametric Tracking Approach for Robust Microwave Filter Tuning," *2023 The IEEE International Conference on Artificial Intelligence, Blockchain and Internet of Things (AIBThings)*, Mount Pleasant, MI, USA, 2023, pp. 1–5, doi: 10.1109/AIBThings58340.2023.10292473.

A Novel Real-Time Parametric Tracking Approach for Robust Microwave Filter Tuning

2023 IEEE International Conference on Artificial Intelligence, Blockchain, and Internet of Things (AIBThings) | 979-8-3503-2234-7/23/$31.00 ©2023 IEEE | DOI: 10.1109/AIBThings58340.2023.10292473

Even Sekhri*
Department of Electrical Power Engieering and Mechatronics
Tallinn University of Technology
Tallinn, Estonia
0000-0002-2578-1910

Mart Tamre
Department of Electrical Power Engieering and Mechatronics
Tallinn University of Technology
Tallinn, Estonia
0000-0002-7489-9683

Rajiv Kapoor
Department of Electronics and Communication Engieering
Delhi Technological University
New Delhi, India
0000-0003-3020-1455

Rahul Kumar
Department of Electronics and Communication Engieering
Delhi Technological University
New Delhi, India
0000-0002-5068-5488

***Abstract*—The robust tracking of tuning parameters is crucial in enhancing the efficiency of automated filter tuning. The existing automated filter tuning methods use the phase plot information at the center frequency of filter and extract tuning parameters represented by the marker position. This paper presents a vision-based approach for tracking the tuning parameters over the Smith chart display of Vector Network Analyzer (VNA) using Deep Learning (DL). Using a camera to detect the marker allows the ease in presenting the proof of concept without accessing or modifying the commercial VNA's software. The realm of microwave cavity filter tuning has yet to incorporate real-time parametric tracking of tuning parameters on a Smith chart. For training the DL network, a labeled dataset has been curated. Manual tuning of a 5th order cavity filter (a filter with 5 tuning screws) was used to test the proposed method. Results obtained in this research demonstrates that the proposed method outperforms the state-of-the-art techniques in terms of tracking performance. The mAP value was determined to be 98.2% using YOLOv5. The robustness of the suggested method has been demonstrated through rigorous testing of the proposed technique on the polar plot display of the VNA. This methodology holds the potential for complete automation of the filter tuning process.**

Keywords—filter tuning, marker detection, microwave filter tuning, parametric tracking, robust tracking, Faster-CNN, Single-Shot Detector (SSD), YOLOv5

I. INTRODUCTION

Microwave (MW) cavity bandpass filters are commonly employed to isolate the desired signal amidst a crowded frequency spectrum. These filters require tuning to compensate for design imperfections and manufacturing errors [1]. Tuning a filter using the phase response of the reflection coefficient (S_{ii}, where i = number of ports) is a common way of tuning all-pole filters [2]. To determine the phase change, the tuning parameter variations at the center frequency of the filter are observed. Using the Smith chart plot on the Vector Network Analyzer (VNA) equipment is another approach to monitor the phase change. Researchers striving to automate the filter tuning process often overlook Smith chart-based tuning due to two primary reasons: a) the complexity involved in dealing with the "infinity" term on the short-circuit side of the Smith chart; and, b) the simultaneous variation of the resistance value and reactance value (capacitive reactance or inductive reactance) while tuning the filter. However, by precisely tracking the marker movement on the Smith chart, there is a possibility for achieving autonomous filter tuning.

The research community has put forth numerous techniques for Computer-Aided Tuning (CAT) of MW filters, offering a wide array of options for the tuning process including filter diagnosis [2][3][4][5][6][7], Time Domain (TD) [8][9], Group Delay (GD) [10], Space Mapping (SM) [11][12][13][14], Fuzzy Logic (FL) [15][16][17][18], Artificial Neural Network (ANN) [19][20][21][22], etc. TD-based tuning solutions needed a human operator to actually tune the filter. The filter diagnosis-based solutions rely on circuit models, which are inherently inexact. The automated filter tuning was attempted on data-driven algorithms based on SM [12] and FL [18]. The accuracy of SM-based filter tuning approach is dependent on the complexity of the coarse model and the fine model. The commercialization of FL-based filter tuning was hampered by the necessity of a large number of 'IF-THEN' linguistic fuzzy rules. Despite the wide range of CAT-based filter tuning techniques and automated filter tuning solutions documented in the literature, none of the existing approaches have addressed the tracking of tuning parameters variation at the filter's center frequency. Also, the utilization of Smith chart for automated filter tuning has not been considered.

With the significant boost in computational power over the recent years, DL-based algorithms have gained prevalent traction in the fields of object detection and tracking [23]. DL-based approaches not only possess powerful learning capabilities but also excel at handling challenges such as occlusion, scale transformation, and varying background etc. The DL-based object detection approaches can be divided into two categories i.e., region-based methods; and regression model-based methods. The region-based methods include Region-based Convolutional Neural Network (R-CNN) [24], Spatial Pyramid Pooling network (SPP-net) [25], Fast R-CNN [26], Faster R-CNN [27], Region-based Fully Convolutional Networks (R-FCN) [28], Feature Pyramid Networks (FPN) [29], Mask R-CNN [30] etc. Each region-based method follows a two-step process. In the initial step, an attention mechanism scans the entire image, mimicking the operation of a human brain. In the second step, focus is directed towards the Region of Interest (ROI). In contrast, regression-based methods like MultiBox [31], AttentionNet [32], G-CNN [33], Different versions of YOLO [34], Single Shot Detector (SSD) [35], Deconvolutional Single Shot Detector (DSSD) [36], and Deep Supervised Object Detectors (DSOD) [37] use regressive technique in a single stage for drawing the bounding boxes. However, aforementioned algorithms have primarily been developed for the detection and/or tracking of specific entities such as persons, cars, Unmanned Aerial Vehicles (UAVs), animals, and more. The use of any of these tracking techniques as a VNA marker detector (a representative entity of tuning

parameter variation) still remains unexplored and lacks published research.

The current research proposes a novel and robust method for tracking the variation in the tuning parameters on the Smith chart using YOLOv5. To train the DL model, a meticulously labeled dataset containing approximately 5000 images was specifically created (uploaded at IEEE dataport [38]). To increase the accuracy, a pre-processing stage was carried out to select the Region of Interest (ROI). The accuracy was further improved by incorporating multilevel thresholding in the pre-processing phase. The performance of the proposed method was compared with state-of-the-art tracking techniques. The accuracy of the results serves as compelling evidence for the robustness of the proposed methodology.

The remainder of the paper is structured as follows: Section II presents the proposed marker tracking methodology. The results of the current research work are discussed in Section III, along with a comparative analysis with other state-of-the-art tracking methodologies. Section IV provides the conclusion of the research conducted, along with a delineation of future prospects and potential areas for further exploration.

II. Proposed Methodology

A. Dataset generation

For tuning the filter using the marker tracking approach, a labeled marker dataset was created using Keysight Fieldfox RF Analyzer 9914A – 6.5 GHz [39]. The dataset images were taken whilst the cavity filter was being manually tuned. After collecting the images, they were labeled. The total dataset comprises of 4967 labeled images. The procedure for gathering the images for dataset is depicted in Fig. 1.

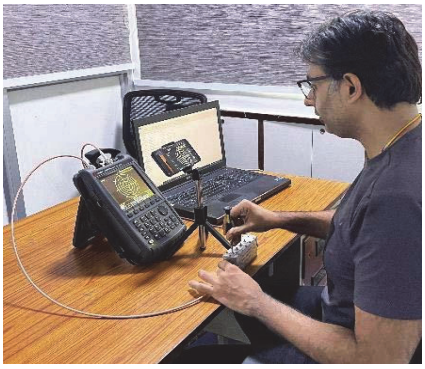

Fig. 1. Dataset generation while manual tuning the filter. A smartcamera looking at VNA is capturing the frames

The bifurcation of the dataset in terms of number of images and training-validation-test dataset split is presented in Table I.

TABLE I. Dataset Details

Category	Number	Split
Training Dataset	3475	70%
Validation Dataset	992	20%
Testing Dataset	500	10%
Total	4967	100%

B. Deep Network Training

Before training the network, the labeled images were not preprocessed. Cross-validation stage was not utilized in this work, either. The implementation of the deep networks was performed using the system possessing the configuration Ryzen-9 5800 HS CPU, 16 GB RAM and NVIDIA - RTX3060 with 6 GB GPU.

With a batch size of 16; 640 x 640 sized images; and 100 epochs, the model was trained using YOLOv5. This model was trained with Stochastic Gradient Descent (SGD) optimizer with a learning rate of 0.01 and a decaying factor of 0.005. Completion of one epoch meant that both Feed Forward (FF) and Back Propagation (BP) have finished for the entire dataset for training. With a learning rate of 0.01 it took 1 h 37 min to train the YOLOv5 model. The precision-recall curve obtained after training the deep network is illustrated in Fig. 2. The descending slope confirms the effectiveness of the network training.

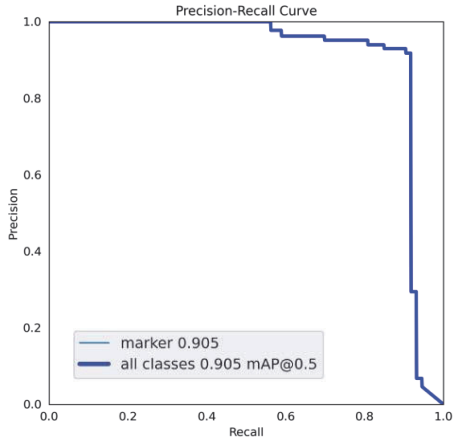

Fig. 2. The Precision-Recall Curve

C. Detection of Marker

After training of the deep network, the trained model was evaluated on the Smith chart of the VNA. A 5-pole cavity filter (filter having 5 tuning screws) that was being manually tuned was connected to the VNA. The phase change of the input reflection coefficient (S_{11}) on Smith chart plot was tracked in real-time.

For tracking the marker, a smartphone's camera was used as an IP web-camera to acquire the real-time video of a VNA's Smith chart plot. Adding a camera into the system allows us to present the proof of concept without accessing or changing the commercial VNA's software. As mentioned in Section II B, the dataset was trained on the raw images. However, for testing the model, the ROI was selected to remove the noise, thus, increasing the accuracy of results. Though some incorrectly classified marker occurrences were seen, the tracking results were considered to be encouraging. Therefore, another segmenting approach i.e. a multi-level thresholding step was added as an additional pre-processing step to further improve the accuracy of the marker tracking. The overall tracking scheme is presented in Fig. 3.

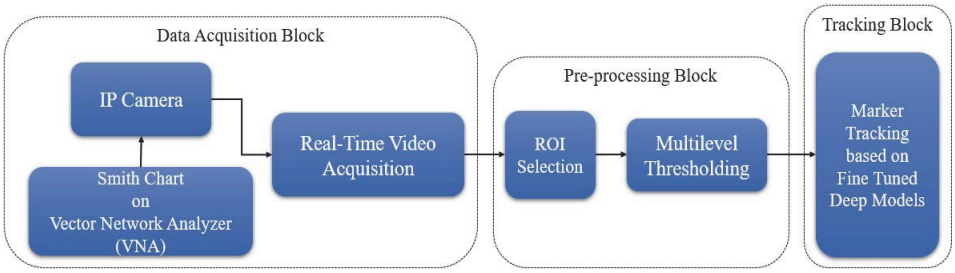

Fig. 3. Tuning Parameter Variation Detection Process

Adding multi-level thresholding assisted in tracking the marker accurately. The multi-thresholding technique also ensured that the marker is clearly visible throughout the filter tuning and is not obscured by several circles on the VNA. The resultant images after applying the pre-processing steps on the acquired images are presented in Fig. 4 and Fig. 5.

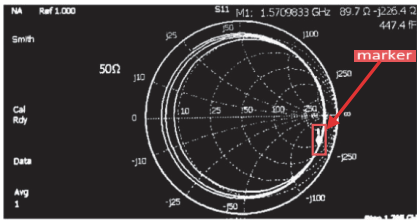

Fig. 4. Defining the marker entity and its position before initiating the tuning (VNA not calibrated)

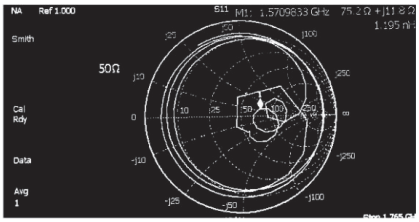

Fig. 5. Marker position when the last screw is about to be tuned

Fig. 4 presents the initial position of the marker prior to tuning the filter and Fig. 5 presents the scenario when the last screw is nearly tuned.

The overall setup for tracking the marker in real-time is displayed in Fig. 6. The marker is being tracked on the considered system while the filter is being manually tuned.

Fig. 6. The overall setup for tracking the marker in real-time

III. Results and Comparative Analysis

After video acquisition and preprocessing, the movement of marker within the ROI was tracked while tuning the filter. The trained DL-based model drew a bounding box around the center frequency marker as depicted in Fig. 7 and Fig. 8. The marker tracking result shown in Fig. 7 is for the case when the first screw was tuned starting from the marker's initial position (shown in Fig. 4). All the tuning screws were tuned sequentially in this work, starting from the filter's input side to its output side i.e. from first resonator to the last resonator. Fig. 8 depicts the marker being tracked while the filter's final tuning screw is turned (all the previous screws have been tuned). A video showing the real-time marker tracking on the Smith chart is publicly available[1].

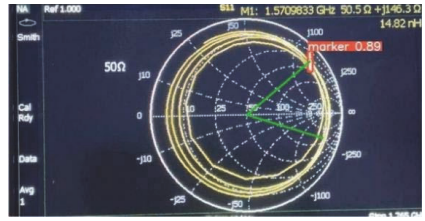

Fig. 7. Marker being tracked while tuning the first screw is getting tuned

Fig. 8. Marker tracking when last screw is tuned

The green lines in Fig. 7 and Fig. 8 show the marker tracking results w.r.t. a reference line. Among both green lines, the reference line is the one which is drawn between the center of Smith chart (50 Ω point) and the centroid of marker at its initial position (shown in Fig. 4). This reference line holds its position throughout the tracking process. When the filter is tuned manually, the second green line tracks the marker movement on the VNA's Smith chart in real-time.

The output of the YOLOv5-based model was compared to those of the Faster R-CNN and SSD techniques. The specifics of training the YOLOv5 model are previously covered in

[1] https://drive.google.com/file/d/1wzAYKqaHbO9KfMKuJodRXBITJSt6x7-n/view?usp=sharing

Section II B. The same batch size and image size were considered for the comparative analysis. While training the Faster R-CNN model, the Stochastic Gradient Descent (SGD) optimizer with a momentum value of 0.9 and the weight adjusting parameter of 10 were used. With a learning rate of 0.001, and 1500 epochs, the Faster-CNN model took almost 5 h 40 min for completion of training. The SSD model used RMSProp optimizer and the SSD model training took 4 h 43 min when 1500 epochs, decay factor 0.9, and learning rate 0.001 were defined.

Table II provides the comparative analysis of the results. The outcomes are for the scenario in which the aforementioned pre-processing steps were also implemented while testing the different tracking methodologies.

TABLE II. COMPARITIVE ANALYSIS

Tracking Technique	Entity	Value
With YOLOv5 (Proposed)	mAP	98.2%
	Precision	97.7%
	Recall	97.3%
Faster R-CNN [27]	mAP	95.8%
	Precision	94.7%
	Recall	93.4%
Single-Shot Detector (SSD) [35]	mAP	94.0%
	Precision	93.2%
	Recall	93.1%

As evident from Table II, the mAP, Precision and Recall values of the model trained using YOLOv5 are better as compared to Faster R-CNN and SSD techniques. Using YOLOv5 tracking, the maximum mAP of 98.2% was attained during testing. While testing the trained YOLOv5 model, only one misclassification occurrence is seen in the video link mentioned in footnote 1 (on previous page). By increasing the dataset, the tracking accuracy can further be increased.

To test the robustness of the proposed methodology, the tracking was tested on polar display of the marker without implementing the pre-processing techniques used. The overall performance got reduced by approximately 1.27% when pre-processing step was excluded. As evident from Fig. 9, the confidence level of the marker also went down when compared to Fig. 7 and Fig. 8. The polar display of the VNA shows the concentric reflection circles (whereas the Smith chart display presents superimposed resistance and reactance circles). The tuning parameter tracking results for the polar chart are made publicly available[2]. Even though the dataset was generated using the Smith chart display, the proposed methodology nevertheless produced promising tracking results on a VNA polar plot, demonstrating its robustness.

Fig. 9. Tracking the tuning parameters in polar plot without implementing the preprocessing block presented in Fig 3.

During the evaluation of the methodology on a polar chart, it was observed that the accuracy of marker detection was lower compared to that on the Smith chart. Furthermore, there were occasional misclassifications and brief instances where the marker disappeared from the frame. By incorporating a polar chart image dataset and expanding the number of images in the dataset, the efficiency of tracking-based filter tuning can be enhanced.

IV. CONCLUSION AND FUTURE SCOPE

Accurate marker tracking is pivotal for achieving efficient tuning of the MW filters. This research focused on developing a robust vision-based technique to track the marker position in the Smith chart of the VNA. A labeled dataset was curated to train the deep network. While testing the proposed methodology on a cavity filter with 5 tuning screws, YOLOv5 showed the highest mAP value of 98.2% when compared with other state-of-the-art tracking techniques. The methodology was also tested on the VNA's polar chart without implementing the pre-processing stage and without creating the dataset specifically related to polar chart display of the VNA. The demonstrated accuracy of the results serves as testament to the robustness of the proposed method.

In future, this research will be expanded to encompass automated filter tuning through a marker tracking-based approach. Researchers also aim to curate a more extensive dataset, which will serve to improve the tracking accuracy and boost the marker's confidence level while tracking. Additionally, a specific module will be introduced to commercial VNA's software for tracking the tuning parameter variations.

REFERENCES

[1] R. J. Cameron, "Computer-Aided Diagnosis and Tuning of Microwave Filters," in *Microwave Filters for Communication Systems: Fundamentals, Design and Applications, Second Edition*, 2018, pp. 609–642.

[2] H. T. Hsu, H. Yao, K. A. Zaki, and A. E. Atia, "Computer-Aided Diagnosis and Tuning of Cascaded Coupled Resonators Filters," *IEEE Trans Microw Theory Tech*, vol. 50, no. 4, pp. 1137–1145, 2002.

[3] H. Hsu, H. Yao, K. A. Zaki, and A. E. Atia, "Computer-Aided Diagnosis and Tuning of Cascaded Coupled Resonator Filters," *IEEE Trans Microw Theory Tech*, vol. 50, no. 4, pp. 1137–1145, 2002, doi: 10.1109/22.993417.

[4] G. Pepe, F. Gortz, and H. Chaloupka, "Computer-Aided Tuning and Diagnosis of Microwave Filters using Sequential Parameter Extraction," in *2004 IEEE MTT-S International Microwave Symposium Digest, Fort Worth, TX, USA*, 2004, pp. 1373–1376. doi: 10.1109/MWSYM.2004.1338824.

[5] M. Meng and K. L. Wu, "An Analytical Approach to Computer-Aided Diagnosis and Tuning of Lossy Microwave Coupled Resonator Filters," *IEEE Trans Microw Theory Tech*, vol. 57, no. 12, pp. 3188–3195, 2009, doi: 10.1109/TMTT.2009.2033868.

[6] W. Meng and K. L. Wu, "Analytical Diagnosis and Tuning of Narrowband Multicoupled Resonator Filters," *IEEE Trans Microw Theory Tech*, vol. 54, no. 10, pp. 3765–3771, 2006, doi: 10.1109/TMTT.2006.881623.

[7] S. Wu, C. Liu, W. Cao, and M. Wu, "A New Method for Hybrid Diagnosis and Tuning of Coaxial Cavity Filter," in *2017 36th Chinese Control Conference (CCC 2017), Dalian, China*, 2017, pp. 9692–9696. doi: 10.23919/ChiCC.2017.8028902.

[8] J. Dunsmore, "Tuning Band Pass Filters in the Time Domain," in *1999 IEEE MTT-S International Microwave Symposium Digest,*

[2] https://drive.google.com/file/d/1G8V77oR8zpIWrSALvRlRqjUMv4sJ4gzw/view?usp=sharing

Anaheim, CA, USA, 1999, pp. 1351–1354. doi: 10.1109/MWSYM.1999.779638.

[9] J. Dunsmore, "Advanced Filter Tuning using Time Domain Transforms," in *29th European Microwave Conference, EuMC 1999, Munich Germany*, 1999, pp. 72–75. doi: 10.1109/EUMA.1999.338412.

[10] J. B. Ness, "A Unified Approach to the Design, Measurement and Tuning of Coupled-Resonator Filters," *IEEE Trans Microw Theory Tech*, vol. 46, no. 4, pp. 343–351, 1998, doi: 10.1109/22.664135.

[11] S. Li and P. D. Laforge, "A Post-Fabrication Tuning Method for a Varactor-Tuned Microstrip Filter using the Implicit Space Mapping Technique," in *IEEE MTT-S International Microwave Symposium, Phoenix, AZ, USA*, Pheoniz, AZ, USA, 2015, pp. 1–4. doi: 10.1109/MWSYM.2015.7167087.

[12] J. C. Melgarejo, J. Ossorio, S. Cogollos, M. Guglielmi, V. E. Boria, and J. W. Bandler, "On Space Mapping Techniques for Microwave Filter Tuning," *IEEE Trans Microw Theory Tech*, vol. 67, no. 12, pp. 4860–4870, 2019, doi: 10.1109/TMTT.2019.2944361.

[13] S. Li, X. Fan, P. D. Laforge, and Q. S. Cheng, "A Post-fabrication Tuning Method using Space Mapping and Surrogate Modeling Techniques," in *2019 49th European Microwave Conference, (EuMC 2019), Paris, France*, Paris, France: European Microwave Association (EuMA), 2019, pp. 392–395. doi: 10.23919/EuMC.2019.8910767.

[14] S. Li, X. Fan, P. D. Laforge, and Q. S. Cheng, "Surrogate Model-Based Space Mapping in Postfabrication Bandpass Filters' Tuning," *IEEE Trans Microw Theory Tech*, vol. 68, no. 6, pp. 2172–2182, 2020, doi: 10.1109/tmtt.2020.2977022.

[15] V. Miraftab and R. R. Mansour, "Computer-Aided Tuning of Microwave Filters using Fuzzy Logic," *IEEE Trans Microw Theory Tech*, vol. 50, no. 12, pp. 2781–2788, 2002, doi: 10.1109/TMTT.2002.805291.

[16] V. Miraftab and R. R. Mansour, "Tuning of Microwave Filters by Extracting Human Experience using Fuzzy Logic," in *2005 IEEE MTT-S International Microwave Symposium Digest, Long Beach, CA, USA*, Long Beach, CA, USA: IEEE, 2005, pp. 1605–1608. doi: 10.1109/MWSYM.2005.1517011.

[17] V. Miraftab and R. R. Mansour, "Automated Microwave Filter Tuning by Extracting Human Experience in terms of Linguistic Rules using Fuzzy Controllers," in *2006 IEEE MTT-S International Microwave Symposium Digest, San Francisco, CA, USA*, 2006, pp. 1439–1442. doi: 10.1109/MWSYM.2006.249541.

[18] V. Miraftab and R. R. Mansour, "Fully Automated RF/Microwave Filter Tuning by Extracting Human Experience using Fuzzy Controllers," *IEEE Transactions on Circuits and Systems - 1: Regular Papers*, vol. 55, no. 5, pp. 1357–1367, 2008, doi: 10.1109/TCSI.2008.916614.

[19] J. J. Michalski, "Artificial Neural Networks Approach in Microwave Filter Tuning," in *Progress In Electromagnetics Research M*, 2010, pp. 173–188.

[20] T. Kacmajor, P. Kant, and J. J. Michalski, "Microwave Filter Tuning for Different Center Frequencies based on Artificial Neural Network and Phase Compensation," in *2014 20th International Conference on Microwaves, Radar and Wireless Communications (MIKON 2014), Gydnia, Poland*, 2014, pp. 1–4. doi: 10.1109/MIKON.2014.6899833.

[21] J. J. Sun, S. Sun, X. Yu, Y. P. Chen, and J. Hu, "A Deep Neural Network based Tuning Technique of Lossy Microwave Coupled Resonator Filters," *Microw Opt Technol Lett*, vol. 61, no. 9, pp. 2169–2173, 2019, doi: 10.1002/mop.31866.

[22] S. B. Wu and W. H. Cao, "Tuning Model for Microwave Filter by using Improved Back-Propagation Neural Network based on Gauss Kernel Clustering," *International Journal of RF and Microwave Computer-Aided Engineering*, vol. 29, no. 8, pp. 1–10, 2019, doi: 10.1002/mmce.21787.

[23] Z. Q. Zhao, P. Zheng, S. T. Xu, and X. Wu, "Object Detection with Deep Learning: A Review," *IEEE Trans Neural Netw Learn Syst*, vol. 30, no. 11, pp. 3212–3232, Nov. 2019, doi: 10.1109/TNNLS.2018.2876865.

[24] R. Girshick, J. Donahue, T. Darrell, and J. Malik, "Rich feature hierarchies for accurate object detection and semantic segmentation," in *Proceedings of the IEEE Computer Society Conference on Computer Vision and Pattern Recognition*, IEEE Computer Society, Sep. 2014, pp. 580–587. doi: 10.1109/CVPR.2014.81.

[25] K. He, X. Zhang, S. Ren, and J. Sun, "Spatial Pyramid Pooling in Deep Convolutional Networks for Visual Recognition," in *European Conference on Computer Vision, Zurich, Switzerland*, 2014, pp. 346–361. [Online]. Available: http://arxiv.org/abs/1406.4729v1.

[26] R. Girshick, "Fast R-CNN," in *2015 IEEE International Conference on Computer Vision (ICCV)*, IEEE, Dec. 2015, pp. 1440–1448. doi: 10.1109/ICCV.2015.169.

[27] S. Ren, K. He, R. Girshick, and J. Sun, "Faster R-CNN: Towards Real-Time Object Detection with Region Proposal Networks," in *NIPS'15: Proceedings of the 28th International Conference on Neural Information Processing Systems - Volume 1*, IEEE Computer Society, Jun. 2015, pp. 91–99. doi: 10.1109/TPAMI.2016.2577031.

[28] J. Dai, Y. Li, K. He, and J. Sun, "R-FCN: Object Detection via Region-based Fully Convolutional Networks," in *30th Conference on Neural Information Processing Systems (NIPS 2016), Barcelona, Spain*, 2016, pp. 379–387. [Online]. Available: https://github.com/daijifeng001/r-fcn.

[29] T. Y. Lin, P. Dollár, R. Girshick, K. He, B. Hariharan, and S. Belongie, "Feature pyramid networks for object detection," in *Proceedings - 30th IEEE Conference on Computer Vision and Pattern Recognition, CVPR 2017*, Institute of Electrical and Electronics Engineers Inc., Nov. 2017, pp. 936–944. doi: 10.1109/CVPR.2017.106.

[30] K. He, G. Gkioxari, P. Dollár, and R. Girshick, "Mask R-CNN," in *2017 IEEE International Conference on Computer Vision (ICCV), Venice, Italy*, IEEE Computer Society, Feb. 2017. doi: 10.1109/TPAMI.2018.2844175.

[31] D. Erhan, C. Szegedy, A. Toshev, and D. Anguelov, "Scalable object detection using deep neural networks," in *Proceedings of the IEEE Computer Society Conference on Computer Vision and Pattern Recognition*, IEEE Computer Society, Sep. 2014, pp. 2155–2162. doi: 10.1109/CVPR.2014.276.

[32] D. Yoo, S. Park, J.-Y. Lee, A. S. Paek, and I. S. Kweon, "AttentionNet: Aggregating Weak Directions for Accurate Object Detection," in *2015 IEEE International Conference on Computer Vision (ICCV)*, IEEE, Dec. 2015, pp. 2659–2667. doi: 10.1109/ICCV.2015.305.

[33] M. Najibi, M. Rastegari, and L. S. Davis, "G-CNN: An Iterative Grid Based Object Detector," in *Proceedings of the IEEE Computer Society Conference on Computer Vision and Pattern Recognition*, IEEE Computer Society, Dec. 2016, pp. 2369–2377. doi: 10.1109/CVPR.2016.260.

[34] P. Jiang, D. Ergu, F. Liu, Y. Cai, and B. Ma, "A Review of Yolo Algorithm Developments," in *Procedia Computer Science*, Elsevier B.V., 2021, pp. 1066–1073. doi: 10.1016/j.procs.2022.01.135.

[35] W. Liu *et al.*, "SSD - Single Shot MultiBox Detector," in *14th European Conference on Computer Vision, Amsterdam, The Netherlands*, B. Leibe, J. Matas, N. Sebe, and M. Welling, Eds., in Lecture Notes in Computer Science, vol. 9905. Cham: Springer International Publishing, 2016, pp. 21–37. doi: 10.1007/978-3-319-46448-0.

[36] C.-Y. Fu, W. Liu, A. Ranga, A. Tyagi, and A. C. Berg, "DSSD : Deconvolutional Single Shot Detector," *arXiv e-prints*. Jan. 23, 2017. [Online]. Available: http://arxiv.org/abs/1701.06659

[37] Z. Shen, Z. Liu, J. Li, Y. G. Jiang, Y. Chen, and X. Xue, "DSOD: Learning Deeply Supervised Object Detectors from Scratch," in *Proceedings of the IEEE International Conference on Computer Vision*, Institute of Electrical and Electronics Engineers Inc., Dec. 2017, pp. 1937–1945. doi: 10.1109/ICCV.2017.212.

[38] E. Sekhri, "Labelled Marker Dataset from Smith Chart for Image Processing based Intelligent Tuning of Microwave Cavity Filters," *IEEE Dataport*, May 15, 2023.

[39] Keysight, "N9914A FieldFox Handheld RF Analyzer, 6.5 GHz," *Official Documentation*, May 15, 2023.

Publication VI

E. Sekhri, M. Tamre and R. Kapoor, "Data-Driven Approaches Based Microwave Filter Tuning – A Review," in *Springer Book Series - Lecture Notes in Network and Systems.* Springer Verlag, 2023, pp. 1–14.

Data-Driven Approaches Based Microwave Filter Tuning – A Review

Even Sekhri[1][0000-0002-2578-1910], Mart Tamre[1][0000-0002-7489-9683] and Rajiv Kapoor[2][0000-0003-3020-1455]

[1] Tallinn University of Technology, Tallinn, 19086, Estonia
[2] Delhi Technological University, New Delhi 110040, India
evensekhri@gmail.com

Abstract. The process of post-production tuning of microwave (MW) filters is imperative to meet the desired frequency requirements. Currently, this intricate task is carried out by the expert technicians who possess the necessary training and expertise to manually tune these filters. A rapid surge in communication requirements due to an increased number of users in the last 25 years posed a need to automate the filter tuning process. Current research endeavors to comprehensively investigate the research studies conducted in the domain of data-driven microwave filter tuning. The data-driven methods rely on historical or experimental data to build the complex models, thus, has attracted the researchers engaged in the advancement of data-driven techniques for tuning the microwave filters. With the aim to meticulously examine and synthesize the various approaches, methodologies and findings proposed by the researchers in this field, this research undertaking aspires to serve as a pivotal reference for scholars, engineers and practitioners trying to automate the filter tuning process using state-of-the-art data-driven techniques.

Keywords: ANN, Cavity Filter, Data-Driven Techniques, Filter Tuning, Fuzzy Logic, Liner Decomposition, Linear Matrix Operators, Machine Learning, Neuro-Fuzzy System, Reinforcement Learning, SVM, Supervised Learning

1 Introduction

Microwave (MW) bandpass filters hold significant importance in Wireless Base Stations (WBSs) as they are responsible for isolating the desired frequency from the complex communication spectrum. In order to meet the evolving communication requirements, industries produce a wide variety of commercially available and customized filters. However, despite the careful design and manufacturing process, the frequency response of the assembled filters is not as desired. To compensate the discrepancies and for meeting the stated frequency response, these filters need to undergo a precise tuning process [1]. The tuning elements are adjusted until the desired output waveform is achieved. To achieve sharp out-of-band rejection, cross-coupled filters [2] or Frequency-Variant Couplings [3] are used. The fine tuning of these filters requires the expertise of trained technicians, despite the availability of tuning guidelines outlined in

[4]. Further, the filter tuning process is solely based on the experience of these technicians, thus, considered to be an art.

For automating the filter tuning process, COM DEV Ltd. presented their solutions in [5], [6] and [7] but their solution needed a script and did not consider all the potential screw positions. The intricate task of tuning the filters becomes even more complex due to diverse array of design, encompassing different topologies, shapes and sizes tailored to meet specific frequency response requirements. This level of variability makes it impractical to rely solely on traditional methods for a generalized tuning process. As a result, there is a compelling need to delve into data-driven approaches for filter tuning. This is because the data-driven methods have the capability to handle processes where a direct relationship between the variables is not elusive.

This work represents an initial endeavor to review and consolidate the existing body of knowledge on data-driven techniques for tuning MW filters. This comprehensive literature review encompasses an extensive range of data-driven approaches presented by various research groups over the past 38 years. To the best of researcher's knowledge, this review is first of its kind, as no prior reports have provided such an exhaustive analysis in this field. The existing data-driven filter tuning techniques are categorized into seven different categories. The tuning of active filters is beyond the scope of this review. The last literature review on MW filter tuning, published in 1991 [8], exclusively focused on lumped element-based low pass filters only.

The structure of the paper is outlined as follows: Section 2 provides an overview of the current challenges encountered in the MW filter tuning process. In section 3, the existing data-driven techniques for MW filter tuning process are presented. These techniques are bifurcated into seven different categories, and the limitations of each methodology are also discussed. The findings derived from this comprehensive study are discussed in section 4. Lastly, section 5 concludes the paper by summarizing the key insights and drawing overall conclusions from the research.

2 Challenges

Microwave filters are sensitive to the mechanical adjustments of the screws, which introduces a significant challenge during the tuning process. The expertise of trained technicians is crucial, as the relationship between screw position and the corresponding filter response is intricate and complex. However, this task not only becomes monotonous over time but also poses wrist-joint related problems and challenges to the sustainability of technicians in the industry. Consequently, there is a pressing need to automate the filter tuning process.

Data-driven approaches offer a promising solution, as they can discern the complex relationships between screw positions and frequency waveform of the filter. By leveraging these data-driven techniques, the reliance on expert-level technicians can be reduced, potentially addressing the challenges faced during the manual tuning. This motivation prompted the authors of the current research paper to conduct a thorough review of various data-driven techniques related to MW filter tuning.

3 Various Data-Driven Filter Tuning Strategies

3.1 Machine Learning

In [9], the application of ML was explored for Finite Impulse Response (FIR) waveguide filter tuning, utilizing pattern recognition algorithms and adaptive signal processing techniques. While implementing this algorithm, features were collected from a perfectly tuned filter as well as from a filter which is deliberately detuned by a known quantity. This dataset, encompassing feature information and detuning amount, was inputted into a Recursive Least Square (RLS) algorithm. The algorithm then estimated the weight factor of the filters linked to the parallel-connected adaptive combiners. The algorithm's output specified the tuning element requiring adjustment and the necessary adjustment magnitude. The S_{11} polar plot served as the tuning basis, providing phase and signal amplitude information. The implemented RLS algorithm aimed to minimize the Mean Square Error (MSE) to reduce detuning by adjusting only the screw causing the maximum error in each iteration. This method was robust, also enabling Group Delay (GD) tuning. However, the technique had several drawbacks: the influence of coupling screws was not investigated; the publication lacked the details about calibration and other manipulations performed on all coupling screws during implementation; and, a skilled technician performed the coarse filter tuning and this method was only applicable in the fine-tuning stage.

3.2 Fully Logic (FL)

FL [10] can aid in the creation of a comprehensive model that encompasses objective knowledge (mathematical models and measurement data) and subjective knowledge (rules based on expert insights). In FL, numerical data is interpreted as 'Linguistic Rules' where a membership value of ‘0’ signifies that the element doesn't belong to the set, and ‘1’ indicates the opposite.

The complexity of the filter tuning process prevents the direct use of Boolean or Classical Logic. Thus, researchers have investigated the use of fuzzy logic or sets for filter tuning applications. The initial proposition of using FL in filter tuning was attributed to technicians in the industry who use knowledge like 'Sets Theory' to adjust coupling values. These technicians are adept at interpreting the measured response from the VNA and determining which 'Set' the present coupling element belongs to. This method has made it possible to create a comprehensive model that incorporates not only empirical data but also theoretical models and human expertise.

Researchers presented two FL methods for filter tuning: FL without human experience and FL with human experience. Subsections discuss both categories successively.

Not Considering the Human Experience

The S-parameters of the filter are sampled at fixed frequencies and used as input into the model in FL. A Coupling Matrix (CM) is the result of the model's tuning variables. Filter detuning can be traced back to the tuning elements by comparing the produced CM with the corresponding ideal CM.

A Mamdani-type FLS [11] was presented in [12] and [13]. S-parameters and coupling elements were respectively the linguistic antecedents and consequences of "if-then" rules. I/O fuzzy sets were assigned triangular membership functions. Training pairings helped extract CM and identify detuned tuning elements. This method had considerable drawbacks: the method used two FLSs for less and highly detuned problems, and required enough data pairs before building the FLS.

Authors of [14] diagnosed and tuned the filters using a Sugeno type FLS [15] with a single FLS capable to deal with slightly detuned as well as highly detuned filters. The researchers used a Gaussian Membership Function. Subtractive clustering [16] was used to minimize "if-then" rules and discover the center of each membership function. The S-parameters could generate the CM elements at predefined frequency sampling locations in the FLS which aided in finding the detuned screw element. The key drawbacks of [12], [13] and [14] were the requirement to develop sophisticated fuzzy logic rules, the proposed method's inability to attain the correct tuning state, and the lack of technician experience consideration.

Considering Human Experience

The intent behind incorporating the human-expert knowledge for filter tuning was to model the filter as well as the thought process of experts during filter tuning. Using human experiences, an intelligent, efficient, and fast-automated algorithm for tuning filters was anticipated.

The authors in [17] presented a method incorporating the knowledge of a filter tuning expert for the first time. Human intelligence served as a Fuzzy Logic Controller. The First-Order Sugeno FLS [15] in this work used Gaussian type membership functions and variable standard deviations. After successful tuning of a filter by an expert, the corresponding input-output data-pairs were used to build a FLS. After tuning several filters, many such FLS were built i.e. there were several sub-controllers which helped in avoiding the conflicting rules, few data-pairs, and option to increasing more data-pairs. Data pairs were categorized using Subtractive Clustering [16]. The approach identified detuned tuning elements. Nevertheless, successful implementation of the method required sufficient learning data scenarios, but gathering all possible scenarios is practically impossible, rendering the method unsuccessful in meeting the desired objective. Also, this work only utilized the S_{11} parameter of the filter which limited its use in tuning real-world filters.

A two-step filter tuning method consisting of coarse tuning stage and fine-tuning stage was presented in [18]. Both tiers used fuzzy controllers separately. For the first time the human intelligence was captured as linguistic "if-then" rules utilizing triangle membership functions during filter tuning. GD was used to measure the phase offset before initiating the tuning process, with the phase response aiding in the ‘coarse tuning’ stage. The defined 'if-then' rules assisted the Fuzzy Logic Controllers in initially ‘coarse tuning’ and then ‘fine tuning’ the filter. The authors of this method presented the possibility of adding more expert rules. In [19], a completely automated filter tuning system based on FL used the same approach as [18] but could handle more complex filter topologies. However, the approach couldn't address resonator loss, and the

solution was practical in limited settings. Thus, this procedure was not apt for industrial filter tuning.

Simulated Intelligent Fuzzy Logic

Recently, a method to tune a 4th order waveguide cavity filter was presented in [20]. The authors used Mamdani type FLS with triangular membership function while implementing this method. However, the methodology was evaluated in a simulated Matlab environment and used a simpler filter to prove the effectiveness of their method. This method is not apt to tune the complex commercial filters.

Adaptive Fuzzy

The accuracy of filter tuning using FLS relies solely on the number of scenarios used in defining the fuzzy rules. To avoid this dependency and to come-up with a robust tuning system, variable universe adaptive FL was presented in [21] in which the universe could contract or expand. However, each screw was iteratively as well as sequentially tuned for meeting the desired frequency response. The main issue with sequential tuning process is the propagation of error.

A heuristic FLS which was based on dynamic attention was presented later [22] which could modify the tuning goals dynamically and could adaptively regulate the evaluation function without altering the defined fuzzy rules. The proposed method was accurate, fast and effective in tuning the complex filters. Nonetheless, the versatility of the proposed FLS was limited by its lack of adaptability in optimizing the critical parameters and its inability to self-learn the strategies of tuning.

3.3 Artificial Neural Networks (ANNs)

ANNs, being remarkable universal approximators, have become a reliable tool for the multidimensional design and tuning of MW components. These networks establish a distinct mapping between the S-parameters and the tuning screw discrepancy, leading to an inverse black-box model. ANNs can learn from training samples obtained from correctly tuned filter units or "golden filter" units. This trained model then uses raw (detuned) S-parameters as inputs to approximate the tuning screw error. Research in this domain is split into two key categories: a) Supervised Learning, and b) Reinforcement Learning.

Supervised Learning based Filter Tuning

The initial use of ANNs for tuning MW filters was detailed in [23]. They built an inverse model between S-parameters and screw deviations using a Back Propagation (BP) FF-ANN. Despite some limitations, the proposed algorithm managed to tune the filter to some extent. This method was further refined by the same author in [24] using multiple golden filters for improving the generalization abilities, better training vectors, and efficient tuning algorithm. However, while implementing [23] and [24], the inter-resonator couplings were pre-tuned, and the correct ANN architecture was not investigated.

[25] expanded on the previous works ([23] and [24]), providing an analysis of the ANN structure for FT applications, which included an optimal method for selecting the number of frequency sampling points. However, this approach still had limitations, particularly regarding the selection of tuning screws (as couplings between resonators were pre-adjusted), which hindered its commercial use. Innovative techniques, like the use of Principal Component Analysis (PCA) in [26] and Wavelets in [27], were later introduced to efficiently tune the filters. PCA reduced the input layer neurons, speeding up the ANN training without impacting the network's generalization ability. Shortening the ANN input vector length with Daubechies Wavelet (D4) compressed the S-Parameters. Thus, the ANN structure was trained faster without losing generalization capacity. Nevertheless, the Wavelet-based method could only handle simpler ANN topologies and not higher-order cross-coupled filters.

The authors of [23, 24] and [25] had chosen a Feed-Forward (FF) ANN structure with a single hidden layer as the network blueprint. These papers leveraged S_{11} characteristics for filter tuning and employed an IAFTT Robot [28] to gather training data by detuning the filter. Even if the training vectors were improved using [26] and [27], the key issue with this approach was that the model could not be updated in real time, and the algorithm was restricted by filter topology.

Another NN inverse modeling-based filter tuning approach based on 3-layered FF architecture was presented in [29]. The S-parameters of a cross-coupled filter were mapped to the relevant tuning screw position. In order to account for N tuning elements (i.e., resonator cavities, inter-resonator couplings, and cross-couplings), N inverse sub-filter models were created. Each tuning element of a finely tuned physical filter was detuned in both directions to collect the training vector set for the NN architecture. Only one sub-filter was used at a time, hence there was only one neuron in the output layer. The next sub-filter was taken into consideration when the trained ANN had provided the necessary amount of adjustment to tune the sub-filter under consideration. It was suggested that the filter's tuning process should move from its input side to its output side. However, the practical application of this technology was constrained by the requirement for a large quantity of training datasets.

To deal with tuning of filters with different center frequencies, an inverse modeling was also introduced by the researchers [30]. This model enhanced the generalization capabilities but was still limited to S_{11} parameter for tuning, thus, unable to provide a comprehensive solution for automatic filter tuning.

Reinforcement Learning (RL)-based Filter Tuning

RL models, inspired by animal learning processes, were introduced to the field of machine learning. The RL models use Neural Networks to reinforce learning through a Temporal Difference (TD) approach. The TD process was first mathematically outlined in [31] and further developed into Q-learning in [32]. When the Q-learning agent explores the states of the environment while learning to maximize the positive reward in the future, the bias and weights of the ANN architecture are iteratively updated.

Getting inspiration from the work presented by DeepMind [33], the authors of [34] trained a Deep Q-Network (DQN) with a 20-20-4 Feed Forward-Back Propagation Neural Network (FF-BPNN) structure. Despite certain limitations like discontinuous

reward function, the solution tripping into local minima, and being restricted to consideration of only S_{11} parameter, this research marked the first step towards RL-based filter tuning.

Following this, various improvements to RL-based filter tuning were introduced by the research community. This included: CNN-based filter tuning method using Lagrangian multiplier [35] ensured the global minima; the use of Deep-Deterministic Policy Gradient (DDPG) algorithm [36] used continuous action space in conjunction with [37]; and, double deep Q-learning (DDQN) techniques [38] discarding the maximization bias problem. However, all these methods were also restricted to S_{11} characteristics only. Tuning the filters while simultaneously considering the S_{11} and S_{12} parameters, researchers proposed a method based on tuning using a DQN network [39]. This method used discontinuous reward function as in [34] and DDPG algorithm as in [36]. However, this method still had limitations, particularly when it came to higher-order filters.

Recently a method capable of learning of human tuning strategies using continuous RL was presented [40] where the authors collected the training data from one channel of the combiner using a robotic system. All the other previous methods where RL was used to simulate the filter tuning, the simpler reward functions were used. In [40], the authors compared the tuning performance and tuning time with 03 different reward functions. The addition of human-inspired shaping reward function reduced the exploration, thus, ensuring better system performance. Nevertheless, the methodology was limited by its simpler model and captivating the changes in the curve only in the vertical direction. Additionally, just like other RL-based filter tuning methods, this method was also limited to simulation environment only.

3.4 Filter tuning using a Neuro-Fuzzy System (NFS)

For tuning the filters using a hybrid of Neural Networks and Fuzzy Logic (of Sugeno type), researchers introduced a novel multi-dimensional estimator [41]. The adaptive network-based fuzzy inference system (ANFIS) [42] was found capable of correlating the S-parameters of a filter with the variance in tuning screws. This system required fewer learning vectors while also delivering smaller Learning Error (LE) and Generalized Error (GE) compared to the GE value from [23] that used only the ANN structure. The couplings were considered to be pre-tuned. However, the methodology's drawbacks included its lengthy training process, the authors only considered the S_{11} characteristics, and inability of the model in getting updated in real time.

3.5 Filter tuning using Linear Matrix Operator

To avoid the prolonged training process as in the case of ANN and NFS based techniques, a strategy based on linear mapping was introduced in [43]. With the linear matrix operator, the model could illustrate the connection between the alterations in S-parameters and changes in the tuning screw position. The samples utilized in this research were gathered using IAFTT [28]. PCA was used for dimensionality reduction. The matrix to establish linear mapping was determined using the Least-Squares Method

(LSM) [44], with the approximation error minimized through 'outliners elimination'. However, its limitations included the random collection of datasets, the consideration of only cavity tuning within a limited range, the inter-resonator coupling and cross-couplings were pre-tuned, and not considering the inter-resonator coupling while collecting the datasets.

3.6 Filter tuning based on Linear Decomposition of Reflection Characteristics

The concept of employing the Linear Decomposition technique in filter tuning applications assumes that the relationship between data pairs can be expressed by a sum of polynomial functions. The research in [45] successfully mitigated two major limitations of ANN-based and Linear Matrix Operator-based techniques – the necessity for random detuning of a filter for data pair collection, and the requirement for numerous data pairs. Yet, this research had its own limitations, including the consideration of only the S_{11} parameter, the tuning of only the cavity screws (inter-resonator couplings and cross-couplings were not considered), and its implementation on slightly detuned filters only. The research in [46] expanded upon [45] by considering: S_{11} as well as S_{21} characteristics of the filter response, and considering the cross-couplings. The linear optimizer developed in this research was based on a coarse set that could generate deviations corresponding to cavities and cross-couplings. The proposed method did not need training but the overall response of this methodology was slower as compared to the ANN-based filter tuning methods when finding the amount of detuning.

3.7 Filter tuning using Support Vectors

In the domain of microwave (MW) filter tuning, Support Vector Regression (SVR)-based models have been developed to construct electromagnetic (EM) coupling models. The use of Support Vector Algorithms presents several advantages over ANNs including their ability to find an optimal solution even with a small sample size.

In [47], the first wavelet kernel mechanism model-based Least Squares Support Vector Regression (LS-SVR) was used to create a model to understand the relationship between the tuning screw length changes and the corresponding changes in the coupling matrix (CM). The limitation here was that screw positions were approximated rather than directly measured, and discrepancies existed between ideal models and real products. Additionally, the method was applicable only for simple filter topologies where each output port could be examined separately. In response to this, Multi-output LS-SVR (MLS-SVR) was developed to handle devices with multiple output MW Filters. For example, the use of Multi-Kernel Linear Programming Support Vector Regression (MKLP-SVR) allowed for an effective EM coupling model for filter tuning [48]. The data related to success as well as failure of the manual filter tuning process was recorded. Despite its effectiveness in terms of moderately complex filters, this method relied heavily on time consuming optimization routines which are not suitable for automating the filter tuning process.

Further research led to the development of a hybrid model, MKPLP-SVR [49], which incorporated prior knowledge and multi-kernels in LP-SVR. The Coupling

Matrix (CM) was extracted using [50] and [51]. The model was trained using the data collected during the manual tuning process. This methodology was evaluated on electrically tunable filters. However, this model was not without its challenges. Firstly, the CM was extracted in an ideal state, the method did not provide an accurate CM when the filter was highly detuned. Furthermore, the criteria of model and hyperparameter selection were not discussed.

Further modifications led to the development of another hybrid MKPLP-SVR modeling approach for filter tuning [52], combining the Coarse Model and the SVR model. When tested on electrically tunable filters, the proposed methodology could improve the accuracy and extrapolation capability of the model. But this method could also not deal with highly detuned filters.

A common limitation of all these support vector-based filter tuning methods i.e. [47], [48], [49] and [52] could only tune slightly detuned filter only. To address this limitation, authors of [53] proposed a model for highly detuned filters was proposed, using a pole-residue-based Multi-output Least Squares Support Vector Regression (MLS-SVR) methodology [54]. However, this approach was also limited by its reliance on simulation software data, which might not always accurately reflect real-world scenarios. The method was also restricted to simpler filter topologies, limiting its practical application.

4 Discussion

The first publication related to data-driven approach was reported in 1989 by Mirzai et al. which used ML to tune the waveguide filters but could only assist the manual tuning during the fine-tuning stage. To find a fully automated solution, later, the focus of researchers was then shifted towards FL-based techniques which allowed the possibility of adding human experience in terms of the fuzzy rules. But FL-based filter tuning relied on the CM extraction process and could tune only the simpler filter topologies. Due to advancements in algorithms and computation power, the researchers started considering ANNs to map the relationship between screw deviations and corresponding S-parameters of the filters. With the use of data-truncation techniques like PCA and wavelets, the architecture training time was reduced but the key problem with this technique was that the trained model could only tune exactly the same filter from which the training vector was generated. RL-based filter tuning solutions were only limited to simulations only due to its reliance on the reward function and problems in training the agent to learn all the possible states. Filter tuning based on NFS needed lengthy training time and the model could not be updated in real-time. For avoiding the network training process, the researchers presented a linear matrix operator and linear decomposition of reflection characteristics as potential solutions but selective approach in deciding the tuning elements and slower response of the algorithms restricted the further use of these methods. SVMs were also considered to find the solution to problem in hand but they could not deal with tuning of complex filters. Recently, the paradigm has shifted towards adaptive fuzzy-based techniques as it offers an effective and versatile approach for dealing with this complex and uncertain filter tuning task. An increase in research

interest for data-driven filter tuning techniques can also be inferred from Fig. 1 which depicts a decade-wise distribution of the publications presented by the research community.

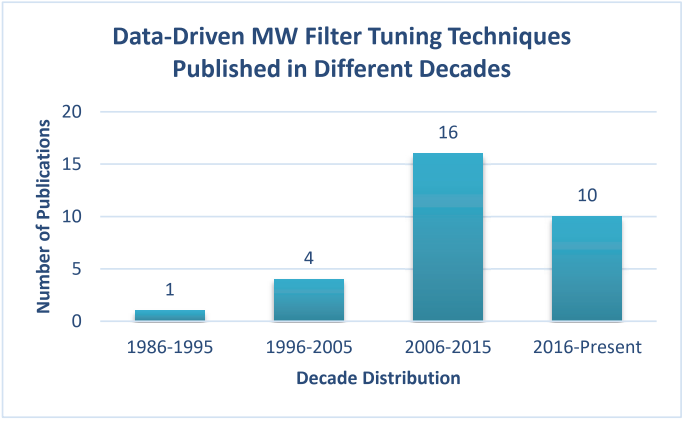

Fig. 1. Various data-driven techniques of MW filter tuning presented by the research community

The data-driven techniques can handle the complex relationship between tuning elements and electrical response of the MW filters. The upward trend seen in Fig. 1 for exploring the data-driven techniques of filter tuning can be attributed to the fact that the data-driven approaches are not restricted by the filter topology or the size of filter when finding the hidden relation between the variables.

5 Conclusion

Data-driven approaches offer notable advantages in terms of efficiency, speed and accuracy – making them well-suited for handling complex relationships between the variables. Recognizing these benefits, the authors of the current research conducted an extensive literature review spanning the past 38 years, exploring various data-driven techniques for MW filter tuning. The reviewed data-driven approaches were categorized into seven categories, thereby furnishing a comprehensive panorama of available methodologies. A notable finding from the research analysis was an upward trend in the research interest over the last two decades. This trend can be attributed to advancements in computing power and emergence of powerful algorithms capable of handling vast amounts of complex data. Some key advantages of the data-driven techniques are adaptability and ease of customizations that allows for scalability. These characteristics distinguish them from traditional filter tuning methods, which often lack such flexibility. By harnessing data-driven techniques, the bottleneck in filter production lines can potentially be eliminated, paving the way for automating the filter tuning process.

To summarize, the extensive review of literature reveals the potential of data-driven techniques in MW filter tuning. Their efficiency, adaptability, and scalability made them a promising avenue for addressing challenges faced in traditional filter tuning methods.

References

1. Cameron, R.J., C. M. Kudsia, Mansour, R.R.: Tunable Filters. In: Microwave Filters for Communication Systems: Fundamentals, Design and Applications, Second Edition. pp. 731–783 (2018).
2. Brian Thomas, J.: Cross-Coupling In Coaxial Cavity Filters - A Tutorial Overview. IEEE Trans Microw Theory Tech. 51, 1368–1376 (2003). https://doi.org/10.1109/TMTT.2003.809180.
3. Zhang, Y.L.: Improved Matrix Synthesis for Inline Filters with Transmission Zeros Generated by FVC. Progress In Electromagnetics Research M. 76, 9–17 (2018). https://doi.org/1.2528/PIERM18101502.
4. Lindner, A., Biebl, E., Strasse, A.: A Manual Tuning Method for Coupled Cavity Filters. In: Proceedings of 36th European Microwave Conference, Manchester, UK. pp. 1340–1342 (2006).
5. Yu, M.: Computer Aided Tuning. COM DEV Internal Report. (1994).
6. Yu, M.: A Fully Automated Filter Tuning Robot for Wireless Base Station Diplexers - Presentation. In: IEEE International Microwave Symposium - Workshop: Computer Aided Filter Tuning, (IMS 2003), Philadelphia, Pennsylvania (2003). https://doi.org/10.13140/2.1.4648.1923.
7. Yu, M.: Robotic Computer-Aided Tuning (COM DEV Ltd.). Microw J (Int Ed). 136–138 (2006). https://doi.org/10.11139/cj.29.3.507-531.
8. Jervis, B.W., Crofts, M.: Comparison of Computer-Aided Tuning Algorithms Applied to the Amplitude Response of Passive Analogue Filters. IEE Proceedings G - Circuits, Devices and Systems. 138, 363–371 (1991). https://doi.org/10.1049/ip-g-2.1991.0062.
9. Mirzai, A.R., Cowan, C.F.N., Crawford, T.M.: Intelligent Alignment of Waveguide Filters using a Machine Learning Approach. IEEE Trans Microw Theory Tech. 37, 166–173 (1989).
10. Zadeh, L.A.: Fuzzy Sets. Information and Control. 8, 338–353 (1965).
11. Mamdani, E.H.: Application of fuzzy algorithms for control of simple dynamic plant. In: Proceedings of the IEEE. pp. 1585–1588 (1974).
12. Miraftab, V., Mansour, R.R.: Computer-Aided Tuning of Microwave Filters using Fuzzy Logic. In: 2002 IEEE MTT-S International Microwave Symposium Digest, Seattle, WA, USA. pp. 1117–1120 (2002). https://doi.org/10.1109/TMTT.2002.805291.
13. Miraftab, V., Mansour, R.R.: Computer-Aided Tuning of Microwave Filters using Fuzzy Logic. IEEE Trans Microw Theory Tech. 50, 2781–2788 (2002). https://doi.org/10.1109/TMTT.2002.805291.
14. Miraftab, V., Mansour, R.R.: A Robust Fuzzy-Logic Technique for Computer-Aided Diagnosis of Microwave Filters. IEEE Trans Microw Theory Tech. 52, 450–456 (2004). https://doi.org/10.1109/TMTT.2003.820895.
15. Takagi, T., Sugeno, M.: Fuzzy Identification of Systems and Its Applications to Modeling and Control. IEEE Trans Syst Man Cybern. SMC-15, 116–132 (1985). https://doi.org/10.1109/TSMC.1985.6313399.

16. Chiu, S.L.: Fuzzy model identification based on cluster estimation. Journal of Intelligent and Fuzzy Systems. 2, 267–278 (1994). https://doi.org/10.3233/IFS-1994-2306.
17. Miraftab, V., Mansour, R.R.: Tuning of Microwave Filters by Extracting Human Experience using Fuzzy Logic. In: 2005 IEEE MTT-S International Microwave Symposium Digest, Long Beach, CA, USA. pp. 1605–1608. IEEE, Long Beach, CA, USA (2005). https://doi.org/10.1109/MWSYM.2005.1517011.
18. Miraftab, V., Mansour, R.R.: Automated Microwave Filter Tuning by Extracting Human Experience in terms of Linguistic Rules using Fuzzy Controllers. In: 2006 IEEE MTT-S International Microwave Symposium Digest, San Francisco, CA, USA. pp. 1439–1442 (2006). https://doi.org/10.1109/MWSYM.2006.249541.
19. Miraftab, V., Mansour, R.R.: Fully Automated RF/Microwave Filter Tuning by Extracting Human Experience using Fuzzy Controllers. IEEE Transactions on Circuits and Systems - I : Regular Papers. 55, 1357–1367 (2008). https://doi.org/10.1109/TCSI.2008.916614.
20. Aghanim, A., Lasri, R., Oulhaj, O.: Implementation of a fuzzy controller to tune the response of a waveguide cavity filter. e-Prime - Advances in Electrical Engineering, Electronics and Energy. 2022, 1–7 (2022). https://doi.org/10.1016/j.prime.2022.100078.
21. Peng, S., Cao, W., Bi, L., Yuan, Y., Wu, M.: A tuning strategy for microwave filter using variable universe adaptive fuzzy logic system. In: Proceeding - 2021 China Automation Congress, CAC 2021, Beijing - China. pp. 6061–6066. Institute of Electrical and Electronics Engineers Inc. (2021). https://doi.org/10.1109/CAC53003.2021.9727379.
22. Bi, L., Cao, W., Hu, W., Wu, M.: A Dynamic-Attention-Based Heuristic Fuzzy Expert System for the Tuning of Microwave Cavity Filters. IEEE Transactions on Fuzzy Systems. 30, 3695–3707 (2022). https://doi.org/10.1109/TFUZZ.2021.3124643.
23. Michalski, J.J.: Artificial Neural Networks Approach in Microwave Filter Tuning. In: Progress In Electromagnetics Research M. pp. 173–188 (2010).
24. Michalski, J.J.: Artificial Neural Network Algorithm for Automated Filter Tuning with Improved Efficiency by Usage of Many Golden Filters. In: 2010 18th International Conference on Microwave Radar and Wireless Communications (MIKON 2010), Vilnius, Lithuania. pp. 1–3 (2010).
25. Michalski, J.J., Kacmajor, T., Gulgowski, J., Mazur, M.: Consideration on Artificial Neural Network Architecture in Application for Microwave Filter Tuning. Piers Online. 7, 271–275 (2011).
26. Kacmajor, T., Michalski, J.J.: Principal Component Analysis in Application for Filter Tuning Algorithms. In: 2011 IEEE MTT-S International Microwave Workshop- Series on Millimeter Wave Integration Technologies, Sitges, Spain. pp. 121–123. , Sitges, Spain (2011).
27. Michalski, J.J., Kacmajor, T.: Filter Tuning Algorithm with Compressed Reflection Characteristic by Daubechies D4 Wavelet Transform. In: 2011 41st European Microwave Conference (EuMC 2011), Manchester, UK. pp. 778–781 (2011).
28. Intelligent Automatic Filter Tuning Tool (IAFTT): European Patent Application No. P382895 assigned by Polish National Patent Office, (2007).
29. Michalski, J.J.: Inverse Modeling in Application for Sequential Filter Tuning. Progress In Electromagnetics Research. 115, 113–129 (2011).
30. Kacmajor, T., Kant, P., Michalski, J.J.: Microwave Filter Tuning for Different Center Frequencies based on Artificial Neural Network and Phase Compensation. In: 2014 20th International Conference on Microwaves, Radar and Wireless Communications (MIKON 2014), Gydnia, Poland. pp. 1–4 (2014). https://doi.org/10.1109/MIKON.2014.6899833.
31. Sutton, R.S., Barto, A.G.: Reinforcement Learning: An Introduction. MIT Press, Cambridge, MA, USA (1998). https://doi.org/10.1179/175622708X282910.
32. Watkins, C.J.C.H.: Learning from Delayed Rewards, (1989).

33. Mnih, V., Kavukcuoglu, K., Silver, D., Rusu, A.A., Veness, J., Bellemare, M.G., Graves, A., Riedmiller, M., Fidjeland, A.K., Ostrovski, G., Petersen, S., Beattie, C., Sadik, A., Antonoglou, I., King, H., Kumaran, D., Wierstra, D., Legg, S., Hassabis, D.: Human-level Control Through Deep Reinforcement Learning. Nature. 518, 529–533 (2015). https://doi.org/10.1038/nature14236.
34. Wang, Z., Yang, J., Hu, J., Feng, W., Ou, Y.: Reinforcement learning approach to learning human experience in tuning cavity filters. In: 2015 IEEE International Conference on Robotics and Biomimetics (ROBIO 2015), Zhuhai, China. pp. 2145–2150 (2015). https://doi.org/10.1109/ROBIO.2015.7419091.
35. Sekhri, E., Tamre, M., Kapoor, R.: Optimal Q-learning approach for tuning the cavity filters. In: 2019 20th International Conference on Research and Education in Mechatronics (REM 2019), Wels, Austria. pp. 1–4. IEEE, Wels, Austria (2019). https://doi.org/10.1109/REM.2019.8744118.
36. Wang, Z., Ou, Y., Wu, X., Feng, W.: Continuous Reinforcement Learning With Knowledge-Inspired Reward Shaping for Autonomous Cavity Filter Tuning. In: 2018 IEEE International Conference on Cyborg and Bionic Systems, Shenzhen, China. pp. 53–58 (2018).
37. Wang, Z., Jin, S., Yang, J., Wu, X., Ou, Y.: Real-Time Tuning of Cavity Filters by Learning from Human Experience: A Vector Field Approach. In: 2016 12th World Congress on Intelligent Control and Automation (WCICA 2016), Guilin, China. pp. 1931–1936 (2016). https://doi.org/10.1109/WCICA.2016.7578618.
38. Sekhri, E., Kapoor, R., Tamre, M.: Double deep Q-learning approach for tuning microwave cavity filters using locally linear embedding technique. In: 2020 15th International Conference on Mechatronic Systems and Materials, (MSM 2020), Bialystok, Poland. pp. 1–6. IEEE, Bialystok, Poland (2020). https://doi.org/10.1109/MSM49833.2020.9202393.
39. Lindstah, S., Lan, X.: Reinforcement learning with imitation for cavity filter tuning. In: 2020 IEEE/ASME International Conference on Advanced Intelligent Mechatronics (AIM-2020), Boston, USA. pp. 1335–1340 (2020). https://doi.org/10.1109/AIM43001.2020.9158839.
40. Wang, Z., Ou, Y.: Learning Human Strategies for Tuning Cavity Filters with Continuous Reinforcement Learning. Applied Sciences (MDPI). 12, (2022). https://doi.org/10.3390/app12052409.
41. Kacmajor, T., Michalski, J.J.: Neuro-Fuzzy Approach In Microwave Filter Tuning. In: IEEE MTT-S International Microwave Symposium Digest, Baltimore, MD, USA. pp. 1–4 (2011). https://doi.org/10.1109/MWSYM.2011.5972771.
42. Jang, J.S.R.: ANFIS: Adaptive-Network-Based Fuzzy Inference System. IEEE Trans Syst Man Cybern. 23, 665–685 (1993). https://doi.org/10.1109/21.256541.
43. Michalski, J.J.: On Linear Mapping of Filter Characteristic to Position of Tuning Elements in Filter Tuning Algorithm. Progress In Electromagnetics Research. 123, 279–298 (2012).
44. Wolberg, J.: Data analysis using the method of least squares. Springer, Germany (2006).
45. Kacmajor Tomasz; Michalski Jerzy Julian: Approximation of Filter Characteristic to Tuning Element Positions Using Coarse Set. In: 2012 19th International Conf. on Microwaves, Radar and Wireless Communications, Warsaw, Poland. pp. 684–687. , Warsaw, Poland (2012).
46. Kacmajor, T., Michalski, J.J.: Filter Tuning Based on Linear Decomposition of Scattering Characteristics. Progress in Electromagnetics Research. 135, 451–464 (2013). https://doi.org/10.2528/PIER12112603.
47. Han, L., Wu, K., Chen, X.-P., He, F.: Influence and Tuning of Tunable Screws for Microwave Filters Using Least Squares Support Vector Regression. International Journal of RF and Microwave Computer-Aided Engineering. 20, 422–429 (2010). https://doi.org/10.1002/mmce.

48. Zhou, J., Huang, J.: Intelligent Tuning for Microwave Filters Based on Multi-Kernal Machine Learning Model. In: 2013 5th IEEE International Symposium on Microwave, Antenna, Propagation and EMC Technologies for Wireless Communications. pp. 259–266. , Chengdu, China (2013).
49. Zhou, J., Duan, B., Huang, J.: Support-Vector Modeling of Electromechanical Coupling for Microwave Filter Tuning. International Journal of RF and Microwave Computer-Aided Engineering. 23, 127–139 (2013). https://doi.org/10.1002/mmce.20683.
50. Liao, C.K., Chang, C.Y., Lin, J.: A Vector-Fitting Formulation for Parameter Extraction of Lossy Microwave Filters. IEEE Microwave and Wireless Components Letters. 17, 277–279 (2007). https://doi.org/10.1109/LMWC.2007.892970.
51. Macchiarella, G.: Extraction of Unloaded Q and Coupling Matrix from Measurements on Filters with Large Losses. IEEE Microwave and Wireless Components Letters. 20, 307–309 (2010). https://doi.org/10.1109/LMWC.2010.2047455.
52. Zhou, J., Huang, J., Li, P., Li, N.: Hybrid Modeling of Microwave Devices using Multi-Kernel Support Vector Regression with Prior Knowledge. International Journal of RF and Microwave Computer-Aided Engineering. 25, 219–228 (2015). https://doi.org/10.1002/mmce.20852.
53. Cao, W.H., Liu, C., Yuan, Y., Wu, M., Wu, S.B.: Parametric Modeling of Microwave Filter using Combined MLS-SVR and Pole-Residue-Based Transfer Functions. International Journal of RF and Microwave Computer-Aided Engineering. 28, 1–10 (2018). https://doi.org/10.1002/mmce.21246.
54. Xu, S., An, X., Qiao, X., Zhu, L., Li, L.: Multi-Output Least-Squares Support Vector Regression Machines. Pattern Recognit Lett. 34, 1078–1084 (2013). https://doi.org/10.1016/j.patrec.2013.01.015.

Publication VII

E. Sekhri, M. Tamre and R. Kapoor, “An Efficient Assistance in Cavity Filter Tuning using Filter Screw Classification,” in *Springer Book Series - Lecture Notes in Electrical Engineering.* Springer Verlag, 2023, pp. 1–14.

An Efficient Assistance in Cavity Filter Tuning using Filter Screw Classification

Even Sekhri[1][0000-0002-2578-1910], Mart Tamre[1][0000-0002-7489-9683] and Rajiv Kapoor[2][0000-0003-3020-1455]

[1] Tallinn University of Technology, Tallinn, 19086, Estonia
[2] Delhi Technological University, New Delhi 110040, India
evensekhri@gmail.com

Abstract. The research community is primarily focused on automating the filter tuning process. Effectively distinguishing the tuning screws from the mounting screws present on the surface of cavity filters is one of the key factors to improving the efficiency of automated filter tuning process. Since the tuning state of the filter is altered only by rotating the tuning screws, it is imperative to detect and localize the position of these tuning screws. This paper presents a supervised Machine Learning (ML)-based approach to differentiate between the tuning screws and mounting screws of a cavity filter. The proposed methodology underwent evaluation on a commercial cavity filter, achieving an impressive precision of 96.66%. Other state-of-the-art supervised learning-based algorithms have been tested against the Support Vector Machine (SVM) classifier. The empirical findings unequivocally demonstrate the superiority of the proposed methodology in comparison to alternative approaches. The findings of this research work can assist in automating the filter tuning process.

Keywords: Cavity Filter, Classification, Decision Trees, Filter Tuning, KNN, Machine Learning, Screw Classification, SVM, Supervised Learning

1 Introduction

Mechanical tuning of Microwave (MW) cavity filters, using the tuning screws, is the most common way to compensate the manufacturing flaws, differences in material properties, mechanical tolerances etc. The frequency response of the filter can be altered by altering the insertion depth of tuning screws [1]. The filter tuning process aims to set the filter to a state which ensures the separation of desired frequency band from the congested communication spectrum. Currently, trained technicians carry out the filter tuning process [2].

Typically, a cavity filter is constructed of a metallic block. To prevent energy leakage, a metallic plate is used to cover the filter. Fig. 1 shows a used cavity filter. One can observe the presence of several screws on the assembled filter's top plate. These screws can be broadly classified into two categories – tuning screws and mounting screws. The tuning screws alter the performance of the filter [3], while the mounting screws just hold the top metallic plate over the filter structure.

Fig. 1. A Commercial Cavity Filter

In the context of a cavity filter, the term 'tuning screws' includes screws like tuning screws, coupling screws, cross-coupling screws, and duplexer screws. Each tuning element has a particular function and can come in a variety of shapes, sizes, and materials. The tuning screws located just over the resonators assist in achieving the resonance frequency and, the coupling screws are used to adjust the EM coupling strength between the neighboring cavities. It should be noted that not all types of tuning screws are always present on the cavity filter unit. The type(s) of tuning screws to be mounted over the filter are chosen by the filter designers while taking the design requirements into consideration [4]. The tuning screws and coupling screws used in the filter type depicted in Fig. 1 have the same shape, material, and size, and they are collectively referred in this work as "tuning screws".

The goal is to construct a Fully Automated Tuning (FAT) system for filters that can extract the exact position coordinates of each tuning screw using a vision system. This system further sends this data to the filter tuning algorithm, which in turn instructs the robot manipulator to travel to the designated coordinates and accurately turn the corresponding tuning screw(s) to alter the tuning state of the filter. The process is repeated until the desired frequency response of the filter is attained. Every screw fitted over the cavity filter must be efficiently classified as either a tuning screw or a mounting screw while automating the filter tuning process.

The Machine Learning (ML) classification is a supervised learning-based approach for building a model to divide the given data into desired number of distinct classes. Artificial Neural Networks (ANNs) [5], Bayesian Networks [6], Decision Trees [7], K-Nearest Neighbors (KNNs) [8], Support Vector Machine (SVM) [9] are a few of the widely used classification techniques documented in the literature. The presence of noise in the data used for training process has an impact on the trained ANN model [10]. Although decision tree-based classifiers are faster than ANNs, they do not offer flexibility to modeling parameters. KNNs are easy to implement but are slow when dealing with huge amounts of the input data. KNNs are also sensitive to irrelevant parameters present in the system. Owing to their strong theoretical foundation, and excellent generalizability, SVMs perform superior to other methods mentioned [11].

SVM, a supervised learning model widely used for binary classification tasks, was introduced by Vapnik and Chervonenkis in 1964 [12]. Its popularity has soared due to

its superior performance in high-dimensional spaces, robustness against overfitting, and flexibility in modeling diverse sources of data [13]. The SVM algorithm finds an optimal hyperplane to separate the data into different classes. The goal is to find the hyperplane with the maximum margin [14]. This maximum margin hyperplane notion is crucial since it improves the model's generalizability and mitigates overfitting [15]. The foundational idea behind SVMs is Structural Risk Minimization (SRM), a concept from the theory of statistical learning. By minimizing the generalization error of the model (instead of frequently used mean squared error), SRM aims to maximize the margin between several classes, enabling them to generalize effectively on unseen data [16]. to tackle noisy data and outliers, Cortes and Vapnik [17] introduced the idea of soft margins which significantly enhanced the SVM's applicability.

SVMs have been effectively used in variety of fields, including text categorization [18], image recognition [19], fault diagnosis [20], and image classification [21]. However, despite their effectiveness, SVMs are often criticized for their poor computational efficiency and lack of interpretability [22]. The development of Sequential Minimal Optimization (SMO), which more efficiently solves the SVM optimization problem, is one study which focused on resolving these limitations [23].

In this paper, SVMs have been used to distinguish the tuning screws from the mounting screws. A unique imaging setup with preset parameters has been employed. The performance of the SVM classifier has been evaluated against other supervised learning-based classifiers.

The remainder of the paper is structured as follows: the suggested methodology is discussed at length in Section 2. After implementing the preprocessing steps, the preprocessed image is then used in the subsequent steps to classify the tuning screws and mounting screws. Section 3 provides the findings of this research work. The conclusions are drawn in Section 4 followed by the future scope.

2 Methodology

2.1 Setup

The images used in this research work were captured using a Logitech C525 HD 720p webcam and they were then processed. Since a powerful light source was necessary for proper illumination and for homogeneous reflection on the mounting plate (to create higher contrast), Halogen lighting was used during the experiments. The overall setup is depicted in Fig. 2. The various parameters used in Fig. 2 were defined to be as following:

$$\alpha = 45°$$
$$L_0 = 250\ mm$$
$$W_0 = 350\ mm$$
$$W_1 = 190\ mm$$
$$L_1 = 240\ mm$$
$$L_C = 38\ mm$$

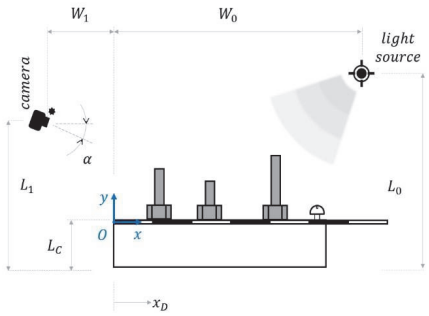

Fig. 2. Experimental Setup used in this work

In order to prevent any screws being occluded i.e. covering up the one(s) behind it, the camera mounting angle i.e. $\alpha = 45°$ was chosen.

2.2 Preprocessing

The procedure for preprocessing the acquired image processing is shown in Fig. 3. The acquired RGB image of the commercial MW cavity filter is first converted into a binary image. The rusty mounting surface seen in Fig. 1 (we have considered a used MW filter in this work) was compensated by adjusting the brightness and contrast of the binary image. The 'value plane' was subsequently used to extract the grey image. The key reason for choosing this plane was that the tops of the screws were a little brighter than the rest of the filter assembly. Finally, after thresholding, all the screws were successfully separated from the filter surface. The resulting processed image was then used for further analysis.

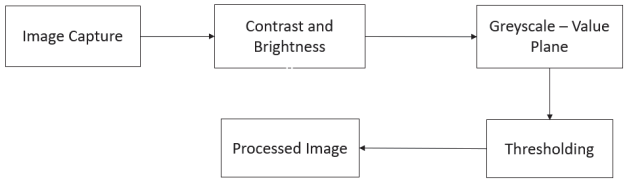

Fig. 3. Image Preprocessing Steps

2.3 Screw Classification

The Hessian matrix provides insights about the local variations and structures within the data. In multivariate calculus, the Determinant of Hessian (DoH) refers to a matrix

composed of second-order partial derivatives of a determinant function. For the image represented by *f(x,y),* the DoH is calculated as presented by (1).

$$\det \mathbf{H} = \begin{vmatrix} f_{xx} & f_{xy} \\ f_{yx} & f_{yy} \end{vmatrix} \tag{1}$$

In this work, when the processed image was given to the proposed solution, DoH method provided area as a feature vector. The screw dimensions were then manually measured and labeled as tuning screws or mounting screws depending on the area of the feature vector. Additionally, the classification of tuning and mounting screws was made easier by extracting the height parameter from the feature vectors provided by DoH. Labeling took 92 minutes to complete. This linear SVM classifier, which was trained using the parameters presented in Table 1, used this labeled data for training the model. The SMO solver, which minimizes the one-norm problem by considering a series of 2-point minimizations, was used to implement the SVM algorithm.

Table 1. SVM Algorithm Parameters

Entity	Value
Lagrangian Multiplier	26 x 1 array
Bias Term for Hyperplane	-13.9878
Solver	SMO

After the model is trained using the labeled data, the screws in the given image can be classified. The overall methodology for classifying the screws is presented in Fig. 4.

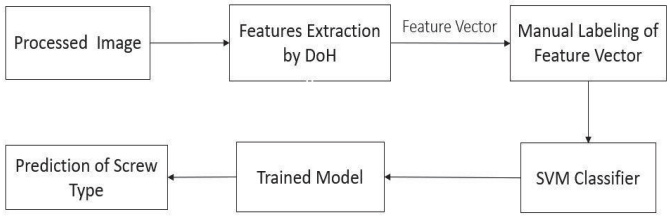

Fig. 4. Screw Classification Methodology

3 Results

The proposed methodology was tested on a commercial cavity filter with a total of 144 screws. Out of these, 58 screws were the tuning screws and rest were the tuning screws. The original image and the corresponding processed image of the filter considered for testing the are displayed in Fig. 5 on the left and the right side respectively. The goal of

implementing the supervised learning algorithms on the processed image is to have a bounding box around the tuning screws.

Fig. 5. The Original Image (Left), and Processed Image (Right)

The processed image and the feature vectors from DoH are given as an input to the trained SVM model and the resultant image with the predictions is shown in Fig. 6 where the bounding boxes are encapsulating the tuning screws. It can be seen in Fig. 6 that the proposed SVM model predicted a total of 60 tuning screws in the processed image. Two false-positive results were predicted by SVM algorithm.

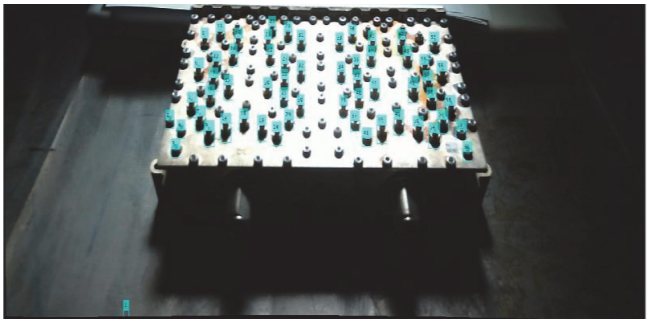

Fig. 6. Tuning Screws Predicted by SVM

The performance of the SVM algorithm was compared with the state-of-the-art supervised ML-based algorithms viz. k-Nearest Neighbor (KNN) and Decision Tree (DT). While implementing the KNN algorithm, the number of neighbors were defined to be 5 and the Euclidean distance between the nearest neighbors is used as a criterion. In the DT algorithm, the cross-validation was not considered. The predictor selection for DT was set to consider all the splits. The predictions made by KNN model and DT model are presented in Fig. 7 and Fig. 8 respectively.

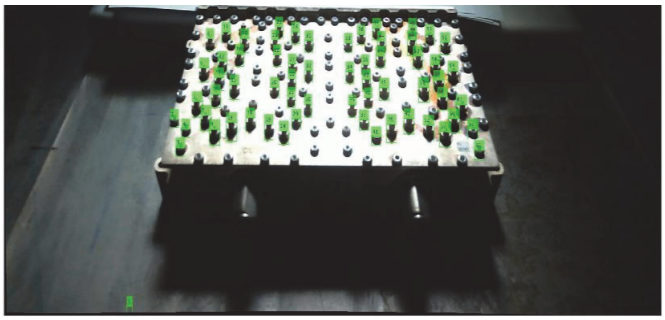

Fig. 7. Tuning Screws Predicted by KNN Classifier

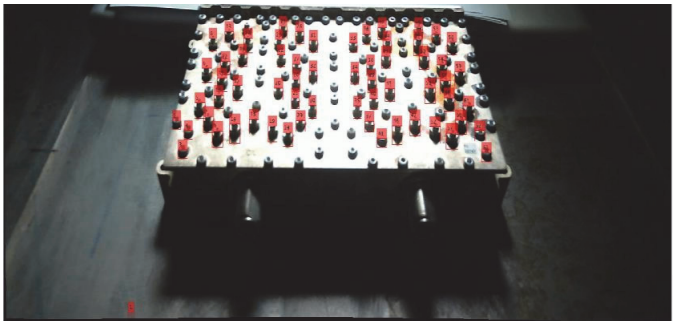

Fig. 8. Tuning Screws Predicted by DT Classifier

The results obtained by implementing KNN and DT algorithms on the processed image show the presence of 5 false-positive results i.e. a total of 63 tuning screws were predicted by both the algorithms. The comparative analysis of different algorithms is compiled in Table 2 where it is evident that the proposed SVM model provided better results in terms of the precision as compared to other algorithms.

Table 2. Comparative Analysis of Tuning Screw Detection Precision

ML Algorithm	Number of Screws Detected by the proposed classifier	Precision
SVM	60	96.66%
KNN	63	92.06%
DT	63	92.06%

4 Conclusion

This work presents a supervised learning-based method to differentiate the tuning screws of a microwave (MW) cavity filter from the mounting screws. The efficacy of automating the filter tuning process relies heavily on the precise maneuvering of the robotic manipulator over the tuning screws. The outcomes of this research present compelling evidence showcasing the feasibility of employing a machine learning-based model for accurate classification of tuning screws and mounting screws. The SVM algorithm demonstrates the classification precision value of 96.66%, surpassing other state-of-the-art algorithms. To augment the system's performance in the future, the researches aim to incorporate an optimal and efficient algorithm for measuring the height of the tuning screws with an optimal and efficient algorithm.

References

1. Cameron RJ (2018) Computer-Aided Diagnosis and Tuning of Microwave Filters. In: Microwave Filters for Communication Systems: Fundamentals, Design and Applications, Second Edition. pp 609–642
2. Lindner A, Biebl E, Strasse A (2006) A Manual Tuning Method for Coupled Cavity Filters. In: Proceedings of 36th European Microwave Conference, Manchester, UK. pp 1340–1342
3. Han L, Wu K, Chen X-P, He F (2010) Influence and Tuning of Tunable Screws for Microwave Filters Using Least Squares Support Vector Regression. International Journal of RF and Microwave Computer-Aided Engineering 20:422–429. https://doi.org/10.1002/mmce
4. Levy R, Snyder R V., George M (2002) Design of Microwave Filters. In: IEEE Transactions on Microwave Theory and Techniques. pp 783–793
5. Aggarwal CC (2018) Neural Networks and Deep Learning. Springer International Publishing
6. Marcot BG, Penman TD (2019) Advances in Bayesian network modelling: Integration of modelling technologies. Environmental Modelling and Software 111:386–393
7. Trabelsi A, Elouedi Z, Lefevre E (2019) Decision tree classifiers for evidential attribute values and class labels. Fuzzy Sets Syst 366:46–62. https://doi.org/10.1016/j.fss.2018.11.006
8. Zhang Y, Cao G, Wang B, Li X (2019) A novel ensemble method for k-nearest neighbor. Pattern Recognit 85:13–25. https://doi.org/10.1016/j.patcog.2018.08.003
9. Cervantes J, Garcia-Lamont F, Rodríguez-Mazahua L, Lopez A (2020) A comprehensive survey on support vector machine classification: Applications, challenges and trends. Neurocomputing 408:189–215. https://doi.org/10.1016/j.neucom.2019.10.118
10. Zhang M, Qu H, Xie X, Kurths J (2017) Supervised learning in spiking neural networks with noise-threshold. Neurocomputing 219:333–349. https://doi.org/10.1016/j.neucom.2016.09.044
11. Liang X, Zhu L, Huang DS (2017) Multi-task ranking SVM for image cosegmentation. Neurocomputing 247:126–136. https://doi.org/10.1016/j.neucom.2017.03.060
12. Vapnik VN, Chervonenkis AY (1964) A note on a class of perceptrons. Automation and Remote Control 25:103–109
13. Steinwart I, Christmann A (2008) Support Vector Machines (Information Science and Statistics). Springer Science + Business Media, New York

14. Bennett KP, Campbell C (2000) Support Vector Machines: Hype or Hallelujah? SIGKDD Explorations 2:1–13
15. Burges CJC (1998) A Tutorial on Support Vector Machines for Pattern Recognition. Data Mining and Knowledge Discovery 2:121–167
16. Vapnik V (1998) Statistical Learning Theory. John Wiley & Sons, Chichester
17. Cortes C (1995) Support-Vector Networks. Mach Learn 20:273–297
18. Joachims T (1998) Text Categorization with Support Vector Machines: Learning with Many Relevant Features. In: Proceedings of the 10th European Conference on Machine Learning (ECML). pp 137–142
19. Chapelle O, Haffner P, Vapnik VN (1999) Support Vector Machines for Histogram-Based Image Classification
20. Yin Z, Hou J (2016) Recent advances on SVM based fault diagnosis and process monitoring in complicated industrial processes. Neurocomputing 174:643–650. https://doi.org/10.1016/j.neucom.2015.09.081
21. Chandra MA, Bedi SS (2021) Survey on SVM and their application in image classification. International Journal of Information Technology (Singapore) 13:1-11. https://doi.org/10.1007/s41870-017-0080-1
22. Guyon I, Weston J, Barnhill S (2002) Gene Selection for Cancer Classification using Support Vector Machines. Mach Learn 46:389–422
23. Platt JC (1999) Fast Training of Support Vector Machines using Sequential Minimal Optimization. Advances in Kernel Methods - Support Vector Learning 185–208

Publication VIII

E. Sekhri, R. Kapoor and M. Tamre, “Review of State-of-the-Art Microwave Filter Tuning Techniques and Implementation of a Novel Tuning algorithm using Expert-based Hybrid Learning,” *Wireless Personal Communications*, pp. 1–57, 2024, doi: 10.1007/s11277-024-10894-x

Wireless Personal Communications
https://doi.org/10.1007/s11277-024-10894-x

Review of State-of-the-Art Microwave Filter Tuning Techniques and Implementation of a Novel Tuning Algorithm Using Expert-Based Hybrid Learning

Even Sekhri[1] · **Rajiv Kapoor**[2] · **Mart Tamre**[1]

Accepted: 29 January 2024

Abstract
Present-day demand and supply of connectivity necessitate the rapid production of Microwave (MW) filter units. The production of these filters is then followed by the step of utmost importance in the assembly line, viz., the 'tuning of the filter', as tuning is crucial to meeting the selectivity requirements of the band. Since the advent of filters, tuning has always been done manually, and hence it is considered a bottleneck by experts in the field. Thus, the need to automate the system is highly implied. The goal of the current work is to outline various MW filter tuning techniques that have been advocated by the community of researchers. The limitations of the said research works and their comparative analysis are also encapsulated in tabular form in the present paper. The paper ends with the implementation of an Expert-Based Hybrid Deep Learning Algorithm to fully automate the filter tuning process.

Keywords Cavity filters · Computer-aided tuning (CAT) · Filter tuning · Microwave filter tuning · RF filter tuning · Review paper

1 Introduction

Microwave/Radio frequency (MW/RF) filters, used for segregating the desired frequency from a plethora of frequencies, are the mainstays of space and ground-based wireless communication systems. A rapid surge in the demand for telecommunication systems resulted in manufacturing copious amounts of MW/RF filter layouts, which include but are not limited to waveguide filters, co-axial filters, microstrip-line filters, dielectric resonator filters, varactor-based filters, and so on. Of these, coaxial cavity bandpass filters are the most widely used in Wireless Base Station (WBS) filter installations. Furthermore, the casing of any filter comprises several coupled resonators. Since higher-order filters with cross-coupled topology meet the sharp frequency requirements of today's time, they are

✉ Rajiv Kapoor
rajivkapoor.dtu@gmail.com

[1] Tallinn University of Technology, Tallinn, Estonia

[2] Delhi Technological University, Delhi, India

commonplace in real-world applications. This cross-coupling facilitates the creation of Transmission Zero (TZ) [1]. Other than meeting sharp frequency selectivity requirements, these TZs also contribute to design flexibility; optimal in-band response; achieving Chebyshev response; and reducing the size of the filter (which further means low insertion losses, scaling down of manufacturing time, and an overall low cost). Furthermore, the presence of real TZ weeds out unwanted interfering signals, and complex TZs synthesize to equalize the Group Delay (GD). The algorithm to determine maximum attainable TZs for a particular topology had been presented in [2]. Fairly recent research sheds light on the effectiveness of Frequency-Variant Couplings (FVCs) in meeting the strict frequency requirements for which TZs were initially used [3].

The design and manufacturing errors that occur during the assembly of these filters mar the expected frequency requirements, making the tuning process inevitable [4]. Since time immemorial, various strategies, including mechanical, electronic, and magnetic systems, have been used to tune filters. However, the tuning elements, which include screws and varactors, are provided on the casing of the filter unit. The major factor that confers changes in resonance frequency coupling between the cavities and the overall frequency response of a filter is the insertion depth of tuning elements. The goal henceforth is to find optimal positions of the tuning elements so that the desired tuning specifications are met. Synoptically, we can safely say that by nature, filter tuning is an optimization problem.

Further, filters can be differentiated based on their layouts, bandwidth insertion loss, mid-band frequency, ripples, slope selectivity, etc. With such a huge variety of filters existing in the market, non-generalization of the tuning process can be safely inferred, i.e., one technique cannot serve the purpose of tuning all types of filters. In addition, the overall response of comb line filters is affected by the tuning structure [5] and the walls [6]. During tuning, the time elapsed and the difficulty level increases exponentially when complex filters (i.e., filters with higher-order and/or with cross-coupled topology) are to be tuned. This is because of the highly non-linear relationship existing between the filter's frequency response and the tuning elements [7].

The deterministic nature of the tuning process demands trained technicians and human operators. These human operators observe the scattering parameters response of the filter displayed on a Vector Network Analyzer (VNA). Although some guidelines for assisting these technicians are available in [8], intensive training is still mandated to acquire the necessary skillset. Furthermore, it is worth noting that completion of training in no way guarantees proficiency in the field, as some trainees, even after receiving months of training, fail to tune simple filters. In other words, these technicians are not certified MW engineers, and favorable outcomes are heavily based on their training and experience. Another pertinent factor worth noting is that if a technician is proficient in tuning one type of filter, there is no assurance that he/she will be able to tune other types as well. Considering all the aforementioned factors, filter tuning is now considered an "art" that needs time, training, and expertise. Industry's continuous need for competent and skilled tuning experts is a further worry, as finding new technicians is an arduous task. Also, as tuning requires heavy use of wrists, technicians often injure their wrists, and the industry has to bear the expense of their surgeries.

The attempts to find automated or semi-autonomous methods of filter tuning were initiated around the early 90 s. Using parameter extraction techniques, COM DEV Ltd. presented an intelligent filter tuning software in 1994 [9]. This software was deployed on the production line in 1995 [10], and could help technicians tune satellite multiplexers. Later, this solution was improved and was named 'RoboCAT'. In 2003, RoboCAT was used in commercial filter tuning [11] where the Coupling Matrix (CM) was extracted using phase

cloning and time domain techniques. However, the major limitations of the tuning solution provided by COM DEV Ltd. were—the decision making was script-driven; in the case when maximum tuning time was reached, an error flag was generated by the software, and the tuning software was made to restart; and the scenario of complete insertion or complete removal of the tuning screw was not considered. Considering all the above-stated shortcomings, one can easily infer that the solution provided by COMDEV Ltd. cannot be treated as autonomous or autonomous; hence, the need to find a more flexible, reliable, and self-sustaining solution is required.

Several researchers have proposed unique and distinctive solutions to solve or decipher the problem of the filter tuning process. This paper intends to review and summarize the major findings, furtherance, and development of various proposed techniques. What further adds to the compilation of this paper is the fact that the last of this kind was published three decades ago [12]. Furthermore, the mentioned paper was distinctly related to the present research as it only focused on LC (i.e., Inductor-Capacitor) based Low Pass Filters.

Every study, no matter how well it is conducted and constructed, has certain limitations. This research is also not without its pitfalls. The major limitation of this paper is that it focuses exclusively on filter tuning of band-pass filters and in line, the diagnostic methods that aid CAT of band-pass filters are also considered. Besides, most barring a few kinds of research considered in the present paper focus solely on the mechanical tuning of filters. But some research works presented in the 'Support Vectors Assisted Filter Tuning' category i.e., section '4*F. 6)'* of this paper were also tested over the electrical filters as well, so they have been included in this review.

Additionally, active filters, ferroelectric filters, superconducting filters, and varactor-based filters were beyond the scope of this paper and hence aren't considered here. The tuning of microstrip filters is also not reviewed (because the correct tuning of microstrip filters can be achieved during the design stage, i.e., by varying the dimensions of resonators, by changing the thickness of the dielectric substrate, by making gap ports in series for tuning, by adding cells, drilling holes, etc.). No tuning elements are directly attached to microstrip filters usually. Likewise, since master and doctorate theses failed to provide any autonomous solution to the problem at hand, the researchers decided not to include them in the periphery of the present research. To avoid copyright infringements, patents are also not reviewed in this document. The research publications that were solely dedicated to MW filter design are not looked at here.

The blueprint of the present research is as follows; Sect. 2 of the document extensively surveys the literature available in the field of filter-tuning. Section 3 compares and contrasts various techniques to tune the filters; the major limitations of these techniques are also presented in the same section. Section 4 presents the discussion on the recent trends and advocates the usage of Deep Learning as the future of the filter-tuning process. Concluding remarks are indicated in the final section of the article.

Note: The terms resonator, cavity resonator, and cavity have been used interchangeably in this paper.

2 Detailed review

The past few decades are testimony of the efforts laid in the advancement of filter tuning, with a battalion of researchers presenting varied techniques that can be used to tune the filters. Figure 1 shows the bifurcation of these techniques. The present section will deal with these methods one at a time.

The layout of the current section is as follows: the first paragraph of each category will provide a short introduction to a specific technique, followed by the research works reviewed by the authors under that.

2.1 Filter Tuning in Time Domain (TD)

For tuning of MW filters using the TD approach, a special discrete Inverse Fast Fourier Transform (IFFT) of the frequency response of reflection characteristics, i.e., $S_{ii}(\omega)$ is calculated. The resulting TD response, i.e., $S_{ii}(t)$, distinguishes the evaluated resonator resonance and inter-resonator coupling aperture response for both filter ports. Distinct 'Peaks' and 'Dips' seen on a network analyzer help in tuning each of the resonators individually. Referring to Fig. 2, each dip corresponds to resonator and the peaks represent inter-resonator coupling.

For $t<0$, these dips and peaks are meaningless; therefore, the first dip and the first peak closest to $t=0$ are considered the first resonator and the first coupling, respectively. In TD, the response of turning each tuning screw can be immediately seen, and hence can be

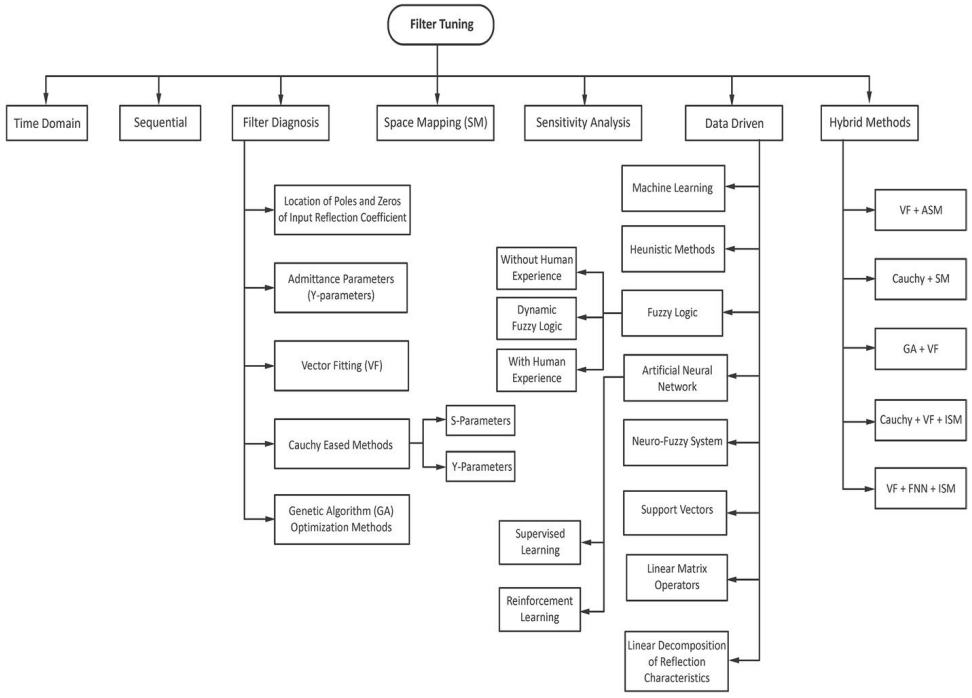

Fig. 1 Various filter tuning techniques

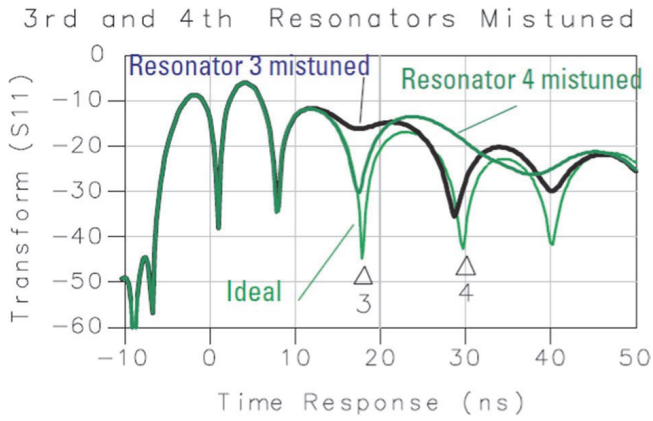

Fig. 2 Filter tuning in time domain [14]

accounted for. Such visualization and cause-and-effect relationship cannot be obtained in Frequency Domain (FD) based methods.

The first publication where the TD method was used for MW filter tuning was presented in 1999 [13]. The response of the reflection characteristics (S_{ii}) of a perfectly tuned filter (also called a 'golden filter') was compared with the response of the Device Under Test (DUT), that is, the filter that we are interested in tuning to find the correct position of the tuning screws. The technique was validated on a 5-cavity in-line coupled resonator filter. Later, in [14], the same author came up with three more examples that demonstrate the ease of the TD method in tuning the coupled-resonator BP filter deterministically. Turning a screw caused the change only in one portion of the curve, and it was shown that the sharpness of the depth of the dip was directly proportional to the extent of resonator tuning. Both these research works ([13] and [14]) were limited to filters with low losses and filters without cross-couplings. In [14], only the theoretical steps for tuning cross-coupled filters and the duplexers were presented, but those steps were not tested via simulations or experiments. The solution to one key limitation of the publications [13] and [14], namely, the tuning of duplexers, was then later presented by the same author in publication [15].

To overcome another limitation of [13] and [14] i.e., the tuning of cross-coupled filters (having symmetrical or asymmetrical transmission zeros) was dealt with in publications [16] and [17]. The effects of the presence of a cross-coupling were also well presented, and it was shown that for such complex (cross-coupled) filters, the depth of dips does not symbolize the current tuning state of the filter. To tune such untuned complex filters, a 'golden filter' or the simulated S-parameters of the desired filter were needed. Two approaches for strongly coupled filters were also presented in [17] but both of these approaches were not verified by any example.

Although the TD-based methods presented in [13, 14, 16] and [17] were flexible and robust, the major fallibilities of all these research works included: a) the coupling value considered for a cross-coupling was quite less than the main-line coupling and b) the tuning direction was uncertain. To overcome this uncertainty about the tuning direction, an advanced TD tuning method that relied on the phase of the reflection parameters was presented in [18]. The direction of phase-shift directly related itself to the difference between the resonance frequency and the center frequency. This information (i.e., whether the value is above or below the center frequency) helped to tune the filter quickly. But the method

presented in [18] could only be implemented on low-order all-pole filters. It could not be used to tune commonly used complex filters.

It is important to note that, with the exception of the TD methods mentioned in [13, 14, 16, 17], and [18], all of the other filter tuning methods presented in this document are based on FD tuning. For having a detailed literature review and a clear understanding of the reader, the authors of this review intentionally left out the bifurcation based on TD methods and FD methods.

As opposed to TD tuning methods which rely solely on reflection characteristics (S_{ii}) parameter of the filters for tuning, the FD tuning methods use reflection characteristics and/or transmission characteristics (i.e. S_{ii} and/or S_{ij}) to tune the filters. All the FD tuning methods use a common type of frequency response curve to tune the filters. Such a simulated frequency response is depicted in Fig. 3 which represents the insertion loss and return loss for a 5th order filter in FD. In Fig. 3, the red solid curve shows the transmitting signal, and the blue dashed curve presents the reflecting signal.

2.2 Sequential Filter Tuning

The publications mentioned under this category are the ones in which the authors advocated to either 'short' (strongly detune) the resonators or to tune the resonator and coupling screws in a particular order and/or direction. The intent behind using this technique was that with such a 'divide-and-conquer' technique, the tuning time will drop; the tuning difficulty will reduce, and the tuning process will be simplified.

The first sequential filter tuning method was proposed in 1951 [19], where an alternating short-circuit-based technique was proposed. This process dealt with minimizing the return loss for tuning the filter (as the 'short' resonator will stop the transmission of the signal in the forward direction). Regarding the direction of adjustment, the authors

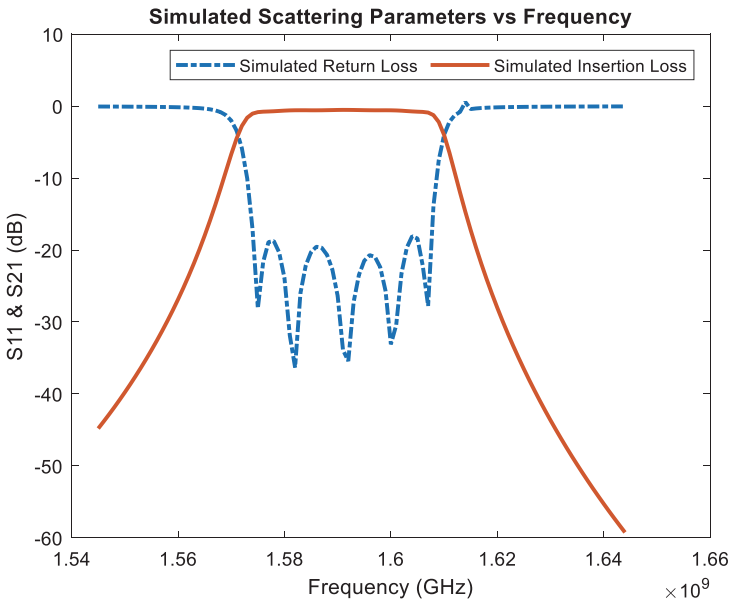

Fig. 3 Filter tuning in frequency domain

proposed that the adjustment must be performed from the input side of the filter (I / P) to the output side (O / P) by analyzing the voltage value at the center frequency of the filter. According to changes in input impedance (i.e., open or short), the author proposed observing the maximum voltage of all the 'odd' resonators and the minimum voltage for all the 'even' resonators. The method could tune BP filters, but a similar method could be extended to other types of filters as well (i.e., High-pass filters, Low-pass filters, and Band-reject filters). However, the key limitations of this research work were—the tuning process was manual; no information about the coupling values was available; a loosely coupled detector was required to measure the amplitude; this method was inefficient for tuning filter designs including resonators with varied resonant frequencies, and the process was highly iterative.

Atia and Williams in [20] presented another sequential tuning method wherein they had combined their methodology with the work presented by Dishal in [19]. The authors of [20] proposed to measure the resonant frequency and inter-resonator coupling of short-circuited filters using the filter synthesis technique proposed by them in [21]. The values were measured when the phase response of the input reflected coefficient (i.e., S_{11}) crossed 0° or 180° on the polar plot. This methodology was quite accurate, but achieving the same resonant frequency by synchronous tuning of every resonator required many trials, which made this process time-consuming. In addition, this method could not tune the filters with different resonant frequencies of the resonators. Also, during implementation, this method needed special care when dealing with cross-coupled cavities. The methodology presented in [20] was later used in [22] for tuning the singly as well as doubly terminated filters. Using the information of measured input impedance (matched to the condition of resonance), the resonant cavities and coupling elements were adjusted, but the tuning process was slow and tedious.

The work presented in [20] was then used for filter tuning purposes in 1986 [23], where a CAT system and the synthesis of lossless networks were presented. The method proposed in [23] was in conjunction with LCX i.e., Inductance, Capacitance, and Reactance synthesis which could determine the inter-cavity couplings as well as the resonant frequencies for a short-circuited network. However, the major shortcomings of [23] were—each cavity needed an I/P and O/P probe, and hence frequent cable changes were to be made; there was a need for prior characterization and calibrations of the tuning elements; and optimization routines were needed to optimize the filter's transfer function.

By modifying the method proposed in [19] and using the knowledge from [20], J. B. Ness in 1998 proposed a unique sequential method for tuning highly detuned resonators in [24]. The filter was divided into various sub-circuits. Then, the theoretically extracted Group Delay (GD) information of each sub-circuit was used one by one while maintaining the GD symmetry simultaneously. For a quick recall to the reader, theoretically, the GD of a reflected signal refers to the time delay of the amplitude and is a function of frequency. And, mathematically, GD is defined as a negative phase derivative with respect to (w.r.t.) angular frequency. This GD information was used for tuning resonant frequencies as well as inter-resonator coupling values of a filter starting from the input end to the output end. For fetching accurate results, while computing the absolute GD of one resonator, all the other resonators needed to be shorted completely, and hence, the magnitude of the GD of reflection characteristics was used for extracting the corresponding coupling values of the filter. However, the method in [24] was restricted to in-line filters only; and dealing with cross-coupled filters was tricky. Later, the scope of [24] was extended to parallel and cross-coupled filters in [25], but the proposed tuning process was complex, and the 'shorting' process was infeasible for practical cases.

Unlike [24] and [25] (where reflection characteristics were used to measure 'absolute' or 'actual' GD), the authors in [26] shorted the filter and measured 'relative' GD using transmission (i.e. forward) characteristics. The measurement was done with 'careful and limited' shorting (detuning) of the resonators so that the GD still exists. The relative GD was derived using the Hilbert Transformation [27] of the forward coefficient module. This allowed the use of low-cost hardware, i.e., a Scalar Network Analyzer (SNA) instead of using a Vector Network Analyzer (VNA), which is an expensive instrument. The method in [26] could eliminate the need for a directional coupler, which was mandatory to use in [20, 22], and [23]. However, the precision of this method suffered when incomplete or uncontrolled detuning was caused. Also, this method was not effective in tuning the higher-order filters.

The methods presented in [24] and [25] could deal with one reflection *S*-parameter only, but the methodology in [16] could use both I/P and O/P reflection coefficients (i.e., S_{11} and S_{22}, respectively) for tuning a filter. The same authors published the extended version of [16] in publication [28]. The proposed method could deal with singly terminated and doubly terminated filters that have an asymmetric frequency response with GD equalization. For *N* number of tuning elements, 'N' inverse sub-filter models were built. In terms of the tuning direction, this method could provide flexibility since tuning from both sides was possible (i.e., using the I/P reflection coefficient (S_{11}) or by using the O/P reflection coefficient (S_{22})). The key limitations of [16] and [28] were—the method was time-consuming; only moderately complex in-line and waveguide filters could be tuned; and like other methods discussed above under this category, this method could not deal with higher-order cross-coupled filters.

To assist the tuning technicians in tuning the cross-coupled filters, a sequential tuning concept depending on frequency domain data cloning was presented in [29]. This work had used the circuit model presented in [20] to develop this tuning method (although, for accuracy, even a golden filter could also be used instead of using an approximate circuit model). In [29], it was mandatory to manually short or to highly detune the resonators, but couplings were allowed to be set to 'weak state'. The method could tune the filters using linear scaled polar plots. In terms of tuning direction, the filter was tuned sequentially from both outer sides (I/P and O/P screws) towards the middle screw. However, the limitations like the careful selection of frequency cloning points; inaccuracies due to—increased order; increased complexity (position of cross-couplings), etc.; bandwidth limitations; and the need for manual shorting of resonators were the main reasons for restricting the implementation of this work in filter tuning application.

In the TD methods [13, 14, 16], and [17], the authors proposed tuning the filters in a particular order. The author proposed the tuning direction to be 'inward', that is, starting from the outer tuning screws of both sides and gradually moving towards the center screw(s). Publications [13] and [14] presented TD-based filter tuning of all-pole filters, while complex filters were discussed in publications [16] and [17]. In publications [16] and [17], it was required to find the node frequency. For quick recall, the resonant frequency with every coupling connected is known as the node frequency (i.e., main and cross-couplings, being grounded for each resonator). For finding the node frequency of complex filters, the author of publications [16] and [17] proposed to set the VNA to dual-channel mode i.e., with one channel in FD; and the other one in TD. To perfectly tune the filter, a repeated process of setting the VNA's center frequency to each node frequency was a mandatory step for reaching the maximum dip level. The need for changing the center frequency from time-to-time restricted the implementation of this sequential filter tuning methodology in the industry.

Another sequential tuning method, based on the Neural Network (NN), was presented in [30]. In this work, the authors presented a NN inverse model for mapping the S-parameters of a cross-coupled filter to the corresponding tuning screw position. So, 'N' inverse sub-filter models were built for *N* number of tuning elements (i.e., resonator cavities; the inter-resonator couplings; and the cross-couplings). For collecting the training vector set for the NN architecture, each tuning element of a perfectly tuned physical filter was made to detune slightly in both directions. The collected training vectors were limited to reflected S-parameters of the input side only, but they could be extended to other parameters as well. A 3-layered (input-hidden-output layers) Feed-Forward (FF) architecture was used in this work. Since only one sub-filter was taken at a time, the output layer had only one neuron. The trained ANN could provide the amount of adjustment needed to tune the sub-filter under consideration, and then the next sub-filter was considered. The tuning direction was proposed to propagate from the I/P side to the O/P side of the filter. But the need for a vast number of datasets for training purposes limited the implementation of this method at the industrial level.

2.3 Filter Tuning Based on Filter Diagnosis

The filters we see today are based on the initial model proposed by Atia and Williams in the 1970s [31] and can be expressed in the form of a Coupling Matrix (CM). CM reflects GD as well as the magnitude of the filter's frequency output response. The elements of CM have a one-to-one correspondence with tuning elements and can assist in the filter tuning process. So, filter diagnosis (i.e., extracting the CM elements) is an essential and crucial step for effective tuning of a filter. The difference between the desired CM and the extracted CM can determine the tuning direction as well as the magnitude of turn needed for each tuning screw. The desired CM is an ideal CM that meets the stated requirements with a realized topology. For filter diagnosis, various techniques have been proposed in the literature. They are based on following methods: 1) Location of Poles and Zeros of the Input Reflection Coefficient; 2) Admittance Parameters (Y-Parameters); 3) Vector Fitting (VF); 4) Cauchy Method; and 5) Optimization process for CM extraction. All these techniques are described sequentially in the following sub-sections.

2.3.1 Filter Diagnosis Using the Location of Poles and Zeros of the Input Reflection Coefficient

During the implementation of this technique, all tuning screws are initially inserted deeply within the filter cavities (also called 'shorting') to bring a large difference between the initial frequency response and the desired response. This methodology allows the use of polar plots for tuning. While attempting to tune the filter, the polar display of VNA is observed until the reflection coefficient starts to appear as a 'spot'. During this time, the frequency is swept many times the bandwidth (around the desired center frequency), and then the phase reference plane is adjusted to find the best spot on the sweep. The phase reference plane is subsequently modified to locate the optimal location on the sweep after the frequency is swept numerous times the bandwidth (around the intended center frequency). This is then considered the reflection coefficient's 'zero' or 'reference' position. Only after performing this calibration process, the tuning procedure is initiated.

In [32], a CAT algorithm based on regular network functions of an equivalent filter circuit was presented to find the relationship between filter response and tuning screw

depth. The developed model could provide the compensation matrix (also called correction matrix). Finding the locations of poles and zeros, and tuning direction was based on the phase of the input reflection coefficient (with short-circuited output). It is important to mention here that in the case of direct measurement, the definition of poles and zeros refers to 0° and ± 180° phase-crossings of the input reflection coefficient. However, the major limitations of the work presented in [32] were: the strongly detuned filters could not be tuned; the proposed algorithm could provide assistance in the tuning phase but the actual tuning was to be finally performed by a human operator; removing the 'short' and correspondingly connecting the absorber was an important step to tune the last element (which earlier was ineffective due to shorting); and the authors neglected the further tuning of the filter once the tuning was in the acceptable tuning range (i.e., even if the filter was still not perfectly tuned at that state).

To avoid the cumbersome method of finding the location of the poles and zeros using phase crossings of 0° and 180°, a filter diagnosis method based on FD was presented in [33]. This work was a generalized form of the work presented in [20]. In [33], after performing the calibration task, the resonant frequencies and inter-cavity couplings of the cascaded coupled resonators were determined. By comparing the extracted values with the measured values, the desired frequency response was obtained. This method was suitable for tuning the cross-coupled cascaded filters. However, the proposed method was not capable of providing a convergent solution when the resonant frequency of one resonator was strongly dependent on the neighboring resonators. Therefore, the method was limited to lower-order filters only.

The work in [33] was extended in [34], where phase-loading effects were also removed for accurate filter tuning. Closed-form recursive formulas for determining the resonant frequency and inter-cavity couplings (using an equivalent-circuit model) were provided in [34] and [35]. The authors of the publication [34] used a modified equivalent-circuit model, while the authors of [35] used symmetrically bisected networks (singly terminated). As in [24], the phase-derivative w.r.t. frequency (i.e., GD) was used in [34] and [35] for determining poles and zeros accurately. In [24], GD information was used for co-relating coupling values between the physical model and the circuit model. The use of phase-derivative removed the phase-loading effect unintentionally in [34, 35], and [24] but it was not systematic. For quick reference of the reader, while simulating GD, 'poles' are the values of frequencies at which phase-derivative is minimum. And, correspondingly, where the phase derivative value is maximum, are the 'zeros'. The authors of [34] and [35] provided design examples and measurement examples to demonstrate the effectiveness of their method. However, the main shortcomings of [34] and [35] were: the effects of phase-shift and losses were not discussed; both these methods relied on a mathematical model that was not exact; the method was limited to cascaded and symmetrically coupled filters only; and there was a requirement for having an additional transmission line at the O/P or I/P port of the filter because the reference plane for phase-measurement was not easily accessible. Due to these limitations, both methods were unsuitable for practical use.

Similar to the methods discussed in [34] and [35], the CM extraction method presented in [36] also needed an additional transmission length. By using information about the location of poles and zeros, a simple computer program was developed. The method in [36] was implemented on directly coupled Dielectric Resonator (DR) filters. The concept of using 'coupling matrix rotation' was presented for the first time in this publication. The Q_u value of the resonant cavity (i.e., the loss for each resonator) was consistent in the CM extraction process. However, it was restricted to specific filter topologies only.

2.3.2 Filter Diagnosis Using Admittance Parameters (Y-Parameters)

When connected to a measurement device (usually a VNA), the output obtained from MW filters is in the form of scattering parameters (abbreviated as S-parameters). But some researchers proposed the conversion of these S-parameters to Y-parameters for tuning the filters. The reason for this conversion can be attributed to the fact that Y-parameters are more accurate; are in dimensionally reduced form, and their model sensitivity is better. The poles and residues obtained from the transfer function of Y-parameters can then be synthesized easily to fetch the corresponding CM by the techniques proposed in [37] and [38].

The analytical method of extracting CM using partial-fraction expansion of the Y-parameters was investigated in [39] in which poles and residues were used. This method did not need extra calibrations for determining the loading effects. The notion of constant phase-loading was introduced in this paper; however, it was not explained how to determine the constant's value. In addition, a very basic procedure for the extraction of Q_u was presented, and the application of this method was limited only to lossless cases. Later, these problems were addressed in [40] but the authors of [40] mainly introduced the concept of phase-loading and only provided the basic procedure of extracting unloaded Q value.

The concept of phase-loading introduced in [39] and [41] was later explained in terms of theory and implementation (mathematical model as well as the analytical formulas) by the same authors in [42]. The CM extraction method presented in [42] was appropriate for lossy filters with non-uniform Q_u. This work provided information regarding de-embedding techniques for unknown transmission lines section and dealt with the degenerate poles in terms of Y-parameters. The process was deterministic without needing any initial guess of the value. The proposed algorithm could determine the tuning element responsible for detuning, but the main limitations of this work were: the method could not deal with Source-Load (S-L) coupling of the filters; the procedure for phase-shift removal required careful selection of frequency samples; the method was applicable mainly to low-loss filters only as the poles were not easily distinguished from the magnitude of Y-parameters; even if the method had been proposed for filters with non-uniform Q_u values, the implementation was restricted to filters having nearly the same Q_u (i.e., short range of variation only); and the assumption of having 'pure real residues' for the system while fetching the 'imaginary portion of poles' of the Y-parameters limited the use of this method. This is because such an assumption is not true for filters with non-uniform Q values.

To overcome two major limitations of [42], that is, to avoid the need to deal with degenerate poles of Y-parameters; and to deal with S-L coupling, the researchers proposed another method in [43]. The method presented in [43] could deal with the lossy cross-coupled BP filters and could also avoid the noise issues that occurred during the measurements. Characteristic polynomials were obtained using the S-Parameters based Cauchy Method (discussed later in sub-section '*4a'* of this paper) after removing the phase-shift effects of the measured S-parameters. These phase-shift effects were caused by the unknown length of the transmission lines at I/P and O/P ports. Then, these S-parameters were converted to Y-Parameters (having normalized characteristic impedance) using standard conversion procedures presented in [44] for obtaining the CM and unloaded Q_u. However, in [43], the Q_u factors were inaccurately obtained and hence the process was inefficient.

To increase the efficiency of the CM extraction process, the Y-Parameters-based Cauchy method [45] (discussed later in sub-section '*4b'* of this document) was used to obtain the characteristic polynomials of a lossy cross-coupled filter. The method in [45] was capable of being used for filter tuning as it did not require the removal of filter losses while

extracting the CM and uneven Q_u value of each resonator. However, the main limitations of this work were: the phase-shift still needed to be removed, and this method required careful selection of frequency points for finding an accurate CM, which restricted the commercial usage of this method.

2.3.3 Filter Diagnosis Using Vector Fitting (VF)

Vector fitting [46] or its modification [47] uses a measured or numerically simulated filter response to create reduced-order models. The approximate rational function polynomial generates a partial fraction expansion form instead of directly fitting the data into polynomials, and VF guarantees the stability of poles and zeros (as they are iteratively identified). So, the researchers tried to use this methodology in the field of MW filter tuning.

A diagnosis method for the synthesis of Y-parameters of lossy cross-coupled filters with a transverse network model was presented in [48]. The method could identify the position of poles and residues of obtained Y-parameters. The real part of the obtained complex poles provided all the information regarding the approximated uniform Q-factor, while the residues of partial expansion of the Y-Parameters were assumed to be real. The authors of this method just talked about the diagnosis of filters with S-L coupling but did not present any examples to justify it. Another limitation of this work was that Q_u was assumed to be constant. Such an assumption is not correct for commercial communication filters.

To deal with lossy filters with uneven Q_u values, researchers proposed another method in [49]. The method could provide accurate Q_u values and could also extract complex poles and residues. To do this, the rational polynomials for a general practical filter were solved in terms of Y-parameters by using measured or simulated S-parameters. However, the main issues with this research were: frequency samples could be specified only on the positive side; inclusion of error occurred while performing BP to LP transformation of the obtained poles and residues, and obtaining these complex poles and residues was an iterative procedure.

2.3.4 Filter Diagnosis Using Cauchy Method

'Simple Cauchy Method' is a fast, accurate and convenient technique for converting measured or simulated S-parameters of lossless, reciprocal 2-port passive devices to reduced ordered rational functions (i.e., interpolants or extrapolates) [50]. It is possible to use the reduced number of data samples for such conversion [51]. Starting from the BP response, these rational functions are further used to generate a polynomial model in the normalized LP frequency domain (having the minimum order of the model and minimum error) [52]. The number of resonators and the total number of TZs are the ones which are responsible for deciding the degree of characteristic polynomials. The Cauchy method uses a Vandermonde Matrix for converting the systems of equations into a simplified matrix form. But unlike other passive devices, for MW filters, two sample sets, i.e., ($S_{11}(f)$) and ($S_{21}(f)$) (wherein f being the frequency variable) are fitted simultaneously. According to filter theory in [53], both these S-parameters should share a set of common poles (building two independent models is not the optimal way because some useful information might get lost or not fully exploited). Thus, to deal with MW filters, the 'Simple Cauchy Method' was modified by research community for considering both the sample sets simultaneously. Some authors used a special polynomial '$K(s)$', also known as a characteristic function or filtering function. This $K(s)$ is the ratio of Transmission Zero (TZ) to Reflection Zero

(RZ). In general, the use of *K(s)* ensures that the sets of zeros are independent of losses in the filter. This 'Modified Cauchy Method' has been termed as 'Cauchy Method' in this document.

It is important to note that for solving the systems using Cauchy Method, the technique of Total Least Square (TLS) [54] is often used in conjunction with Singular Value Decomposition (SVD). The use of TLS ensures optimum solution when the matrix of a given system is noisy, and the use of SVD makes the method capable of solving over-determined systems. Usually, the characteristics of polynomials are solved using a two-step procedure. In this two-step procedure, the numerator coefficients of the polynomials are obtained in the first step using TLS and/or SVD. Then, in the second step, Feldkeller's equation (which is an energy conservation equation) is used to find the common denominator coefficient.

For filter diagnosis, researchers have proposed two variations of the Cauchy methods. They are—a) S-parameters based Cauchy method, and b) Y-parameters based Cauchy method. The publications published under both methods are discussed below sequentially.

2.3.4.1 S-Parameters based Cauchy Method In [55], both ($S_{11}(f)$) and ($S_{21}(f)$) were simultaneously used for finding the filter model. While obtaining the CM, the authors also considered the S-L coupling coefficients. In this work, TLS was used to solve the system, but the main limitations of this research work were—the stability of the rational model was not guaranteed; there was no constraint on the behavior of the model outside the frequency measurement band; and this work was limited to modeling the filter only (i.e., did not consider filter tuning within the scope).

Later, the methodology proposed in [55] was used to assist in filter tuning in [56]. A fast algorithm based on model optimization had been proposed in this work, where the researchers could generate the polynomial models of S-parameters by using a two-step procedure. The authors of [56] used a special polynomial ratio i.e. $K(s)$ instead of using normal S-parameters. After extracting the model, the algorithm approximated the second-order effects on the response of the filter and eventually derived two different CMs (including S-L coupling), i.e.: a) Extracted CM; and b) Objective CM. After comparing these matrices (in every tuning iteration), the Jacobian Inverse of the obtained error vector related the circuital errors with the physical deviations of tuning screws. The method proposed in [56] used the 'Simple TLS Method'. After using TLS, the use of SVD solved the over-determined system. Finally, CM synthesis was done using analytical methods, and this method could tune cross-coupled filters. The main limitations of the work presented in [56] were—the very simple design was chosen for validation; initial adjustments were made; the method required lossless measured data; the proposed method was unable to determine the amount of loss in the filter; the use of *K(s)* required posterior reconstruction of common poles; and the method was limited to no or low loss filters only (as lossless Feldkeller's equation had been used).

The work presented in [57] is an improved version of [56] and could extract the characteristic polynomials of lossless and lossy filters. The numerators and denominators were solved in one step only in this research work. The key differences between [56] and [57] were—the authors of [57] used the 'Constrained TLS Method', and [57] did not consider the polynomial ratio of *K(s)*. The main limitations of the work presented in [57] were: the proposed method could not diagnose the filters having S-L coupling; the second-order effects (i.e., the presence of spurious pass-bands as well as the frequency-depending couplings) could not be dealt with; the lossy polynomials given by this method were not apt for the synthesis of lowpass prototypes using the well-established techniques in [37] and [38]

(because phase-shift is included when raw data of *S*-parameter measurements are used); and, the TZs were not realizable.

To overcome the limitation of [57], a special condition for having realizable TZs presented in [58]. In [58], the forward transmission coefficients (i.e., S_{21}) alternated between pure imaginary and pure real values. The model proposed in [58] was a reduced-order model and was independent of the type of measurements (i.e., lossless or lossy measurements). In addition, the method could synthesize the lossless circuit model from the measured data of a lossy system. The combination of TLS + SVD was used to obtain polynomial characteristics (as was used in [56]) to obtain a good match between the measured values and the model values. However, to find this good match, this method required careful selection of the frequency points (i.e., frequency points close to the desired passband, as the presence of second-order effects may reduce the accuracy). Furthermore, the researchers used constant Q_u values in this work. But the methods proposed in [57] and [58] could deal with low to moderate loss filters only (but not the commercial filters) and be limited to filter modeling only.

The methods proposed in [56] and [57] were tested for the tuning of GSM filters in [59]. The equations were solved using TLS + SVD (as in [56] and [58]) and then Feldkeller's equation was used to find characteristic polynomials. This method could successfully identify the detuned elements by comparing the extracted CM with the desired CM using the characteristic function *K(s)*. The desired CM was obtained using a golden filter unit. But during the CM synthesis process, matrix rotations [60] were needed. The use of the golden unit was also important in determining the tuning sequence on Device under Test (DuT). The main benefits of this whole process were—no optimization was required after synthesizing the CM, and a minimal amount of pre-tuning was needed. However, the method was limited to the pre-tuning stage only.

To increase the capability of the methodology presented in [56–58], and [59], that is, to also consider lossy filters, the researchers proposed a method in [61]. In this work, the characteristic polynomials corresponding to the lossy S-parameters were extracted using measured or simulated data. The filtering function *K(s)* was used in [61] and the effects of losses were removed by shifting the poles and zeros of *K(s)* to find a lossless model or lossless polynomials as the first step. In this work, the characteristic polynomials were found using a two-step procedure. SVD was initially used to solve the system matrix, and then Feldkeller's equation was used to obtain the rational functions in the second step. General CM was synthesized using [38], but the final CM was then extracted using eigenvalue-based optimization [62]. From the extracted CM, the proposed method could provide the external quality factors (i.e., Q_{EXT}) and the unloaded Q (i.e., Q_u). However, in [61], all resonators were assumed to have the same Q_u and the method was restricted to low loss filters only.

To overcome the limitations of [61], i.e., to accurately deal with the filters with large losses, the researchers proposed a method in [63]. The authors of [57] also talked about removing losses from the extracted polynomials, but the process proposed by them was slow or had lower accuracy. The method presented in [63] used a modified BP to LP transformation from the frequency domain to the normalized lowpass domain i.e., from f-domain to s-domain (including losses defined by Q_u) for extracting the CM. This transformation provided a lossless response of the filter by shifting the roots of lossy polynomials to the right-hand side of the s-plane. From this lossless response, CM was extracted. Again, *K(s)* was used and the three characteristic polynomials (i.e., *F, P,* and *E*) were solved with a two-stepped procedure. Numerator polynomials *F* and *P* were obtained using TLS + SVD. Then, in the second step, Feldkeller's equation was used to find the denominator *E*. The

application of Feldkeller's Equation was better as compared to the ones used in [57] and [58] (as they have F and P in normalized lossy domain with some approximations in Feldkeller's Equation). With the method presented in [63], losses associated with all the resonators in a filter could be obtained, and there was no need to apply the de-embedding techniques presented in [42]. However, the main limitations of the method presented in [63] were: the method was again limited to cases where Q_u was the same for all resonators (i.e., uneven Q effect was not handled effectively); this method failed to diagnose filters possessing the S-L coupling; this method could not deal with second-order effects (i.e., the presence of spurious passbands as well as frequency-dependent couplings); and phase-shift effects were not considered.

It is important to note that for extracting an accurate CM, the phase-shift effects need to be removed. Phase-loading and transmission lines at the filter's I/P and O/P ports are the sources of phase-shift effects. The widely used CM synthesis method presented in [38] doesn't provide a correct CM unless the phase-shift effects are not removed. In this regard, some methods, such as those presented in [34, 35] and [42] were proposed for phase-shift removal. To remove phase-shift effects, the methods presented in [34] and [35] required additional transmission lines, while the work presented in [42] needed careful selection of frequency samples, and therefore these methods could not be used practically. Other methods where phase-shift effects were removed using GA (Genetic Algorithm) optimization were then presented in [64, 65], and [66]. The use of an optimization routine could improve the accuracy of CM and Q values.

To remove the phase-shift effects and to obtain Q_u values, the authors of [64] used 3-parameter optimization; researchers of [65] presented a 5-parameter optimization procedure (characteristic polynomials are solved in one step using the method presented in [57]); and then, the authors of [66] used a 6-parameter optimization procedure (in two stages). The authors in [64] didn't consider the effect of the presence of S-L coupling at all, but this effect was later considered in [65]. The work presented in [66] is an extension of the reference [65] where S-L coupling was handled specifically for the case when the number of transmission zeros is equal to the order of the filter. In all these methods (i.e., in [64, 65] and [66]),,the common things were: a) the modified BP to LP transformation presented in [63] was used for converting the measured or simulated S-parameters from the f-domain to the s-domain; b) after removing the phase-shift, the characteristic polynomials were obtained in one step using [57] by simultaneously solving the system's equations using TLS + SVD; c) for meeting the accuracy levels, all these methods needed the frequency samples to be chosen near the passband; and measurement of noise was not necessary. Having the samples far from the passband may lead to poor accuracy because of the second-order effects; d) all the methods presented were simpler than the ones proposed in [42] as there was no need to deal with degenerated poles of the Y-parameters and they didn't require any additional Transmission Lines (TL) as was needed in [34] and [35]. However, the authors of [64] and [65] assumed the same value of Q_u for all resonators. The assumption of having the same Q_u was removed in the second stage of the optimization of [66], but this methodology was complicated, and it needed a lot of time to reach the optimal solution. Furthermore, the convergence rate of GA is slow when variables are approaching the solution.

To further increase the accuracy of [66], a different variation of the Cauchy Method was proposed in [67]. For obtaining an accurate lossy CM, the Differential Evolution (DE) optimization was used, wherein uneven Q_u and non-ideal effects were taken as the unknown parameters to be optimized. DE was found to be fast in converging and was accurate as compared to GA (as there were fewer parameters in DE which needed adjustment).

In addition, the initial values did not have a great influence on the final results. In addition to GA, the authors also implemented Particle Swarm Optimization (PSO) to prove the effectiveness of the proposed method. The method also presented the relationship between non-ideal and ideal S-parameters (the non-ideal effects were obtained using [42]). The BP to LP transformation was different as compared to [51] for finding the model of the lossy polynomial. In the used transformation, the resonator loss effect (by uneven Q_u) was not considered. The measured S-parameters were transformed to ideal form. In this work, *K(s)*; TLS + SVD; and Feldkeller's equation were used to find characteristic polynomials. Later, CM (with losses included) was synthesized from the characteristic polynomials. However, this method assumed that the forward and reverse characteristics were equal, which is not true for highly detuned states. Furthermore, Feldkeller's equation was not suitable to find the characteristic polynomials.

A different variation of the Cauchy-based method was proposed in [43], which allowed the filter diagnosis (while also considering S-L coupling) with the help of Y-parameters. In this investigation, 05 complex coefficients were solved in one step using SVD. Initially, S-parameters were used to obtain the characteristic polynomials after removing the phase-shift effects with the help of 4-parameter GA optimization. These characteristic polynomials later helped in calculating the Y-parameters and then CM was extracted for the desired filter topology. The method could deal with uneven Q_u filters, but the Q_u factors were not accurately obtained using this method. Furthermore, this research was restricted to the S_{11} and S_{21} parameters only.

The method presented in [68] considered the measurement of S_{11}, S_{21}, and S_{22} data together for the first time and could deal with uneven Q_u filters. A point to note here is that the non-reciprocal nature of the filters is not affected by considering the lossy effects, which implies that the condition $S_{21} = S_{12}$ still holds. In this work, the Y-parameters were used to determine rational polynomials, and those Y-parameters were converted to S-parameters using standard formulas for finding the coefficients. Then, by using TLS + SVD, the CM was obtained by performing a few matrix transformations presented in [69]. The imaginary part of the CM provided information about the level of power dissipation, while the real part of the CM indicated the current coupling values. For mapping, the BP response to the corresponding LP prototype domain, the transformation presented in [61] was used. However, the method was complex and time expensive as it needed the calculation of the positive scaling factor also.

The S-parameters-based Cauchy methods could not provide the solution to the fundamental problem of having a CAT system. Hence, some authors tried working with Admittance parameters (Y-parameters) based on Cauchy methods to come up with the solution. Such research works are discussed in the next sub-section of the paper.

2.3.4.2 Y-Parameters Based Cauchy Method The Y-parameters have reduced dimensions and offer enhanced stability in extracting the CM. Unlike the case of use of the S-parameters based Cauchy Method (like the ones discussed in the previous subsection), we do not need to deal with the removal of filter losses while extracting the CM and uneven Q_u value of each resonator when Y-Parameters are used.

In [45], the Cauchy method was used for the first time exclusively in terms of Y-parameters (i.e., conversion to or from S-parameters was not required). This analytical method could deal with filters with uneven Q_u for each resonator. The characteristic polynomials *U, V,* and *W* were obtained in one single step. While the CM and uneven *Qu* were extracted, the filter losses were not to be considered separately. Poles and residues could also be

obtained in just one step only i.e., iteration cycles were not needed. However, even in case of the use of Y-parameters, the phase-shift still needed to be removed, and this method required the frequency samples to be chosen near the passband for accurate results.

2.3.5 Filter Diagnosis Using Optimization

The basis of this filter diagnosis technique is to optimize the defined circuit model's parameters to ensure that the response it produces matches the intended response. The main idea is to compare the parameters between an ideal filter and those that are extracted from a filter model (or from a real filter). By comparing these parameters, the tuning element(s) which is(are) responsible for the detuning can be identified and the defined objective function (error function) is minimized at the sampled frequency points. The process continues until the error between the ideal and measured/extracted coupling elements is reduced to an acceptable value. This methodology allows for the tuning of all elements simultaneously, and the error is compensated at each iteration.

In [70], a method was presented to determine center frequencies and coupling coefficients using element optimization routines. Initially, the filter response was measured, and then an optimized circuit model was generated using network element values to meet the measured filter response. This optimized model helped to perform the diagnosis and alignment of the filter. The process was repeated until the desired filter response was achieved. The major drawbacks of this approach were that the method was: a) iterative (hence time-consuming); b) needed precise calibration and previous characterization; and c) it could not be generalized to different filter topologies.

In [16] and its extended version [71], the researchers presented a tuning algorithm based on an approximated/equivalent network representation that consisted of lumped elements. The representation was derived using the prototype network model presented in [53] (as one of the examples) and the model investigated the effects of I/O couplings. The values of lumped elements were obtained using standard filter tables for deriving the models, and resistive elements were used to include the losses. The model values were extracted from S-parameters using gradient-based optimization. The optimization routine was aimed at minimizing the Mean Squared Error (MSE) between the measured and simulated responses at the selected frequency points in [16] and [71]. Variations of the S-parameters were assumed to be linear w.r.t. frequency. The algorithm could provide optimized tuning elements and correct tuning screw positions using another gradient-based optimization. However, the major pitfalls of [16] and [71] were—there was a need for pre-adjustments and the careful selection of initial values for optimization. The response of the DUT needed to be close to the desired response, and only the magnitudes of the S-parameters (i.e., S_{11}, $S_{21,}$ and S_{22}) were considered when implementing this method.

Instead of using an equivalent network as in [16] and [71], the researchers proposed the direct use of generalized filter prototype models for parameter extraction in [72] and its extended version [73]. The method presented in [72] was limited to direct-coupled filters only, whereas higher-order and cross-coupled filters were also considered in [73]. Both these research works ([72] and [73]) considered the magnitude and phase of the S-parameters. The phase shift by the I/P and O/P probes was modeled by adding transmission lines on both sides (I/P and O/P sides) of the filter (which is not possible when EM simulations are used). This non-linear gradient-based optimization could minimize the MSE between the extracted and desired responses. The values of the extracted parameters were then used to adjust the tuning screws. After the sensitivity analysis, the optimal parameter values were finally found using

another gradient-based optimization procedure. However, this method needed a pre-tuned filter whose response (S-parameter response) was quite close to the ideal response, i.e., pre-tuning was important.

Later, in [74] and [75], the researchers used the Model-Based Parameter Estimation (MBPE) technique [76] for reducing the frequency-domain response of the measured S-parameters to the corresponding polynomial coefficients to obtain TZs and RZs. The key idea of using MBPE was to minimize the cost of measurement and computation (to acquire and represent the frequency response) within the specified frequency range. The concept of using a constrained search minimization routine (i.e., sequential quadratic programming (SQP) [77]) was used for filter diagnosis and tuning in [74] and [75]. The locations of the RZs and TZs were determined and then optimized using multilevel optimization, but the ripple losses and return losses of the filter were not considered in either of these research works. The method of TLS based on SVD had been used for handling the overdetermined system (linear), which made the method insensitive to the noise in measurements. In [74], the measured S-parameters were approximated using a polynomial ratio with real coefficients, but the ratio was not accurate. The ratio (and henceforth the modeling) can be accurate only when the polynomials have a complex coefficient. In addition, [74] did not investigate the diagnosis and tuning of a real/measured filter. In [75], the researchers used an adaptive frequency sampling (for MBPE) that was sensitive to parasitic effects. The rational function model of the S-parameters was built and then CM was extracted. This led to error diagnosis and filter tuning of lossless or low loss filters based on the estimated lumped-element model and multi-level optimization. But methods proposed in [74] and [75] were restricted to limited solutions because they relied on pre-tuned filters whose frequency response was quite close to the ideal response (ensuring that the system wasn't trapping into local minima). Consequently, this method failed to provide the correct solution for actual filter tuning.

The non-linear optimization algorithms presented in [16] and [28] could provide information about the detuned parameter and the amount of detuning. The solution in [16] was implemented in the filter production line of Tesat-Spacecom GmbH & Co. KG. But many multi-level parameter optimization cycles were needed, which made this process time-consuming; and the methodology could be implemented only on low-ordered filters with simpler topologies.

In [23], pattern search optimization was needed to optimize the singularity of the filter transfer function. A model was used to find the resonant frequencies and the inter-cavity couplings. This was the first CAT method presented to tune the MW filters. But the method was quite basic and time consuming.

The method presented in [23] was later used in [33] to find the optimized values of resonant frequency and inter-cavity coupling at the specified number of frequencies. But this method was also suitable for lower-order filters only.

The ROBOCAT presented in [11] relied on the Coupling Matrix (CM) extraction process for filter tuning. The method of phase cloning was used in conjunction with the time domain to come up with this non-linear optimization-based tuning method. But the process was also quite time-consuming and had other limitations that were presented earlier in this review paper.

2.4 Space Mapping (SM)-Based Filter Tuning

Application of the Space Mapping (SM) technique in the field of MW filters can be traced back to the year 1994 [78] when EM optimization problems were solved using this

approach. Later, the research community also presented an advanced version of this technique, i.e., Aggressive Space Mapping (ASM) [79] and Implicit Space Mapping (ISM) [80]. For the convenience of the reader, the SM has been briefly recalled here. SM has two separate models, where the physics-based model that is fast but has low accuracy is called the 'coarse model'; while the model that is computationally intensive and accurate is termed as 'fine model'. The coarse model handles the burden of the main optimization simulations, while the fine model is used for validation purposes. Iterative updates of the mapping provide a quick and accurate matching between both models. Details of the SM approach have been presented in [81]. A review of methods for reducing the differences between the coarse model and the fine model by managing the preset parameters, and continuously optimizing the coarse model to reach the defined ideal target was presented in [82].

In [83], the ASM methodology was used to tune a 04-pole waveguide filter based on an electromagnetic model (EM). For practical applications, ASM is commonly used due to its ease of implementation and simplicity [83]. However, such EM-based models are computationally heavy compared to the total time taken for the direct measurements, and thus are not used for commercial filter tuning applications.

In [84], a simple SM approach presented in [85] was used for generating a 'Compensation Matrix'. This matrix provided the relationship between the CM elements and the deviation of the tuning screw. The use of the SM approach helped in excluding the cross-dependencies between resonators and adjacent couplings. Thus, the approach to iteratively finding the correct tuned state was improved. The inverse compensation matrix gave access to the compensation effect. The coarse model had entries related to CM, whereas the advanced fine model had information about tuning screw positions. This method showed cross-dependencies between various adjacent elements, but this method assumed a linear relationship between CM elements and tuning screw depth. Thus, the method was restricted to simple and lower ordered filters only.

In [86], the SM technique was used to create a surrogated model for tuning the filter. The mapping was iteratively updated to approximate the fine-model solution using a surrogate. The surrogate was established using an EM-based circuit simulation software named ADS, while the fine model was a manufactured component. In this work, the tuning parameters were needed to be pre-set to acceptable reference values in the beginning. In addition, the initial parameters of the surrogated model were taken from the datasheets as well as from the theoretical aspects. Such a pre-characterization is not possible with the tuning of real-world filters, and the simulation cannot completely establish the tuning rules for real filters. These pitfalls limited the commercial use of this method.

To overcome the limitations of [87] and [86]; and also, to deal with unexpected variations in filter behavior, the authors in [88] used a circuit-based coarse model instead of an EM model. This constrained surrogate model was established by combining an ISM-based coarse model with a linearly approximated measured response w.r.t. tuning parameter change (i.e., change from the basis point). Then, the recursive multipoint parameter extraction techniques proposed in [89] and [90] ensured the reliability of this surrogated model as well as the uniqueness of the solution obtained from each parameter extraction step. The robustness of the proposed approach was improved by simultaneously mapping the response as well as its first derivative w.r.t. tuning parameters. Since the number of fine model perturbations is directly related to the possibility of finding a unique solution, [16] was used to add the perturbations when iterations failed. But this work considered only a single basis point, and hence the model was not very reliable. Additionally, this algorithm converged only when the basis point considered was close to the desired point.

2.5 Filter Tuning Based on Sensitivity Analysis

The idea behind using the concept of Sensitivity Analysis in filter tuning is to find the coupling model that can reveal the relationship between the tunable screws and the frequency response of the filter. In 1945, Bode [91] highlighted the importance of having information on network analysis. He showed that network sensitivity can be reduced by feedback. Generally, sensitivity comprises the relationship between the change in the defined function and its variable parameters. In the case of filter tuning, the function could be a model to map the filter response when the positions of the tuning screws were varied.

In [92], a CAT algorithm for MW filter tuning had been proposed. This algorithm combined the use of sensitivity analysis and linear-search technique on MW filters for predicting—the detuned component; tuning direction; and amount of tuning needed. The authors of this work calculated the response sensitivity of each component (i.e., variable component) at each specified frequency. This method was superior to techniques involving the usage of pattern-search or sequential linear search. In [92], the adjustment size was determined using a linear search. The procedure was to seek a different component in every iteration until the desired response was achieved. But this method was not aggressive as perturbations from only known values were considered. In addition, no backup plan was presented in the event of a primary system failure. Thus, this method could not be applied in commercial applications.

In [32], an equivalent filter circuit-based CAT algorithm was proposed to find the relationship between the filter response and the depth of the tuning screw. The developed model used the combination of a compensation matrix and a sensitivity matrix for tuning. The tuning criterion was derived using a method that depended on the phase of the input reflection coefficient of a singly terminated filter. However, this method suffered because—repeated sensitivity measurements were needed; pre-tuning/calibration was mandatory to adjust the level of detuning of the elements (to a nearly linear state); the strongly detuned filters could not be tuned; the presence of humans was inevitable (to tune the filter); fine-tuning was needed to obtain reasonable solutions; and, the method was based on a filter model which was not exact.

To avoid the complex processes of filter modeling, previous characterization and calibration, another filter tuning algorithm based on sensitivity analysis was presented in [93]. This algorithm used the Gauss–Newton solution of the equations to provide the required adjustment as an output. The algorithm could be successfully implemented on various filter networks that met the condition of having a linear relationship between filter response and the tuning element. However, such a linear relationship is valid for only a small tuning range, and therefore this method was implemented only in the fine-tuning stage (as the coarse tuning in this research work was performed using [19]).

Gradient-based optimizations were used in [16]—[73] to find the filter model values from the measured S-parameters. An approximated network representation (consisting of lumped elements) was presented in [16] and its extended version in [71] to come up with a tuning algorithm. The research work presented in [72] and its extended version [73] rather used the basic model proposed in [31]. The sensitivity of each tuning screw was determined by the corresponding element value in the model. This mathematical coupling model revealed the relationship between tuning screw position and the filter's response for CAT. However, pre-tuning was done before applying the proposed algorithm in the selected frequency range, and hence the tuning range was restricted.

A *Y*-parameter-based CM extraction method which was applied to lossless filters had been presented in [42]. The authors of this publication advocated the use of Sensitivity Analysis for all coupling elements present in the extracted CM. However, this step was needed only in the fine-tuning stage, i.e., when the difference between the ideal and extracted coupling elements was very small. Like in [42], the method presented in [86] could also use the sensitivity information during the fine-tuning stages only.

2.6 Data-Driven Approach for Filter Tuning

When provided with abundant data, all the data-driven models like Machine Learning (ML), Fuzzy Logic (FL), Artificial Neural Network (ANN), Support Vectors, etc. can build the relationship coupling model between S-Parameters and screw deviations. The performance of this obtained model is directly proportional to the amount of input data and the method (or the algorithm) used. Data-driven methods usually consider the filter a 'black box' and do not analyze the collected S-parameters. Thus, the ideal benefit of using this approach is that, in this case, the error that occurs while generating the mathematical model of a physical filter is eliminated.

In the following sub-sections, all data-driven approaches proposed for filter tuning applications have been compiled sequentially.

2.6.1 Machine Learning (ML)

In [94], researchers tried to tune the waveguide filters using the ML approach, where the pattern recognition algorithm and adaptive signal processing techniques were used. The initial/coarse tuning was done by the human operators, and the final tuning (the fine-tuning) was carried out with the help of adaptive combiners. While implementing this algorithm, the features were collected both from a perfectly tuned filter; and from a filter that was detuned by a known amount. This dataset (i.e., information about features and the amount of detuning) was given as an input to a Recursive Least Square (RLS) algorithm. This algorithm then estimated the weight factor of the Finite Impulse Response (FIR) filters attached to adaptive combiners. These combiners were implemented using many FIR filters connected in parallel. Consequently, the algorithm indicated the tuning element to be adjusted and the amount of adjustment needed to be performed as an output. The proposed RLS algorithm minimized the MSE for reducing the amount of detuning. The polar plot of S_{11} was chosen as the basis of tuning as it contains information about the phase as well as the amplitude of the signal. In each iteration, only the screw that generated the maximum error value was adjusted. The proposed algorithm was robust in the sense that GD could also be tuned with this method. Nevertheless, the major limitations of this work were: a skilled technician was needed to tune the filter; the publication did not mention the amount of calibration and other manipulations that were performed on all the coupling screws while implementing this method; the influence of coupling screws was not investigated in this work; this method did not provide the whole solution to the problem (as some tolerances were ignored); and, the method could be used in the fine-tuning stage only.

2.6.2 Heuristic Filter Tuning (Derivative-free)

For avoiding modeling; sensitivity analysis; and, any kind of special measurement, the authors in [94] used the combination of two derivative-free optimization-based methods,

i.e., Simulated Annealing (SA) [95] and Direct Search (DS) [96] to tune the filter. SA was used for pre-tuning and then DS was used during the fine-tuning stage. The tuning screw positions were defined as independent variables in the optimization routine. For experimentation purposes, the Intelligent Automatic Filter Tuning Tool (IAFTT) [97] was used. But major limitations of this work were: the authors only considered the input reflection characteristics (S_{11} parameter) of the filter as a tuning criterion and numerous repeated turnings of the same screws were needed, which is unsuitable for having a CAT system.

2.6.3 Fuzzy Logic (FL)

Boolean/Classical Logic cannot be used directly in filter tuning applications because of the complexity of this process. So, researchers tried fuzzy logic/sets for filter tuning applications. FL can help to have a comprehensive model which comprises 1) objective knowledge (i.e., mathematical model and measurement data); and 2) subjective knowledge (i.e., rules based on expert information). In FL, the numerical data are interpreted as 'Linguistic Rules' where the membership value of '0' implies that the element is not belonging to the set and vice versa for the value '1'. The initial idea of using FL in filter tuning was attributed to the fact that technicians responsible for filter tuning in the industry use knowledge such as 'Sets Theory' to adjust coupling values. These technicians are experts in this task and possess the sense of quickly observing the measured response they are seeing in VNA to conclude the specific 'Set' to which this current coupling element belongs. This technique opened the possibilities of integrating measured data, theoretical models, and human experience into one unique model.

When dealing with the problem of filter tuning using FL, the researchers proposed two different kinds of methodologies. They are—a) FL without considering the human experience, and b) FL with human experience taken into consideration. Both these categories are now discussed one by one in the following sub-sections.

2.6.3.1 FL without considering Human Experience While using FL, the S-parameters of the filter at pre-defined frequency sampling points are given as input to the model. This model then provides tuning variables as its output, which further provides us with a CM. By comparing the generated CM elements with the corresponding ideal CM, the tuning elements which are responsible for filter detuning can be obtained.

In [98] and its extended version [100], the Mamdani type Fuzzy Logic System (FLS) was presented (Mamdani type is referred to as the one in which centroid defuzzification gives crisp outputs). The linguistic antecedents of the 'if–then' rules were the S-parameters, while the linguistic consequences were the coupling elements. The authors set the I/O fuzzy sets with triangular membership functions. Training pairs helped in the CM extraction process, which further helped in knowing the de-tuned tuning elements. However, the major drawbacks of this approach were the following: the method did not tell the amount of adjustment needed; the method had difficulty in tuning higher-order filters and filters with cross-couplings; since no iteration was performed once the FLS was ready, the method required enough data pairs before building the FLS; and this method used two separate FLSs for dealing with less detuned problems and highly detuned problems.

Different than the method proposed in [98] and [99], the method in [100] used only one Sugeno type FLS for diagnosis and tuning of slightly detuned as well as highly detuned problems (Sugeno type FLS is the one which is more flexible and uses a weighted average of each rule's output for the final output). In this research work, the

Gaussian Membership Function was used. To minimize the number of 'if–then' rules, and to find the center of every membership function, the subtractive clustering [101] technique was used by the researchers, where each cluster defined a rule itself. The designed FLS used S-parameters to generate the CM elements at the predetermined frequency sampling points. CM elements helped identify the screw element that caused detuning. However, the main limitations of this research work were—there was a need to establish complex fuzzy logic rules; the proposed method was not effective enough to reach the level of correct tuning state; and the experience of the technicians was not taken into consideration in [98, 99] and [100].

2.6.3.2 FL with Human Experience Consideration The use of human-expert knowledge for filter tuning was inevitable and was discussed in FL-based systems presented in [16, 102], and [103]. The intent behind using this approach was to model the filter as well as the thinking process of experts while they are tuning the filters. Using human experience, an intelligent, efficient, and fast-automated algorithm for tuning the filters was expected.

The authors in [16] presented a method in which the knowledge of a filter tuning expert was used to propose a filter tuning algorithm for the first time. Human intelligence was used as a Fuzzy Logic Controller. The First Order Sugeno type FLS presented in this work used Gaussian type membership functions and variable standard deviations. The technique of Subtractive Clustering [101] had been explored for grouping the data pairs to several rules. The method could identify the tuning elements that were the source of detuning, but in this work, only the return loss of the filter was used, i.e., the S_{11} parameter. For the method to be successfully implemented, the learning data required enough scenarios. But having all the possible scenarios is practically impossible and hence this method failed to meet the desired objective. Also, the method was restricted to the in-line topology-based lossless filters only, which again limited the implementation of this process for tuning the real-world filters.

The filter tuning method proposed in [102] used a two-step tuning procedure: (1) Coarse tuning; and (2) Fine tuning. On both these levels, fuzzy controllers were used separately. During filter tuning, human intelligence was captured for the first time in terms of linguistic 'if–then rules' by using triangular membership functions. The method was quite similar to the one proposed by Ness in 1998 [24] where GD information was used to tune the couplings and the resonating frequency (when all resonators were shorted before tuning the filters). But in [102], the purpose of using GD was to measure the phase offset before initiating the tuning process, and the phase response helped in the 'coarse tuning' stage. The defined if–then rules helped the Fuzzy Logic Controllers to initially 'coarse tune' and then 'fine tune' the filter. The authors of this method also presented the possibility of adding more expert rules. The author had designed specialized hardware and software to enable complete automation of the project. Nevertheless, this method was also restricted to lossless in-line configuration filters.

Later, a customized fully automated filter tuning system based on FL was presented in [103], which used the same concept as in [102] but could deal with more complex filter topologies. Similar to [102], linguistic 'if–then rules' with triangular membership functions were also used in [104]. But the main limitations of this work were: the method could not deal with resonator loss; the implementation was again limited to the tuning of in-line filter configuration only; the solution could be used in limited conditions, and there was difficulty in extracting the filter parameters. Therefore, this methodology could not be used in the industrial filter tuning process.

It is important to mention here that in all the FL-based methods (i.e., [98]—[103]) presented above, extracting the CM was a must to tune the filters correctly.

2.6.3.3 Dynamic Fuzzy Logic The only thing that affects the accuracy of filter tuning with FLS is the number of cases used to define the fuzzy rules. In [104], variable universe adaptive FL was introduced, which allows the universe to contract or expand. This helps in overcoming this dependency and provides a reliable tuning scheme. However, each screw had to be adjusted sequentially and progressively in order to achieve the desired frequency response. The sequential tuning procedure suffers from error propagation as its main problem.

In another study [105], an innovative fuzzy logic system (FLS) was proposed that incorporated dynamic attention for improved performance. This approach offered the advantage of adaptively regulating the evaluation function and modifying tuning goals in real-time, all without requiring modifications to the existing set of fuzzy rules. The suggested methodology also provided a precise, rapid, and efficient technique for tuning complex filters. Nevertheless, it should be noted that this FLS had limitations in terms of its capacity to autonomously learn tuning procedures and adjust critical parameters during optimization processes.

2.6.4 Artificial Neural Networks (ANNs) Based Filter Tuning

When talking about a multidimensional universal approximator for MW component design and their tuning, ANNs are considered to be the most reliable ones. Using ANNs, the unambiguous mapping between the S-parameters and the tuning screw deviation is built to yield an inverse black-box model. ANNs can be trained using 'training samples' from a properly tuned filter unit or a 'golden filter' unit. Later, using this trained inverse model, raw (detuned) S-parameters can be given as input to the approximator, and the output will be the individual tuning screw error (i.e., the deviation needed in tuning screws to meet the desired filter characteristics). Research in this area is divided into two categories: a) Supervised Learning; and b) Reinforcement Learning. The next sub-sections are dedicated to these different approaches.

2.6.4.1 Supervised Learning In publications [106, 107], and [108], a Feed-Forward (FF) ANN structure with a single hidden layer had been chosen as the network architecture. All of these publications considered S_{11} characteristics to tune the filter and used IAFTT Robot [97] for detuning the filter to collect training data. A common term, namely generalization error (GE), has been used in all these publications, which refers to the ability of an ANN structure to tune the 'test elements' even if those inputs were not used while training the ANN. The smaller GE value ensures a better ability of the algorithm to tune the filter correctly. However, this further means that there should be a sufficiently high number (i.e., as high as possible) of 'training vectors'.

The use of ANN for tuning the MW filter was first presented in [106], where an inverse model between S-parameters and screw deviations was built using a Back Propagation (BP) FF-ANN. Researchers could analyze the generalization abilities of the model for the case where learning vectors were extracted from one filter and the tests were performed on other filters (but both having the same topology). Unlike [30], the samples were collected randomly in this work. When detuned S-parameters were presented to the NN structure, the proposed algorithm could provide the amount of tuning needed for all the tuning elements

simultaneously. ANN, being a universal approximator, could tune the filter, but the algorithm presented in this publication was very basic, i.e., almost all filters needed some fine tuning (even some of the filters could not be properly tuned by the proposed algorithm). Also, the analysis regarding the correct ANN structure was not studied.

The approach presented in [106] was extended further by the same author in [107] to improve the generalization abilities of the proposed ANN structure with the usage of many golden filters. This helped in preparing better quality training vectors to improve the overall efficiency of the ANN tuning algorithm, i.e., by reducing the GE. However, the main limitations of [106] and [107] were—the generated model could not be updated in real-time, the algorithm was required according to the filter topology; only cavities were tuned while the couplings were fixed (i.e., the couplings were pre-tuned); and only S_{11} characteristics were used. In addition, just like [106], this work also didn't analyze the correct ANN architecture.

The scope of the work published in [106] and [107] was further expanded in [108], where the authors presented an analysis of the structure of the ANN for FT applications. In this work, the method for choosing an optimal number of frequency sampling point was presented. Thus, the optimal number of input neurons needed to train the ANN structure according to the selected topology was presented. After having the optimal number of neurons, the following benefits were obtained: the ANN structure had been optimized and the number of weights could be reduced; the GE was reduced; and the algorithm learning time was improved. However, the inter-resonator couplings were assumed to be pre-tuned (as in [107]) and only the cavity screws were tuned with this approach. This selective approach in choosing the screws limited the use of this method commercially.

The use of PCA in ANN-based filter tuning (non-linear) was first presented in [109]. PCA helped in truncating the less effective data points and reduced the number of input vector dimensions without downgrading the generalization ability of ANN. Another method to reduce the number of neurons in the Input Layer of an ANN structure is to use Wavelets [110]. The Daubechies Wavelet (D4) was transformed to compress the S-Parameters by shortening the ANN's input vector length. By doing so, the ANN structure could be trained faster, and the generalization ability was not lost. However, the Wavelet-based technique was applicable to simpler ANN topologies only and cannot deal with higher-order cross-coupled filters.

All the methods presented above were applied to simple filters or duplexers with a clearly defined center frequency. Later, an inverse model was proposed to tune the filters with different center frequencies was proposed for the first time in [111]. It had been shown that the working signal must undergo a phase transformation (after performing the frequency shift proposed in this work). Among the five proposed phase compensation methods, the 3-line method gave the minimum Root Mean Squared Error (RMSE). This 3-line method was applied to model the phase-difference between the complex signals before and after the change in frequency. This compensation was then used to tune variable-frequency filters (i.e., the filters that can be tuned in a certain frequency range). This method could provide better generalization abilities, but was again limited to the S_{11} parameter only, and hence could not solve the fundamental problem of automatically tuning the filters.

2.6.4.2 Reinforcement Learning (RL) The use of RL in ML today's models is inspired by the learning process of animals. In principle, when an animal is given a reward (positive or negative) for doing a particular action, it triggers (and simultaneously trains) its biological neurons. Then the animal tries to retake the positive actions to obtain the

maximum amount of positive reward. This is how the trend is reinforced. The idea of using this biology-inspired method in problem-solving algorithms had been made possible with the help of Neural Networks (NNs). The process itself is a Temporal Difference (TD) approach and was first presented in a mathematical sense in [112]. Later, this mathematical approach was further developed in [113] and was named Q-learning. The Q-learning 'agent' (i.e., the algorithm) works in an 'environment' (i.e., a simulation environment). An agent explores the environment by taking 'actions' (i.e., possible movements) and by entering different 'states' (i.e., inputs of the learning ANN model). The agent simultaneously obtains the corresponding positive or negative 'rewards' (that is, Q values) for entering that state. This is how better values of weights and bias of an ANN structure are updated iteratively while the agent learns to maximize the positive future reward.

The use of reinforcement for modeling of the filter tuning process was presented for the first time in [114]. This work was motivated by the research work presented by DeepMind [115] (which in itself was a modified version of [116]). In [115], it was shown that the proposed algorithm could beat human experts in playing Atari games by learning those games using ANN models. The authors in [114] simulated a 20–20-4 FF-ANN. This network was used as a Deep Q-Network (DQN) and was trained using a Back Propagation Neural Network (BPNN) algorithm. Before training, the use of PCA technique reduced the dimensionality of input data. In the filter example, the authors used a 04-channel combiner but considered only one channel of the combiner. The researchers used 02 main screws (resonators) to test their algorithm. The major limitations of this research work were—1) only S_{11} characteristics were considered; 2) the reward strategy was discontinuous and not well defined; and 3) the solution often fell into local minima. Later, we (the authors of this review paper) presented an optimal filter tuning method in [117] where the use of a Lagrangian multiplier in DQN ensured that the DQN algorithm finds the Global Minima. The algorithm presented in [117] was quick and efficient compared to [114], and a CNN architecture was used in this work. However, this research work was also limited to S_{11} characteristics only; and the reward strategy was not continuous.

Later, the researchers used the Deep-Deterministic Policy Gradient (DDPG) algorithm to tune the filter in continuous action space. The authors of [118] included knowledge of the controlled 'Vector field' approach [16] for having a better reward function and good generalization abilities. The vector field had been initially obtained by tuning all the screws independently. The work in [118] considered 04 screws for tuning the filter with their algorithm, but again, the key issue with this research work was that the authors limited the scope of this work to the return loss characteristics of the filter only. Also, the decision of step size as well as the idea of curve truncation while using a controlled vector field approach was not straightforward.

We proposed another approach of using double deep Q-learning (DDQN) for filter tuning in [119]. The use of the DDQN algorithm ensured that there was no maximization bias, and the algorithm could learn the optimum strategy to tune the filter. The Locally Linear Embedding (LLE) technique [120] was used in this research work for reducing the dimension of the collected data. This proposed algorithm was quick and accurate as compared to other proposed algorithms based on RL, but this work was again limited to S_{11} characteristics only.

Different from other ANN-based methods, Recently, the authors of [121] proposed a method where S_{11} and S_{12} parameters were used together to correctly tune the filters. The authors used a discrete reward function in their algorithm (as in [114]) and had used the DDPG algorithm proposed in [116]. The outcome of their algorithm was provided by a

DQN algorithm, but again, the method was restricted to lower-order filters only and cannot be implemented on real-world filters directly.

In a recent study [122], researchers introduced a new approach that enables machines to learn from human tuning strategies through continuous reinforcement learning (RL). To gather training data, the authors employed a robotic system to collect information from one channel of the combiner. Previous methods that utilized RL for filter tuning predominantly relied on simpler reward functions. However, in their study [122], the authors conducted a comparison of tuning performance and time using three distinct reward functions. Notably, they observed that incorporating a reward function inspired by human behavior resulted in reduced exploration and consequently improved system performance. However, the methodology faced limitations due to its simplistic model and its ability to capture only the vertical changes in the curve. Moreover, similar to other methods that rely on reinforcement learning for filter tuning, this approach was constrained to a simulated environment exclusively.

2.6.5 Filter Tuning Based on Neuro-Fuzzy System (NFS)

The method presented in [123] was motivated by [106], where the researchers wanted to come up with a new multi-dimensional approximator for filter tuning application. The idea of using Fuzzy Logic (Sugeno type) and Neural Networks hybridization was initially proved to be a universal approximator for various applications by Jang in 1993 [124]. Such a system exploits the capabilities of ANNs to get the parameters of a FLS and provides—online-learning, fast learning, small computational complexity, and smaller errors. In [123], the proposed adaptive network-based fuzzy inference system (ANFIS) structure could map the S-parameters of a filter to the deviation of the tuning screws. This system used a decreased number of learning vectors and also produced a smaller Learning Error (LE) and Generalized Error (GE) compared to the GE value obtained when only the ANN structure was used in [106]. However, in general, the method was presented only in terms of the reflection coefficient, i.e., $S_{11,}$ and assumed the couplings to be pre-tuned. The authors mentioned that the proposed algorithm could be used when forward characteristics are used, but the consideration of main and cross-couplings was a must. However, the pitfalls of this methodology were that the training process was time consuming, and the model could not be updated in real-time.

2.6.6 Support Vectors Assisted Filter Tuning

Support Vector Algorithms are powerful even if they are based on tiny sampled statistical theory for learning. Such algorithms can find an optimal solution (i.e., SVR-based models do not fall into local minima) even by using a small number of samples, and hence are advantageous as compared to ANNs. Various researchers used this technique to come up with EM-based coupling models that could aid in filter tuning.

For filter tuning, the first wavelet kernel mechanism model based on Least Squares Support Vector Regression (LS-SVR) was presented in [7]. The LS-SVR technique is apt to have a mathematical model when we have smaller samples of high-dimensional nonlinear data. In [7], the authors came up with a model that deals with the relationship between the change in the length of the tuning screw and the corresponding change in CM. The major shortcomings of this work were: instead of measuring the screw positions directly, the positions were rather approximated by solving the optimization

problems; and some discrepancies always exist between an ideal model and a real product. These two factors led to error generation and affected the generalizability of the proposed model. In addition, the proposed method was limited to simple filter topologies only, where each output port could be considered separately.

In the case of devices with multiple output MW Filters, the traditional SVR approach (like LS-SVR) is not effective enough as it treats every output separately. By treating the outputs separately, the relationship between different outputs cannot be obtained. Different LS-SVRs are needed to individually learn each output and correspondingly improve modeling accuracy. The various Multi-output LS-SVR (MLS-SVR) algorithms proposed by researchers in filter tuning applications have been described in the following paragraphs.

In [125], by using Multi-Kernel Linear Programming Support Vector Regression (MKLP-SVR), an efficient EM coupling model for filter tuning has been presented. While human experts were performing the manual tuning of the filter, the data about the success and failures of that tuning process was recorded. In this work, the researchers used existing knowledge of the S-parameters in terms of the corresponding CM discussed in [126] to come up with this intelligent method. The model presented in [125] revealed the relationship between the tuning screws and the electrical performance of the filter. To have a multi-output regression model, they used multi-kernels and the method presented in [7]. For extracting CM, the authors of this work used the technique presented in [48]. The method proposed in [125] was effective and could even deal with cross-coupled filters of moderate order. However, the main limitation of this research work was that the method relied on expensive optimization routines to obtain the required amounts of deviations needed to tune the filters.

Different from the MKLP-SVR model presented in [125], a hybrid modeling method that incorporated prior knowledge and multi-kernels in LP-SVR, i.e., an MKPLP-SVR model was proposed in [127]. In [125], the methodologies presented in [48] and [63] were used for the extraction of CM. The data for training the model was collected from measurements carried out during tuning process (and then there was even a possibility of expanding the data by experiments or by a prior simulator model). The proposed methodology was tested on an electrically tunable filter. However, the major shortcomings of this work were—1) CM was extracted in an ideal state; 2) the approach does not provide an accurate CM when the filter is in a highly detuned state; and 3) the criteria of model and hyperparameter selection for the algorithm proposed in this research work was not discussed. To further increase the accuracy of the model with the shortage of data, another hybrid MKPLP-SVR modeling approach was later proposed in [128]. It is important to mention here that only the modeling technique was hybrid but not the methodology used (and for this reason, the publications [127] and [128] are not listed in the category of '*G. Hybrid Methods for Filter Tuning*' (discussed later in this review). The authors of [128] advocated the use of two models complementing each other, that is, a) the Coarse Model (empirical formulas or equivalent models), and b) the SVR model. The coarse models are fast but are inaccurate. Hence, the SVR model was trained to learn and simultaneously correct the difference between the two models. The proposed model could use prior knowledge to improve the accuracy of the model and the extrapolation capabilities of the model even outside of the training data. A 4-pole electrically tunable filter was used as an example for validation purposes. But again, the approach presented in [128] could only provide the S-parameters in terms of a CM (but not directly as S-parameters read from VNA, as was in the case of [7, 125], and [127]). Also, all these methods, i.e. [7, 125, 127], and [128] were suitable only when the filter was slightly detuned.

To come up with a model for highly detuned filters, the authors of [129] used a pole-residue-based Multi-output Least Squares Support Vector Regression (MLS-SVR) [130] methodology. This method used the information about poles and residues as they are less sensitive and more accurate than other rational coefficients. To obtain an accurate CM, the input to the proposed algorithm was the changes in the length of the tuning screws and the information about the frequency. And the outputs were poles or residues of the Y-parameters (converted from S-parameters for reducing the dimensions and increasing the accuracy) by using a modified version of the VF method presented in [47]. The extracted CM considered phase-shift inconsistency as well as cavity losses. A full-wave EM simulation software named 'HFSS' was used to generate the training data set. However, data from software (physics-based EM models) generally does not reflect the exact tuning rules of real-life filters. Also, the method was limited to be used with simpler filter topologies only, which restricted the practical implementation of this method.

2.6.7 Linear Matrix Operator Based Filter Tuning

Unlike other data-driven model-based approaches, a methodology based on linear mapping was proposed in [131]. Using the Linear Matrix Operator, the model could map the relationship between variations in S-parameters while changing the tuning screw's height. The samples used in this research work were collected using IAFTT [97]. The matrix to determine the linear mapping was determined with the help of the Least-Squares Method (LSM) [132], and the approximation error was minimized in this work by using the procedure of 'outliners elimination'. Eliminating the outliner helps to remove 'unsuitable' candidates for building the linear operator. These 'unsuitable' candidates or the 'outliners' are the ones that are far from the rest of the data, or they are responsible for impairing the quality of the approximation. In [131], the tuning efficiency was improved by using Principal Component Analysis (PCA), which helped to transform the information from a data space to a feature space. PCA helped in dimensional reduction (or compression) of the data, which further led to a quicker tuning process. Compared to ANN-based filter tuning methods, the method presented in [131] was quick because it did not require a lengthy training process. However, the main limitations of this research work were—the datasets were collected randomly; the authors only considered the tuning of the cavities and that too in the limited range; the cross-couplings and the main couplings were pre-tuned, and they were not used for collecting the datasets. Hence, this method was not apt to tune a raw filter.

2.6.8 Filter Tuning Using Linear Decomposition of Reflection Characteristics

The basic idea of using the Linear Decomposition technique in filter tuning application was that the research community assumed that the relation between data-pairs could be expressed by functions composed of a sum of the polynomials.

In [16], two major limitations of ANN-based and Linear Matrix Operator-based techniques were removed, i.e., 1) the need to conduct a random detuning of a filter for collecting data-pairs for training, and 2) the need for a lot of data-pairs. In the approximator proposed in [16], very coarse data pairs of tuning screw deviations and the corresponding S-parameters were collected in a 'controlled manner' using a robot. While extracting data pairs, only one screw was turned at a time in this research work. However, there were three major limitations in this research work: 1) only the S_{11} parameter was considered; 2) only the cavity screws were tuned, that is, it was assumed that there was no need to tune the

coupling and cross-coupling screws; and 3) the proposed solution could be implemented on slightly detuned filters only.

The work in [16] was extended in [133], where the authors considered reflection and transmission characteristics of the filter response to tune the filters that were closer to the real-world filter tuning application. The method of collection of S-parameters was the same for both these publications, and the model for the relationship between S-parameters and corresponding screw positions was a sum of an argument polynomial function. Furthermore, the linear optimizer built in this research work was based on a coarse set that could generate deviations corresponding to cavities and cross-couplings (cross-coupled filters were not considered in [16]). The method was fast as compared to CM Extraction-based tuning methods because the training was not needed, but the response of this optimizer was slower than ANN-based tuning methods to find the proper screw deviation values.

2.7 Hybrid Methods for Filter Tuning

Filter tuning using the combination of two or more different approaches was implemented by various authors. Theoretically, by using a hybrid approach, better results are expected as compared to results that are obtained while using a single approach/methodology. Such publications are listed in this section of the article.

2.7.1 Filter Tuning Using VF + ASM Technique

The authors of the publication [134] proposed a hybrid method in which the VF method and the ASM technique were used together to adjust the filters. VF was responsible for extracting the filter parameters (filter diagnosis) from a general cross-coupled network in terms of Y-Parameters. Then, the ASM technique was used to calculate the optimal screw positions, and hence ASM guaranteed the correctness of the tuning direction (clockwise or counterclockwise). The method was validated on higher-order filters, but the key issue with this approach was that quite a lot of sample points were needed to achieve the desired amount of accuracy, and hence, the method was slow.

2.7.2 Filter Tuning Using Cauchy Method + SM-Based Techniques

In [135] and [16], a combination of the Cauchy Method and the ASM Method was presented for filter tuning. The frequency-based sampled S-parameters were converted to rational functions (i.e., a ratio of polynomials) with the help of the Cauchy method. Then, CM was extracted from those polynomials. The optimized ASM model helped in determining the correct direction of screw turning in both these research works. The method in [135] was fast and simpler compared to the method presented in [134]. Furthermore, the method in [135] considered the S-L coupling factor and was reproducible. However, the method presented in [135] was iterative and required the condition of having sampling frequency points close to the passband and should be adjusted iteratively. The method in [16] talked about Asymmetrical Phase shifts that were not considered in [134] and [135]. In [16], phase-shift was removed before applying the Cauchy Method. However, the main limitations of [135] and [16] were that the application of the method was limited only to lower-order filters with no or fewer cross-couplings only.

In [136], a hybrid tuning method based on human experience and the ISM-based data optimization method was proposed. When the detuning level was high, the initial tuning

was carried out by a human operator whose task was to meet the desired frequency range only (i.e., 'coarse tuning'). This manual step helped to eliminate the computational complexity that may arise due to huge initial deviations. After coarse tuning, the fine-tuning is usually time-consuming for humans, and to deal with the 'fine tuning' stage, the authors of this work used the ISM algorithm. The inputs to the proposed algorithm were extracted coupling values, i.e., the values generated using the Cauchy method (after removing the phase effects and loss effects with the help of the GA Algorithm). The modified transformation presented in [63] was used, and a two-step procedure was used to find the polynomial of the common denominator once the numerators were obtained. The algorithm established the mapping between CM value variation and the deviation of tuning screws. However, the main drawback of this approach was that the resonators were assumed to have the same Q_u.

2.7.3 Filter Tuning Using GA + VF Techniques

The method in [137] proposed to use GA optimization to remove the phase-shift from the measured (or simulated) Y-parameters of a coupled narrow-band BP filter. Then, the use of the VF methodology helped in determining complex poles and residues from the Y-parameters for extracting the CM. The standard transformation formulas presented in [44] were used to convert the S-parameters to the Y-parameters. The frequency transformation presented in [61] was used to convert the bandpass domain to the lowpass domain. The work presented in [137] used a lesser number of optimized variables as compared to [65] and [66] and could deal with filters with uneven Q_u and S-L couplings, but this method also could not deal with filters having high Q values. Also, the method worked correctly only when frequency samples were chosen around the passband.

2.7.4 Filter Tuning Using Cauchy Method + NN + ISM Techniques

In [138], the initial tuning (when the filter was highly detuned) was performed using poles and zeros of the input reflection parameter. The phase of the poles and zeros of the input reflected parameters was improved by using iterative optimization. The S-parameters taken from VNA were converted to Y-parameters using the standard transformation formulas presented in [61]. Phase-shift removal ensured that the positioning of poles and zeros of the Y-parameters was improved. Then, the Y-parameters-based Cauchy method [45] was used to extract the CM elements in the second stage of tuning (i.e., in the fine-tuning stage) to reduce the residual errors. After finding the characteristic polynomials, the Y-matrix was found using the partial expansion method discussed in [38]. Then, a tuning model was established using a complex NN structure where the Gradient-Descent method was used for training purposes. Finally, the mapping relationship between the ideal and actual model was obtained using ISM. This relationship could provide the magnitude and direction of the tuning needed to successfully tune the filter. Iterative optimization of the cost function discussed in [82] was used to find the correct position of the tuning screws. However, the extracted CM then needed a rotation transform to be performed, and the method was limited to coaxial filters only.

2.7.5 Filter Tuning Using VF + FNN + ISM Techniques

The authors of [138] then proposed another hybrid method to tune the cavity filters in [139]. The tuning was again divided into two stages, i.e., 'initial tuning' and 'fine tuning'. To avoid the system being trapped in local minima, the Quantum Greed Algorithm [140] was used in this work. Then, after the removal of the phase shift, CM was extracted using the VF technique. The key benefits offered by the VF technique for CM Extraction were that the technique was: simple; quick; and the poles and zeros positions were optimized iteratively, hence they were accurate. In addition, the higher-power polynomial coefficients did not pose any problem in CM Extraction. The combined Fuzzy and Neural Network (FNN) based on the T-S model ensures the accuracy of the tuning model. The use of iterative ISM methodology on top of this FNN tuning model provides the optimal screw positions.

3 Detailed Comparison

In Sect. 2, the authors of the current investigation presented and discussed a detailed analysis of the available research. This section aims to synthesize the key limitations of each type of technique discussed in the previous section (see Table 1). The decade-wise segregation of research publications in the field of filter tuning application has also been presented in Fig. 4. Each colored block in Fig. 4 presents one publication of that particular category in the decade (i.e. the reader can count the number of publications in a particular category by counting the blocks).

The comparative analysis of various techniques has been summarized in Table 2. The various filter tuning techniques are analyzed on the basis of following parameters:

- The tuning technique used.
- The complexity of the implemented algorithm.
- Ability to reach the optimized tuning state.
- Ability to tune complex filters which can help in attaining sharp band selectivity.

The literature analysis is presented in Sect. 3 and the information compiled in Table-1 indicates that there is a lot of scope in finding an effective method of tuning the MW filters. The comparative analysis of various filter tuning techniques presented in Table 2 can be used for deciding the future steps. The next section presents a summary of recent trends in tuning the MW filters and the reasons underlying those trends.

4 Discussion

The downfall of Selective Techniques

The trends depicted in Fig. 4 show a downward trend in the research interest in Time Domain (TD), sensitivity analysis, and sequential filter tuning techniques. The TD tuning is not suitable to tune the complex filter and requires a reference frequency response and a tuning technician is needed to tune the filters. The sequential filter tuning methods suffer

Table 1 The key limitations of the techniques discussed in this review

Type	Name of the Technique	Limitations
A	Filter Tuning in Time Domain	The main limitations of using the TD methodology in filter tuning are: finding the exact values of the coupling and resonant frequency is not possible; a golden filter is mandatory to fetch an ideal response; the use of a golden filter augmented the reliance on a particular kind of filter; fine-tuning is required to meet the expected specifications; the need of having an operator to tune the filters is still inevitable; the method is incapable of dealing with filters having asymmetrical frequency response (like multiplexers for satellite communications); and, there isn't a single tuning screw adjustment, which is the ideal scenario. because multiple turning of the screws leads to Passive Inter-Modulation (PIM) effects and may cause damage to the filter as well
B	Sequential Filter Tuning	In general, although sequential tuning methods can assist the process by breaking the complex problem of filter tuning into smaller sub-problems, the problem of the propagation of cumulative error restricts the commercial use of this methodology. Thus, 'fine-tuning' becomes a mandatory step. In addition, the need to short the resonators or completely remove the screws is disadvantageous in CAT; segregation of the resonators from the filter structure is difficult (especially for dielectric resonator filters)

Table 1 (continued)

Type	Name of the Technique			Limitations	
C	Filter	1	Location of Poles and Zeros of the Input Reflection Coefficient	In general, the procedure of using poles and zeros for filter tuning is highly iterative. The correctness of the parameters extracted using this approach is directly related to the accuracy of the locations determined for poles and zeros. Increasing the number of resonators brings-in errors as well, which implies that this technique cannot be used on higher-order filters. Also, the accuracy of the system primarily depends on calibration procedures for defining the reference plane for phase measurement	The main limitations with all the methods based on filter modeling are—the mathematical models are usually not accurate but are just the approximated versions only. Finding an accurate network model (where all tuning elements are correctly represented) is either difficult or sometimes impossible. These approximated models do not consider the fact that varying the position of just one tuning element usually affects the performance of neighboring elements as well. In addition, the model-based methods cannot be generalized to other filter topologies Another limitation of using this methodology includes the fact that conventional CM does not consider performance degradation due to practical uncertainties and the variation in material characteristics

Table 1 (continued)

Type	Name of the Technique			Limitations
	Diagnosis	2	Y-Parameters	As with the filter diagnosis based on commonly used S-parameters, the use of Y-parameters also requires the removal of phase loading effects for obtaining the poles and residues. The removal of phase loading is important because it is not incorporated in the filter model, but it is always present in a physical filter unit. Also, this method needs careful manipulations due to which this methodology is not suitable to have a CAT system
	Filter	3	Vector Fitting (VF)	To extract a correct CM using VF methodology, further transformations are needed like the one proposed in [62]. Alternatively, the extracted CM needs further optimization. Also, the VF methodology requires the frequency samples to be defined in the positive direction only, and hence this methodology is not suitable for having a CAT system

Table 1 (continued)

Type	Name of the Technique				Limitations
	Diagnosis	Cauchy Method	4a	S-Parameters based Cauchy Method	In all research works in which the Cauchy method has been used, the last step is to synthesize the CM using well-established methods presented in [37, 38], and the book [44]. The key issue with the Cauchy method (for filter diagnosis and tuning) is that the Vandermonde matrix used in the Cauchy method cannot deal with higher-order systems since this matrix becomes ill-conditioned and its accuracy is degraded when the number of unknowns becomes high [141]. Some useful strategies to handle this problem have been discussed in [142] but the accuracy is still not up to the mark that this method can be used to have an automatic filter tuning solution In [143], another modification of the Cauchy method was presented that could deal with higher-order systems, in which the authors proposed the preconditioning of the main matrix of the system using an appropriate scaling technique. It was suggested in [144] and [145] that matrix equilibration is important to increase numerical computations. So, the method proposed in [143] is lengthy, computationally heavy, and cannot perform well when the detuning level is high Also, in general, the Cauchy method loses its accuracy because of the presence of 2nd order effects
	Filter Diagnosis		4b	Y-Parameters based Cauchy Method	

Table 1 (continued)

Type	Name of the Technique			Limitations
		5	Optimization-based Filter Tuning Methods	The general issues with all the optimization-based filter tuning methods are—they cannot deal with highly detuned filters; the spurious and unwanted couplings between neighboring elements are not accurately detected; the process of finding the global minima is complicated; attaining the global minima majorly relies on the number and initial guess of the optimization variables and the defined initial values. One way to overcome some of these problems is to use the approach presented in [146]. The authors of [146] proposed an algorithm in which a Multiple hidden layered Extreme Learning Machine (MELM) with a Differential Evolution Particle Swarm Optimization (DESPO) algorithm was presented for finding the parametric model. This model could present the relationship between the change in screw length and the corresponding change in CM parameters Alternatively, a tuning model based on improved Back-Propagation Neural Network (BPNN) and Gauss Kernel Clustering presented in [147] can also be used where the use of the Shuffled Frog-Leaping algorithm can optimize the weights of the BPNN architecture. These models might still not be able to solve the problem completely, but they can provide some assistance for tuning the filters

Table 1 (continued)

Type	Name of the Technique	Limitations
D	Space Mapping based Filter Tuning	While using SM as a solution for filter tuning, the accuracy of the solution depends on the information of the fine model, or it needs a lot of pre-assigned parameters, due to which the convergence may be bad, or the algorithm may even fail. Additionally, the mapping quality is strongly dependent on the chosen process for Parameter Extraction (PE). For quick reference, PE is a procedure by which the parameters of the coarse/surrogate model are optimized and matched to the measurement result. Having an incorrect PE process leads to incorrect results. The exact PE extraction process has not been reported yet, and hence this methodology cannot be used commercially
E	Sensitivity Analysis based Filter Tuning	The use of Sensitivity Analysis for filter tuning purposes requires repeated measurements of sensitivities. Sensitivity analysis is followed by an optimization algorithm to get accurate results. The publications discussed in this category were based only on simulations, and thus, the practical aspects of tuning, i.e., the fact that a screw when turned changes the frequency and coupling of screws in the neighborhood, were not considered. Furthermore, the models presented by the researchers were linear and therefore confined to a limited range. However, in actuality, there is a non-linear relationship existing between the I/P and O/P of the filter. Thus, this methodology can be used mainly during the 'fine-tuning' stage only; is time-expensive; and is not suitable for tuning highly detuned filters

Table 1 (continued)

Type	Name of the Technique			Limitations	
F	Data Driven	1	Machine Learning	For the efficient and consistent performance of an ML algorithm, a huge amount of accurate training data is usually needed. Collecting such data is expensive in terms of time, computational memory, and money. Another major concern using this technique is the inclination of the data toward a specific type of instrument (filter topology)	All the data-driven methods discussed here, i.e., ML, Heuristic Methods, FL, ANNs, and SVMs, work by learning the models from the pre-recorded data. The accuracy of the data-driven models is directly proportional to the abundance of correct data available. The main issues like lack of data; incomplete data; missing data portions; and scattered data, etc., badly affect the performance of data-driven techniques. Also, there is a huge dependency on the algorithms used (which then also affects the performance of the model) and they often cannot be generalized to other topologies. Additionally, the processing and calculation time increases exponentially when a large amount of training data is provided

Table 1 (continued)

Type	Name of the Technique				Limitations
		2	Heuristic Methods (Derivative-free)		The use of direct search optimization routine results is not an ideal way of filter tuning as the optimization routines are time-consuming and rely heavily on the initial values. Also, the use of heuristic methods results in numerous turns of a screw. Repetitive screw turnings are not ideal for having a CAT system because this often leads to PIM issues in the filter
	Data Driven	Fuzzy	3a	Fuzzy Logic without using Human Experience	The problems with fuzzy-based methods for tuning the filters are: the method can deal with in-line and lossless filters only; the method relies on initial values of Q-factor and CM elements; this approach cannot reveal any information about the amount by which the tuning element is deviating and how much adjustment level is needed for those tuning screws to reach the desired tuning state; the method needed enough linguistic rules to be defined for achieving accurate results. Defining too many linguistic rules brings in more complex computations and, consequently, more delay. Also, a complex accurate model between the CM elements and tuning screws is difficult to obtain. To remove the reliance on the number of 'If–Then' rules, dynamic fuzzy methods were presented by the research community, but the methods failed to optimize the parameters
			3b	Fuzzy Logic with Human Experience	
		Logic	3c	Dynamic Fuzzy	

Table 1 (continued)

Type	Name of the Technique				Limitations
	Data Driven	Ann	4a 4b	Supervised Learning Reinforcement Learning	ANN is still the most reliable multi-dimensional approximator and was used for tuning MW devices. However, the key problematic issues with this approach are: 1) the need to have a large amount of training data is inevitable; and 2) generalization is not possible. ANN models are independent of filter structure and are data-driven, but the one trained model is limited to its usage for filters of the same kind. Filters with different topologies will need another dedicated trained model; 3) the optimal solution cannot be obtained if the present data lies outside the boundaries of the data used for training the model; 4) it is not possible to update the tuning model in real-time; 5) the obtained training model can have over-fitted data because of the traditionally used Back-Propagation method and the choice of the initial weights, and 6) while using RL, having too many layers can cause an exponential increase in the delay. Additionally, there is a need for a time-consuming training phase. The research to find an ANN-based CAT solution for filters is still ongoing actively

Table 1 (continued)

Type	Name of the Technique			Limitations
		5	Neuro-Fuzzy System (NFS)	This needs pre-processing of data and the convergence of the parameters is low. In addition, ANFIS models cannot be easily interpreted
		6	Support Vectors	When applied to filter tuning problems, the Support Vector models built by researchers are not direct, i.e., S-parameters are represented by a CM but not in their original form drawn from a VNA. The other factor that caused errors is that screw positions are approximated using the results obtained from the solutions of optimization problems. Also, the generalization abilities of the proposed methods are poor when only filter structure is modeled but not human intelligence
		7	Linear Matrix Operator	Although the training stage is not necessary to use while implementing this methodology, the volume and quality of the data gathered has a significant impact on how well this strategy performs
		8	Linear Decomposition of Reflection Characteristics	In this methodology, the need for a training phase was eliminated because the response of the system is based on the linear decomposition of the S-parameters. But there is a need for an optimization routine in this methodology which adds delay in providing the final value, i.e., the amount of detuning needed

Table 1 (continued)

Type	Name of the Technique			Limitations
G	Hybrid	1	VF + ASM	Initially, the main intention of using the hybrid methods of filter tuning was that it would assist in the optimal tuning of the MW filters. However, using two or more techniques simultaneously brought not only their individual pros but also their cons. Most combinations of the techniques are based on filter modeling or parameter extraction processes, which are not exact
		2	Cauchy + SM-based	
		3	GA + VF	
		4	Cauchy + NN + ISM	
		5	VF + FNN + ISM	

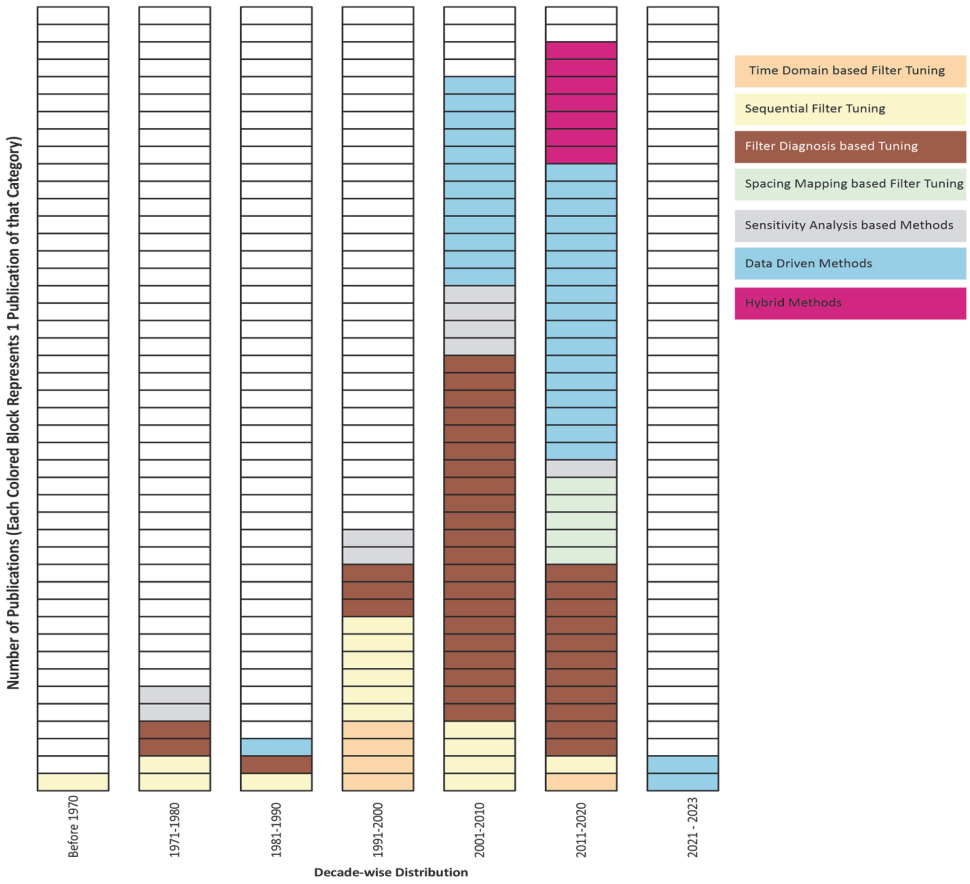

Fig. 4 Decade-wise research trends of the various techniques presented

from cumulative error propagation issues. The tuning methods based on sensitivity analysis require numerous measurements and various optimization iterations, and hence they are suitable for the 'Fine Tuning' stage only.

4.1 Technological Choices of Researchers

The trend shown in Fig. 4 is that the techniques based on Space Mapping (SM) and Hybrid Methods have gathered the attention of researchers in recent times. SM-based solutions are highly reliant on the accuracy of fine model and PE process whereas the hybrid methods are computationally expensive.

Another trend revealed by Fig. 4 is the interest of researchers in implementing data-driven methods to tune the filters. The reason for this inclination is the increased computational power offered by the CPUs and GPUs of these days as well as the availability of efficient algorithms.

After carrying out the literature review it was found that a Hybrid Learning category is still missing in the literature for the filter tuning applications. Hybrid Learning is a new category which fuses theoretical tuning knowledge with video analysis-based learning from

Table 2 The comparative analysis of various filter tuning techniques

Technique			Computational Complexity	Optimized Tuning	Sharp Band Selectivity
A. Time Domain			Moderate	No	No
B. Sequential			Low	No	No
C. Filter Diagnosis	Location of Poles and Zeros of S11		High	No	No
	Admittance Parameters		Moderate	No	Yes
	Vector Fitting (VF)		High	No	Yes
	Cauchy Method	S-parameters	High	No	Yes
		Y-parameters	High	No	No
	Genetic Algorithm (GA) Optimization		High	Yes	Yes
D. Space Mapping (SM)			High	No	No
E. Sensitivity Analysis			High	Yes	No
F. Data Driven	Machine Learning		High	No	No
	Heuristic Methods		Moderate	No	No
	Fuzzy Logic	Without human experience	Moderate	No	No
		With human experience	Moderate	No	Yes
		Dynamic Fuzzy Logic	High	Yes	No
	Artificial Neural Network (ANN)	Supervised Learning	High	Yes	No
		Reinforcement Learning	High	Yes	Yes
	Neuro-Fuzzy System		High	No	No
	Support Vectors		High	Yes	Yes
	Linear Matrix Operator		Moderate	No	No
	Linear Decomposition of Reflection Characteristics		Low	No	No

Table 2 (continued)

Technique		Computational Complexity	Optimized Tuning	Sharp Band Selectivity
G. Hybrid Methods	VF + Aggressive SM	High	Yes	Yes
	Cauchy + SM			
	GA + VF			
	Cauchy + VF + Implicit SM			
	VF + Fuzzy Neural Network + Implicit SM			

the best tuning technician. This technique is manually followed by the industries where the best tuning technician teaches others to tune the filters correctly.

The following sub-section presents the implementation of such an expert-based hybrid learning technique to tune the filters efficiently.

4.2 Expert Driven Hybrid Deep Learning

To overcome the limitations observed from the literature review, a new filter tuning method is needed. Using the experience of authors of the current investigation with data-driven filter tuning methods (presented in [115] and [118]), a new method in which fusion of theoretical knowledge and knowledge from video analysis of best tuning technician has been proposed.

Figure 5 presents an expert-driven hybrid deep learning algorithm in which a combination of theoretical and practical knowledge were used for tuning the filters. The filter under consideration was an iris-coupled 5th order commercial filter equipped with solid cylindrical resonator posts. This theoretical knowledge from filter design was used as one of the learning criteria and the video analysis from the videos were used to collect the features for learning. Multiple filters were tuned by one of the best tuning technicians, and several videos were captured. Data related to S_{11} and S_{21} parameters of a filter were accumulated simultaneously. The hybrid learning method in which the theoretical and practical learning was fused proved to be highly beneficial in the initial stage of tuning (when the filter was highly detuned). This is because the RL agent had some initial idea of the environment, and the decision regarding the exploration and exploitation strategy was made accordingly. The use of Semi-Decoupled Deep Q-Network (SD-DQN) [148] ensured the stability aspect which was missing in [118]. The policy generated by the proposed algorithm helped in tuning the filter accurately and efficiently. While implementing the algorithm, the discount factor was set to be 0.95 and the replay buffer was set to 150,000. The maximum permissible screw turns were set to four full rotations i.e. 1440°. A convolutional neural network (CNN) architecture with 2 hidden layers and ReLU activation function was used. The simulation was run on a system with the hardware configuration 16 GB RAM, Ryzen-9 5800 HS CPU and NVIDIA RTX3060 – 6 GB GPU. The results obtained after tuning the filter using the proposed algorithm are presented in Fig. 6.

In Fig. 6, the dotted red line presents the insertion loss, and the solid blue line presents the return loss after the 5th order filter is tuned. The return loss target line is drawn with magenta color and the black line defines the insertion loss limit. The filter is considered to be tuned when the reflection curve is below the target line of -18 dB and the insertion

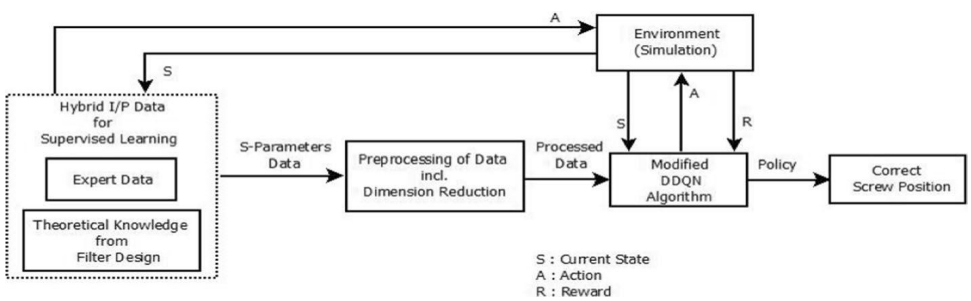

Fig. 5 The proposed fusion algorithm

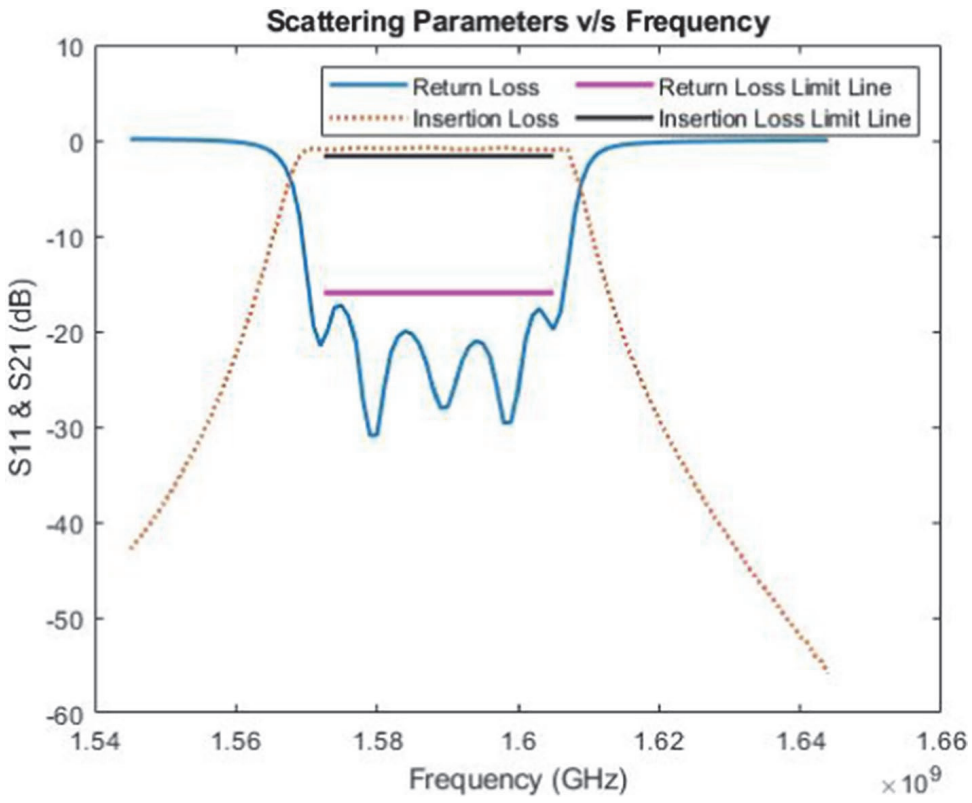

Fig. 6 Frequency response with the proposed algorithm

curve is over the -1 dB value. It can be observed that both these criteria are simultaneously met in Fig. 6 i.e. the filter has been tuned using the proposed hybrid learning method.

After differentiating the tuning screws from the plate mounting screws using the methodology presented in [149], this expert driven hybrid deep learning algorithm can be used to automate the filter tuning process.

5 Conclusion

Conclusively, the prime objective of the current research paper was to review and compile the research works conducted in the field of MW/RF filter tuning. To this aim, approximately 150 papers published in various journals and conferences were reviewed by the authors. Additionally, a novel architecture with modified Deep Learning specifically for MW filter tuning has been proposed. All researchers collectively emphasize that filter tuning is a complex and expensive process, and finding a suitable automated filter tuning process can remove the bottlenecks in the production of these filters. In this paper, the authors have highlighted the blockages of filter tuning, and a discussion of limitations associated with different topologies has also been mentioned. Additionally, the comparative analysis of various filter tuning techniques is also presented. The paper ends with the novel

expert-based hybrid learning method for tuning the MW filters. The proposed method could tune a 5th order all pole cavity filter more effectively.

Author Contributions The conceptualization of this paper was a collaborative effort among all three authors. The first author conceived the idea of paper; developed, tested, and validated the novel tuning algorithm; and compiled the manuscript. The second author provided the vision for the novel expert-based hybrid learning algorithm and also contributed to testing, and multiple reviews. The third author was part of the overall execution of the objective.

Funding Research was supported by Tallinn University of Technology, Tallin, Estonia.

Availability of Data and Material (Data Transparency) It is an extensive literature survey paper with an implementation of a novel approach. All required data has been mentioned in the manuscript and no other data is required.

Code Availability (Software Application or Custom Code) It is an extensive Literature survey paper. This is not applicable.

Declarations

Conflict of Interest There is no conflict of interests among all authors of any kind.

References

1. Brian Thomas, J. (2003). Cross-coupling in coaxial cavity filters—A tutorial overview. *IEEE Transactions on Microwave Theory and Techniques, 51*(4), 1368–1376. https://doi.org/10.1109/TMTT.2003.809180
2. Amari S., and Bornemann J, (2000). Maximum number of finite transmission zeros of coupled resonator filters with source/load-multiresonator coupling and a given topology. In Asia-Pacific Microwave Conference Proceedings, APMC 2000, Sydney, NSW, Australia, Sydney, Australia. pp. 1175–1177. doi: https://doi.org/10.1109/apmc.2000.926040
3. Zhang, Y. L. (2018). Improved matrix synthesis for inline filters with transmission zeros generated by FVC. *Progress In Electromagnetics Research M, 76*, 9–17. https://doi.org/10.2528/PIERM18101502
4. Ruiz-Cruz, J. A., Wang, C., & Zaki, K. A. (2008). Advances in microwave filter design techniques. *Microwave Journal, 51*, 26–44.
5. Yao H. W., Wang C., and Zaki K. A., (1996). Effects of tuning structures on combline filters. In 1996 26th European Microwave Conference, EuMC 1996, Prague, Czech Republic. pp. 427–430. doi: https://doi.org/10.1109/EUMA.1996.337605.
6. Chuma, J. M., & Mirshekar-Syahkal, D. (2002). Effects of walls on coupling between coupled combline resonators. *IEE Proceedings: Microwaves, Antennas and Propagation, 149*(1), 53–56. https://doi.org/10.1049/ip-map:20020180
7. Han, L., Wu, K., Chen, X.-P., & He, F. (2010). Influence and tuning of tunable screws for microwave filters using least squares support vector regression. *International Journal of RF and Microwave Computer-Aided Engineering, 20*(4), 422–429. https://doi.org/10.1002/mmce
8. Lindner A., Biebl E., and Strasse A.,(2006). A manual tuning method for coupled cavity filters. In *Proceedings of 36th European Microwave Conference, Manchester, UK*. pp. 1340–1342.
9. Yu M., (1994). Computer aided tuning. COM DEV Internal Report.
10. Yu, M. (2006). Robotic computer-aided tuning (COM DEV Ltd.). *Microw J (Int Ed)*. https://doi.org/10.11139/cj.29.3.507-531
11. Yu, M., (2003). A fully automated filter tuning robot for wireless base station diplexers – presentation. In *IEEE International Microwave Symposium - Workshop: Computer Aided Filter Tuning, (IMS 2003), Philadelphia, Pennsylvania*. doi: https://doi.org/10.13140/2.1.4648.1923.
12. Jervis, B. W., & Crofts, M. (1991). Comparison of computer-aided tuning algorithms applied to the amplitude response of passive analogue filters. *IEE Proceedings G - Circuits, Devices and Systems, 138*(3), 363–371. https://doi.org/10.1049/ip-g-2.1991.0062

13. Dunsmore J., (1999). Tuning band pass filters in the time domain. In 1999 IEEE MTT-S International Microwave Symposium Digest, Anaheim, CA, USA. pp. 1351–1354. doi: https://doi.org/10.1109/MWSYM.1999.779638
14. "Simplified Filter Tuning Using Time Domain, Application Note, AN 1287–8, 1999, (Republished in 2000 by Agilent as 5968–5328E)."
15. Dunsmore, J. (2000). "Duplex filter tuning using time domain transforms, *2000 30th European Microwave Conference*. *EuMC, 2000*, 6–9. https://doi.org/10.1109/EUMA.2000.338794
16. Dunsmore J., (1999). Advanced filter tuning using time domain transforms. In 29th European Microwave Conference, EuMC 1999, Munich Germany. pp. 72–75. doi: https://doi.org/10.1109/EUMA.1999.338412
17. "Network Analysis Solutions Advanced Filter Tuning Using Time Domain Transforms, Application Note 5980–2785EN, 1999 (Republished by Keysight in 2017)."
18. Burger S. and Hoeft M., (2014). Improved filter tuning in the time domain. In 1st Australian Microwave Symposium, ASM 2014, Melbourne, VIC, Australia, Melbourne, VIC, Australia: IEEE. pp. 27–28. doi: https://doi.org/10.1109/AUSMS.2014.7017349
19. Dishal, M. (1951). Alignment and adjustment of synchronously tuned multiple-resonant-circuit filters. *Proceedings of the IRE, 39*(11), 1448–1455. https://doi.org/10.1109/JRPROC.1951.273611
20. Atia, A. E., & Williams, A. E. (1975). Measurements of intercavity couplings. *IEEE Transactions on Microwave Theory and Techniques, 23*(6), 519–522. https://doi.org/10.1109/TMTT.1975.1128614
21. Atia, A., Williams, A., & Newcomb, R. (1974). Narrow-band multiple-coupled cavity synthesis. *IEEE Trans Circuits Syst, 21*(5), 649–655. https://doi.org/10.1109/TCS.1974.1083913
22. Chen, M. H. (1977). Short-circuit tuning method for singly terminated filters. *IEEE Transactions on Microwave Theory and Techniques, 25*(12), 1032–1036.
23. Accatino L., (1986). Computer-aided tuning of microwave filters. In 1986 IEEE MTT-S International Microwave Symposium Digest, Baltimore, MD, USA. pp. 249–252
24. Ness, J. B. (1998). A unified approach to the design, measurement and tuning of coupled-resonator filters. *IEEE Transactions on Microwave Theory and Techniques, 46*(4), 343–351. https://doi.org/10.1109/22.664135
25. Ness, J. B. (1998). Alignment of cross-coupled resonator filter using the group delay technique. *Microwave and Optical Technology Letters, 18*(3), 174–179.
26. Zahirovic N., and Mansour R. R., (2008). Sequential tuning of coupled resonator filters using hilbert transform derived relative group delay. In 2008 IEEE MTT-S International Microwave Symposium Digest, Atlanta, GA, USA. pp. 739–742
27. P. Perry and T. J. Brazil, (1996). Hilbert-transform-derived relative group delay measurement of frequency conversion systems. In IEEE MTT-S Int. Microw. Symp. Dig, San Francisco, CA, USA: IEEE, pp. 1695–1698. doi: https://doi.org/10.1109/MWSYM.1996.512267.
28. Pepe, G., Görtz, F. J., & Chaloupka, H. (2005). Sequential tuning of microwave filters using adaptive models and parameter extraction. *IEEE Transactions on Microwave Theory and Techniques, 53*(1), 22–31. https://doi.org/10.1109/TMTT.2004.839342
29. A. Lindner, H. Kugler, and E. Biebl, (2007). Manual filter tuning by cloning frequency domain data. In *European Microwave Conference, EUMC 2007, Munich Germany*. pp. 329–331. doi: https://doi.org/10.1109/EUMC.2007.4405193
30. Michalski, J. J. (2011). Inverse modeling in application for sequential filter tuning. *Progress In Electromagnetics Research, 115*, 113–129.
31. Atia, A. E., & Williams, A. E. (1971). New types of waveguide bandpass filters for satellite transponders. *The COMSAT Technical Review, 1*(1), 21–44.
32. J. Marquardt and G. Muller, (1977). Computer-aided tuning of microwave circuits. In IEEE MTT-S International Microwave Symposium Digest, San Diego, CA, USA, San Diego, CA, USA, USA. pp. 147–150. doi: https://doi.org/10.1109/MWSYM.1977.1124388.
33. Atia A. E., and Yao H., (2000). Tuning & measurements of couplings and resonant frequencies for cascaded resonators. In *2000 IEEE MTT-S International Microwave Symposium Digest, Boston, MA, USA*. pp. 1637–1640
34. Hsu, H. T., Yao, H., Zaki, K. A., & Atia, A. E. (2002). Computer-aided diagnosis and tuning of cascaded coupled resonators filters. *IEEE Transactions on Microwave Theory and Techniques, 50*(4), 1137–1145.
35. Hsu, H. T., Zhang, Z., Zaki, K. A., & Atia, A. E. (2002). Parameter extraction for symmetric coupled-resonator filters. *IEEE Transactions on Microwave Theory and Techniques, 50*(12), 2971–2978. https://doi.org/10.1109/TMTT.2002.805283

36. Ghadiya A., and Soni S., (2014). Sequential parameter extraction of direct-coupled resonator filter. In *2014 Fourth International Conference on Communication Systems and Network Technologies, Bhopal, India*, IEEE. pp. 25–29. doi: https://doi.org/10.1109/CSNT.2014.14.
37. Cameron, R. J. (1999). General coupling matrix synthesis methods for chebyshev filtering functions. *IEEE Transactions on Microwave Theory and Techniques, 47*(4), 433–442.
38. Cameron, R. J. (2003). Advanced coupling matrix synthesis techniques for microwave filters. *IEEE Transactions on Microwave Theory and Techniques, 51*(1), 1–10.
39. Meng, W., & Wu, K. L. (2006). Analytical diagnosis and tuning of narrowband multicoupled resonator filters. *IEEE Transactions on Microwave Theory and Techniques, 54*(10), 3765–3771. https://doi.org/10.1109/TMTT.2006.881623
40. Kabir, H., Wang, Y., Yu, M., & Zhang, Q. J. (2010). High-dimensional neural-network technique and applications to microwave filter modeling. *IEEE Transactions on Microwave Theory and Techniques, 58*(1), 145–156. https://doi.org/10.1109/TMTT.2009.2036412
41. Meng, M., & Wu, K. L. (2009). An analytical approach of extracting coupling matrix and unloaded Q of a bandpass filter. *IEEE MTT-S International Microwave Symposium Digest*. https://doi.org/10.1109/MWSYM.2009.5165954
42. Meng, M., & Wu, K. L. (2009). An analytical approach to computer-aided diagnosis and tuning of lossy microwave coupled resonator filters. *IEEE Transactions on Microwave Theory and Techniques, 57*(12), 3188–3195. https://doi.org/10.1109/TMTT.2009.2033868
43. Wang, R., Li, L. Z., & Peng, L. (2014). Diagnosis of lossy resonator filters with source-load coupling using Y-parameters. *International Journal of RF and Microwave Computer-Aided Engineering, 24*(6), 713–717. https://doi.org/10.1002/mmce.20816
44. Cameron, R. J., Kudsia, A. C. M., & Mansour, R. R. (2007). *Microwave filters for communication systems —fundamentals, design and applications (2nd edn)*. USA: Wiley. https://doi.org/10.1002/9781119292371
45. Wang, R., Li, L.-Z., & Peng, L. (2015). Improved diagnosis of lossy resonator bandpass filters using Y-parameters. *International Journal of RF and Microwave Computer-Aided Engineering, 25*(9), 807–814. https://doi.org/10.1002/mmce.20919
46. Gustavsen, B., & Semlyen, A. (1999). Rational approximation of frequency domain responses by vector fitting. *IEEE Transactions on Power Delivery, 14*(3), 1052–1061. https://doi.org/10.1016/0001-8708(78)90008-7
47. Gustavsen, B. (2006). Improving the pole relocating properties of vector fitting. *IEEE Transactions on Power Delivery, 21*(3), 1587–1592. https://doi.org/10.1109/TPWRD.2005.860281
48. Liao, C. K., Chang, C. Y., & Lin, J. (2007). A vector-fitting formulation for parameter extraction of lossy microwave filters. *IEEE Microwave and Wireless Components Letters, 17*(4), 277–279. https://doi.org/10.1109/LMWC.2007.892970
49. Hu, H., & Wu, K. L. (2014). A generalized coupling matrix extraction technique for bandpass filters with uneven-Qs. *IEEE Transactions on Microwave Theory and Techniques, 62*(2), 244–251. https://doi.org/10.1109/TMTT.2013.2296744
50. Adve, R. S., & Sarkar, T. K. (1993). Generation of accurate broadband information from narrowband data using the cauchy method. *Microwave and Optical Technology Letters, 6*(10), 569–573. https://doi.org/10.1002/mop.4650061002
51. Dhaene T., Ureel J., Fache N., and De Zutter D., (1995). Adaptive frequency sampling algorithm for fast and accurate S-parameter modeling of general planar structures. In *Proceedings of 1995 IEEE MTT-S International Microwave Symposium Digest*, Orlando, FL, USA. pp. 1427–1430. doi: https://doi.org/10.1109/mwsym.1995.406240.
52. Adve, R. S., Sartar, T. K., Rao, S. M., Miller, E. K., & Pflug, D. R. (1997). Application of the cauchy method for extrapolating/interpolating narrow-band system responses. *IEEE Transactions on Microwave Theory and Techniques, 45*(5), 837–845. https://doi.org/10.1109/22.575608
53. Matthaei G. L., Young L., and Jones E. M. T., (1964). *Microwave Filters, Impedance-Matching Networks, and Coupling Structures*. Norwood, MA, 02062: Artech House
54. Van Huffel S., and Vandewalle J. P. L., (1991). The total least squares problem: computational aspects and analysis. Philedelphia: Society for Industrial and Applied Mathematics.
55. Lamperez A. G., Sarkar T. K., and Palma M. S., (2002). Filter model generation from scattering parameters using cauchy method. In 2002 32nd European Microwave Conference, Milan, Italy. pp. 1–4.
56. García-Lampérez, A., Llorente-Romano, S., Salazar-Palma, M., & Sarkar, T. K. (2004). Efficient electromagnetic optimization of microwave filters and multiplexers using rational models. *IEEE Transactions on Microwave Theory and Techniques, 52*(2), 508–521. https://doi.org/10.1109/TMTT.2003.822021

57. Lampérez, A. G., Sarkar, T. K., & Palma, M. S. (2004). Generation of accurate rational models of lossy systems using the cauchy method. *IEEE Microwave and Wireless Components Letters, 14*(10), 490–492. https://doi.org/10.1109/LMWC.2004.834576
58. Macchiarella, G., & Traina, D. (2006). A formulation of the cauchy method suitable for the synthesis of lossless circuit models of microwave filters from lossy measurements. *IEEE Microwave and Wireless Components Letters, 16*(5), 243–245. https://doi.org/10.1109/LMWC.2006.873583
59. Traina D., Macchiarella G., and Bertelli J., (2006). Computer-aided tuning of GSM base-station filters-experimental results. In 2006 IEEE Radio and Wireless Symposium, San Diego, CA, USA. pp. 587–590. doi: https://doi.org/10.1109/RWS.2006.1615225.
60. Tamiazzo, S., & Macchiarella, G. (2005). An analytical technique for the synthesis of cascaded N-tuplets cross-coupled resonators microwave filters using matrix rotations. *IEEE Transactions on Microwave Theory and Techniques, 53*(5), 1693–1698. https://doi.org/10.1109/TMTT.2005.847065
61. Esmaeili M., and Borji A., (2010). Diagnosis and tuning of multiple coupled resonator filters. In 2010 18th Iranian Conference on Electrical Engineering, ICEE 2010, Isfahan, Iran, IEEE. pp. 124–129. doi: https://doi.org/10.1109/IRANIANCEE.2010.5507088.
62. Kozakowski, P., Lamecki, A., Sypek, P., & Mrozowski, M. (2005). Eigenvalue approach to synthesis of prototype filters with source/load coupling. *IEEE Microwave and Wireless Components Letters, 15*(2), 98–100. https://doi.org/10.1109/LMWC.2004.842838
63. Macchisrella, G. (2010). Extraction of unloaded Q and coupling matrix from measurements on filters with large losses. *IEEE Microwave and Wireless Components Letters, 20*(6), 307–309. https://doi.org/10.1109/LMWC.2010.2047455
64. Wang, R., & Xu, J. (2011). Computer-aided diagnosis of lossy microwave coupled resonators filters. *International Journal of RF and Microwave Computer-Aided Engineering, 21*(5), 519–525. https://doi.org/10.1002/mmce.20537
65. Wang, R., & Xu, J. (2011). Extracting coupling matrix and unloaded Q from scattering parameters of lossy filters. *Progress In Electromagnetics Research, 115*, 303–315. https://doi.org/10.2528/PIER11021604
66. Wang, R., Xu, J., Wei, C. L., Wang, M. Y., & Zhang, X. C. (2011). Improved extraction of coupling matrix and unloaded Q from S-parameters of lossy resonator filters. *Progress in Electromagnetics Research, 120*, 67–81. https://doi.org/10.2528/PIER11072804
67. Cao, W. H., Liu, C., Yuan, Y., & Wu, M. (2018). Extracting coupling matrix from lossy filters with uneven-Qs using differential evolution optimization technique. *International Journal of RF and Microwave Computer-Aided Engineering, 28*(6), 1–10. https://doi.org/10.1002/mmce.21269
68. Zhao, P., & Wu, K. L. (2016). A new computer-aided tuning scheme for general lossy coupled-resonator bandpass filters based on the cauchy method. *HKIE Transactions, 23*(1), 52–62. https://doi.org/10.1080/1023697X.2015.1129292
69. Guyette, A. C., Hunter, I. C., & Pollard, R. D. (2006). The design of microwave bandpass filters using resonators with non-uniform Q. *IEEE Transactions on Microwave Theory and Techniques, 54*(11), 3914–3921. https://doi.org/10.1109/TMTT.2006.884627
70. Thal, H. L. (1978). Computer-aided filter alignment and diagnosis. *IEEE Transactions on Microwave Theory and Techniques, 26*(12), 958–963.
71. Harscher, P., & Vahldieck, R. (2001). Automated tuning of waveguide filters using adaptive network models. *IEEE Transactions on Microwave Theory and Techniques, 49*(11), 2125–2130.
72. Harscher P., Vahldieck R., and Amari S.,(2001). Automated test and tuning system for microwave filters. In IEEE MTT-S International Microwave Symposium Digest (Cat. No.01CH37157), Phoenix, AZ, USA. pp. 1543–1546. doi: https://doi.org/10.1109/MWSYM.2001.967197.
73. Harscher, P., Vahldieck, R., & Amari, S. (2001). Automated filter tuning using generalized low-pass prototype networks and gradient-based parameter extraction. *IEEE Transactions on Microwave Theory and Techniques, 49*(12), 2532–2538. https://doi.org/10.1109/22.971646
74. Kahrizi M., Safavi-naeini S., and Chaudhuri S. K., (2000). Computer diagnosis and tuning of filters using model-based parameter estimation and multi-level optimization. In 2000 IEEE MTT-S International Microwave Symposium Digest (Cat. No.00CH37017), Boston, MA, USA. pp. 1641–1644.
75. Kahrizi, M., Safavi-naeini, S., Chaudhuri, S. K., & Sabry, R. (2002). Computer diagnosis and tuning of rf and microwave filters using model-based parameter extraction. *IEEE Transactions on Circuits and Systems - I: Fundamental Theory and Applications, 49*(9), 1263–1270.
76. Miller, E. K., & Burke, G. J. (1991). Using model-based parameter estimation to increase the physical interpretability and numerical efficiency of computational electromagnetics. *Computer Physics Communications, 68*(1–3), 43–75. https://doi.org/10.1016/0010-4655(91)90193-O
77. Boggs, P. T., & Tolle, J. W. (1995). Sequential quadratic programming. *Acta Numerica, 4*, 1–51. https://doi.org/10.1017/S0962492900002518

78. Bandler, J. W., Biernacki, R. M., Chen, S. H., Grobelny, P. A., & Hemmers, R. H. (1994). Space mapping technique for electromagnetic optimization. *IEEE Transactions on Microwave Theory and Techniques, 42*(12), 2536–2544. https://doi.org/10.1109/22.339794
79. Bandler, J. W., Biernacki, R. M., Chen, S. H., Hemmers, R. H., & Madsen, K. (1995). Electromagnetic optimization exploiting aggressive space mapping. *IEEE Transactions on Microwave Antennas Propagation, 43*(12), 2874–2882.
80. Bandler, J. W., Cheng, Q. S., Nikolova, N. K., & Ismail, M. A. (2004). Implicit space mapping optimization exploiting preassigned parameters. *IEEE Transactions on Microwave Theory and Techniques, 52*(1), 378–385. https://doi.org/10.1109/TMTT.2003.820892
81. Bandler, J. W., et al. (2004). Space mapping: The state of the art. *IEEE Transactions on Microwave Theory and Techniques, 52*(1), 337–361. https://doi.org/10.1109/TMTT.2003.820904
82. Cheng Q. S., Bandler J. W., and Koziel S., (2015). A review of implicit space mapping optimization and modeling techniques. In 2015 IEEE MTT-S International Conference on Numerical Electromagnetic and Multiphysics Modeling and Optimization (NEMO 2015), Ottawa, ON, Canada, IEEE. pp. 1–3. doi: https://doi.org/10.1109/NEMO.2015.7415041.
83. Rayas-Sánchez, J. E. (2016). Power in simplicity with ASM: Tracing the aggressive space mapping algorithm over two decades of development and engineering applications. *IEEE Microwave Magazine, 17*(4), 64–76. https://doi.org/10.1109/MMM.2015.2514188
84. Miek D., and Höft M., (2018). Compensation of cross-dependencies in computer aided tuning of microwave filters by simplified space mapping approach. In 2018 IEEE MTT-S International Conference on Numerical Electromagnetic and Multiphysics Modeling and Optimization (NEMO 2018), Reykjavik, Iceland. pp. 1–4.
85. Muller A., Soto P., and Boria V. E., (2017). Design procedure for coaxial combline filters based on segmentation and space mapping strategies. In 2017 IEEE MTT-S International Conference on Numerical Electromagnetic and Multiphysics Modeling and Optimization for RF, Microwave, and Terahertz Applications (NEMO 2017), Seville, Spain. pp. 13–15. doi: https://doi.org/10.1109/NEMO.2017.7964171.
86. S. Li, X. Fan, P. D. Laforge, and Q. S. Cheng, (2019). A post-fabrication tuning method using space mapping and surrogate modeling techniques. In 2019 49th European Microwave Conference, (EuMC 2019), Paris, France, Paris, France: European Microwave Association (EuMA). pp. 392–395. doi: https://doi.org/10.23919/EuMC.2019.8910767.
87. A. Rodriguez *et al.*, (2017). Robust optimization and tuning of microwave filters and artificial transmission lines using aggressive space mapping techniques. In 2017 IEEE MTT-S International Microwave Symposium (IMS 2017), Honolulu, HI, USA. pp. 1501–1504. doi: https://doi.org/10.1109/MWSYM.2017.8058909
88. Li, S., Fan, X., Laforge, P. D., & Cheng, Q. S. (2020). Surrogate model-based space mapping in post-fabrication bandpass filters' tuning. *IEEE Transactions on Microwave Theory and Techniques, 68*(6), 2172–2182. https://doi.org/10.1109/tmtt.2020.2977022
89. Bandler J. W., Biernacki R. M., and Chen S. H., (1996). Fully automated space mapping optimization of 3D structures. In 1996 IEEE MTT-S International Microwave Symposium Digest, San Francisco, CA, USA. pp. 1–4. doi: https://doi.org/10.1109/mwsym.1996.511048
90. Bakr, M. H., Bandler, J. W., & Georgieva, N. (1999). An aggressive approach to parameter extraction. *IEEE Transactions on Microwave Theory and Techniques, 47*(12), 2428–2439. https://doi.org/10.1109/mwsym.1999.779470
91. Bode H. W., (1945). Network analysis and feedback amplifier design. doi: https://doi.org/10.1183/09031936.00138507.
92. Pinel, J. F. (1971). Computer-aided network tuning. *IEEE Transactions on Circuit Theory, 18*(1), 192–194.
93. Marshall, P. M., & Tissi, P. (1991). A new algorithm for the accurate alignment of microwave networks. *IEEE Transactions on Microwave Theory and Techniques, 39*(10), 1754–1758. https://doi.org/10.1109/22.88547
94. Cegielski T., and Michalski J., (2008). Heuristic methods for automated microwave filter tuning. In 2008 17th International Conference on Microwaves, Radar and Wireless Communications (MIKON 2008). pp. 1–4.
95. Kirkpatrick, S., Jr., Gelatt, C. D., & Vecchi, M. P. (1983). Optimization by simulated annealing. *Science, 220*(4598), 671–680.
96. Lewis, R. M., Torczon, V., Trosset, M. W., & William, C. (2000). Direct search methods : then and now. *Journal of Computational and Applied Mathematics, 124*(1–2), 191–207.
97. "Intelligent Automatic Filter Tuning Tool (IAFTT): European Patent Application No. P382895 assigned by Polish National Patent Office," 2007

98. Miraftab V., and Mansour R. R., (2002). Computer-aided tuning of microwave filters using fuzzy logic. In IEEE MTT-S Int. Microw. Symp. Dig. pp. 1117–1120. doi: https://doi.org/10.1109/MWSYM.1986.1132161.
99. Miraftab, V., & Mansour, R. R. (2002). Computer-aided tuning of microwave filters using fuzzy logic. *IEEE Transactions on Microwave Theory and Techniques, 50*(12), 2781–2788. https://doi.org/10.1109/TMTT.2002.805291
100. Miraftab, V., & Mansour, R. R. (2004). A robust fuzzy-logic technique for computer-aided diagnosis of microwave filters. *IEEE Transactions on Microwave Theory and Techniques, 52*(1), 450–456. https://doi.org/10.1109/TMTT.2003.820895
101. Chiu, S. L. (1994). Fuzzy model identification based on cluster estimation. *Journal of Intelligent and Fuzzy Systems, 2*(3), 267–278. https://doi.org/10.3233/IFS-1994-2306
102. Miraftab V., and Mansour R. R., (2006). Automated microwave filter tuning by extracting human experience in terms of linguistic rules using fuzzy controllers. In 2006 IEEE MTT-S International Microwave Symposium Digest, San Francisco, CA, USA, 2006, pp. 1439–1442. doi: https://doi.org/10.1109/MWSYM.2006.249541
103. Miraftab, V., & Mansour, R. R. (2008). Fully automated RF/Microwave filter tuning by extracting human experience using fuzzy controllers. *IEEE Transactions on Circuits and Systems - I : Regular Papers, 55*(5), 1357–1367. https://doi.org/10.1109/TCSI.2008.916614
104. Peng S., Cao W., Bi L., Yuan Y., and Wu M., (2021). A tuning strategy for microwave filter using variable universe adaptive fuzzy logic system. In Proceeding - 2021 China Automation Congress, CAC 2021, Beijing - China, Institute of Electrical and Electronics Engineers Inc., pp. 6061–6066. doi: https://doi.org/10.1109/CAC53003.2021.9727379.
105. Bi, L., Cao, W., Hu, W., & Wu, M. (2022). A dynamic-attention-based heuristic fuzzy expert system for the tuning of microwave cavity filters. *IEEE Transactions on Fuzzy Systems, 30*(9), 3695–3707. https://doi.org/10.1109/TFUZZ.2021.3124643
106. Michalski, J. J. (2010). Artificial neural networks approach in microwave filter tuning. *Progress In Electromagnetics Research M, 13*, 173–188.
107. Michalski J. J, (2010). Artificial neural network algorithm for automated filter tuning with improved efficiency by usage of many golden filters. In 2010 18th International Conference on Microwave Radar and Wireless Communications (MIKON 2010), Vilnius, Lithuania. pp. 1–3.
108. Michalski, J. J., Kacmajor, T., Gulgowski, J., & Mazur, M. (2011). Consideration on artificial neural network architecture in application for microwave filter tuning. *Piers Online, 7*(3), 271–275.
109. Kacmajor T., and Michalski J. J., (2011). Principal component analysis in application for filter tuning algorithms. In 2011 IEEE MTT-S International Microwave Workshop- Series on Millimeter Wave Integration Technologies, Sitges, Spain, Sitges, Spain. pp. 121–123
110. Michalski J. J., and Kacmajor T., (2011). Filter tuning algorithm with compressed reflection characteristic by daubechies D4 wavelet transform. In 2011 41st European Microwave Conference (EuMC 2011), Manchester, UK, 2011, pp. 778–781
111. Kacmajor T., Kant P., and Michalski J. J., (2014). Microwave filter tuning for different center frequencies based on artificial neural network and phase compensation. In 2014 20th International Conference on Microwaves, Radar and Wireless Communications (MIKON 2014), Gydnia, Poland, 2014, pp. 1–4. doi: https://doi.org/10.1109/MIKON.2014.6899833.
112. Sutton, R. S., & Barto, A. G. (1998). *Reinforcement learning: An Introduction*. Cambridge: MIT Press. https://doi.org/10.1179/175622708X282910
113. Watkins C. J. C. H., (1989). Learning from delayed rewards, Ph.D Thesis, King's College, Cambridge University, UK
114. Wang Z., Yang J., Hu J., Feng W., and Ou Y., (2015). Reinforcement learning approach to learning human experience in tuning cavity filters. In 2015 IEEE International Conference on Robotics and Biomimetics (ROBIO 2015), Zhuhai, China. pp. 2145–2150. doi: https://doi.org/10.1109/ROBIO.2015.7419091.
115. Mnih, V., et al. (2015). Human-level control through deep reinforcement learning. *Nature, 518*(7540), 529–533. https://doi.org/10.1038/nature14236
116. V. Mnih *et al.*, (2013). Playing atari with deep reinforcement learning. *NIPS Deep Learning Workshop*. pp. 1–9
117. Sekhri E., Tamre M., and Kapoor R., (2019). Optimal Q-learning approach for tuning the cavity filters. In 2019 20th International Conference on Research and Education in Mechatronics (REM 2019), Wels, Austria, Wels, Austria: IEEE, 2019, pp. 1–4. doi: https://doi.org/10.1109/REM.2019.8744118.

118. Wang Z., Ou Y., Wu X., and Feng W., (2018) Continuous reinforcement learning with knowledge-inspired reward shaping for autonomous cavity filter tuning. In 2018 IEEE International Conference on Cyborg and Bionic Systems, Shenzhen, China, pp. 53–58.
119. Sekhri E., Kapoor R., and Tamre M., (2020) Double deep Q-learning approach for tuning microwave cavity filters using locally linear embedding technique. In 2020 15th International Conference on Mechatronic Systems and Materials, (MSM 2020), Bialystok, Poland, Bialystok, Poland: IEEE, 2020, pp. 1–6. doi: https://doi.org/10.1109/MSM49833.2020.9202393.
120. Roweis, S., & Saul, L. (2000). Nonlinear dimensionality reduction by locally linear embedding. *Science, 290*(5500), 2323–2326. https://doi.org/10.1126/science.290.5500.2323
121. Lindstah S., and Lan X, (2020) Reinforcement learning with imitation for cavity filter tuning. In 2020 IEEE/ASME International Conference on Advanced Intelligent Mechatronics (AIM-2020), Bosto*n, USA*, 2020, pp. 1335–1340. doi: https://doi.org/10.1109/AIM43001.2020.9158839.
122. Wang, Z., & Ou, Y. (2022). Learning human strategies for tuning cavity filters with continuous reinforcement learning. *Applied Sciences (MDPI)*. https://doi.org/10.3390/app12052409
123. Kacmajor T., and Michalski J. J., (2011) "Neuro-fuzzy approach in microwave filter tuning. In IEEE MTT-S International Microwave Symposium Digest, Baltimore, MD, USA, 2011, pp. 1–4. doi: https://doi.org/10.1109/MWSYM.2011.5972771.
124. Jang, J. S. R. (1993). ANFIS: adaptive-network-based fuzzy inference System. *IEEE Transactions on Systems, Man, and Cybernetics, 23*(3), 665–685. https://doi.org/10.1109/21.256541
125. Zhou J, and Huang J., (2013) Intelligent Tuning for Microwave Filters Based on Multi-Kernal Machine Learning Model. In 2013 5th IEEE International Symposium on Microwave, Antenna, Propagation and EMC Technologies for Wireless Communications, Chengdu, China, 2013, pp. 259–266
126. Hong, J., & Lancaster, M. J. (2001). *Microstrip filters for rf/microwave applications*. John Wiley & Sons Inc.
127. Zhou, J., Duan, B., & Huang, J. (2013). Support-vector modeling of electromechanical coupling for microwave filter tuning. *International Journal of RF and Microwave Computer-Aided Engineering, 23*(1), 127–139. https://doi.org/10.1002/mmce.20683
128. Zhou, J., Huang, J., Li, P., & Li, N. (2015). Hybrid modeling of microwave devices using multi-kernel support vector regression with prior knowledge. *International Journal of RF and Microwave Computer-Aided Engineering, 25*(3), 219–228. https://doi.org/10.1002/mmce.20852
129. Cao, W. H., Liu, C., Yuan, Y., Wu, M., & Wu, S. B. (2018). Parametric modeling of microwave filter using combined MLS-SVR and pole-residue-based transfer functions. *International Journal of RF and Microwave Computer-Aided Engineering, 28*(5), 1–10. https://doi.org/10.1002/mmce.21246
130. Xu, S., An, X., Qiao, X., Zhu, L., & Li, L. (2013). Multi-output least-squares support vector regression machines. *Pattern Recognit Lett, 34*(9), 1078–1084. https://doi.org/10.1016/j.patrec.2013.01.015
131. Michalski, J. J. (2012). On linear mapping of filter characteristic to position of tuning elements in filter tuning algorithm. *Progress In Electromagnetics Research, 123*, 279–298.
132. Wolberg, J. (2006). *Data analysis using the method of least squares*. Springer.
133. Kacmajor, T., & Michalski, J. J. (2013). Filter tuning based on linear decomposition of scattering characteristics. *Progress in Electromagnetics Research, 135*, 451–464. https://doi.org/10.2528/PIER12112603
134. Zhang, Y.-L., Su, T., Li, Z.-P., & Liang, C.-H. (2013). A fast tuning method for microwave filter using VF-ASM technology. *Progress In Electromagnetics Research M, 30*, 25–37. https://doi.org/10.2528/PIERM13012201
135. Zhang, Y.-L., Su, T., Li, Z.-P., & Liang, C.-H. (2013). A hybrid computer-aided tuning method for microwave filters. *Progress In Electromagnetics Research, 139*, 559–575.
136. Wu, S., Liu C, Cao W, and Wu M, "A new method for hybrid diagnosis and tuning of coaxial cavity filter. In 2017 36th Chinese Control Conference (CCC 2017), Dalian, China, 2017, pp. 9692–9696. doi: https://doi.org/10.23919/ChiCC.2017.8028902
137. Wang, R., Li, L.-Z., Peng, L., Tu, X.-Q., & Zhong, X.-X. (2016). Diagnosis of coupled resonator bandpass filters using VF and optimization method. *Progress In Electromagnetics Research M, 51*, 195–203. https://doi.org/10.2528/PIERM16083001
138. Wu, S., Cao, W., Wu, M., & Liu, C. (2018). A tuning method for microwave filter via complex neural network and improved space mapping. *World Academy of Science, Engineering and Technology: International Journal of Electronics and Communication Engineering, 12*(3), 222–228.
139. Wu, S., Cao, W., Liu, C., & Wu, M. (2018). A computer-aided tuning method for microwave filters by combing T-S fuzzy neural networks and improved space mapping. *Computer Modeling in Engineering and Sciences, 116*(3), 433–453. https://doi.org/10.31614/cmes.2018.03309

140. Yang, Z., Peng, M., Cao, Y., & Zhang, L. (2014). A new multi-objective reliability-based robust design optimization method. *Computer Modeling in Engineering and Sciences, 98*(4), 409–442. https://doi.org/10.3970/cmes.2014.098.409
141. Golub, G. H., & Van Loan, C. F. (1996). *Matrix Computations 3rd edition*. The Johns Hopkins University Press.
142. Traina, D., Macchiarella, G., & Sarkar, T. K. (2007). Robust formulations of the cauchy method suitable for microwave duplexers modeling. *IEEE Transactions on Microwave Theory and Techniques, 55*(5), 974–982. https://doi.org/10.1109/TMTT.2007.895394
143. Traina, D., & Macchiarella, G. (2007). New general formulation of the cauchy method for the accurate model extraction of higher order microwave systems. *Microwave and Optical Technology Letters, 49*(8), 1957–1961. https://doi.org/10.1002/mop
144. Wilkinson, J. H. (1961). Error analysis of direct methods of matrix inversion. *Journal of ACM (JACM), 8*(3), 281–330. https://doi.org/10.1145/321075.321076
145. Bauer, F. L., (1963). Optimally scaled matrices. In Numerische Mathematik. 5, pp. 73–87.
146. Wu, S., & Cao, W. (2019). Parametric model for microwave filter by using multiple hidden layer output matrix extreme learning machine. *IET Microwaves, Antennas and Propagation, 13*(11), 1889–1896. https://doi.org/10.1049/iet-map.2018.5823
147. Wu, S. B., & Cao, W. H. (2019). Tuning model for microwave filter by using improved back-propagation neural network based on Gauss Kernel clustering. *International Journal of RF and Microwave Computer-Aided Engineering, 29*(8), 1–10. https://doi.org/10.1002/mmce.21787
148. Halat S, and Mehdi M (2021), "Modified double DQN: addressing stability,. doi: https://doi.org/10.48550/arXiv.2108.04115.
149. E. Sekhri, M. Tamre, R. Kapoor, and D. C. Liyanage, "Novel Band-Subtraction Technique to Differentiate Screws for Microwave Cavity Filter Tuning," in *International Conference on Electrical, Computer, Communications and Mechatronics Engineering (ICECCME 2023), Tenerife, Canary Islands, Spain*, Institute of Electrical and Electronics Engineers Inc., 2023, pp. 1–6. doi: https://doi.org/10.1109/ICECCME57830.2023.10253048.

Even Sekhri received the B. Tech degree in mechanical engineering from Kurukshetra University, India in 2009. In 2013, he received his first master's degree i.e. M. Tech degree in manufacturing, automation and robotics from Manav Rachna International University, Faridabad, India. Later, he received his second master's degree i.e. MSc in Mechatronics from Tallinn University of Technology (TalTech), Tallinn, Estonia in 2017. Currently, Even Sekhri is a Ph.D. student as well as he is working as an Engineer with the TalTech, Tallinn, Estonia. He is currently working on several projects. He has extensive experience with a total experience of almost 14 years wherein he has published four (04) books. Also, he has authored and co-authored research articles in various renowned international journals and conferences. His research areas include microwave filters, machine vision, machine learning, image processing, control systems and so on.

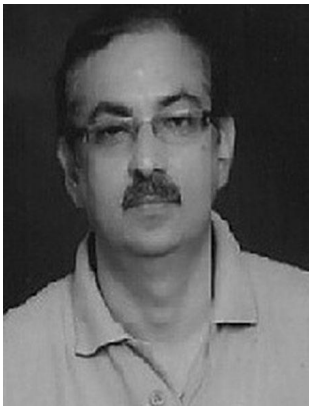

Rajiv Kapoor received the B.E., M.E. and the Ph.D. degree in electronics and communication engineering from Punjab Engineering College, Panjab University, Chandigarh, India, in 2004. He is currently a Professor with the Department of Electronics and Communication Engineering, Delhi Technological University (DTU), New Delhi, India. He is currently working on multiple industry-sponsored projects and has got 11 patents published and 5 patents awarded. He has extensive industry and academic experience of approximately 35 years. He has published nine books and has got H-Index of 28 with more than 300 publications in the journals and conferences of repute. He has designed a number of products like for Medical Electronics, Communication Engg and some are at TRL level 7 or above. He has his Industry sponsored Laboratory for Product Design. His research interests include computer vision, machine learning, signal and image processing, sensor design, and so on specially to help the society, poor people and Farmers with novel and affordable technologies.

Mart Tamre received the MSc Engineering Diploma in Mechanical Engineering (Fine Mechanics) from Tallinn University of Technology (TalTech), Tallinn, Estonia in 1982, and the Ph.D. degree in 1995 from TalTech, Tallinn, Estonia. He is currently working as a Professor of Mechatronics with Department of Electrical Power Engineering and Mechatronics, TalTech, Tallinn, Estonia. He has 40 years of experience in academics and industry and currently he is working on several government, EU, and industry-sponsored projects. He is a member of numerous professional societies incl. IEEE, and he has work experience from many removed Universities like MIT (US), Wales Univ. (UK), etc. He has authored and co-authored over 100 research papers in various renowned international journals and conferences. He has also authored chapters in various books and contributed to numerous inventions. His research areas include electronics and filters, hyperspectral Imaging, image classification, artificial intelligence, robot control and vision, machine vision, etc.

Appendix 2

Model training curves

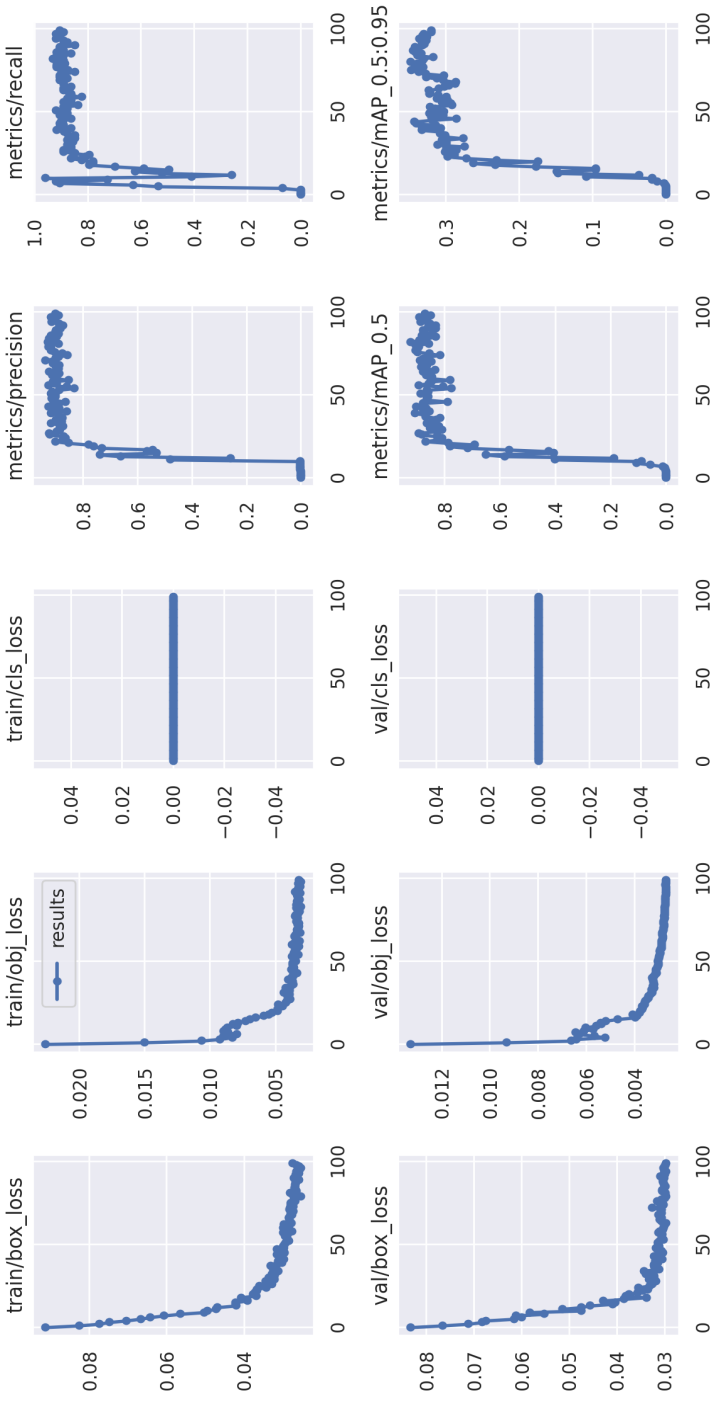

Appendix 3

Training hyperparameters for training YOLOv5

Table Appendix3: Training hyperparameters

Hyperparameter	Value	Hyperparameter	Value
lr0	0,01	fl_gamma	0,0
Lrf	0,01	hsv_h	0,015
Momentum	0,937	hsv_s	0,7
weight_decay	0,0005	hsv_v	0,4
warmup_epochs	3,0	degrees	0,0
warmup_momentum	0,8	translate	0,1
warmup_bias_lr	0,8	scale	0,5
Box	0,05	shear	0,0
Cls	0,5	perspective	0,0
cls_pw	1,0	flipud	0,0
Obj	1,0	fliplr	0,5
obj_pw	1,0	mosaic	1,0
iou_t	0,2	mixup	0,0
anchor_t	4,0	copy_paste	0,0

Curriculum vitae

Personal data

Name:	Even Sekhri
Date of birth:	03.03.1988
Place of birth:	Ambala (India)
Citizenship:	Indian

Contact data

E-mail:	even.sekhri@taltech.ee/evensekhri@gmail.com

Education

2018–2024	Tallinn University of Technology, Estonia – PhD
2017–2018	Open School, Tallinn University of Technology, Estonia – Student
2015–2017	Tallinn University of Technology, Estonia – MSc in Mechatronics (Cum Laude)
2010–2013	Manav Rachna International University, India – MTech in Manufacturing, Automation and Robotics (Evening Shift)
2005–2009	Ambala College of Engineering and Applied Research, India – BTech in Mechanical Engineering
1992–2005	Schooling from The Central Boars of Secondary Education (CBSE), India

Language competence

English	Fluent
Hindi	Native

Professional employment

2015–Present	Tallinn University of Technology, Estonia – Engineer (Projects, Supervisor of MSc theses, Teacher for MSc and BSc courses)
2015–2015	Chandigarh Group of Colleges, Jhanjeri, India – Assistant Professor (Projects, Supervisor of BTech theses, Teacher in Mechanical Engineering department for BTech courses)
2014–2014	ITS Engineering College, Greater Noida, India – Assistant Professor (Projects, Supervisor of BTech theses, Teacher in Mechanical Engineering department for BTech courses)
2010–2014	Manav Rachna International University, Faridabad, India – Assistant Professor during Morning Shift (Projects, Supervisor of BTech theses, Teacher in Mechanical Engineering department for BTech courses)
2009–2010	Swami Divyanand Polytechnic of Engineering, Mullana, India – Lecturer (Projects, Supervisor of Diploma Dissertations, Teacher in Mechanical Engineering department for Diploma courses)

Elulookirjeldus

Isikuandmed

Nimi:	Even Sekhri
Sünniaeg:	03. märts 1988
Sünnikoht:	Ambala (India)
Kodakondsus:	India

Kontaktandmed

E-post:	even.sekhri@taltech.ee/evensekhri@gmail.com

Hariduskäik

2018–2024	Tallinna Tehnikaülikool – PhD
2017–2018	Tallinna Tehnikaülikooli Avatud Ülikool – tudeng
2015–2017	Tallinna Tehnikaülikool – MSc mehhatroonika eriala (Cum Laude)
2010–2013	Manav Rachna Rahvusvaheline Ülikool, India – MTech, tootmine, automaatika ja robootika (õhtune)
2005–2009	Ambala Tehnika- ja rakendusuuringute kolledž, India – BTech, masinaehitus
1992–2005	Central Board of Secondary Education (CBSE), India – keskharidus

Keelteoskus

Inglise keel	Kõrgtase
Hindi keel	Emakeel

Teenistuskäik

2015–tänaseni	Tallinna Tehnikaülikool, Inseneriteaduskond – Insener
2015–2015	Chandigarhi kolledžite rühm, Jhanjeri tehniline ülikoolilinnak, India – Abiprofessor (Projektid, BTech lõputööde juhendaja, BTech kursuste masinaehitusosakonna õpetaja)
2014–2014	ITS Engineering College, Greater Noida, India – Abiprofessor (Projektid, BTech lõputööde juhendaja, BTech kursuste masinaehitusosakonna õpetaja)
2010–2014	Manav Rachna Rahvusvaheline ülikool, Faridabad, India – Abiprofessor hommikuse vahetuse ajal (projektid, BTech lõputööde juhendaja, BTech kursuste masinaehitusosakonna õpetaja)
2009–2010	Swami Divyanand Tehnika Polütehnikum, Mullana, India – Lektor (õppejõud) (projektid, diplomitööde juhendaja, diplomikursuste masinaehitusosakonna õpetaja)

ISSN 2585-6901 (PDF)
ISBN 978-9916-80-139-0 PDF)